# Investigation in the Pyrolysis of Corrugated Cardboard and Waxed Cardboard into Fuels and Products

A Dissertation

Presented in Partial Fulfillment of the Requirements for the

Degree of Doctor of Philosophy

with a

Major in Natural Resources

in the

College of Graduate Studies

University of Idaho

by

Farid Sotoudehnia

Major Professor: Armando G. McDonald, Ph.D.

Committee Members: Randall Brooks, Ph.D.; Kamal Kumar, Ph.D.; Steven Shook, Ph.D.

Department Administrator: Charles Goebel, Ph.D.

May 2021

## Authorization to Submit Dissertation

This dissertation of Farid Sotoudehnia submitted for the degree of Doctor of Philosophy with a Major in Natural Resources and titled "Investigation in the Pyrolysis of Corrugated Cardboard and Waxed Cardboard into Fuels and Products," has been reviewed in final form. Permission, as indicated by the signatures and dates below, is now granted to submit final copies to the College of Graduate Studies for approval.

Major Professor: _____ Date: 04/22/2021

Armando G. McDonald, Ph.D.

Committee Members: _____ Date: 4/27/2021

Randall H. Brooks, Ph.D.

_____ Date: 4/22/2021

Kamal Kumar, Ph.D.

_____ Date: 4/22/2021

Steven Shook, Ph.D.

Department
Administrator: _____ Date: 4/22/21

Charles Goebel, Ph.D.

# Abstract

Waste corrugated cardboard and waxed cardboard comprise a substantial portion of municipal solid waste. More than 17 million tons of paper products end up in landfills every year, and this number is expected to grow significantly with the increase in human population in the next few decades. Methods of product and energy recovery from waste can serve as means of not only reducing the environmental and economic impacts of landfilling, but also ensuring sufficient energy resources for future generations. Both waste cardboard and waxed cardboard are suitable resources for thermochemical conversion. Utilizing pyrolysis, a set of experiments was developed to establish waste-to-product and waste-to-energy pathways for cardboard and waxed cardboard. In the first step, waste cardboard was extensively characterized and then pyrolyzed in an auger reactor. The pyrolysis products were characterized. The liquid product (oil) could be used as bunker fuel or further refined to harvest valuable compounds such as levoglucosan. Cardboard solid product (char) was found to be suitable for use in composite materials and as soil amendment. In the second step, waxed cardboard was characterized and pyrolyzed and the pyrolysis products (wax-oil and char) were characterized and analyzed. The wax was effectively recovered. The main compounds found in wax-oil were alkanes, alkenes, and dienes ($C_9$ to $C_{36}$). Higher pyrolysis temperatures resulted in the breakdown of larger carbon chains into smaller chain alkanes. The wax-oil contained an abundance of long-chain hydrocarbons and small number of oxygenated compounds that made it suitable for further upgrading into fuels. In the final step, the wax-oil samples were thermally and catalytically pyrolyzed on a custom-made small tubular batch reactor, and the resultant liquid products were analyzed against gasoline to evaluate their performance as a transport fuel. The products of thermal pyrolysis of the samples were mainly comprised of dienes and short-chain olefins, oxygenated compounds, and minor amounts of aromatic compounds. Their functional groups resembled those found in paraffin. The catalytic pyrolysis liquid products were similar to gasoline in chemical composition and functional groups and could be used as a "drop in" fuel. The addition of zeolite Y as the catalyst facilitated the conversion of long-chain hydrocarbons to short-chain alkanes and aromatics. The catalyst was able to be recovered and reused, which is an important feature for industrial use in catalytic pyrolysis.

**Acknowledgements**

I would like to express my deepest gratitude to my advisor, Dr. Armando McDonald, for his continuous support and guidance during my Ph.D. studies. His dedication to science and depth of knowledge is exemplary, and he has certainly set an example of excellence as a researcher and mentor for me.

I would also like to express my appreciation to Drs. Randall Brooks, Kamal Kumar, and Steven Shook for serving in my committee and for their valuable feedback and suggestions.

I would like to thank the Forest, Rangeland and Fire Sciences Department Chair, Dr. Charles Goebel, for his support and encouragement throughout the course of my Ph.D.

I am forever grateful to Dr. Thomas Gorman for believing in me and always having my back.

I would like to acknowledge Dr. Bob Stillinger Scholarship, Office of Research and Economic Development, and College of Natural Resources at the University of Idaho for making this work possible. I would also like to thank Drs. Thomas Williams and Eric Aston for their contributions to this work.

I sincerely thank my wonderful colleagues and lab mates at the Forest and Sustainable Products Lab for their professional and moral support. You all have made this journey more enjoyable. I am especially thankful to Mr. Dan Mottern, who have thought me many life lessons throughout the years. I am also grateful to Dan's daughter, Ella, whose presence has brightened my days in the lab on many occasions.

I owe a debt of gratitude to my family and friends. Their support and love have kept me energized and motivated. Thank you!

**Table of Contents**

## List of Abbreviations

| | |
|---|---|
| ATR | Attenuated total reflection |
| ß | Heating rate |
| CCB | Corrugated cardboard |
| CCI | Cellulose crystallinity index |
| CeI | Cellulose index |
| CI | Carbonyl index |
| $\Delta H_m$ | Melting enthalpy |
| $\Delta H_0$ | Melting enthalpy of 100% crystalline polymer |
| DSC | Differential scanning calorimetry |
| DTG | Derivative thermogravimetry |
| $E_a$ | Activation energy |
| ESI-MS | Electrospray ion trap mass spectrometry |
| FTIR | Fourier transform infrared spectroscopy |
| GC-MS | Gas chromatogram mass spectrometry |
| HI | Hydroxyl index |
| $I_D$ | D-Raman peak |
| $I_G$ | G-Raman peak |
| $M_n$ | Number average molar mass |
| $M_w$ | Weight average molar mass |
| $M_z$ | Z-average molar mass |
| Py-GC-MS | Pyrolysis gas chromatography mass spectrometry |
| SEM | Scanning electronic microscopy |
| Ө | Half-angle of diffraction |
| TGA | Thermogravimetric analysis |
| $T_m$ | Melting temperature |
| WCCB | Waxed corrugated cardboard |
| $X_c$ | % Degree of crystallinity |
| XRD | X-ray diffraction |

## List of Tables

# List of Figures

## Chapter 1. Introduction and Literature Review

### 1.1    Motivation

The world is transitioning toward a circular economy, and municipal solid waste (MSW) management is one of the areas with significant value creation potential [1]. MSW poses serious environmental, health, and economic concerns globally [2].
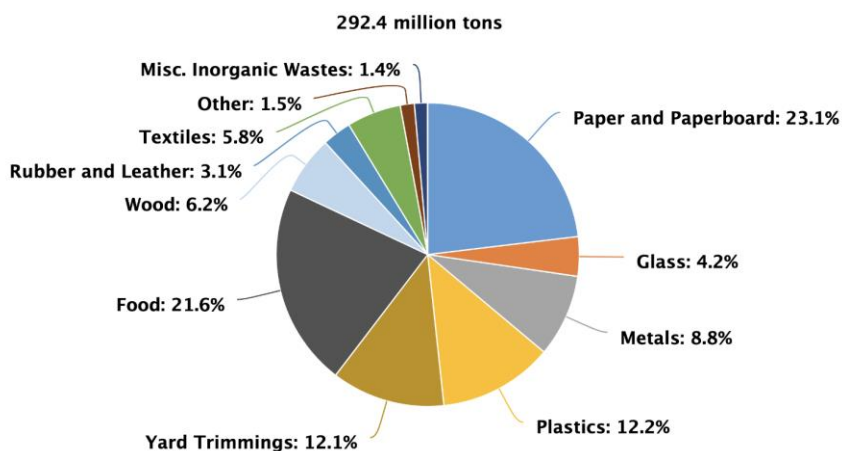


Figure 1.1. Total MSW generated by material in 2018. Source: epa.gov.

According to the Environmental Protection Agency (EPA), paper products, including cardboard, comprise the largest component of MSW in the USA (Figure 1.1). While a considerable portion of paper products is recycled, about 30% end up in the landfills [3]. In 2018, landfills received 17.2 million tons of paper products, an astonishing 11.8% of all MSW landfilled [4].

About 5% of all cardboard is coated or impregnated with wax to enhance its compression strength and durability under humid, wet conditions [5]. This wax coating is generally a plastic-like compound such as polyethylene (PE) [6] or paraffin [7]. Waxed cardboard is primarily used by retailers and rarely by consumers, and therefore, has the potential to be commercially collected. Waxed corrugated cardboard (WCCB) cannot be recycled, and in fact, can adversely impact the environment and ecosystems if comingled with non-coated corrugated cardboard (CCB) [5].

With the increase in human population, it is expected that MSW generation will increase in the next few decades. Even though the landfills have come a long way in minimizing the environmental impacts of MSW, and engineered landfills are now subject to stringent regulations to protect the environment [8], there are still concerns about the disposal of non-readily biodegradable MSW such as waxed cardboard.
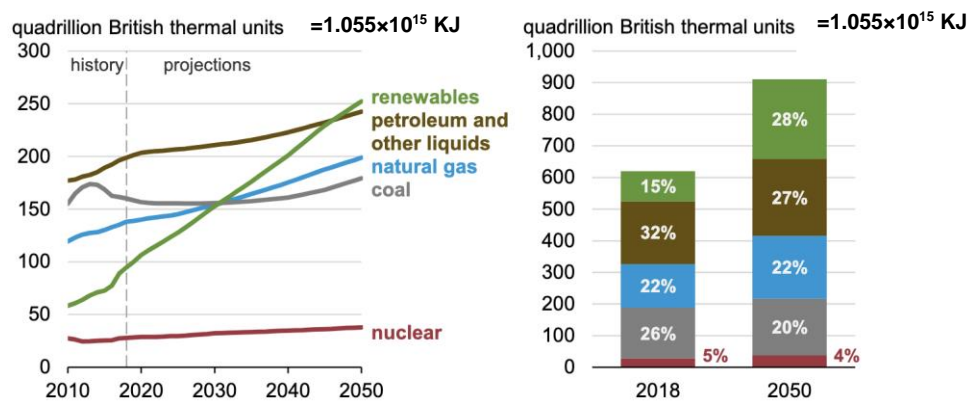


Figure 1.2. Global primary energy consumption by energy source (2010-2050) (1 BTU= 1.055 KJ). Source: eia.gov.

The United States Energy Information Administration (EIA) projects a 50% increase in global energy usage buy the year 2050 (Figure 1.2) [9]. Petroleum-based fuels will not be able to keep up with an increase in consumption rate [10]. To ensure having sufficient energy sources, it is crucial to find ways to harvest energy from renewable resources and to recover energy from sources traditionally considered waste. The large body of literature on both topics, renewable resources and waste-to-energy, as well as governmental [11] and non-governmental initiatives [12] are testaments to the necessity.

Our goal in this dissertation is to propose a feasible pathway to recover products and energy from waste cardboard and waxed cardboard. In the next section, we will provide some background information on the structure of cardboard and waxed cardboard and then introduce a number of potential processes that can facilitate the waste-to-product and waste-to-energy pathways.

## 1.2 Background and literature review

### 1.2.1 Cardboard and waxed cardboard

Corrugated fiberboard is often referred to as CCB and is comprised of several layers of paperboard, typically two outer layers and an inner corrugated layer (medium) (Figure 1.3). A starch-based adhesive is used to join the medium to one of two outer paperboard layers [13].
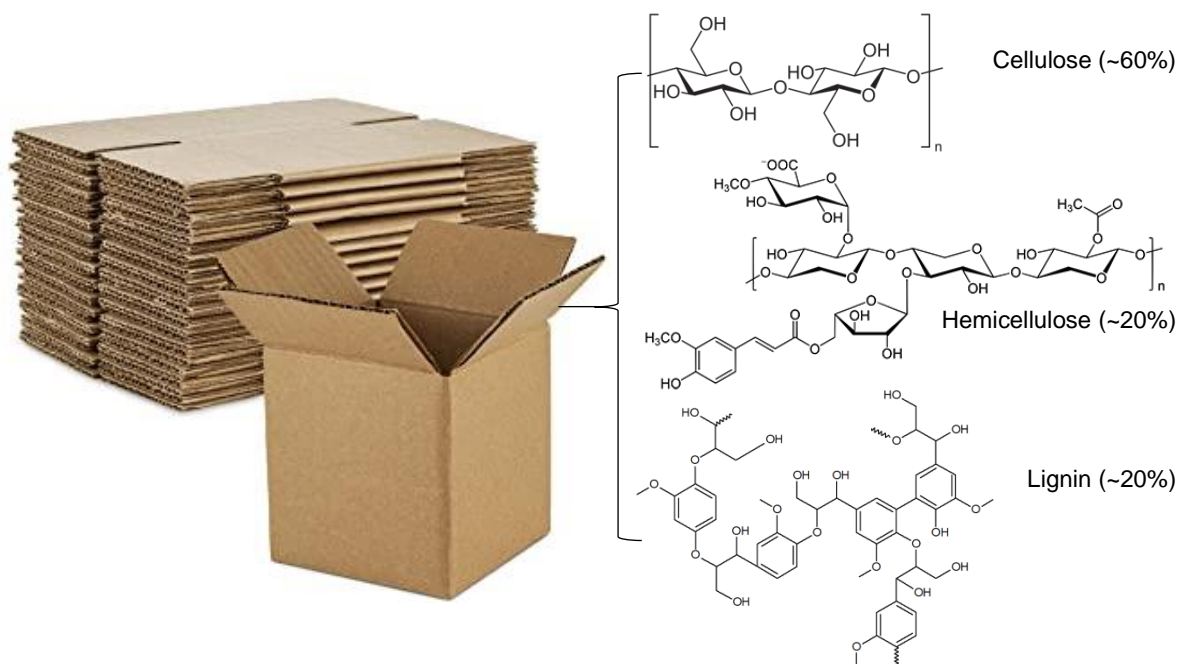


Figure 1.3. Cardboard structural composition.

The pulp used in the construction of CCB is composed primarily of cellulose, hemicellulose, and lignin [14], making CCB a structurally close relative of lignocellulosic materials, such as wood (Figure 1.3). As a lignocellulosic compound, cardboard has shown potential when added as a solid fuel component [15].

Waxed corrugated cardboard (WCCB), as the name suggests, is cardboard that has been coated with a layer of wax. The wax can be paraffin or PE, both petroleum-derived polymers, and is the main reason for non-recyclability of WCCB.

### 1.2.2 Thermochemical conversion processes

Surveying the literature to find potential technologies that can be used successfully on both lignocellulosic (cardboard) and petroleum-derived (wax) feedstocks on recovering products

and energy was via thermochemical conversion processes such as combustion, gasification, hydrothermal liquefaction, and pyrolysis (Figure 1.4).
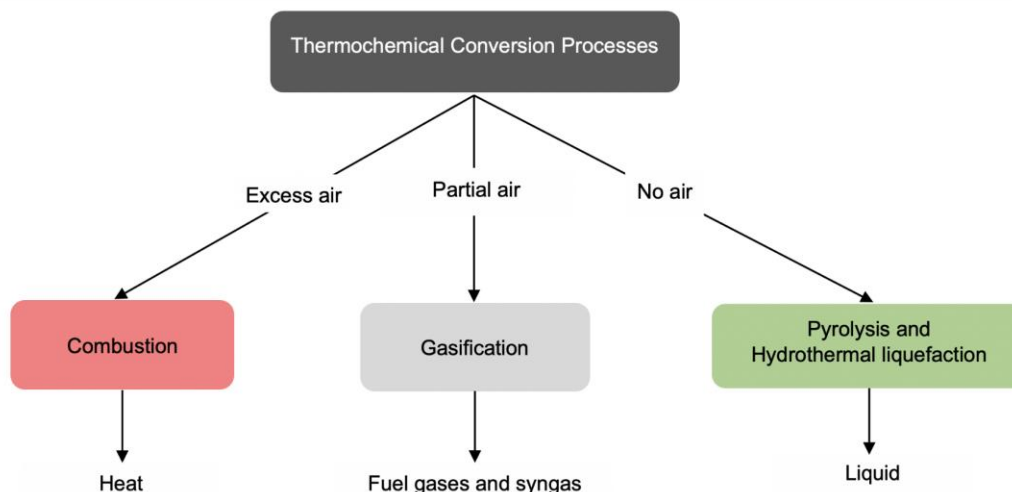


Figure 1.4. Thermochemical conversion processes and products.

## 1.2.2.1 Combustion

Direct combustion is the simplest and oldest way to capture energy. During the combustion process, the feedstock is burned in specialized boilers to generate heat and often steam. The heat and/or steam can then be used for multiple purposes such as heating and producing electricity. Wood and woody biomass is the most suitable for direct combustion. The EPA has reported that 4.2 million tons of waste paper products and 5.6 million tons of plastics have been combusted in 2018 [4]. Direct combustion of lignocellulosic biomass/feedstock constitutes about 95–97% of the world's bioenergy [16]. Modern combustion systems are highly efficient and can control pollutant emissions rather precisely [17]. Even with highly controlled systems, one of the concerns surrounding bioenergy produced through combustion is the release of nitrogen oxides ($NO_x$). Nitrogen oxides can cause damage to human and animal health and natural ecosystems and crops through the formation of photochemical smog, acid rain, and ground-level ozone [18].

## 1.2.2.2 Gasification

Gasification is another thermochemical process that converts carbon rich feedstocks (biomass, coal and MSW) into syngas (i.e., carbon dioxide ($CO_2$), hydrogen ($H_2$), and carbon

monoxide (CO)). Syngas production is optimized during gasification, and little amounts of char and oil are produced. The syngas can be used directly as a fuel (in the case of CO and $H_2$) or can be converted to other desired chemical products including methanol and dimethyl ether [19]. Multiple gasification technologies with enhancements have been proposed in the literature including steam gasification in Dual Fluidized Bed (DFB) gasifiers [20], which provides considerably higher gas qualities than air-blown gasification, and co-gasification of coal and biomass for improved hydrogen yield [21]. Saeba et al. have reported that they have successfully used gasification to obtain syngas from a different mixtures of PE and polypropylene (PP), with pure PE having the highest syngas production potential [22]. The literature on the gasification lignocellulosic feedstock is not as promising and often times favors mixtures of lignocellulosic feedstock, such as coconut shells, and other less environmentally friendly feedstocks such as charcoal [23].

### 1.2.2.3 Hydrothermal liquefaction

Hydrothermal liquefaction (HTL) is yet another thermochemical process that converts feedstock into bio-crude oils. The process takes place in water at moderate temperatures (200- 400 ℃) and high pressures (10- 25 MPa). A liquid bio-crude is the main product of HTL [24]. Toor et al., suggest that the HTL process is comprised of three main steps: (ii) depolymerization, (ii) decomposition, and (iii) recombination into bio-crude, gas, and solid compounds [25]. Many feedstocks can be used in HTL. However, better results have been observed in resources with higher lignin content [26] and plastics [27]. Seshasayee et al. have reported that they have produced energy-dense oils from polyolefins, polycarbonates, and polyesters [27]. Compared to gasification, HTL provides some advantages, namely, HTL does not require the feedstock to be dry or low in moisture content, which eliminates the energy-expensive drying process necessary. However, the use of high pressure can drive up equipment costs and pose as a disadvantage.

### 1.2.2.4 Pyrolysis
### 1.2.2.4.1 Thermal pyrolysis

Pyrolysis is the process of thermochemical decomposition of organic material at high temperatures and in the absence of oxygen to produce oil, char, and gas (e.g., $H_2$, CO, $CO_2$, and $CH_4$). Proportions of products vary according to pyrolysis operating conditions and

feedstock characteristics. During pyrolysis, the temperature and heating rate are usually controlled to optimize the production of oil. The feed particles should also have a controlled moisture content to achieve optimal mass and heat transfer [28]. Liquid product of pyrolysis can be upgraded and enhanced to substitute fossil fuels in many applications including transportation. The literature on pyrolysis shows that high-quality oil can be obtained from different feedstocks including lignocellulosic material [29], microalgae [30], and waste products [31]. However, the pyrolysis oil of lignocellulosic materials, such as paper products, may contain oxygenated compounds due to the feedstock's lower C/H [32]. The literature is rich on the pyrolysis characteristics of cellulosic materials such as printing paper, cardboard, and waste packaging. The reaction products have also been extensively characterized [32]–[35]. Zhou et al. [32] have identified phenolics and benzenes as the two main groups in the oil of printing paper and cardboard. They have also presented the yields of several non-aromatic compounds formed from cyclization reactions at 500 °C. Their findings suggested that combination reactions dominate at the temperature zone of 400 °C to 500 °C, and decomposition reactions dominate at a higher temperature. Phan et al. [35] have reported that the char portion contained the highest energy content in the cardboard. Cardboard biochar has been shown to be a suitable material as a reinforcing filler in composite materials due to its improved weatherability and bio durability [36]. In addition to having been extensively used for lignocellulosic feedstock, pyrolysis has been explored for plastic waste [37].

In contrast to lignocellulosic materials such as cardboard, synthetic polymers such as PE, deliver oils and waxes of higher quality due to their high C content [38]. Studies have shown that co-pyrolysis of lignocellulosic feedstock with synthetic polymers enhances the properties of the obtained oil. Paradela et al. have reported that increase in the plastics content in the blend of pine, plastics, and tires not only increased liquids yield (from 33% to 92% w/w) and favoured the formation of lighter compounds (less distillation residue), but it also favoured the conversion of aromatic compounds into alkanes and alkenes [39]. Rutkowski studied the bio-oil characteristics of beverage carton packaging waste and found that non-catalytic pyrolysis of their feedstock led to the formation of levoglucosan as a major liquid product of cardboard decomposition [40] and long-chain hydrocarbons as the product of thermal decomposition of PE layers [33]. Chen et al. also reported that co-pyrolysis of waste paper and PE significantly enhanced the oil yield and the fuel properties of the obtained oil [38].

Other studies have shown that pyrolysis of plastic waste can result in the generation of a mixture of hydrocarbons under various pyrolysis conditions [41]–[46].

### 1.2.2.4.2  Catalytic pyrolysis

While multiple studies show the feasibility of the pyrolysis process to recover products and value from MSW and other feedstock [33], [38], [39], [41]–[46], there are concerns about the economic and energy consumption feasibility of the process. Moreover, quite often, the pyrolysis process produces liquid oil that contains large carbon chain compounds [47]. The oil may also be of lower quality because of its low octane number and presence of solid residues [48] and impurities such as sulfur, nitrogen, chlorine, and phosphorous [49]. To overcome these issues, catalytic pyrolysis of MSW has become a topic of interest in the past decade [50]. Various catalysts have been utilized such as Red Mud and ZSM-5 [50], FCC [51], HZSM-5 [52], zeolite Y [53], $Fe_2O_3$ [54], and natural zeolite [55] among others to improve the quality of the obtained oil in catalytic pyrolysis.

### 1.2.3  The Catalyst

The primary function of the catalysts is to increase the proportion of lighter hydrocarbons in the oil through cracking reactions [56] and improve the overall process energy efficiency [50] (i.e., achieving higher quality products at lower temperatures).

The first step in catalytic pyrolysis is the thermal cracking on the external surface of the catalyst. The porous structure inside the catalyst works as channels for selective movement and breakdown of large hydrocarbon chains into smaller ones [51].  Generally, the degradation of heavier alkenes occurs in the outer surface of the catalyst, and further degradation and product selectivity take place in the internal pores of the catalyst [57]. The catalyst can be mixed with feedstock in the reactor or with organic vapors produced in a separate catalyst chamber. Lopez et al. [50] and Chen et al. [43] have reported that a liquid phase or direct contact with feedstock improves the cracking process by reducing the reaction temperature and retention time. However, in the case of direct contact, it is difficult to recover the catalyst due to the sticky nature of plastic feedstock [55]. Various catalysts such as zeolite Y and ZSM-5 [50] were used with vapor phase contact with promising results.

Catalyst characteristics such as Brunauer–Emmett–Teller (BET) surface area, pore size, pore volume, and acidity are the main factors of catalysts that affect its activity in the pyrolysis process [57]. Syamsiro et al. have reported that using a catalyst with a high BET surface area allows for more contact between reactants and the catalyst surface, which results in an increased rate of cracking reaction to produce more gases than liquid oil [55].

The three main type of catalysts used in catalytic pyrolysis include fluid catalytic cracking (FCC), silica–alumina catalysts, and zeolites [57]. FCC catalysts are mainly used in the petroleum refineries for cracking of heavy oil into gasoline and liquid oil petroleum. These catalysts have been used in the pyrolysis process successfully [57]. Silica-alumina catalysts are amorphous catalysts that have Lewis acid sites as electron acceptors and Brønsted acid sites with ionizable hydrogen atoms (Figure 1.5) [57]. It has been shown that the acidity of these catalysts affects the production of liquid oil from plastic waste, and lower acidity results in higher yield [58]. Zeolite catalysts are crystalline alumino-silicates molecular sieves that have a 3D framework consisting of cavities and channels. The main characteristic of these catalysts is their ion-exchange capabilities and open pores. Different ratios of $SiO_2/Al_2O_3$ in zeolites determine their reactivity and affects the final products of the pyrolysis process. Zeolite catalysts generally increase volatile hydrocarbon production and have a low rate of deactivation.
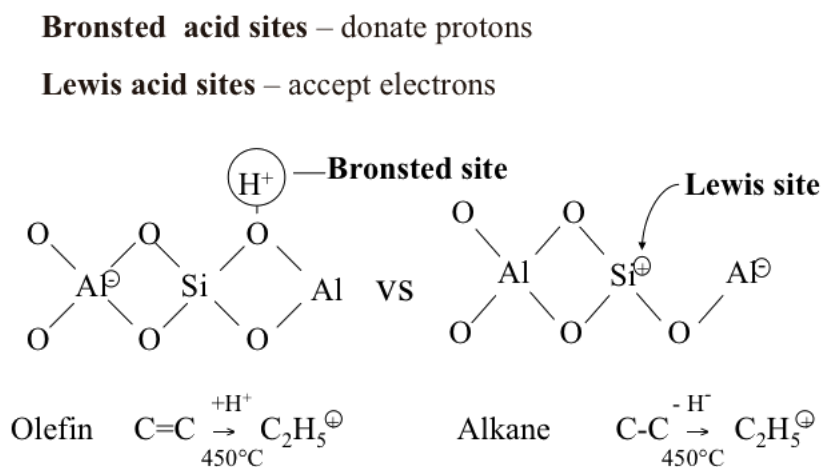


Figure 1.5. Formation of carbocations on acid cites of catalysts.

Among these catalysts, FCC catalysts increase the liquid oil yields and the use of spent catalysts (i.e., those that have been previously used in refineries) instead of fresh make them more economical [59]. It is noteworthy that the introduction of zeolite materials in FCC catalyst formulations (e.g., zeolite Y) resulted in a drastic increase in the gasoline yield in the 1970s and 1980s [60].

Yuan et al. co-pyrolyzed rice husk and polyvinyl chloride (PVC) with $MgO/MgCO_3$, which resulted in significantly decreased acid content and increase hydrocarbon content [61]. Miandad et al. have reported that natural and synthetic zeolite catalysts can be used for catalytic pyrolysis of four major types of plastic wastes such as PE, polystyrene (PS), PP, and polyethylene-terephthalate (PET). Their resultant liquid oils had high higher heating value (HHV, 40.2–45 MJ/kg) that is similar to conventional diesel [62]. Syamsiro et al. have used zeolite Y and natural zeolite catalysts for sequential pyrolysis and catalytic reforming of municipal plastic wastes and produced high-quality liquid products and higher heating value solid products than those of biomass and low-rank coal [55].

Zeolite Y (Figure 1.6) has been the main cracking component of FCC. This because zeolite Y possesses a unique combination of a few important characteristics: (1) high surface area and relatively large pores (~7.3 Å in diameter); (2) strong Brønsted acidity; (3) superior thermal and hydrothermal stability; and (4) low cost and reusability. The internal porous structure can convert longer-chain hydrocarbons to smaller molecules through the formation of carbenium ions via proton transfers in the hydrocarbon's Brønsted and Lewis acid sites (Figure 1.5). To pass through the pores of zeolite Y, the larger molecules in the wax-oil will need to be thermally cracked first before passing through the pores. Lee used multiple zeolite catalysts, including zeolite Y, for the upgrading of pyrolysis wax oil (obtained from municipal plastic waste) in a continuous plug flow reactor at 450 °C [53]. He reported that the catalyst pore dimensions play a vital role in the conversion of wax into light hydrocarbon and catalysts with more than one dimension, such as zeolite Y, show high conversion of wax into light hydrocarbon.
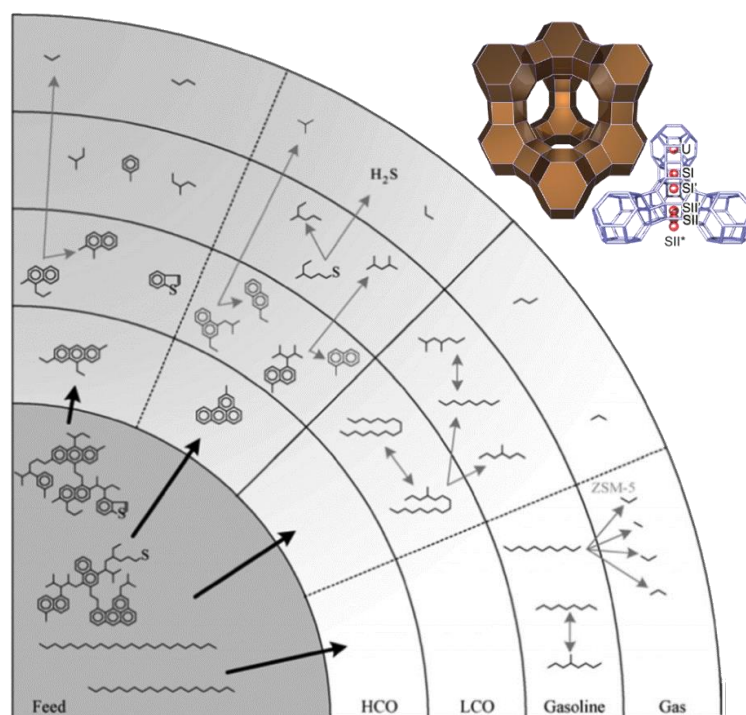
Figure 1.6. Consecutive cracking reactions of complex feedstock leading to the final FCC products. Source: E. T. C. Vogt, B. M. Weckhuysen, "Fluid catalytic cracking: recent developments on the grand old lady of zeolite catalysis."

Given the richness of literature on pyrolysis of both lignocellulosic and plastic feedstock as well as promising reported findings on the co-pyrolysis of the two, it was decided to investigate the pyrolysis of waste cardboard and waxed cardboard. In addition, catalytic pyrolysis using zeolite Y was investigated to improve the quality of the liquid pyrolysis products.

## 1.3    Objectives

The aims of this dissertation are to develop and evaluate waste-to-product and waste-to-energy processes for waste cardboard and waxed cardboard. The specific objectives to accomplish the aims include:

1. Investigation into the thermal behavior and characteristics of cardboard, followed by pyrolysis and product characterization.

2. Investigation into the thermal behavior and characteristics of waxed cardboard, chemical wax extraction, followed by pyrolysis and product characterization.

3. Thermal and catalytic upgrading of chemically and non-chemically recovered wax into liquid product yet potentially can be use as fuel.

4. Characterization of the resultant liquid and evaluation against gasoline.

Chapter 1 is a general introduction and outlines the motivation behind this work and provides a review of current literature on thermochemical conversion processes commonly used for municipal solid waste and strategies to improve processability and properties of the final products. Chapter 2 covers the study of thermal behavior and characteristics of waste cardboard. It also presents the details of the pyrolysis process and product characterizations. Chapter 3 discusses chemical and non-chemical wax extraction methods from waxed cardboard and presents the details of the pyrolysis process and product characterizations. Chapter 4 covers the thermal and catalytic upgrading of extracted wax and evaluation of the liquid product. Chapter 5 summarizes the conclusions and potential further work beyond this dissertation. Chapters 2 through 4 were written as separate journal manuscripts.

# Chapter 2. Characterization of Bio-Oil and Biochar from Pyrolysis of Waste Corrugated Cardboard

## 2.1    Abstract

As the most abundant municipal solid waste, corrugated cardboard (CCB) is a suitable resource for thermochemical conversion into various solid and liquid products.  CCB samples were pyrolyzed at three temperatures (350, 400, and 450 °C) and their pyrolysis products (bio-oil and biochar) were characterized and analyzed. Thermogravimetric analysis (TGA) was utilized to study the thermal degradation behavior of CCB. CCB and biochar samples were subjected to proximate, ultimate, lipid and carbohydrates analyses, and Py–GCMS to characterize their chemical components. The highest biochar yield was 75% at 350 °C, and the highest bio-oil yield was 47% at 450 °C. The biochar physical and chemical properties were also assessed using calorific values, specific surface area, Fourier-transform infrared (FTIR) and Raman spectroscopies, and x-ray diffraction (XRD). Biochar was found to have low ash and nitrogen contents. The bio-oil was characterized by the combination of GCMS, high-performance liquid chromatography (HPLC), and electrospray ionization mass spectrometry (ESI–MS). The molar mass distribution and an estimate of monomer/oligomer ratio were determined from ESI-MS data. The bio-oil contained a complex mixture of pyrans, furans, phenols, and cyclopentanes. Levoglucosan was abundantly found in the bio-oil, suggesting the suitability of cardboard pyrolysis products for further processing into fuels.

## 2.2    Introduction

The world is transitioning towards a circular economy, and municipal solid waste (MSW) management is one of the areas with great value creation potential [1]. Thermal conversion processes that convert MSW into products can be a solution to the problems associated with conventional landfilling of MSW [32].  Among all MSW, corrugated cardboard (CCB) is the waste fraction with the highest collection potential [1], [3], [63]. only CCB has shown great

potential when added as a solid fuel component [15], studies have shown that through pyrolysis, CCB may be a marketable candidate for alternative fuel production [32].

Pyrolysis has shown potential for biomass conversion in the area of renewable energy production [64] and energy recovery, and given the highly cellulosic nature of CCB, [65], [66], similar results can be expected when CCB is pyrolyzed. Pyrolysis generally refers to the irreversible process of thermochemical decomposition of organic materials at high temperatures and in the absence of oxygen. Temperature and residence time are the major factors that affect the proportions of oil, char, and syngas [67]. These factors can be adjusted to favor one product (e.g., biochar) or the other. Multiple studies have been conducted on the thermal conversion processes of cellulose and hemicellulose, including pyrolysis kinetics, the effects of reaction conditions, and the mechanisms of reactions [68]–[73]. Previous research has studied the pyrolysis characteristics of cellulosic materials such as printing paper, CCB, and waste packaging and some of the reaction products were characterized [32]–[35]. Zhou et al. [32] have identified substituted phenolics and benzenes as the two main groups in bio-oil. They have also presented the yields of several non-aromatic compounds formed from cyclization reactions at 500 °C. Their findings suggested that combination reactions dominate at the temperature zone of 400 °C to 500 °C and decomposition reactions dominate at a higher temperature. Phan et al. [35] have reported that the char portion contained the highest energy content in the cardboard. Few studies have investigated in detail the products from CCB pyrolysis and their potential to be used as alternative fuels and other products [35], [65], [74]. Biochar has been shown to be a suitable material as a reinforcing filler in composite materials due to its improved weatherability and bio durability [36].

This study aims to examine the feasibility of converting waste CCB into products. Mixed CCB was obtained from the recycling center and used to produce crude bio-oil and biochar via a pyrolysis process. The CCB sample was characterized by its chemical composition and thermal behavior. Keeping all other pyrolysis conditions constant, the effect of temperature on product yields and quality were studied. The pyrolysis bio-oil products were chemically investigated by a combination of GCMS, ESI-MS, and HPLC. The biochar was characterized by proximate, ultimate, surface area, FTIR and Raman spectroscopies, and x-ray diffraction.

## 2.3    Materials and methods

### 2.3.1    Cardboard production and preparation

CCB material was obtained from the University of Idaho recycling center. Prior to use, the CCB sheets were cut into small pieces (30 x 30 mm$^2$), then Wiley milled to pass through a 3.2 mm screen and dried in an oven for 24 h at 100 °C. The CCB was processed without any modifications to its original composition and may contain minor amounts of paint, plastic linings, glue, and ink.

### 2.3.2    Biomass and biochar characterization

#### 2.3.2.1    Calorific value

The calorific values of CCB and biochar samples (in duplicate) were determined by bomb calorimetry using a Parr oxygen bomb calorimeter (model no. 1261) in accordance with ASTM D5865-04. A Carver Laboratory hydraulic press (1,500 MPa) was utilized to press pre-dried samples (1.0 g) into pellets (6 mm Ø) for analysis.

#### 2.3.2.2    Proximate and ultimate analysis

Proximate analysis was performed on samples following ASTM E870-82 to identify ash, volatile matter (VM), and fixed carbon (FC) contents. For FC and VM, samples were combusted at 950 °C in a muffle furnace for 7 min. The ash content was determined after furnacing at 600 °C for at least 16 h. A Costech ESC 4010 elemental analyzer was used to determine carbon (C), nitrogen (N), and hydrogen (H) contents.

#### 2.3.2.3    Surface area (S$_{BET}$)

The specific surface areas (S$_{BET}$) of all degassed biochar samples (0.25 g, in duplicate) were measured using 30% nitrogen (N$_2$) in helium (He) to obtain an N$_2$ adsorption-desorption isotherm at -196 °C on a Micromeritics FlowSorb 2300 instrument according to ASTM D6556-10. The CCB and biochars were examined by scanning electron microscopy (SEM), after gold coating on a Leo Gemini field emission SEM at 5 kV.

#### 2.3.2.4    Moisture content

The moisture content of the CCB was determined prior to the extraction using Mettler Toledo moisture analyzer. CCB samples (4 g) were Soxhlet extracted using dichloromethane (150 mL) for 16 h and lipid (extractives) content was determined gravimetrically, according to ASTM D1108-96.

**2.3.2.5  Fatty Acid Methyl Ester (FAME) analysis**

Lipids were identified using their FAME derivatives. The samples (2 mg) were heated in a sealed 5 mL reacti-vial[TM] for 90 min at 90 °C in a mixture of methanol/sulfuric acid/chloroform (1.7:0.3:2.0 v/v/v, 2 mL) to convert to their FAME derivatives. Chloroform contained 1-naphthaleneacetic acid as an internal standard (200 µg mL$^{-1}$). Water was then added to the cooled vial, and after vigorous shaking, the organic layer was collected and dried over anhydrous sodium sulfate. The FAME compounds were analyzed by gas chromatography-mass spectrometry (GC–MS) using a FOCUS-ISQ (ThermoScientific) system at a temperature gradient of 40 °C (1 min) to 320 °C at 5 °C min$^{-1}$ equipped with a ZB-5 (30 m x 0.25 mmØ, 0.25 µm coating, Phenomenex) capillary column. The eluted compounds were identified with authentic $C_{12}$ to $C_{20}$ fatty acid standards and by spectral matching with the 2017 NIST mass spectral library.

**2.3.2.6  Lignin and carbohydrate analysis**

The extractive free samples were analyzed for lignin and carbohydrate contents. Klason and acid soluble lignin were determined by digesting extractive-free CCB (200 mg) with sulphuric acid (2 ml, 72%) for 60 min at 30 °C, followed by secondary hydrolysis (4% sulfuric acid, 30 min, 121°C) in an autoclave according to ASTM D 1106-96. Klason lignin content was determined gravimetrically after filtration. Acid soluble lignin was determined by absorbance at 205 nm of the filtered hydrolysate (made up to 250 mL) using an absorption coefficient of 110 L g$^{-1}$ cm$^{-1}$ (Biomate 5, Thermoelectron) [75]. Carbohydrate analysis was performed on the hydrolysis filtrate (5 mL) according to ASTM E 1758-01. The monosaccharides were quantified by HPLC (two Rezex RPM columns, 7.8 mm x 300 mm, Phenomenex) at 85 °C on elution with water (0.5 mL min$^{-1}$) using differential refractive index detection (Waters model 2414) [76]. Total lignin was also determined, in duplicate, using acetyl bromide / UV absorbance method [77]. Oven-dry and extractive-free CCB (5 mg) was incubated with acetyl bromide (25% w/w) in acetic acid (5 mL) together with perchloric acid (0.2 mL, 70%) at 70 °C for 60 min. The solutions were made up to 100 mL containing 2M sodium hydroxide (10 mL) and acetic acid (25 mL). Absorbance at 280 nm was measured (Biomate 5, ThermoElectron) and lignin content was determined using an absorptivity of lignin (ε) of 20.09 L g$^{-1}$ cm$^{-1}$. Total carbohydrate content was also determined, in duplicate, using a modified phenol-sulfuric acid colorimetric method [78]. Oven-dry CCB (10 mg) and cellulose standard

(Sigmacell type 101, 2 to 10 mg) were incubated in sulfuric acid (100 µL, 77%) and then phenol in water (1 mL, 5%) and subsequently concentrated sulfuric acid (5 mL) were added. Absorbance at 490 nm was measured (Biomate 5, Thermoelectron).

### 2.3.2.7 Fourier-Transform InfraRed (FTIR) spectroscopy, X-Ray Diffraction (XRD), and Raman spectroscopy

FTIR spectra were obtained, in quadruplicate, for the CCB, biochar, and bio-oil samples using a Thermo-Nicolet iS5 spectrometer equipped with a ZnSe attenuated total reflection (iD5 ATR) accessory. FTIR spectra were baseline corrected and averaged using the Omnic v9 software (Thermo-Nicolet). Carbonyl index (CI), cellulose index (CeI), and hydroxyl index (HI) were calculated as the ratio of the band intensity (absorbance) at 1,720, 1,024, and 3,342 $cm^{-1}$, respectively, to the band 2,916 $cm^{-1}$ for the $-CH_2-$ group [79]. The cellulose crystallinity index (CCI) was determined from the XRD (Siemens D5000 diffractometer; 5 to 55$^{o}$ using 0.05$^{o}$ steps). CCI was determined from the ratio of the integral intensities, after peak fitting and amorphous baseline subtraction using IgorPro v8 software, of crystalline portions to the total intensity of sample according to CCI = $(1 - (I_{am}/I_{002}))$, where $I_{am}$ is the intensity of the peak at $2\theta = 16°$ and $I_{002}$ is the maximum intensity of the (002) plane diffraction at $2\theta = 22°$ [80], [81]. Raman spectra (3 replicates) were recorded on an Alpha 300R Raman microscope (Witec) at 532 nm excitation and the spectra averaged and baseline corrected. The ratio of D (disordered, 1355 $cm^{-1}$)/G (graphitic, 1580 $cm^{-1}$) band intensities ($I_D/I_G$) was used to calculate an estimation of disordered carbon in the biochar [67].

### 2.3.3 Thermogravimetric analysis (TGA)

TGA was performed on samples (5-6 mg) using a PerkinElmer TGA-7 instrument from 30 to 900 ºC at heating rates ($\beta$) of 5, 10, 15, 20, and 25 °C $min^{-1}$ under nitrogen (30 mL $min^{-1}$) to determine activation energy (*E*) and thermal degradation behavior [28][29]. The TGA and differential thermogravimetric (DTG) data were analyzed using Pyris v11 software. Isothermal TGA was also utilized to determine the mass yield of CCB during pyrolysis at a given temperature. The temperature was ramped from 30 °C at 200 °C $min^{-1}$ to 350, 400, or 450 °C and then held for 60 min.

### 2.3.4 Py-GCMS analysis

Analytical pyrolysis was performed on CCB at 500 °C (in duplicate) using a Pyrojector II unit (SGE Analytical Science) coupled to a GC-MS (Focus-ISQ, Thermo Scientific). The

compounds were separated on the ZB-5 capillary column (30 m × 0.25 mm Ø, 0.25 µm coating, Phenomenex) from 50 (1 min) to 250 °C (10 min) at 5°C min$^{-1}$. The eluted compounds were identified by their mass spectra, authentic standards, and NIST 2017 library matching. The abundance of each compound was calculated relative to the carbon dioxide peak.

### 2.3.5 Pyrolysis

CCB was pyrolyzed at three different temperatures of 350, 400, and 450 °C with a feeding rate of 0.5 kg h$^{-1}$ (K-Tron loss-in-weight feeder). A custom-built auger reactor (Ø 5 cm x 90 cm) was used to perform the pyrolysis experiments with a nitrogen purge (5 L min$^{-1}$) (Figure 2.1). Auger speed was adjusted to obtain a 6.4 s residence time. Vapors were condensed with a two-stage ice-water-cooled tube and shell condenser. Biochar and bio-oil were collected to determine gravimetric yields and for further characterization. The gaseous products were collected in a gas sampling bag and immediately analyzed by GC equipped with a thermal conductivity detector (Gow-Mac 350) and separated using a HayeSep DB packed column (Φ 3.3 mm x 9.1 m) at 25 °C.
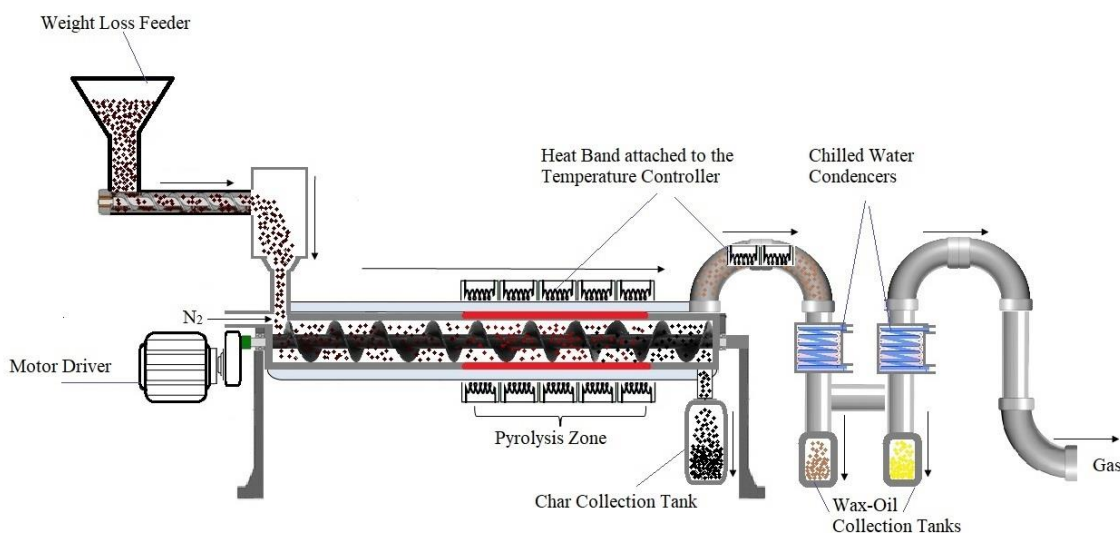


Figure 2.1. Schematic representation of the auger reactor used in this work.

### 2.3.6 Bio-oil characterization

### 2.3.6.1 pH, moisture content, and calorific value

The pH value of the pyrolysis bio-oil was measured with a portable pH meter (Orion-3-Star). The water content of the bio-oils was determined on a Mettler model V30 Karl Fischer titrator. The bio-oil samples were dried using sodium sulfate anhydrous, and their calorific

value was determined as described above.

### 2.3.6.2  Electrospray Ionization-Mass Spectrometry (ESI-MS)

Negative ion ESI-MS was used to determine the molar mass of fresh bio-oil samples using a
Finnigan LCQ-Deca instrument (ThermoQuest). The bio-oil samples (1 mg mL$^{-1}$) in
methanol containing 1% acetic acid and were subjected to ESI–MS (*m/z* 100–2,000) for 3
mins at a flow rate of 10 µL min$^{-1}$. The ion source and capillary voltages were optimized
using a reserpine standard and the instrument autotune function at 4.5 kV and -20 V at
275°C, respectively.  The MS data (averaged over 3 min run) were analyzed using the
Xcalibur software (v2.2) and transferred to Microsoft Excel$^{TM}$ to calculate the number
average molar mass ($M_n$) as $M_n = \sum N_i M_i / \sum N_i$ and the weight average molar mass ($M_w$) as
$M_w = \sum N_i M_i^2 / \sum N_i M_i$ where $N_i$ is the intensity of ions and $M_i$ is the mass after accounting
for the charge.

### 2.3.6.3  Gas Chromatography-Mass Spectrometry (GC-MS) and HPLC

The fresh bio-oils (1 mg in dichloromethane (1 mL) containing anthracene (100 µg mL$^{-1}$) as
an internal standard) were analyzed in duplicate by GC-MS (Focus-ISQ, ThermoScientific).
Separation was achieved on ZB-5 capillary column (30 m × 0.25 mm Ø, 0.25 µm coating,
Phenomenex) using a temperature program of 40 °C (1 min) to 320 ºC at 5 °C min$^{-1}$.
The fresh bio-oils were analyzed for organic acids and anhydro-sugars by HPLC, in
triplicate, using a Rezex ROA organic acid column (7.8 × 30 cm, Phenomenex) equipped
with a differential refractive index detector (Shodex SE31), on elution with 0.005 N aqueous
sulfuric acid (0.5 mL min$^{-1}$) at 65 °C.  The identity of the compounds was determined by
retention time against authentic standards (formic acid, acetic acid, propionic acid, methanol,
levoglucosan, furfurol, furfural, hydroxymethyfurfural, glycerol, glucose, and xylose).

## 2.4    Results and Discussion

### 2.4.1  Cardboard characteristics

 The results of chemical composition, proximate, ultimate, surface area, and calorific value
analyses of CCB and biochars are given in Table 2.1. CCB contained 43.2% C, 0.12% N,
5.8% H, and 4.0% ash. All values are within the range previously reported for cardboard and
lignocellulosic biomass [32], [34], [74], [82]–[85], [86, p. 2]. Ash in paper and CCB is a
result of inorganic additives such as talc [34], [87]. The low N content was expected as

cardboard has very little protein. A FC value of 13% for CCB was obtained and is in the range reported in the literature (0.1%-32.3%) [34], [74], [83], [88]. The calorific value obtained for CCB was 18 MJ kg$^{-1}$, which is comparable to reported values [74], [83]. CCB has an acid soluble and Klason lignin contents of 0.02% and 11.3%, respectively. While the acid-soluble lignin content was found to be very low in this work, Klason lignin content was close to those previously found for cardboard and waste paper in the literature [89], [90]. Lignin content was also determined using the acetyl bromide method at 13.2%. The dichloromethane extractive yield was low at 0.87 % for CCB. FAME analysis of the extract identified palmitic acid (C16:0), stearic acid (C18:0), and oleic acid (C18:1) as the most abundant fatty acids (Table 2.2). The FAME results are consistent with prior findings for lignocellulosic material [91]. Oil, paint, glues, and ink may also be present in CCB, and some contain fatty acids [74].

CCB had a total carbohydrate content of 77.8% determined by the phenol-sulfuric method. Detailed carbohydrate analysis showed the presence of glucose (703 mg/g), xylose, galactose, arabinose, and mannose with a total of 80.9% and comparable with the phenol-sulfuric method and prior findings by Jung et al. [90].

Table 2.1. Proximate and ultimate analysis, surface area analysis, and lignin and carbohydrate contents of corrugated cardboard (CCB) and pyrolysis biochars.

| | CCB | CCB 350 °C Biochar | CCB 400 °C Biochar | CCB 450 °C Biochar |
|---|---|---|---|---|
| % N | $0.12 \pm 0.01$ | $0.11 \pm 0.01$ | $0.16 \pm 0.01$ | $0.18 \pm 0.01$ |
| % C | $43.24 \pm 0.00$ | $46.84 \pm 0.01$ | $51.33 \pm 0.47$ | $54.17 \pm 0.32$ |
| % H | $5.80 \pm 0.03$ | $5.70 \pm 0.01$ | $4.80 \pm 0.06$ | $3.70 \pm 0.03$ |
| % Ash | $4.0 \pm 0.2$ | $5.0 \pm 0.3$ | $5.2 \pm 0.3$ | $12.3 \pm 0.6$ |
| % Fixed carbon | $13.1 \pm 0.7$ | $17.2 \pm 0.9$ | $27.8 \pm 1.4$ | $41.8 \pm 2.1$ |
| Calorific value (MJ kg$^{-1}$) | $18 \pm 0.9$ | $18.4 \pm 0.9$ | $19.7 \pm 1.0$ | $20.4 \pm 1.0$ |
| Surface Area (m$^2$ g$^{-1}$) | $1.5 \pm 0.1$ | $1.2 \pm 0.1$ | $1.6 \pm 0.1$ | $1.6 \pm 0.1$ |
| % Extractives | $0.87 \pm 0.04$ | - | - | - |
| % Klason lignin | $11.3 \pm 0.6$ | - | - | - |
| % Acid soluble lignin | $0.02 \pm 0.005$ | - | - | - |
| % Total lignin (acetyl bromide) | $13.2 \pm 0.6$ | - | - | - |
| % Total carbohydrate (phenol-sulfuric) | $77.8 \pm 0.2$ | - | - | - |
| Glucose (mg/g) | $703 \pm 35$ | - | - | - |
| Xylose (mg/g) | $64.1 \pm 3.2$ | - | - | - |
| Galactose (mg/g) | $2.9 \pm 0.1$ | - | - | - |
| Arabinose (mg/g) | $27.7 \pm 1.4$ | - | - | - |
| Mannose (mg/g) | $11.3 \pm 0.6$ | - | - | - |

Table 2.2. Fatty acid methyl esters (FAME) identified and quantified (mg/g) in corrugated cardboard (CCB).

| Fatty acid | Retention time (min) | M$^+$ (m/z) | CCB (mg/g CCB) |
|---|---|---|---|
| Lauric Acid | 24.70 | 200 | $85.4 \pm 4.3$ |
| Myristic Acid | 28.70 | 228 | $31.8 \pm 1.6$ |
| Palmitic Acid | 32.80 | 270 | $284.0 \pm 14.2$ |
| Linoleic Acid | 34.72 | 294 | $37.0 \pm 1.9$ |
| Oleic Acid | 36.08 | 296 | $105.0 \pm 5.2$ |
| Stearic Acid | 36.56 | 298 | $185.0 \pm 9.2$ |
| Arachidic Acid | 40.01 | 304 | $16.4 \pm 0.8$ |

### 2.4.2   Thermogravimetric analysis (TGA) of CCB

TGA was performed to determine the thermal degradation and kinetic behavior of CCB. The TGA and DTG thermograms of CCB are presented in (Figure 2.2). Pyrolysis of biomass usually consists of three stages: (i) dehydration; (ii) devolatilization, which leads to the formation of biochar, and (iii) the slow transformation of the formed biochar [92]. The first decomposition stage for CCB takes place < 300 °C and is associated with very little mass loss and attributed to evaporation of water and light volatiles [93]. The main weight loss takes place between 300 and 500 °C with two distinct DTG peaks at 345-385 °C and around 470 °C that correspond to the steep weight loss. Therefore, pyrolysis experiments were performed below this temperature. In the end, >95% of the sample degraded. The first peak is consistent with the main devolatilization stage found for other lignocellulosic biomass [84], including uncontaminated cardboard [74]. This stage is primarily associated with cellulose degradation, which occurs between 325 and 400 °C [32], [94], [95]. Cellulose is decomposed to form levoglucosan and other oligomers through trans-glucosidation [96]. The peak around 470 °C is likely associated with decomposition of polymers present in the lining or paint used on the CCB [85]. Above 500 °C, a slow weight loss was observed, which can be attributed to the slow transformation of biochar [74]. The final residue left of the CCB sample was approximately 4%, which is consistent with the reported proximate analysis findings. DTG curves (Figure 2.2) exhibit a peak shift in higher temperatures, likely due to a change in reaction kinetics [97]. The peaks also increase in intensity for higher temperatures. The apparent $E$ was calculated using the isoconversional method based on the linear regression model (Figure 2.3, Table 2.3). The $E$ values found for $10\% \leq \alpha \leq 70\%$ are in the range reported for cellulose [98] and cardboard [85].
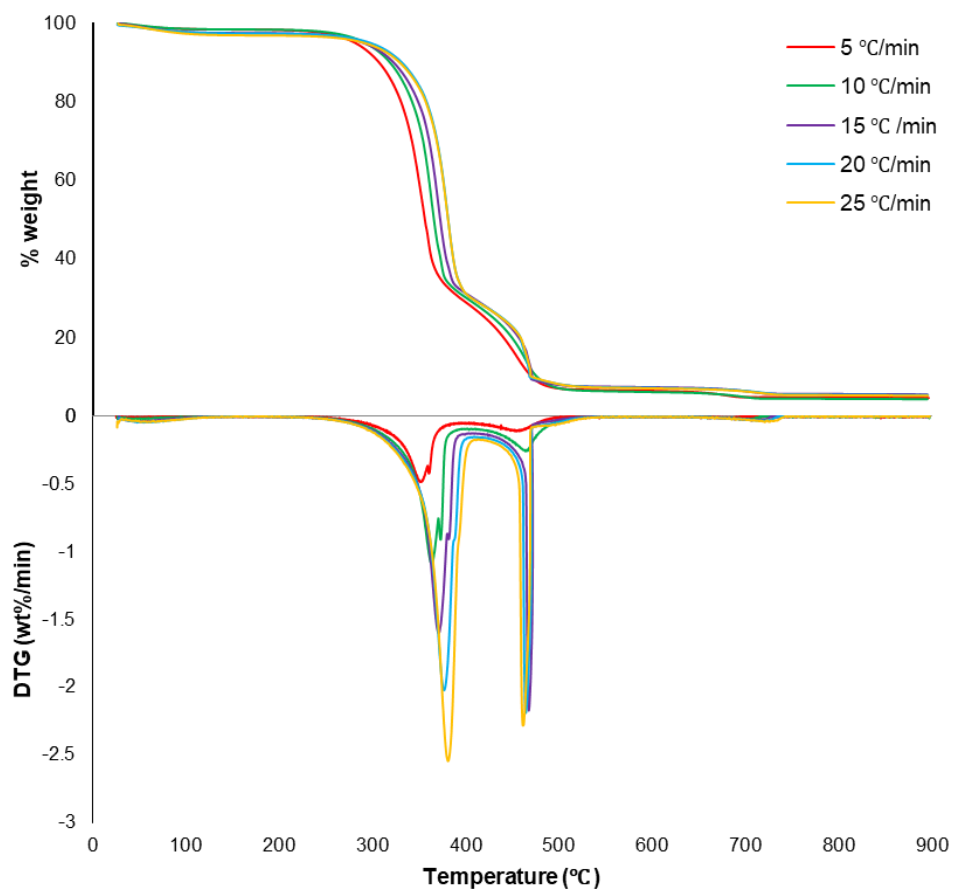
Figure 2.2. (a) TGA and (b) DTG thermograms of corrugated cardboard (CCB) at different heating rates ($\beta$ of 5–25 °C min−1).
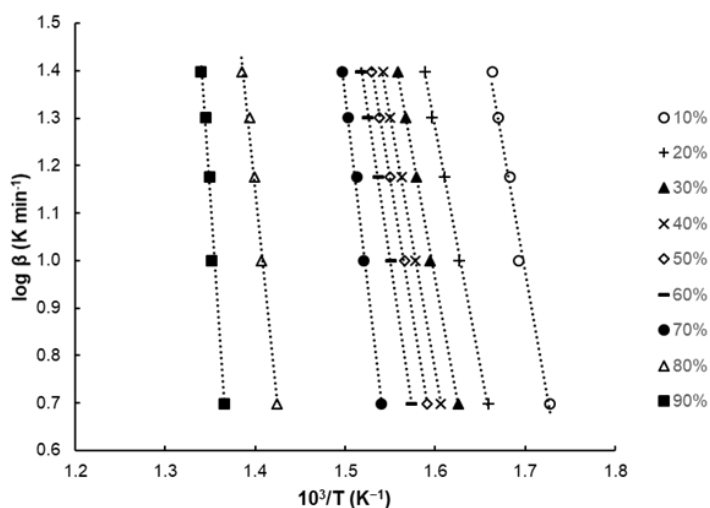
Figure 2.3. Determination of apparent activation energy (E) according to the FWO method at heating rates (β) of 5, 10, 15, 20, and 25 °C min-1 for corrugated cardboard (CCB).

Table 2.3. Activation energy values (E) at various conversion factors (α) for corrugated cardboard (CCB) determined by TGA.

| Conversion (α) | $E$ (J mol$^{-1}$) | $R^2$ |
|---|---|---|
| 10% | 198 | 0.9843 |
| 20% | 180 | 0.9982 |
| 30% | 188 | 0.9986 |
| 40% | 196 | 0.9994 |
| 50% | 207 | 0.9991 |
| 60% | 229 | 0.9985 |
| 70% | 298 | 0.9939 |
| 80% | 338 | 0.9871 |
| 90% | 510 | 0.9757 |

The isothermal TGA experiments were performed to monitor the temporal pyrolysis reaction and showed a 47% yield of biochar at 350 °C, 14% at 400 °C, and 8.5% at 450 °C, confirming a decrease in biochar yield with temperature (Figure 2.4). On extended heating (60 min) the biochar yields were considerably lower at 23.7% at 350 °C and about 6.3% at 400 °C and 450 °C.
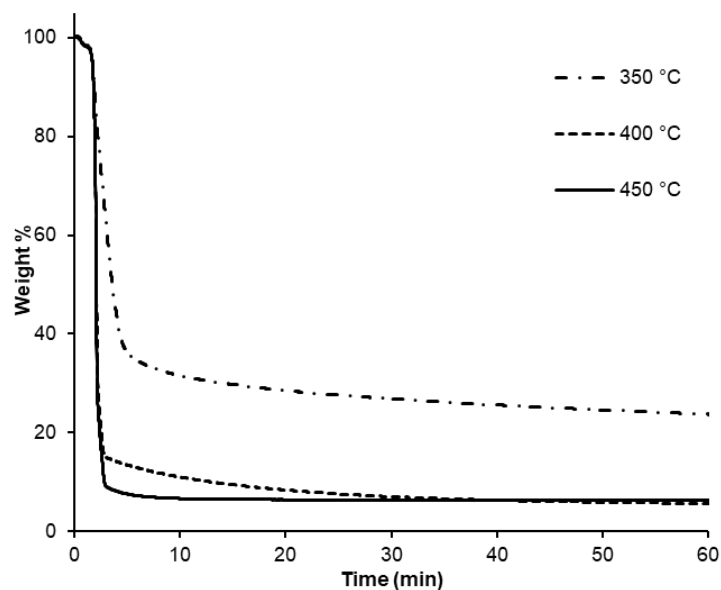
Figure 2.4. Isothermal TGA experiments of CCB ramped at 200 ºC min-1 to 350, 400 and 450 °C.

### 2.4.3  Analytical Py-GCMS of CCB

Analytical Py- GC-MS was performed at 500 °C (higher than the pyrolysis experiments) to determine the potential pyrolysis products from CCB. A list of identified compounds and levels (%) are given in Table 2.4. The most abundant compound was found to be levoglucosan and is consistent with the literature [96], [99], [100]. Aromatic compounds and a variety of pyran and furan derivatives ($C_{5-6}$ ring-containing compounds), and aliphatic oxygenated $C_{2-4}$ organic compounds were also present. The high concentration of levoglucosan suggests a great potential for fuel and chemicals production. Levoglucosan can be isolated and used as a tracer compound to determine smoke distribution [101]. It can also be used for synthesis of pesticides, growth regulators, macrolide antibiotics, and even to produce bio-ethanol [102].

Table 2.4. Identified compounds via Py-GC-MS for corrugated cardboard (CCB), pyrolyzed at 500 °C.

| Compound | Formula | RT (min) | $M^+$ (m/z) | CCB 500 °C (Area %) |
|---|---|---|---|---|
| Carbon dioxide | $CO_2$ | 1.53 | 44 | $6.10 \pm 0.31$ |
| Acetaldehyde | $C_2H_4O$ | 1.72 | 44 | $4.32 \pm 0.22$ |
| 2-Methylbutanal | $C_5H_{10}O$ | 1.98 | 86 | $5.56 \pm 0.28$ |
| Dihydroxyacetone | $C_3H_6O_2$ | 2.42 | 74 | $2.23 \pm 0.11$ |
| trans-Tiglaldehyde | $C_5H_8O$ | 3.35 | 84 | $0.79 \pm 0.04$ |
| 3-Hydroxypropanal | $C_3H_6O_2$ | 3.58 | 74 | $1.06 \pm 0.05$ |
| Butanedial | $C_4H_6O_2$ | 3.76 | 86 | $0.61 \pm 0.03$ |
| Methyl pyruvate | $C_4H_6O_3$ | 3.89 | 102 | $1.09 \pm 0.05$ |
| Furfural | $C_5H_4O_2$ | 4.75 | 96 | $0.88 \pm 0.04$ |
| Dihydro-methyl-furanone | $C_5H_8O_2$ | 5.26 | 98 | $0.29 \pm 0.01$ |
| 4-Hexen-2-one | $C_6H_{10}O$ | 5.54 | 98 | $0.29 \pm 0.01$ |
| Styrene | $C_8H_8$ | 6.09 | 104 | $1.24 \pm 0.06$ |
| 2(5H)-Furanone | $C_4H_4O_2$ | 6.63 | 84 | $0.41 \pm 0.02$ |
| 2-Furanmethanol | $C_5H_6O_2$ | 6.72 | 98 | $0.33 \pm 0.02$ |
| 1,2-Cyclopentanedione | $C_5H_6O_2$ | 6.89 | 98 | $1.01 \pm 0.05$ |
| Acryloylurea | $C_4H_6N_2O_2$ | 7.93 | 114 | $0.82 \pm 0.04$ |
| 1-Methyl-2-cyclohexen-1-ol | $C_7H_{12}O$ | 8.37 | 110 | $0.11 \pm 0.01$ |
| Methyl-dihydro-(2H)-pyran-2-one | $C_6H_8O_2$ | 8.81 | 112 | $0.61 \pm 0.03$ |
| 4-Hydroxy-5,6-dihydro-(2H)-pyran-2-one | $C_5H_6O_3$ | 8.90 | 114 | $1.18 \pm 0.06$ |
| 3-Methyl-1,2-cyclopentanedione | $C_6H_8O_2$ | 9.74 | 112 | $0.27 \pm 0.01$ |
| 3-Methyl-furan-2,4-dione | $C_5H_6O_3$ | 10.25 | 114 | $0.55 \pm 0.03$ |
| Methoxy-phenol | $C_7H_8O_2$ | 11.58 | 124 | $0.35 \pm 0.02$ |
| Ketone, 1-cyclohexen-1-yl methyl | $C_8H_{12}O$ | 11.65 | 124 | $0.70 \pm 0.04$ |
| 1,4-Dioxaspiro [2.4] heptan-5-one | $C_5H_6O_3$ | 12.48 | 114 | $0.30 \pm 0.02$ |
| 1.2-Hexyl-3-methyloxirane | $C_9H_{18}O$ | 14.30 | 142 | $1.50 \pm 0.08$ |
| 4-methyl-Guaiacol | $C_8H_{10}O_2$ | 14.52 | 138 | $0.60 \pm 0.03$ |
| 3-Hydroxy-2-methyl-pyran-4-one | $C_6H_6O_3$ | 14.75 | 126 | $0.21 \pm 0.01$ |
| 1,4:3,6-Dianhydro-α-d-glucopyranose | $C_6H_8O_4$ | 14.98 | 144 | $0.29 \pm 0.01$ |
| 5-Hydroxymethylfurfural | $C_6H_6O_3$ | 15.60 | 126 | $0.87 \pm 0.04$ |
| 2-Hydroxymethyl-5-hydroxy-2,3-dihydro-(4H)-pyran-4-one | $C_6H_8O_4$ | 17.55 | 144 | $3.93 \pm 0.20$ |
| 4-vinyl-guaiacol | $C_9H_{10}O_2$ | 19.91 | 150 | $1.01 \pm 0.05$ |
| Vanillin | $C_8H_8O_3$ | 20.13 | 152 | $0.55 \pm 0.03$ |
| Isoeugenol | $C_{10}H_{12}O_2$ | 21.41 | 164 | $1.07 \pm 0.05$ |
| 4-propyl-guaiacol | $C_{10}H_{14}O_2$ | 21.65 | 166 | $0.09 \pm 0.01$ |
| 1.6-Methoxy-3-methyl-1-benzofuran | $C_{10}H_{10}O_2$ | 22.1 | 162 | $0.19 \pm 0.01$ |
| Levoglucosan | $C_6H_{10}O_5$ | 22.83 | 162 | $19.51 \pm 0.98$ |
| Coniferyl alcohol (trans) | $C_{10}H_{12}O_3$ | 24.61 | 180 | $0.17 \pm 0.01$ |
| Syringol | $C_8H_{10}O_3$ | 24.78 | 154 | $0.46 \pm 0.02$ |

| Compound | Formula | RT (min) | $M^+$ (m/z) | CCB 500 °C (Area %) |
|---|---|---|---|---|
| 3-(1-Ethoxyethoxy)-3-methyl-1-butene | $C_9H_{18}O_2$ | 25.58 | 158 | $1.02 \pm 0.05$ |
| Syringaldehyde | $C_9H_{10}O_4$ | 26.39 | 182 | $0.16 \pm 0.01$ |
| Cyclotridecane | $C_{13}H_{26}$ | 27.04 | 182 | $0.41 \pm 0.02$ |
| Acetosyringone | $C_{10}H_{12}O_4$ | 27.99 | 196 | $0.34 \pm 0.02$ |
| Coniferyl alcohol (cis) | $C_{10}H_{12}O_3$ | 28.09 | 180 | $0.88 \pm 0.04$ |
| 2-methyl-1-hexadecanol | $C_{17}H_{36}O$ | 29.18 | 256 | $1.36 \pm 0.07$ |
| 7-Methyl-Z-tetradecen-1-ol acetate | $C_{17}H_{32}O_2$ | 29.31 | 268 | $0.36 \pm 0.02$ |
| 1-Nonadecene | $C_{19}H_{38}$ | 31.21 | 266 | $0.61 \pm 0.03$ |
| Nonadecane | $C_{19}H_{40}$ | 31.34 | 268 | $0.44 \pm 0.02$ |
| n-Hexadecanoic acid | $C_{16}H_{32}O_2$ | 32.53 | 256 | $0.69 \pm 0.03$ |
| 2-(9-octadecenyloxy)- (Z)- Ethanol, | $C_{20}H_{40}O_2$ | 33.04 | 312 | $0.49 \pm 0.02$ |
| 1-Docosene | $C_{22}H_{44}$ | 33.16 | 308 | $1.33 \pm 0.07$ |
| 1,15-Pentadecanediol | $C_{15}H_{32}O_2$ | 34.91 | 244 | $0.23 \pm 0.01$ |
| Oleic Acid | $C_{18}H_{34}O_2$ | 35.81 | 282 | $0.66 \pm 0.03$ |
| 1,3,5-triphenyl-Cyclohexane | $C_{24}H_{24}$ | 37.05 | 312 | $9.90 \pm 0.50$ |
| 1-Hexacosene | $C_{26}H_{52}$ | 38.51 | 364 | $2.15 \pm 0.11$ |
| Heptacosane | $C_{27}H_{56}$ | 38.61 | 380 | $1.20 \pm 0.06$ |
| Behenic alcohol | $C_{22}H_{46}O$ | 41.73 | 326 | $1.41 \pm 0.07$ |
| Octacosane | $C_{28}H_{58}$ | 41.81 | 394 | $1.24 \pm 0.06$ |
| Phthalic acid, bis(2-ethylhexyl) ester | $C_{24}H_{38}O_4$ | 42.61 | 390 | $0.37 \pm 0.02$ |
| 1,3,5-Triphenyl-1,5-pentanedione | $C_{23}H_{20}O_2$ | 44.10 | 328 | $0.56 \pm 0.03$ |
| 1-Heptacosanol | $C_{27}H_{56}O$ | 45.46 | 396 | $1.14 \pm 0.06$ |
| Nonacos-1-ene | $C_{29}H_{58}$ | 48.04 | 406 | $2.30 \pm 0.11$ |
| Undec-10-ynoic acid, tridec-2-yn-1-yl ester | $C_{24}H_{40}O_2$ | 50.02 | 360 | $0.20 \pm 0.01$ |
| Hentriacontane | $C_{31}H_{64}$ | 51.44 | 436 | $0.76 \pm 0.04$ |
| 17-Pentatriacontene | $C_{35}H_{70}$ | 51.30 | 490 | $0.58 \pm 0.03$ |

### 2.4.4 Pyrolysis yield, products fractionation, and product characterization

The pyrolysis bio-oil, biochar, and gas (by difference) yield values for CCB were determined for the various reaction temperatures (Figure 2.5). The highest bio-oil yield (47%) was obtained from the CCB sample pyrolyzed at 450 °C. While this is higher than the bio-oil yields of cardboard pyrolyzed on a batch reactor [32], and a packed bed reactor [103], catalytic pyrolysis of CCB has been shown to increase liquid yield considerably [33]. The highest biochar yield (75%) was observed in the CCB sample pyrolyzed at 350 °C. This value is also considerably higher than what has been previously reported for cardboard pyrolyzed at higher temperatures (600 °C) in the literature [32], [103]. The pyrolysis gaseous products were analyzed by GC and found mainly to be carbon monoxide, methane and carbon dioxide (Table 2.5).
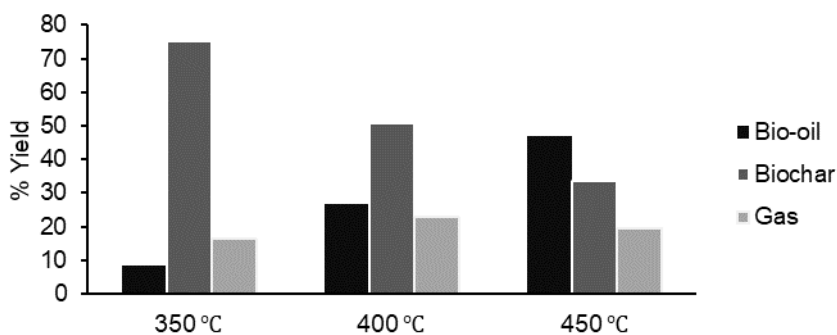


Figure 2.5. Corrugated cardboard (CCB) Pyrolysis product (oil, char, and gas) yields.

Table 2.5. Composition of pyrolysis gas.

| Gas | 350 °C (vol%) | 400 °C (vol%) | 450 °C (vol%) |
|---|---|---|---|
| $H_2$ | | | 1 |
| CO | 78 | 62 | 95 |
| $CH_4$ | 5 | 6 | 1 |
| $CO_2$ | 17 | 32 | 3 |

### 2.4.5   CCB biochar characterization

The CCB biochar samples were characterized by proximate/ultimate analysis, calorific value, and surface area (Table 2.1). Consistent with previous findings [104], %C, FC, and calorific values all increased with pyrolysis temperature in the biochar samples. The calorific values are slightly lower than those reported for cardboard by Phan et al. [35] and Ghorbel et al. [74], likely due to differences in the biomass composition. The calorific value was also much lower than that of diesel oil or blended oil [105], making it less suitable for substitution as a transportation fuel, however, it may be suitable as heating oil. The BET surface areas were comparably low (1.2-1.6 $m^2$ $g^{-1}$) for all biochar and CCB samples and consistent with values found for other lignocellulosic biomass biochars [23].

Average fiber length for CCB (190±100 µm), CCB350 (120±60 µm), CCB400 (80±30 µm) and CCB450 (76±35 µm) was determined by SEM (Figure 2.6). The average fiber length was shown to progressively decrease with pyrolysis temperature. Mild-moderate pyrolysis temperatures (350-400 °C) could produce biochar fibers of suitable length and surface hydrophobicity for use in composites materials [106].
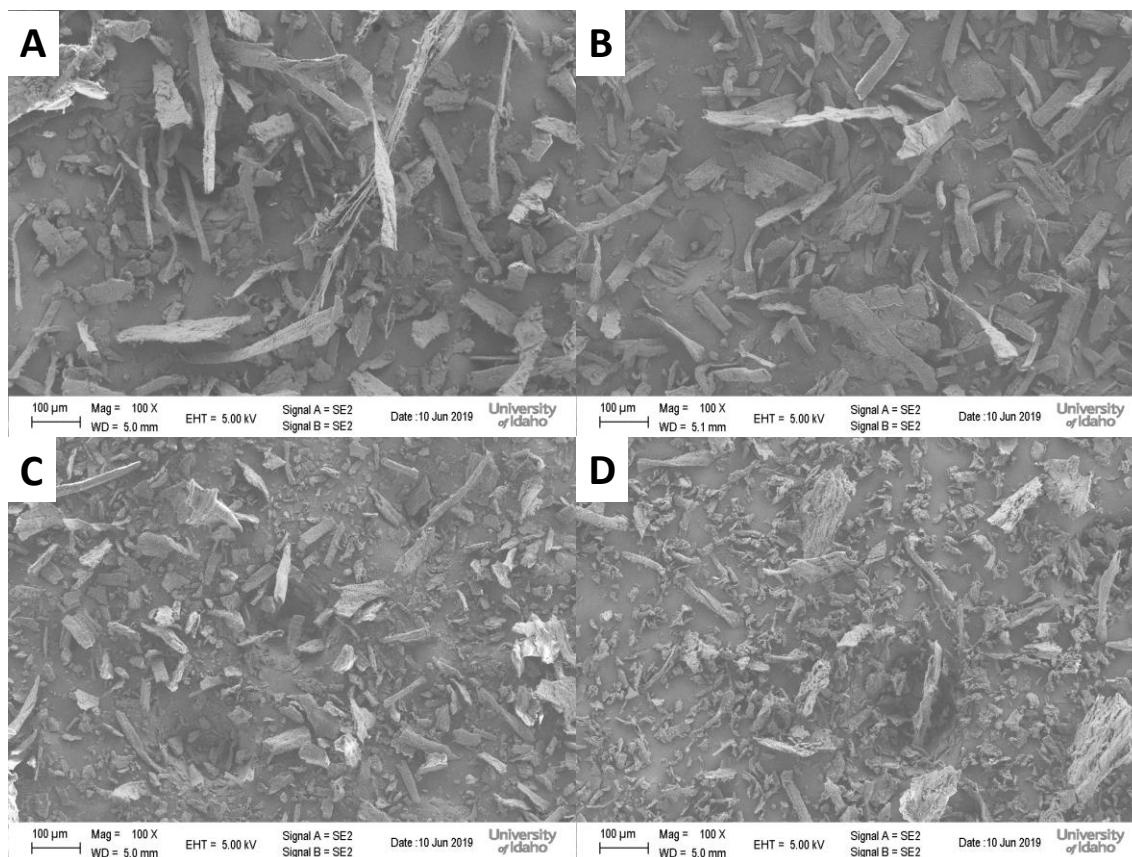
Figure 2.6. Scanning electron micrographs of (a) CCB, (b) CCB350 biochar, (c) CCB400 biochar and (d) CCB450 biochar at 100× magnification.

FTIR analysis was performed to obtain chemical group information of CCB and biochars (Figure 2.7). Band assignments for all samples are based on the literature and are given in Table 2.6 [67]. For the CCB and biochar samples, the broad band at 3600-3200 cm$^{-1}$ is attributed to O-H stretching vibrations in alcohols [107]. The CCB O-H band intensity decreased in the biochar samples with pyrolysis temperature, suggesting that some hydroxyl groups were removed during pyrolysis via dehydration reactions [108]. The existence of asymmetric and symmetric C-H stretching for aliphatic functional groups is established by the bands between 2930 cm$^{-1}$ and 2850 cm$^{-1}$. This is also confirmed by a scissoring $CH_2$ vibration at 1425 cm$^{-1}$ [109], [110]. The band at 1702 cm$^{-1}$ correspond to the C=O stretching [111]. The bands at about 1599 and 1515 cm$^{-1}$ are assigned to aromatic skeletal stretching associated with lignin [112]. An increase in absorption intensities at 1590 cm$^{-1}$ for higher pyrolysis temperatures suggests an increase in aromatic structures [113]. As pyrolysis temperature increased, the band intensities at 1030 cm$^{-1}$ (symmetric C-O stretching)

decreased, which indicates the reduction of cellulose, hemicelluloses, and lignin [113], [114]. The bands between 665 and 874 cm$^{-1}$ are associated with aromatic C-H stretching vibrations and indications of the presence of adjacent aromatic hydrogens in biochars [115]. The relative changes in carbonyl, cellulose, and hydroxyl content to methylene groups that occurred during pyrolysis in the CCB, and biochar were examined by calculating CI, CeI, and HI, respectively (Table 2.6). The CI value increased from 0.09 (for CCB) with temperature to 1.38 (for biochar at 450°C) as a result of oxidation. The HI value decreased from 2.94 (CCB) with temperature to 1.54 (for biochar at 450°C) as a result of hydroxyl group loss by dehydration reactions [108]. The CeI value increased from 2.96 (for CCB) to 3.56 (for CCB400) and then decreased to 2.80 for the CCB450. These findings support that the cellulose content decreased, at 450 °C, with the extent of pyrolysis because of dehydration and degradation reactions. This trend has been seen in the extent torrefaction of mixed paper waste [79].
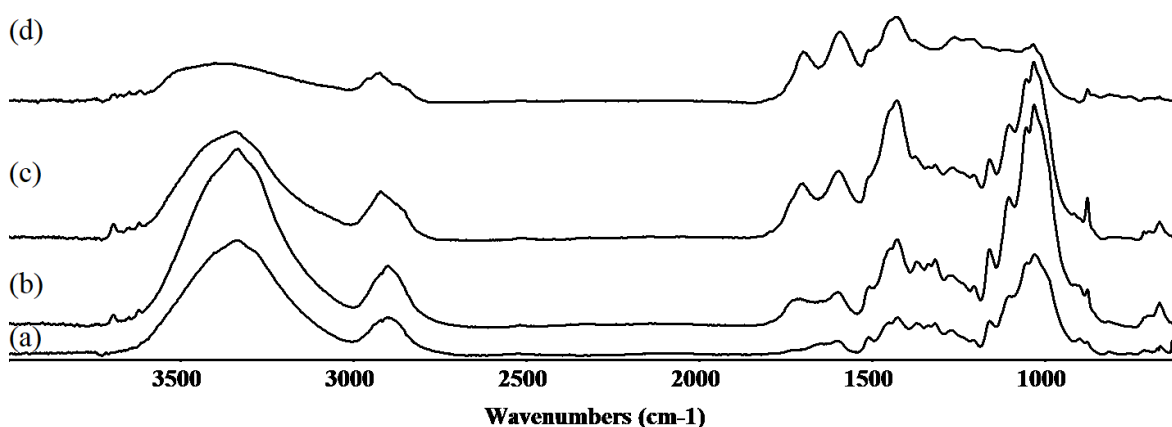


Figure 2.7. FTIR spectra of (a) corrugated cardboard (CCB), (b) CCB350 biochar, (c) CCB400 biochar, and (d) CCB450 biochar.

Table 2.6. FTIR analysis results for cardboard and biochar samples [54]– [62].

| Band assignment | Cardboard | Biochar 350°C | Biochar 400°C | Biochar 450°C |
|---|---|---|---|---|
| | Wavenumber ($cm^{-1}$) | | | |
| O–H stretch, free hydroxyl | | | 3693 | 3618 |
| O–H stretching vibration | 3339 | 3333 | 3341 | 3402 |
| C–H ($CH_3$, $CH_2$) stretching vibration | 2901 | | 2919 | 2921 |
| C-H stretching (Alkene) | | 2898 | | |
| C=O stretch, aldehydes | | 1721 | | |
| −C=C−stretch | | | 1699 | 1668 |
| Aromatic skeletal vibration (C=C) in lignin | 1599 | 1598 | 1595 | 1593 |
| Aromatic skeletal vibration (C=C) | 1512 | 1508 | 1512 | 1508 |
| Deformation of CH, $CH_3$, and $CH_2$ | 1424 | 1425 | 1427 | 1429 |
| O–H or C–H bending | 1370 | 1369 | | |
| C–C and C–O stretching in guaiacol | | | 1267 | 1260 |
| C−H wag(−$CH_2$X) | 1316 | 1315 | | |
| C–O stretching and O–H bending | 1159 | 1158 | 1157 | |
| C–O stretching | 1028 | 1029 | 1031 | 1032 |
| Adjacent aromatic C–H deformation | | | 875 | 874 |
| Phenol O–H out of plane/ deformation /=C–H bending | 664 | 666 | 666 | 666 |

Raman spectroscopy was performed to obtain information as to the carbon structure of the CCB biochar samples. Figure 2.8 shows the Raman spectra of the CCB biochar. The spectra of CCB450 and CCB400 biochar showed two bands at Raman shifts of 1355 $cm^{-1}$ and 1580 $cm^{-1}$ assigned to the D-band and G-band of carbon, respectively [67]. The CCB350 biochar sample showed no Raman bands for carbon. The $I_D/I_G$ values for CCB biochar pyrolyzed at 450 and 400 °C were respectively 1.1 and 1.2 and fall within the range of biochars from various sources (0.8-1.5) [67], [116], [117].
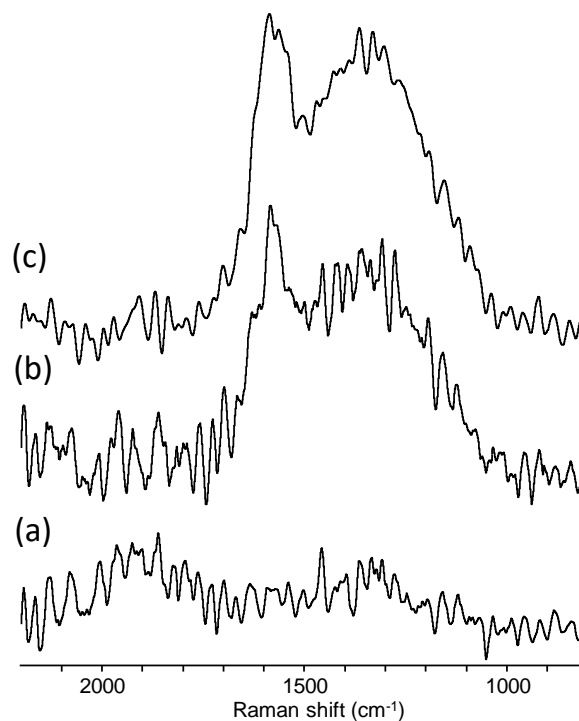
Figure 2.8. Raman spectra for CCB biochar pyrolyzed at (a) 350 ℃, (b) 400 ℃ and (c) 450 ℃.

XRD analysis was performed to confirm the presence of crystalline cellulose in the CCB and biochar samples (Figure 2.9). The samples showed typical XRD patterns of cellulose I; peaks showing at 2θ scale at 16° and 22° were assigned to the planes of (101), (10−1), and (002), respectively. CCI was determined for CCB at 0.46, and after pyrolysis, the crystallinity decreased in the CCB biochar to between 0.35 (350°C) and 0.40 (450°C) (Table 2.7) and is contrary to the CeI values determined by FTIR.
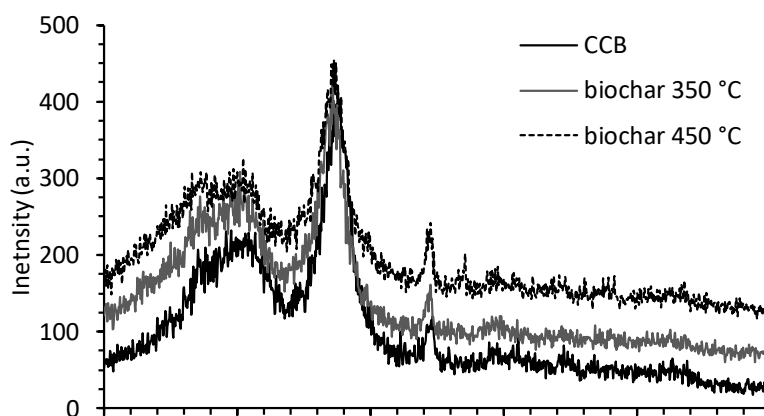


Figure 2.9. X-ray diffractograms of corrugated cardboard (CCB) and pyrolysis CCB350 and CCB450 biochar samples.

Table 2.7. Cellulose crystallinity index (CCI), cellulose index (CeI), carbonyl index (CI), and hydroxyl index (HI) of CCB and biochars.

| Parameter | CCB | Biochar 350 °C | Biochar 400 °C | Biochar 450 °C |
|---|---|---|---|---|
| CCI by XRD | 0.46 | 0.35 | 0.39 | 0.40 |
| CeI by FTIR | 2.96 | 3.45 | 3.56 | 2.80 |
| CI by FTIR | 0.09 | 0.41 | 1.07 | 1.38 |
| HI by FTIR | 2.94 | 2.79 | 1.98 | 1.54 |

## 2.4.6   CCB bio-oil characterization

### 2.4.6.1   Bio-oil properties

The water content, calorific value, and pH of the bio-oils were determined (Table 2.8). The bio-oil generated at 450 °C had the lowest water content (50%) and the highest dried calorific value (21.7 MJ kg$^{-1}$). Water is present in all lignocellulosic bio-oils as it is a product of dehydration reactions during pyrolysis [84]. The water content was higher than reported values for lignocellulosic biomass [118], [119]. However, it was similar to that reported by Hoe et al. [120]. The low pH of the bio-oils (3.17-4.13) was similar to other lignocellulosic bio-oils and due to the presence of carboxylic acids (e.g., acetic and propionic acids)[84].

Table 2.8. Properties of bio-oil obtained from corrugated cardboard (CCB) pyrolyzed at various temperatures.

| Sample ID | Water content (%) | Calorific Value (MJ kg$^{-1}$) | pH |
|---|---|---|---|
| CCB350 Bio-oil | 58.3 | 21.2 | 3.17 |
| CCB400 Bio-oil | 52.0 | 21.5 | 3.25 |
| CCB450 Bio-oil | 50.0 | 21.7 | 4.13 |

### 2.4.6.2 ESI-MS analysis of bio-oil

ESI-MS analysis was employed to determine the molar mass distribution of both volatile and non-volatile compounds (Figure 2.10). In the negative ion ESI-MS the main [M-H]$^-$ ions at m/z 161 and m/z 111 were respectively assigned to levoglucosan and $C_6H_8O_2$ (or $C_5H_4O_3$). Other minor ions [M-H]$^-$ at m/z 123, 137, 151, 163, 177 and 323 were tentatively assigned to guaiacol, hydroxymethyl furfural, ethyl guaiacol, eugenol/isoeugenol, coniferyl aldehyde, and cellobiosan, respectively [121]. The molar mass ($M_w$ and $M_n$) of the bio-oils were determined by negative ion ESI-MS analyses (Table 2.9). The $M_w$ (1028-1150 g mol$^{-1}$) and $M_n$ were high and shown to decrease with pyrolysis temperature. The MS showed a bimodal distribution centered around m/z 160 (monomers) and 800 (oligomers). It was assumed that the majority (85%) of the monomeric compounds were < m/z 300 based on Py-GC-MS results (Table 2.4), however, some compounds > m/z 300 were observed, such as 1,3,5-triphenyl-cyclohexane. An estimate of the monomer to oligomer (and polymer) ratio was calculated from ion intensities $\Sigma$ m/z 100-300 / $\Sigma$ m/z 301-2000 for the bio-oils (Table 2.9). As pyrolysis temperature increased from 350 to 450 °C the monomer/oligomer ratio increased from 0.19 to 0.42, suggesting more thermal cracking to smaller molecular fragments.

Table 2.9. Weight (Mw) and number average molar mass (Mn) of corrugated cardboard (CCB) pyrolysis bio-oils at 350, 400, and 450 °C determined from negative ion ESI-MS data.

|  | $M_n$ (g mol$^{-1}$) | $M_w$ (g mol$^{-1}$) | Monomer/Oligomer |
|---|---|---|---|
| CCB bio-oil 350°C | 877 | 1150 | 0.19 |
| CCB bio-oil 400°C | 829 | 1125 | 0.24 |
| CCB bio-oil 450°C | 692 | 1028 | 0.42 |
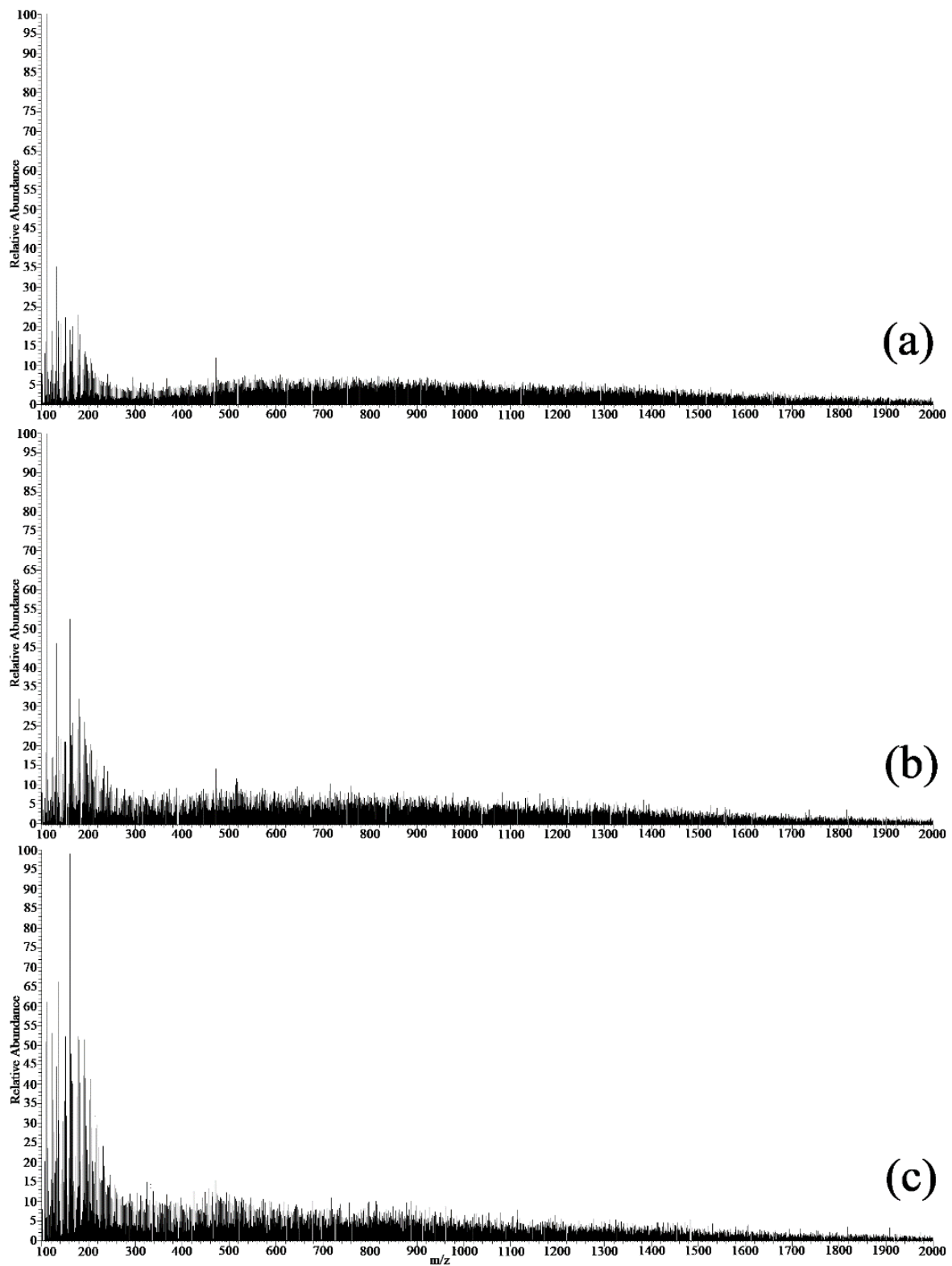
Figure 2.10. Negative ion ESI-MS spectra of corrugated cardboard (CCB) bio-oil obtained at (a) 350 °C, (b) 400 °C, and (c) 450 °C.

### 2.4.6.3   GC-MS analysis of bio-oil

The volatile compounds in the bio-oil were analyzed directly by GC-MS (Figure 2.11). The compounds identified by GC-MS for fresh CB bio-oil are listed in Table 2.10.  Previously reported products of pyrolysis of cellulosic materials primarily consisted of pyrans (e.g., levoglucosan and levoglucosenone), furans (e.g., 5-hydroxymethyl furfural and furfural), and smaller linear hydrocarbons, aldehyde/ketones and acids (e.g., 1-hydroxy-2-propanone, acetaldehyde, acetic acid, and propanoic acid) [72]. Zhou et al. have reported phenolics, benzenes, naphthalenes, benzofurans, and cyclopentenes as the main pyrolysis products of cardboard [32]. Furthermore, phenols and cyclopentenes were also found in abundance. Levoglucosan levels increased substantially at higher pyrolysis temperatures, which is consistent with high values previously reported for pyrolyzed cardboard [83]. Additionally, other compounds (such as 2-hydroxycyclopent-2-en-1-one) also increased with pyrolysis temperature [32]. The formation of cyclopentene is associated with the cyclization of organic compounds caused by the activation and combination of reactive radicals with the other structures [32]. Many of the heavier compounds show a decreasing trend with increasing pyrolysis temperature while the lighter compounds increased. A common noticeable trend is that many compound concentrations (e.g., 2, 6-dimethoxy-phenol, benzaldehyde, and guaiacol) change at 400 °C and stays fairly constant at 450°C. This suggests that many chemical reactions in CCB pyrolysis occur in temperatures ≤ 400 °C [122], which is also supported by TGA data presented earlier.
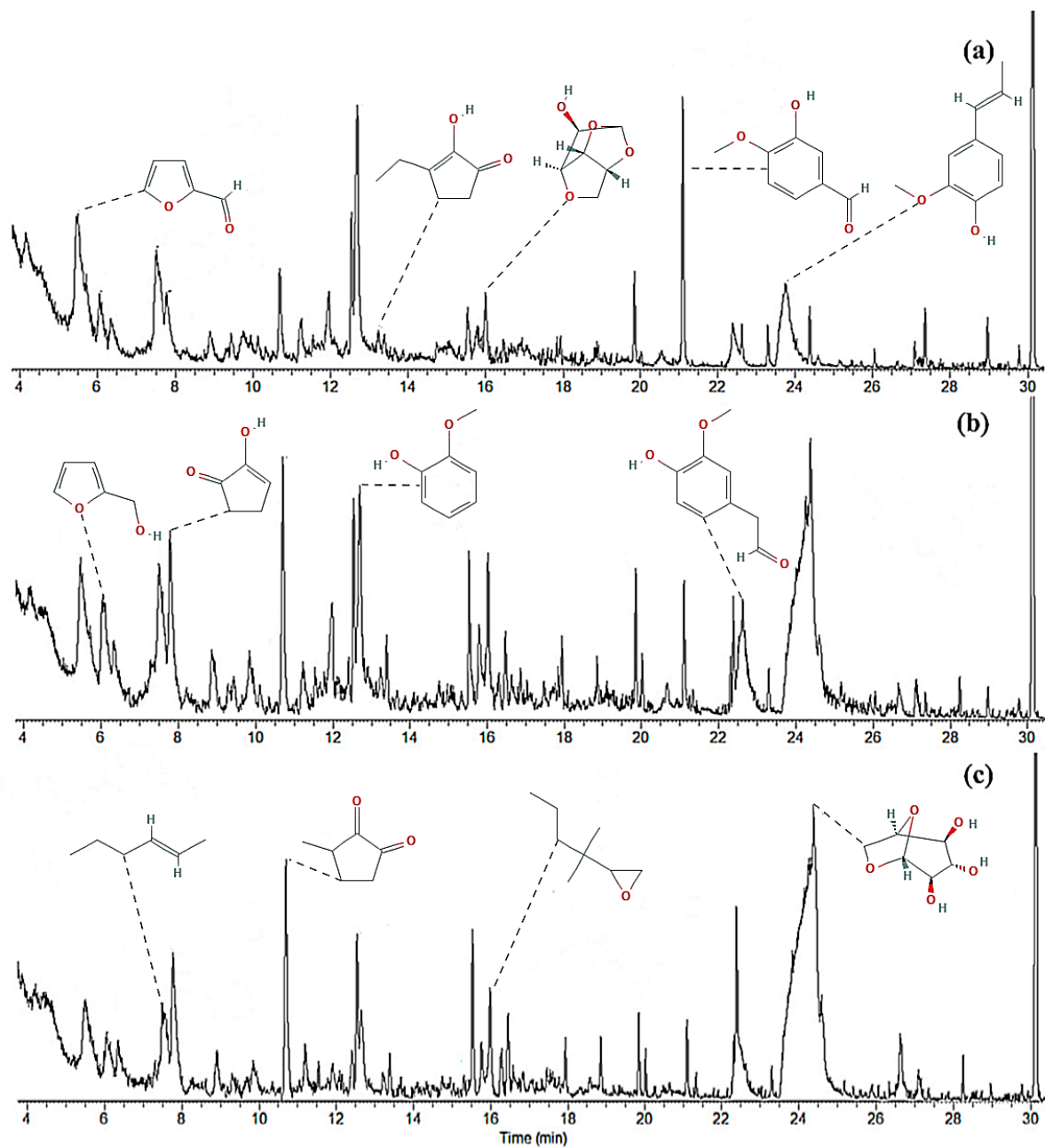
Figure 2.11. GC-MS Chromatograms of corrugated cardboard (CCB) fresh bio-oil at (a) 350 °C, (b) 400 °C, and (c) 450 °C.

Table 2.10. Compounds identified in corrugated cardboard (CCB) fresh bio-oil by GC-MS.

| Compound | Formula | M+ | RT | 350 °C µg/ml | 400 °C µg/ml | 450 °C µg/ml |
|---|---|---|---|---|---|---|
| Furfural | $C_5H_4O_2$ | 96 | 5.48 | $1.94 \pm 0.10$ | $1.89 \pm 0.09$ | $1.92 \pm 0.10$ |
| 2-Furfuryl alcohol | $C_5H_6O_2$ | 98 | 6.05 | $0.45 \pm 0.02$ | $0.91 \pm 0.05$ | $0.83 \pm 0.04$ |
| Butanedial | $C_4H_6O_2$ | 86 | 6.34 | $0.30 \pm 0.02$ | $0.19 \pm 0.01$ | $0.69 \pm 0.03$ |
| 2-Hexene, (E)- | $C_6H_{12}$ | 84 | 7.52 | $1.17 \pm 0.06$ | $1.84 \pm 0.09$ | $1.45 \pm 0.07$ |
| 2-Hydroxycyclopent-2-en-1-one | $C_5H_6O_2$ | 98 | 7.77 | $0.49 \pm 0.02$ | $1.39 \pm 0.07$ | $1.99 \pm 0.10$ |
| 2-Propylfuran | $C_7H_{10}O$ | 110 | 8.88 | $0.24 \pm 0.01$ | $0.53 \pm 0.03$ | $0.50 \pm 0.03$ |
| Phenol | $C_6H_6O$ | 94 | 9.44 | $0.23 \pm 0.01$ | $0.39 \pm 0.02$ | $0.29 \pm 0.01$ |
| 2-Cyclopenten-1-one, 2-hydroxy-3-methyl- | $C_6H_8O_2$ | 112 | 9.74 | $0.28 \pm 0.01$ | -- | -- |
| Heptanal | $C_7H_{14}O$ | 114 | 9.84 | -- | $0.67 \pm 0.03$ | $0.50 \pm 0.03$ |
| Styrene | $C_8H_8$ | 104 | 10.13 | $0.13 \pm 0.01$ | $0.12 \pm 0.01$ | -- |
| 2H-Pyran-2,6(3H)-dione | $C_5H_4O_3$ | 112 | 10.34 | $0.07 \pm 0.00$ | $0.09 \pm 0.00$ | -- |
| 1,2-Cyclopentanedione, 3-methyl | $C_6H_8O_2$ | 112 | 10.7 | $0.44 \pm 0.02$ | $1.33 \pm 0.07$ | $2.08 \pm 0.10$ |
| 1-Acetyloxypropane-2-one | $C_5H_8O_3$ | 116 | 11.22 | $0.31 \pm 0.02$ | $0.45 \pm 0.02$ | $0.43 \pm 0.02$ |
| Butanoic acid, 2-propenyl ester | $C_7H_{12}O_2$ | 128 | 11.95 | $0.03 \pm 0.02$ | $0.68 \pm 0.03$ | $0.30 \pm 0.02$ |
| Furaneol | $C_6H_8O_3$ | 128 | 12.41 | -- | -- | $0.34 \pm 0.02$ |
| Phenol, 2-methoxy- | $C_7H_8O_2$ | 124 | 12.54 | $1.94 \pm 0.10$ | $1.89 \pm 0.09$ | $1.92 \pm 0.10$ |
| 2-Furancarboxaldehyde, 5-(hydroxymethyl)- | $C_6H_6O_3$ | 126 | 13.23 | $0.20 \pm 0.02$ | $0.29 \pm 0.02$ | $0.34 \pm 0.02$ |
| 2-Cyclopenten-1-one, 3-ethyl-2-hydroxy- | $C_7H_{10}O_2$ | 126 | 13.39 | $1.94 \pm 0.10$ | $0.26 \pm 0.01$ | $0.28 \pm 0.01$ |
| Pentane, 3-ethyl-3-methyl- | $C_8H_{18}$ | 114 | 13.67 | $0.06 \pm 0.00$ | $0.09 \pm 0.00$ | $0.12 \pm 0.01$ |
| Octane, 2-methyl- | $C_9H_{20}$ | 128 | 13.87 | $0.02 \pm 0.00$ | $0.04 \pm 0.00$ | -- |
| Guauacol,3-methyl- | $C_8H_{10}O_2$ | 138 | 15.54 | $0.27 \pm 0.01$ | $0.60 \pm 0.03$ | $0.93 \pm 0.05$ |
| 3,4-Dimethylcyclohexanol | $C_8H_{16}O$ | 128 | 15.79 | $0.25 \pm 0.01$ | $0.53 \pm 0.03$ | $0.51 \pm 0.03$ |
| Oxirane, (1,1-dimethylbutyl)- | $C_8H_{16}O$ | 128 | 16 | $0.33 \pm 0.02$ | $0.77 \pm 0.04$ | $0.94 \pm 0.05$ |
| 1,4:3,6-Dianhydro-α-D-glucopyranose | $C_6H_8O_4$ | 144 | 16.47 | $1.94 \pm 0.10$ | $0.32 \pm 0.02$ | $0.55 \pm 0.03$ |
| 3,4-Anhydro-d-galactosan | $C_6H_8O_4$ | 144 | 16.93 | $0.45 \pm 0.02$ | $0.14 \pm 0.01$ | $0.12 \pm 0.01$ |
| Phenol, 4-ethyl-2-methoxy- | $C_9H_{12}O_2$ | 152 | 17.94 | $0.08 \pm 0.00$ | $0.24 \pm 0.01$ | $0.25 \pm 0.01$ |
| 2-Methoxy-4-vinylphenol | $C_9H_{10}O_2$ | 150 | 18.88 | $0.01 \pm 0.00$ | $0.17 \pm 0.01$ | $0.34 \pm 0.02$ |
| 2-Heptanol, 5-ethyl- | $C_9H_{20}O$ | 144 | 18.95 | $0.03 \pm 0.00$ | $0.02 \pm 0.00$ | $0.02 \pm 0.00$ |
| Phenol, 2,6-dimethoxy- | $C_8H_{10}O_3$ | 154 | 19.86 | $0.26 \pm 0.01$ | $0.39 \pm 0.02$ | $0.40 \pm 0.02$ |
| Benzaldehyde, 3-hydroxy-4-methoxy- | $C_8H_8O_3$ | 152 | 21.11 | $0.85 \pm 0.04$ | $0.41 \pm 0.02$ | $0.42 \pm 0.02$ |
| Isoeugenol(cis) | $C_{10}H_{12}O_2$ | 164 | 21.34 | $0.06 \pm 0.00$ | $0.22 \pm 0.01$ | $0.31 \pm 0.01$ |
| Homovanillin | $C_9H_{10}O_3$ | 166 | 22.63 | $0.13 \pm 0.01$ | $1.21 \pm 0.06$ | $0.93 \pm 0.05$ |
| Apocynin | $C_9H_{10}O_3$ | 166 | 23.3 | $0.11 \pm 0.01$ | $0.15 \pm 0.01$ | $0.18 \pm 0.01$ |
| Isoeugenol(trans) | $C_{10}H_{12}O_2$ | 164 | 23.75 | $2.26 \pm 0.11$ | -- | -- |
| Levoglucosan | $C_6H_{10}O_5$ | 162 | 24.38 | $0.17 \pm 0.01$ | $7.69 \pm 0.38$ | $18.88 \pm 0.94$ |
| coniferyl alcohol(trans) | $C_{10}H_{12}O_3$ | 180 | 25.16 | $0.03 \pm 0.00$ | $0.13 \pm 0.01$ | -- |
| Syringol, 4-propenyl(cis) | $C_{11}H_{14}O_3$ | 194 | 26.05 | $0.03 \pm 0.00$ | -- | $0.04 \pm 0.00$ |
| Dihydroconiferyl alcohol | $C_{10}H_{14}O_3$ | 182 | 27.08 | $0.07 \pm 0.00$ | -- | $0.27 \pm 0.01$ |

| Compound | Formula | M+ | RT | 350 °C µg/ml | 400 °C µg/ml | 450 °C µg/ml |
|---|---|---|---|---|---|---|
| Syringaldehyde | $C_9H_{10}O_4$ | 182 | 27.36 | $0.17 \pm 0.01$ | $0.08 \pm 0.00$ | $0.05 \pm 0.00$ |
| Syringol, 4-propenyl(trans) | $C_{11}H_{14}O_3$ | 194 | 28.24 | -- | $0.11 \pm 0.01$ | $0.18 \pm 0.01$ |
| Acetosyringone | $C_{10}H_{12}O_4$ | 196 | 28.97 | $0.15 \pm 0.01$ | $0.1 \pm 0.01$ | $0.07 \pm 0.00$ |
| Syringylacetone | $C_{11}H_{14}O_4$ | 210 | 29.78 | $0.02 \pm 0.00$ | $0.07 \pm 0.00$ | $0.08 \pm 0.00$ |

### 2.4.6.4 Analysis of water dispersible (WD) bio-oil fraction

The list of compounds in the WD CCB bio-oil fraction is presented in Table 2.11. The most abundant compound in all three bio-oil samples was furfurol. Formic acid was also present at a high concentration (167 – 199 mg/g) in all oils. Acetic acid was also detected and most likely generated by deacetylation of hemicelluloses [123]. Interestingly, methanol levels in the 350 °C bio-oil sample were found to be almost six times more than from the bio-oils produced at 400 and 450 °C and results from demethylation of hemicelluloses and lignin. The water-soluble constituents found in the CCB bio-oil samples are similar to those from other lignocellulosic feedstocks [84].

Table 2.11. Identified compounds via HPLC for the aqueous fraction of corrugated cardboard (CCB) obtained at various pyrolysis temperatures.

| Name | RT | 350°C bio-oil (mg/g) | 400°C bio-oil (mg/g) | 450°C bio-oil (mg/g) |
|---|---|---|---|---|
| Glucose | 12.6 | $5.7 \pm 0.3$ | -- | $87.1 \pm 4.4$ |
| Xylose | 13.4 | $7.1 \pm 0.4$ | $11.8 \pm 0.6$ | $21.9 \pm 1.1$ |
| Levoglucosan | 16.4 | $40.6 \pm 2$ | -- | -- |
| Furfurol | 16.8 | $183 \pm 9.2$ | $344 \pm 17.2$ | $497 \pm 24.9$ |
| Glycerol | 17.9 | $47 \pm 2.4$ | $62.6 \pm 3.1$ | $56.5 \pm 2.8$ |
| Formic Acid | 18.2 | $167 \pm 8.4$ | $177 \pm 8.9$ | $199 \pm 10$ |
| Acetic Acid | 19.6 | $58.9 \pm 2.9$ | $115 \pm 5.8$ | $118 \pm 5.9$ |
| Propionic Acid | 22.7 | $8.3 \pm 0.4$ | $10.8 \pm 0.5$ | $12.9 \pm 0.6$ |
| Methanol | 24.2 | $373 \pm 18.7$ | $66.1 \pm 3.3$ | $65.3 \pm 3.3$ |
| Hydroxymethyl furfural | 37.5 | $5.6 \pm 0.3$ | $6 \pm 0.3$ | $8.3 \pm 0.4$ |
| Furfural | 53.1 | $57.3 \pm 2.9$ | $5 \pm 0.3$ | $4.8 \pm 0.2$ |

**2.5    Conclusion**

In this work, cardboard samples collected from the University of Idaho, recycling center was pyrolyzed at various temperatures, and their pyrolysis products (bio-oil and biochar) were subsequently characterized. Bio-oil and biochar yields were maximized at highest and lowest pyrolysis temperatures, respectively. Pyrans, furans, phenols, and cyclopentenes were most abundantly found in cardboard bio-oil. Expectedly, the bio-oil was highly acidic due to its cellulosic nature. The bio-oil also has a high concentration of oxygenated compounds. This suggests that to utilize this bio-oil as an alternative fuel, further upgrading is required—a process which is currently financially burdensome and potentially infeasible. The lower calorific value compared to transportation fuels make it suitable as a heating oil.  However, the pyrolysis process still resulted in the generation of many compounds such as acids, alcohols, levoglucosan and phenols, which may be refined. Levoglucosan can be isolated and used as a tracer compound to determine smoke distribution or fermented into bio-ethanol. Cardboard biochar was found to have little nitrogen and ash content. The biochar hydrophobicity and thermal stability make it a viable candidate for use as a reinforcing fiber in composite materials or used as a soil amendment.

# Chapter 3. Valorization of Waste Waxed Corrugated Cardboard via Pyrolysis for Recovering Wax

"Valorization of Waste Waxed Corrugated Cardboard via Pyrolysis for Recovering Wax."
*Environmental Progress and Sustainable Energy*, vol. 145, 2020, p. 104722.

## 3.1    Abstract

Corrugated cardboard (CCB) comprises a substantial portion of municipal solid waste (MSW), of which ~5% is coated with wax (WCCB) to enhance its performance. WCCB is not able to be recycled, making it a suitable resource for thermochemical conversion to recover wax and produce char. The WCCB was characterized for its extractable wax, lignin, and carbohydrate contents and by thermogravimetric analysis (TGA) to study its thermal degradation behavior. WCCB was preliminarily examined by Py–GCMS to determine volatile product composition. WCCB samples were then pyrolyzed in an auger and tube reactors at 450, 500, and 550 °C, and their pyrolysis products (wax-oil and char) were characterized (GCMS, ESI-MS, and FTIR). WCCB and char samples were subjected to proximate, ultimate, surface area, and carbohydrates analyses. The highest char yield was 36% at 450 °C, and the highest wax-oil yield was 49% at 550 °C. Char was found to have low ash and N contents. The wax-oil fraction contained mainly alkanes, alkenes, and dienes ($C_9$ to $C_{36}$), and chain length decreased with pyrolysis temperature. This wax fraction could be recovered and used as bunker fuel ($C_{12}$-$C_{40}$) or further converted to diesel ($C_{10}$-$C_{20}$).

## 3.2    Introduction

Municipal solid waste (MSW) poses serious environmental, health, and economic concerns globally [2]. It is estimated that the MSW generation will double to 30 million tons by the year 2033 as the urban population grows [57]. According to the Environmental Protection Agency, paper products and corrugated cardboard (CCB) comprise a substantial portion (25%) of the generated MSW [4]. About 5% of all CCB is coated with wax (waxed corrugated cardboard (WCCB)) to enhance its compression strength and durability under humid/wet conditions for produce packaging [5].  While a significant portion of paper and CCB are recyclable, waxed WCCB cannot be recycled, and in fact, can adversely impact the

environment and ecosystems if comingled with non-coated cardboard [5]. Therefore, there is a need for alternative solutions to recover value and materials from WCCB.

Given that most WCCB is coated with paraffin wax [7], and paraffin has properties similar to plastic and other petroleum-derived polymers [124], energy recovery technologies commonly explored for plastic waste recycling such as thermal and catalytic pyrolysis, gasification, and plasma gasification can be viable options for WCCB processing [37]. Furthermore, the wax coating of WCCB has a high H/C ratio and convenient molecular chain structure that make it very suitable for liquid fuel production [125]. Other paper-based packaging products (cups and juice cartons) can be coated with polyethylene to improve their in-service performance [126]. In general, thermal degradation of plastics is expected to yield useful products such as monomers and combustible gases as well as fuels [125], [127].

Pyrolysis is an irreversible process of thermal decomposition of organic materials at high temperatures in an inert atmosphere. The process generally delivers gas, solid (char), and liquid (oil) products. Many factors, such as temperature, residence time, and particle size, affect the ratio and quality of the products [67]. It has been demonstrated that CCB pyrolysis produces highly oxygenated derived oil due to its relatively low carbon content and high oxygen content [40]. Similar results have been reported for biomass resources such as microalgae, residual bacterial biomass, and cassava plants [67], [121], [128]. Synthetic polymers such as polyethylene, on the other hand, deliver oils and waxes of higher quality due to their high C content [38]. Studies have also shown that the co-pyrolysis of lignocellulosic biomass with synthetic polymers enhances the properties of the obtained oil [38], [39], [129]–[133]. Given the lignocellulosic nature of CCB and polymer nature of the wax coating, similar improved results are expected for the pyrolysis products of WCCB.

From a circular economy standpoint, the energy recovered from the thermal conversion of WCCB can help reduce dependency on fossil fuels and can recover part of the energy that has gone into the production of WCCB. From an environmental standpoint, the thermal processing of WCCB would result in the reduction of landfilling and ensure minimal harm to the environment and ecosystems.

This work aims to address the imperative problem of unrecyclable WCCB by examining the feasibility of recovering wax and other products from WCCB that are suitable for further refinement into transport fuels. The WCCB sample was characterized by its chemical composition and thermal behavior. The effect of temperature on char and wax/oil product yields and quality were studied in an auger and tube reactor. The pyrolysis wax-oil products were chemically investigated by a combination of FTIR, GCMS, and ESI-MS. The char was characterized by proximate, ultimate, surface area, FTIR spectroscopy, and x-ray diffraction analyses.

## 3.3    Materials and methods

### 3.3.1    Waxed cardboard retrieval and preparation

WCCB boxes were obtained from the Safeway grocery store in Moscow, ID, cut into approximately 25 mm x 25 mm size pieces, then Wiley milled to pass through a 3.2 mm screen, and lastly dried in an oven for 48 h at 45 °C. Paraffin (J. T. Baker Chemicals) was used as a standard.

### 3.3.2    WCCB and char characterization

#### 3.3.2.1    Calorific value, proximate, elemental, and surface area analyses

A Parr oxygen bomb calorimeter (model no. 1261) was used to obtain the calorific values on pressed pellets (1.0 g, 6 mm Ø using a Carver Laboratory hydraulic press at 1,500 MPa) WCCB and char samples (in triplicate) in accordance with ASTM D5865-04. The WCCB and char ash content, volatile matter (VM), and fixed carbon (FC) were determined by proximate analysis according to ASTM E870-82 in triplicate. Elemental analysis was performed in duplicate using a Costech ESC 4010 instruments to obtain C, N, and H contents. The specific surface areas ($S_{BET}$) of all degassed char samples (0.25 g, in duplicate) were measured on a Micromeritics FlowSorb 2300 instrument according to ASTM D6556-10.

#### 3.3.2.2   Moisture content measurement and wax extraction

Mettler Toledo moisture analyzer was used to obtain the moisture content of the WCCB. The WCCB sample (4.0 g) was Soxhlet extracted in duplicate using $CH_2Cl_2$ (150 mL) for 16 h, and wax content was determined gravimetrically, according to ASTM D1108-96.

### 3.3.2.3 Lignin and carbohydrate content analyses

The wax-free WCCB (200 mg) were analyzed for lignin and carbohydrate contents in duplicate by hydrolysis in sulphuric acid (2 ml, 72%) for 60 min at 30 °C, followed by secondary hydrolysis in sulfuric acid (4% $H_2SO_4$, 30 min, 121°C) in an autoclave, in accordance with ASTM D 1106-96 with some modifications. Klason lignin content was determined gravimetrically after filtration. Acid soluble lignin was determined by absorbance at 205 nm of the filtered hydrolysate (made up to 250 mL) using an absorption coefficient of 110 L $g^{-1}$ $cm^{-1}$ (Biomate 5, Thermoelectron) [75]. Carbohydrate analysis was performed on the hydrolysis filtrate (5 mL) according to ASTM E 1758-01. The monosaccharides were quantified by HPLC (two Rezex RPM columns, 7.8 mm x 300 mm, Phenomenex) at 85 °C on elution with water (0.5 mL $min^{-1}$) using differential refractive index detection (Waters model 2414) [76].

Acetyl bromide / UV absorbance method was also used to determine the total lignin in duplicate [77]. Dried and wax-free WCCB (5.0 mg) was placed in acetyl bromide (25% w/w) in acetic acid (5 mL) and perchloric acid (0.2 mL, 70%) at 70 °C for 60 min. The solutions were made up to 100 mL containing 2M NaOH (10 mL) and acetic acid (25 mL). Absorbance at 280 nm was measured (Biomate 5, ThermoElectron) and lignin content determined using an absorptivity of lignin ($\varepsilon$) of 20.09 L $g^{-1}$ $cm^{-1}$. A modified phenol-sulfuric acid colorimetric method was utilized to obtain the total carbohydrate content in duplicate [78]. Dried WCCB (10 mg) and cellulose standard (Sigmacell type 101, 2 to 10 mg) were incubated in sulfuric acid (100 μL, 77%), then aqueous phenol (1 mL, 5%) followed by concentrated sulfuric acid (5 mL) were added and mixed vigorously. Absorbance at 490 nm was measured (Biomate 5, Thermoelectron).

### 3.3.2.4 Scanning Electron Microscopy (SEM)

SEM was performed on carbon-coated samples using a Zeiss Supra 55 VP-FEG instrument [Carl Zeiss LLC, White Plains, NY] at either 5 or 10 kV. The average fiber length and width were determined using at least 50 values obtained from the fibers present in each image.

### 3.3.2.5 X-Ray diffraction (XRD)

XRD analysis on wax-free WCCB and char were performed on a Siemens D5000 diffractometer using Cu-Ka radiation (wavelength of 0.1542 nm) from $2\theta$ = 2 to 80° at 0.01°

steps. The crystallinity index (CI) for cellulose (CIc) and wax (CIw) were determined using the adjusted deconvolution method [134][135].

Equation 1

$$CI = \left(\frac{\sum A_{cry}}{\sum A_{cry} + \sum A_{am}}\right) x \ 100$$

Where $A_{cry}$ is the adjusted crystalline peak area, and $A_{am}$ is the adjusted broad peak area of the amorphous component. Crystalline peaks for cellulose are found at 101 and 200, and peaks for wax are found at 004, 011, 020, 310, and 311.

### 3.3.2.6  Fourier Transform InfraRed (FTIR) spectroscopy

FTIR spectra on WCCB and char samples were obtained using an iS5 (ThermoNicolet) spectrometer with an attenuated total reflection (ATR) accessory (iD5, Ge crystal) in triplicate. For the wax-oil samples, a ZnSe ATR crystal was used. The spectra were baseline corrected and averaged using the Omnic v9 software (Thermo-Nicolet).

### 3.3.3  Thermogravimetric analysis (TGA)

A PerkinElmer TGA-7 instrument was used to perform TGA on WCCB samples (5-6 mg) from 30 to 900 °C at heating rates (β) of 5, 10, 15, 20, and 25 °C min$^{-1}$ under nitrogen (30 mL min$^{-1}$) to determine the apparent activation energy (*E*) and thermal degradation behavior. The TGA and differential thermogravimetric (DTG) data were analyzed using Pyris v11 software. The *E* was calculated using a model-free technique (Flynn-Wall-Ozawa's (FWO) method [136], [137]) that relied on TGA data. Isothermal TGA was also used to estimate the char mass yield of WCCB during pyrolysis at given temperatures. The temperature was ramped from 30 °C to 450, 500 and 550 °C at 200 °C min$^{-1}$ and then maintained for 60 min.

### 3.3.4  Pyrolysis-GCMS analysis

Analytical pyrolysis was performed in duplicate at 500 °C using a Pyrojector II unit (SGE Analytical Science) coupled to a GC-MS (Trace 1300-ISQ, Thermo Scientific) and the compounds were separated on a ZB-5 capillary column (30 m × 0.25 mm Ø, Phenomenex) from 50 °C (1 min) to 250 °C (10 min) at 5 °C min$^{-1}$. All the compounds were identified by comparing with standards, their mass spectra, and using NIST 2017 library matching. The relative abundance of each compound was calculated relative to the $CO_2$ peak.

### 3.3.5 Pyrolysis

WCCB was pyrolyzed at three different temperatures of 450, 500, and 550 °C in a custom-built auger reactor (Ø 5 cm x 90 cm) (Figure 2.1) with an $N_2$ purge (5 L min$^{-1}$) and a feeding rate of 0.5 kg h$^{-1}$ (K-Tron loss-in-weight feeder) for two hours. Auger speed was adjusted to obtain a 6.4 s residence time. A two-stage ice-water-cooled tube and shell condenser was used to condense the vapors. Char and wax-oil were collected from for characterization. To further investigate the wax-oil chemical composition and to allow for a more controlled product collection, the second set of pyrolysis experiments were performed on a small quartz tube (20 mm ID x 300 mm) reactor (Figure 3.1) with an $N_2$ purge (0.1 L min$^{-1}$). The WCCB sample (0.60 g) was placed inside a quartz boat and quickly inserted inside the heated zone (150 mm). A single-stage cooling U-tube submerged in liquid nitrogen was used to condense the vapors. The wax-oil was collected and subsequently analyzed.
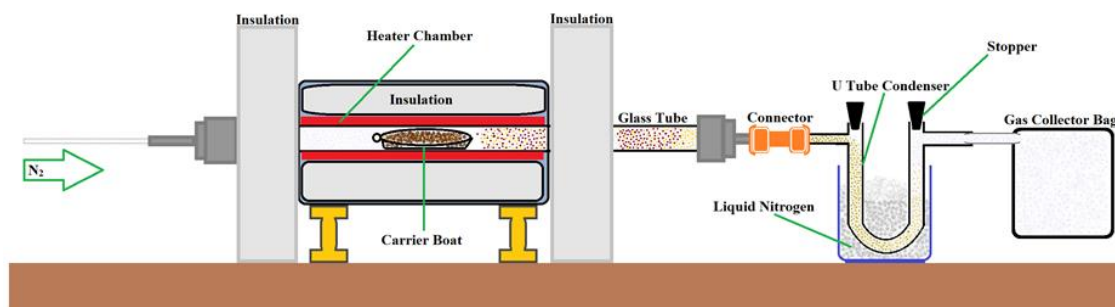


Figure 3.1. Schematic profile view of small tube batch reactor used for pyrolysis of waxed corrugated cardboard (WCCB).

### 3.3.6   Wax-oil characterization

The wax-oil samples were dried using anhydrous sodium sulfate, and their calorific value was determined as described above.

### 3.3.7   Electro Spray Ionization Mass Spectrometry (ESI-MS)

The molar mass of fresh wax-oil samples was determined using a Finnigan LCQ-Deca instrument (ThermoQuest). The wax-oil samples (1 mg mL$^{-1}$) were dissolved in dichloromethane (50%), methanol (49%), and acetic (1%) acid solution and subjected to negative ion ESI–MS (*m/z* 100–2,000) at a flow rate of 10 μL min$^{-1}$. The ion source and capillary voltages were 4.5 kV and 50 V at 275°C, respectively.  The number average molar mass ($M_n$) was calculated as $M_n = \sum N_i M_i / \sum N_i$ and the weight average molar mass ($M_w$) as $M_w = \sum N_i M_i^2 / \sum N_i M_i$ where $N_i$ is the intensity of ions, and $M_i$ is the mass after accounting for the charge.

### 3.3.8   Gas Chromatography-Mass Spectrometry (GC-MS)

The wax-oils (1 mg in CH$_2$Cl$_2$ (1 mL) containing trichlorobenzene (100 μg mL-1) as an internal standard) were analyzed in duplicate by GC-MS (Trace 1300-ISQ, ThermoScientific). Product compounds were separated using a ZB-5 capillary column (30 m × 0.25 mm Ø, Phenomenex) using a temperature program of 40 °C (1 min) to 320 °C (10 min) at 5 °C min$^{-1}$.

## 3.4   Results and discussion

### 3.4.1   Waxed cardboard (WCCB) characterization

The results of the elemental, proximate, ultimate, surface area, and calorific value analyses of WCCB and char samples are given in Table 3.1. WCCB contained 54.6% C, 0.1% N, 8.9% H, and 2.1% ash. These elemental results are clearly in the range for a mixture of lignocellulosic biomass such as cardboard, and plastic such as wax [32], [38], [40], [138]. The small amount of ash (2.1%) may have come from inorganic additives such as talc [34], [87]. The low N content (0.1%) confirms that the WCCB has very little protein. A FC value of 11.9% for WCCB was comparable to the values obtained for cardboard and paper [32], [38], [40]. The calorific value obtained for WCCB was 27 MJ kg$^{-1}$, which is higher than the reported values for cardboard and similar substances such as paper cups [126] and is more consistent with those reported for plastics such as polyethylene terephthalate (PET) [40],

[74], [83], [138]. About 51% of WCCB was wax as determined by extraction (Table 3.1). WCCB was shown to have an acid-soluble and Klason lignin contents of 1.8% and 8.5%, respectively. Lignin content determined using the acetyl bromide method was 8.8%. WCCB had a total carbohydrate content of 35.8% determined by the phenol-sulfuric method. Detailed carbohydrate analysis showed the dominant presence of glucose at 33.3%. Xylose, arabinose, mannose, and galactose were also found. The lignin and carbohydrate values in the CCB portion of WCCB are in agreement with the literature for lignin [40], [89], [90], and for carbohydrates [40], [90].

Table 3.1. Proximate and ultimate analysis, surface area analysis, average fiber length/width, and lignin and carbohydrate contents of waxed corrugated cardboard (WCCB) and pyrolysis chars.

| | WCCB | WCCB450 Char | WCCB500 Char | WCCB550 Char |
|---|---|---|---|---|
| % N | $0.1 \pm 0.005$ | $0.12 \pm 0.01$ | $0.13 \pm 0.01$ | $0.14 \pm 0.01$ |
| % C | $54.6 \pm 2.5$ | $45.4 \pm 2.3$ | $48.9 \pm 2.4$ | $51.1 \pm 2.6$ |
| % H | $8.9 \pm 0.45$ | $7.9 \pm 0.4$ | $7.4 \pm 0.37$ | $6.1 \pm 0.3$ |
| % Ash | $2.1 \pm 0.12$ | $4.5 \pm 0.2$ | $8.1 \pm 0.3$ | $12.1 \pm 0.6$ |
| % Fixed carbon | $11.9 \pm 0.6$ | $27.1 \pm 1.2$ | $42.6 \pm 2.1$ | $62.0 \pm 2.9$ |
| Avg fiber length ($\mu$m) | $650 \pm 29.6$ | $350 \pm 16.1$ | $250 \pm 12.3$ | $200 \pm 9.7$ |
| Avg fiber width ($\mu$m) | $35 \pm 1.6$ | $30 \pm 1.2$ | $20 \pm 0.9$ | $15 \pm 0.7$ |
| Calorific value (MJ kg$^{-1}$) | $27.0 \pm 1.3$ | $27.0 \pm 1.4$ | $29.0 \pm 1.5$ | $30.0 \pm 1.5$ |
| Surface Area (m$^2$ g$^{-1}$) | $0.72 \pm 0.036$ | $0.89 \pm 0.05$ | $0.30 \pm 0.01$ | $0.64 \pm 0.03$ |
| % Wax content (CH$_2$Cl$_2$ extract) | $51 \pm 2.1$ | - | - | - |
| Density (g cm$^{-3}$) | $1.21 \pm 0.003$ | $1.40 \pm 0.002$ | $1.25 \pm 0.001$ | $1.28 \pm 0.06$ |
| % Klason lignin | $8.5 \pm 0.5$ | - | - | - |
| % Acid soluble lignin | $1.8 \pm 0.06$ | - | - | - |
| % Total lignin (acetyl bromide) | $8.8 \pm 0.3$ | - | - | - |
| % Total carbohydrate (phenol-sulfuric) | $35.8 \pm 1.4$ | - | - | - |
| Glucose (mg/g) | $333 \pm 17$ | - | - | - |
| Xylose (mg/g) | $36 \pm 1.9$ | - | - | - |
| Galactose (mg/g) | $1.3 \pm 0.07$ | - | - | - |
| Arabinose (mg/g) | $16.6 \pm 0.8$ | - | - | - |
| Mannose (mg/g) | $8 \pm 0.4$ | - | - | - |

### 3.4.2 Thermogravimetric analysis (TGA) of WCCB

Thermal degradation and kinetic behavior of WCCB was investigated by TGA. The TGA and DTG thermograms of WCCB are presented in Figure 3.2 a and b. Studies have shown that the cardboard portion of WCCB is primarily composed of cellulose, followed by hemicellulose and lignin [65], [66]. The DTG thermogram showed three major peaks. Below 300 °C, very little mass loss occurs, which is attributed to the evaporation of water and light volatiles [93]. The first two significant peaks occurred at 300 °C and 400 °C, which corresponds to the decomposition of cellulose and lignin [32], [94], [95], [139], [140]. The third peak around 500 °C is associated with the decomposition of the wax portion of WCCB [125], [139]. A minor amount of residue was left, which is consistent with the reported proximate analysis findings. The apparent $E$ was calculated using the isoconversional method based on the linear regression of the FWO method in the conversion ($\alpha$) range of 10% to 90% (Table 3.2). An average $E$ of 180 J mol$^{-1}$ is lower than those reported for plastics that used the same method [141] but is in the range reported for cardboard [40], [85].
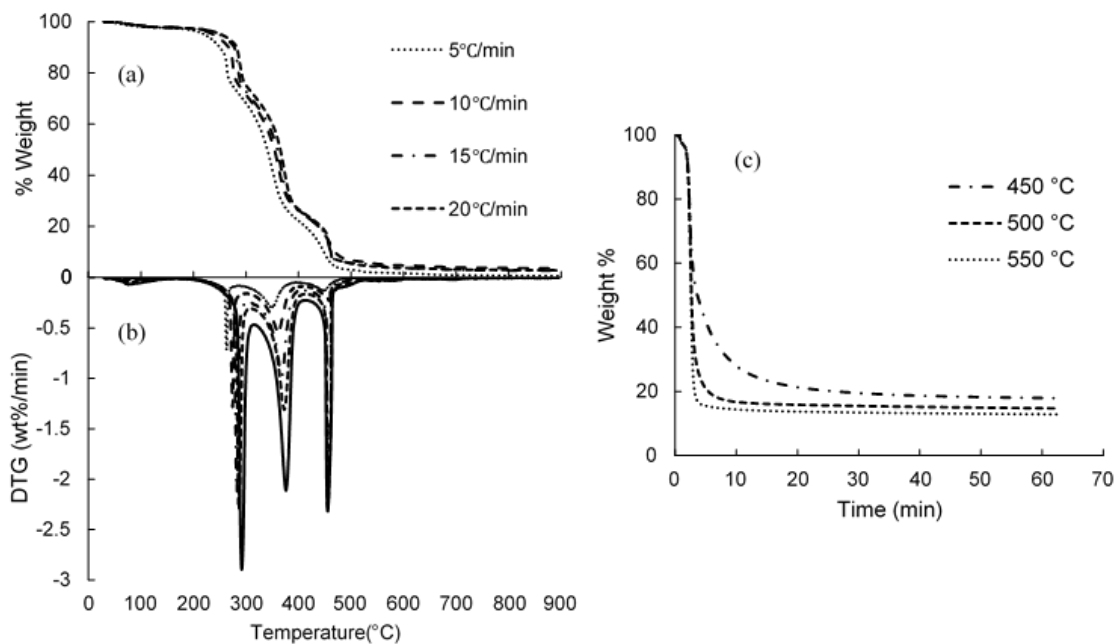


Figure 3.2. (a) TGA, (b) DTG thermograms of waxed corrugated cardboard (WCCB) at different heating rates ($\beta$ of 5–25 °C min$^{-1}$), and (c) isothermal TGA experiments of waxed corrugated cardboard (WCCB) ramped at 200 °C min$^{-1}$ to 450, 500, and 550 °C.

The isothermal TGA experiments were performed to monitor the temporal pyrolysis reaction (Figure 3.2 c). The results showed approximate char yields of 50% at 450 °C, 22% at 500 °C, and 17% at 550 °C, confirming the decrease in char yield with increasing temperature. With extended heating, all samples converged to a comparable value of approximately 20%, representing the final char yield of the WCCB samples.

Table 3.2. Activation energy values (E) at various conversion factors ($\alpha$) for waxed corrugated cardboard (WCCB) determined by TGA.

| Conversion ($\alpha$) | $E$ (J mol$^{-1}$) | $R^2$ |
|---|---|---|
| 10% | 99 | 0.9598 |
| 20% | 121 | 0.9788 |
| 30% | 148 | 0.9623 |
| 40% | 167 | 0.9956 |
| 50% | 191 | 0.9974 |
| 60% | 222 | 0.9879 |
| 70% | 265 | 0.9733 |
| 80% | 155 | 0.997 |
| 90% | 257 | 0.995 |

### 3.4.3    Analytical Py-GCMS of WCCB

Analytical pyrolysis GC-MS was performed at 500 °C to determine the potential pyrolysis products from WCCB. A list of identified compounds and levels are given in Table 3.3. Long-chain hydrocarbons (totaling ~72% at 500 °C) such as octacosane and heptacosane were abundantly found, which is in agreement with GC-MS analysis findings of plastic waste pyrolysis previously reported [125]. The most abundant oxygenated compound found was levoglucosan (5.49% at 500 °C), which is consistent with the literature for cellulose pyrolysis decomposition [96], [99], [100]. The abundance of long-chain hydrocarbons and a low number of oxygenated compounds is promising for fuel products.

Table 3.3. Identified compounds via Py-GCMS for waxed corrugated cardboard (WCCB), pyrolyzed at 500 °C.

| Compound | Formula | RT (min) | M+ (m/z) | WCCB 500°C (Area%) |
|---|---|---|---|---|
| Carbon dioxide | $CO_2$ | 1.66 | 44 | $0.66 \pm 0.03$ |
| Acetaldehyde | $C_2H_4O$ | 1.85 | 44 | $0.72 \pm 0.04$ |
| 2-Methylbutanal | $C_5H_{10}O$ | 2.13 | 86 | $0.94 \pm 0.05$ |
| Phenol, o-methoxy- | $C_7H_8O_2$ | 11.68 | 124 | $0.64 \pm 0.03$ |
| 1.2-Hexyl-3-methyloxirane | $C_9H_{18}O$ | 14.33 | 142 | $0.7 \pm 0.04$ |
| 5-Hydroxymethylfurfural | $C_6H_6O_3$ | 15.61 | 126 | $0.53 \pm 0.03$ |
| 2-Hydroxymethyl-5-hydroxy-2,3-dihydro-(4H)-pyran-4-one | $C_6H_8O_4$ | 17.58 | 144 | $0.77 \pm 0.04$ |
| Isoeugenol | $C_{10}H_{12}O_2$ | 21.41 | 164 | $0.82 \pm 0.04$ |
| Levoglucosan | $C_6H_{10}O_5$ | 22.96 | 162 | $5.49 \pm 0.27$ |
| 3-methyl-3-(1-ethoxyethoxy)-1-eutene, | $C_9H_{18}O_2$ | 25.63 | 158 | $0.68 \pm 0.03$ |
| Coniferyl alcohol | $C_{10}H_{12}O_3$ | 28.1 | 180 | $0.63 \pm 0.03$ |
| Myristic acid | $C_{14}H_{28}O_2$ | 28.54 | 228 | $0.83 \pm 0.04$ |
| Palmitic acid | $C_{16}H_{32}O_2$ | 32.57 | 256 | $1.32 \pm 0.07$ |
| Eicosane | $C_{20}H_{42}$ | 33.29 | 282 | $0.53 \pm 0.03$ |
| Heneicosane | $C_{21}H_{44}$ | 35.14 | 296 | $1.27 \pm 0.06$ |
| Docosane | $C_{22}H_{46}$ | 36.92 | 310 | $3.44 \pm 0.17$ |
| Tetracosane | $C_{24}H_{50}$ | 38.64 | 338 | $8.68 \pm 0.43$ |
| 1-Hexacosene | $C_{26}H_{52}$ | 40.29 | 364 | $13.53 \pm 0.68$ |
| Hexacosane | $C_{26}H_{54}$ | 41.05 | 366 | $1.1 \pm 0.05$ |
| 1-Heptacosene | $C_{27}H_{54}$ | 41.24 | 378 | $0.53 \pm 0.03$ |
| Heptacosane | $C_{27}H_{56}$ | 41.86 | 380 | $16.45 \pm 0.82$ |
| 1-Octacosene | $C_{28}H_{56}$ | 42.84 | 392 | $0.85 \pm 0.04$ |
| Octacosane | $C_{28}H_{58}$ | 43.54 | 394 | $14.1 \pm 0.7$ |
| Sinapyl alcohol | $C_{11}H_{14}O_4$ | 44.1 | 210 | $0.51 \pm 0.03$ |
| Triacontane | $C_{30}H_{62}$ | 44.75 | 422 | $0.55 \pm 0.03$ |
| Dotriacontane | $C_{32}H_{66}$ | 45.62 | 450 | $8.55 \pm 0.43$ |
| Tetratriacontane | $C_{34}H_{70}$ | 48.17 | 478 | $2.25 \pm 0.11$ |
| 54 other compounds (concentration <0.5%) | - | - | - | $12.95 \pm 0.64$ |

### 3.4.4    Pyrolysis yield

The TGA experiments indicated that the WCCB decomposed by ~83% at 550 °C. For this reason, three temperatures of 450, 500, and 550 °C were chosen for pyrolysis experiments. The pyrolysis wax-oil, char, and gas (by difference) yield at various temperatures were determined for both the auger and tube reactor and are presented in Figure 3.3. Previously Wang et al. [142] had confirmed for CCB that the char yield would decrease with the increase of temperature, the oil yield would increase with the increase of temperature up to 550 °C, and it would decrease in higher temperatures to create more gaseous products. The results of this work follow this trend; however, the change is less dramatic in the tube reactor. The highest wax-oil yield in the auger reactor (49%) was obtained at 550 °C, which is comparable to the 51% wax content of WCCB. This value is close to the oil yield of the pyrolysis of the plastic-rich MSW sample reported by Lopez et al. [143] and co-pyrolysis of biomass and plastics [125]. It is, however, lower than the reported yield of tar (oil) by Grieco and Baldi [144] for a mixture of paper and plastic, which is structurally more similar to the WCCB samples. The wax-oil yield for the tube reactor (53%) is more consistent with Grieco and Baldi's results [143]. The high wax-oil yield in the tube reactor experiments is the result of a more effective condensation of vapor products facilitated by liquid nitrogen. As expected, both the auger and tube reactor oil yields were lower than those reported for pure plastics [145]. The highest overall char yield (36%) was observed in the WCCB sample pyrolyzed at 450 °C, suggesting that not all the wax was removed under these conditions. This value is higher than those reported for char yield in literature for MSW. The highest char yield from the batch reactor was 17% at 450 °C. In the tube reactor, near-complete thermochemical conversion was achieved at 550 °C.  In general, the tube reactor used for these experiments was more precise in comparison to the auger reactor as its smaller size and part accessibility allowed for more control over critical factors and more effective condensation and collection processes. The advantage of using the auger reactor was the ability to process a larger volume of material continuously.
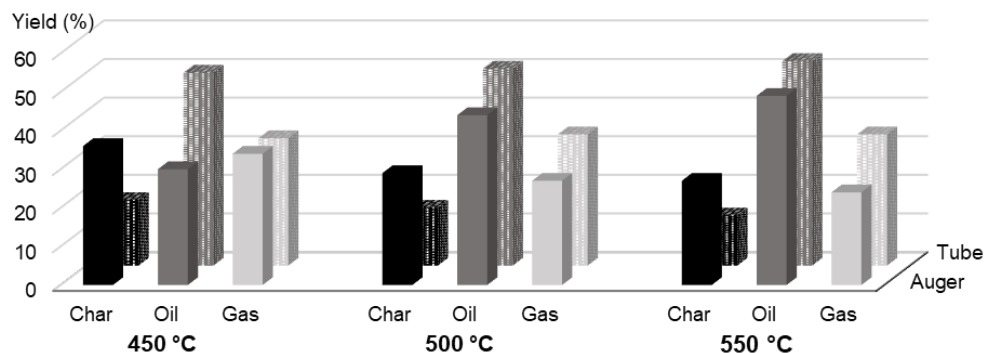
Figure 3.3. Waxed corrugated cardboard (WCCB) pyrolysis product yields from the auger and tube reactors.

### 3.4.5 WCCB wax-oil characterization

### 3.4.5.1 Calorific value

The calorific values for dried WCCB wax-oil samples from the auger reactor were measured at 41 kJ g$^{-1}$ for the wax-oil sample obtained at 450 °C (WCCB450 wax-oil) and 43 kJ g$^{-1}$ for samples collected at 500 and 550 °C (WCCB500 and WCCB550 wax-oils). While these are in the range reported for pyrolysis oils derived from MSW in the literature [146], the values are almost twice the values obtained for regular cardboard oil [40], as expected due to the presence of wax.

### 3.4.5.2 ESI-MS analysis of wax-oil

Negative ion [M-H]$^-$ ESI-MS analysis was used to determine the molar mass distribution of both volatile and non-volatile compounds (Figure 3.4). Significant [M-H]$^-$ peaks at 161, 163, 177, 191 $m/z$ were tentatively assigned to levoglucosan, eugenol/isoeugenol, coniferyl aldehyde, and $C_{11}H_{12}O_3$, respectively [40], [147]. Upon closer examination of the spectra for $100 < m/z < 300$ (Figure 3.4), a series of ions ($m/z$ 14 apart) were clearly observed for the presence of hydrocarbon dienes from $C_8$ ($m/z= 109$) to $C_{21}$ ($m/z = 291$). In addition, a series ion for hydrocarbon alkenes ($C_8$ $m/z= 111$ to $C_{21}$ $m/z = 293$) and alkanes ($C_8$ $m/z= 113$ to $C_{21}$ $m/z = 295$) were also detected. GCMS analysis (section 3.5.3) also showed the presence of alkane, alkene, and diene products. The peak at $m/z$ 473 was seen in the background in all samples, most likely due to an unknown contaminant.

The calculated $M_w$ and $M_n$ of extracted wax and auger pyrolysis wax-oils obtained in duplicate are given in Table 3.4. The $M_w$ for wax decreased progressively from 1077 g mol^{-1} to 948 g mol^{-1} as pyrolysis temperature increased to 550 °C. A decrease in average molar mass is the result of developed thermal degradation by increasing the pyrolysis temperature [67]. An estimate of the proportion of low (monomers, Σ $m/z$ 100-300) to high (oligomers, Σ $m/z$ 301-2000) molar mass compounds was calculated from ion intensities (Table 3.4). These ranges were arbitrarily decided as indicative of low and high molar mass [40]. The wax extract had a monomer/oligomer ratio of 0.11 and increased progressively with pyrolysis temperature to 0.31 at 550 °C, indicating more thermal cracking and a relatively higher proportion of smaller molecular fragments. An increase in the relative abundance of the peaks by increasing temperature is representing higher extraction and better degradation of WCCB at 550 °C pyrolysis.

Table 3.4. Weight (Mw) and number average molar mass (Mn) of WCCB auger pyrolysis wax-oils at 450, 500, and 550 °C determined from negative ion ESI-MS data.

| Sample | $M_n$ (g mol^{-1}) | $M_w$ (g mol^{-1}) | Monomer/Oligomer |
|---|---|---|---|
| Extracted Wax | 850 ± 43 | 1077 ± 54 | 0.11 |
| WCCB450 Wax-Oil | 733 ± 35 | 975 ± 48 | 0.22 |
| WCCB500 Wax-Oil | 731 ± 36 | 971 ± 49 | 0.22 |
| WCCB550 Wax-Oil | 693 ± 31 | 948 ± 47 | 0.31 |
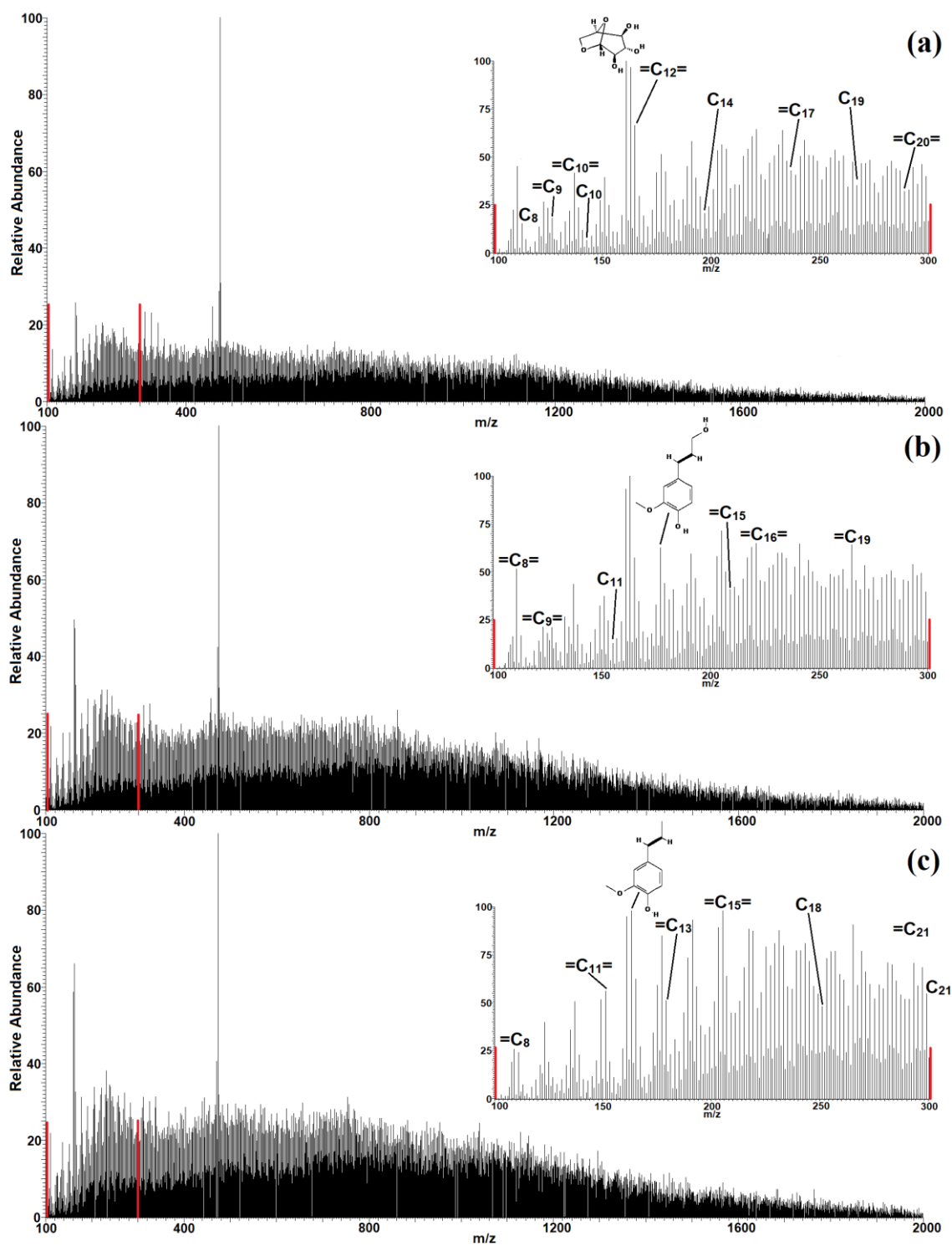
Figure 3.4. Negative ion ESI-MS spectra of (a) WCCB450, (b) WCCB500, and (c) WCCB550 wax-oil samples from the auger reactor. (Cx: Alkane, =Cx: Alkene, =Cx=: Diene).

### 3.4.6   The GC-MS analysis of wax-oil

The volatile compounds in the wax-oil obtained from the pyrolysis of WCCB in the auger reactor were analyzed directly by GC-MS (Figure 3.5), and the identified and quantified compounds are listed in Table 3.5. The recovered pyrolysis wax-oil contained very few oxygenated compounds and was dominated by hydrocarbons ($C_9$-$C_{36}$) at about 97.6% [105]. The high degree of wax recovery during the pyrolysis process was promising and suggests that the wax-oil could be considered for catalytic upgrading to produce transport fuels. Higher pyrolysis temperatures resulted in an increase in smaller hydrocarbon products ($C_9$-$C_{20}$). The main component of cardboard pyrolysis oil, levoglucosan [40] that was also found in Py-GCMS results reported earlier, was absent in the wax oil obtained from the auger reactor. Other oxygenated compounds such as furans (e.g., furfural), aldehyde/ketones, and acids that are commonly found in the pyrolysis products of lignocellulosic biomass [72] were absent in the wax-oil of WCCB. One possible explanation was that the level of oxygenated compounds might have been negligible compared to wax and therefore, not observed. To test this hypothesis, the authors constructed a small tube batch reactor (Figure 3.1) to allow for a more efficient multi-stage collection of the condensed vapors obtained from the pyrolysis of WCCB. The collected oil fraction (end of quartz tube) and wax fractions (U-tube condenser) were analyzed by GC-MS (Figure 3.6).
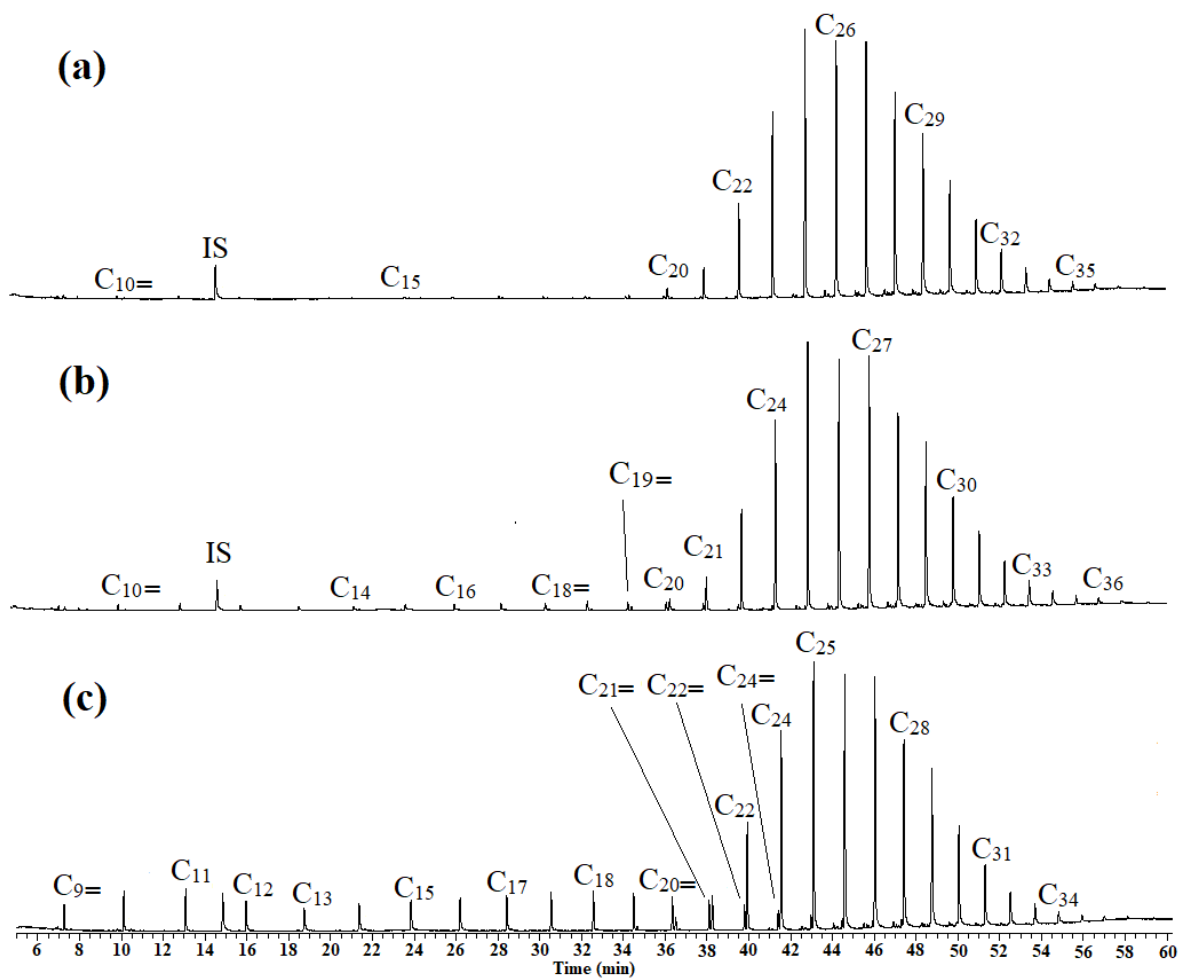
Figure 3.5. GC-MS Chromatograms of (a) WCCB450, (b) WCCB500, and (c) WCCB550 pyrolysis wax-oil samples collected from the auger reactor. (Cx: Alkane, Cx=: Alkene).

Table 3.5. Compounds identified in wax corrugated cardboard (WCCB) fresh wax-oil obtained from the auger reactor by GC-MS.

| Compound | Formula | M+ | RT | WCCB450 µg/ml | WCCB500 µg/ml | WCCB550 µg/ml |
|---|---|---|---|---|---|---|
| 1-Nonene | $C_9H_{18}$ | 126 | 7.26 | 0.38±0.02 | 0.85±0.04 | 4.8±0.24 |
| 1-Decene | $C_{10}H_{20}$ | 140 | 10.1 | 0.53±0.03 | 1.54±0.08 | 8±0.4 |
| Decane | $C_{10}H_{22}$ | 142 | 10.44 | 0.3±0.02 | 0.37±0.02 | 0.31±0.02 |
| Cyclopropane, 1-heptyl-2-methyl- | $C_{11}H_{22}$ | 154 | 13.05 | 0.7±0.04 | 1.87±0.09 | 9.75±0.49 |
| Undecane | $C_{11}H_{24}$ | 156 | 13.39 | - | 0.24±0.01 | 0.31±0.02 |
| Dodecane | $C_{12}H_{26}$ | 170 | 15.93 | 0.73±0.04 | 1.45±0.07 | 9.03±0.45 |
| Tridecane | $C_{13}H_{28}$ | 184 | 18.71 | 1.59±0.08 | 2.63±0.13 | 9.28±0.46 |
| Tetradecane | $C_{14}H_{30}$ | 198 | 21.33 | 1.45±0.07 | 3.08±0.15 | 10.1±0.51 |
| Pentadecane | $C_{15}H_{32}$ | 212 | 23.8 | 1.49±0.07 | 2.9±0.15 | 11.28±0.56 |
| Hexadecane | $C_{16}H_{34}$ | 226 | 26.15 | 1.44±0.07 | 3.15±0.16 | 10.85±0.54 |
| Heptadecane | $C_{17}H_{36}$ | 240 | 28.37 | 1.48±0.07 | 3.2±0.16 | 10.82±0.54 |
| Octadecane | $C_{18}H_{38}$ | 254 | 30.49 | 1.55±0.08 | 3.53±0.18 | 11.3±0.56 |
| 1-Octadecene | $C_{18}H_{38}$ | 254 | 32.5 | 0.81±0.04 | 2.97±0.15 | 9.52±0.48 |
| Nonadecane | $C_{19}H_{40}$ | 268 | 34.43 | 0.77±0.04 | 2.76±0.14 | 9.35±0.47 |
| 1-Nonadecene | $C_{19}H_{40}$ | 268 | 34.6 | 1.02±0.05 | 1.32±0.07 | 0.97±0.05 |
| Eicosane | $C_{20}H_{42}$ | 282 | 36.27 | 0.67±0.03 | 2.66±0.13 | 8.22±0.41 |
| isomer-Eicosane | $C_{20}H_{42}$ | 282 | 36.43 | 2.71±0.14 | 3.62±0.18 | 3.24±0.16 |
| Heneicosane | $C_{21}H_{44}$ | 296 | 38.03 | - | 2.07±0.1 | 7.1±0.35 |
| isomer-Heneicosane | $C_{21}H_{44}$ | 296 | 38.18 | 7.49±0.37 | 10.16±0.51 | 8.79±0.44 |
| Docosene | $C_{22}H_{44}$ | 308 | 39.71 | - | - | 6.79±0.34 |
| 1-Docosene | $C_{22}H_{44}$ | 308 | 39.85 | 25 ± 1.25 | 30.45±1.52 | 25.91±1.3 |
| Tricosane | $C_{23}H_{48}$ | 324 | 41.33 | - | 58.42±2.92 | 4.76±0.24 |
| Tetracosane | $C_{24}H_{50}$ | 338 | 41.46 | 50.9 ± 2.55 | - | 48.76±2.44 |
| Pentacosane | $C_{25}H_{52}$ | 352 | 43.02 | 76.1 ± 3.81 | 82.17±4.11 | 69.7±3.48 |
| Hexacosane | $C_{26}H_{54}$ | 366 | 44.5 | 70.18±3.51 | 81.83±4.09 | 69.02±3.45 |
| Heptacosane | $C_{27}H_{56}$ | 380 | 45.94 | 75.44±3.77 | 84.65±4.23 | 68.04±3.4 |
| Octacosane | $C_{28}H_{58}$ | 394 | 47.32 | 62.33±3.12 | 67.6±3.38 | 53.05±2.65 |
| Nonacosane | $C_{29}H_{60}$ | 408 | 48.65 | 55.3±2.77 | 82.73±4.14 | 48.87±2.44 |
| Triacontane | $C_{30}H_{62}$ | 422 | 49.95 | 35.28±1.76 | 42.38±2.12 | 32.53±1.63 |
| Hentriacontane | $C_{31}H_{64}$ | 436 | 51.2 | 27.44±1.37 | 32.57±1.63 | 21.17±1.06 |
| Dotriacontane | $C_{32}H_{66}$ | 450 | 52.4 | 16.82±0.84 | 20.98±1.05 | 14.24±0.71 |
| Tritriacontane | $C_{33}H_{68}$ | 464 | 53.57 | 8.74±0.44 | 12.82±0.64 | 8.47±0.42 |
| Tetracosane, 11-decyl- | $C_{34}H_{70}$ | 478 | 54.71 | 4.86±0.24 | 10.21±0.51 | 5.84±0.29 |
| Pentatriacontane | $C_{35}H_{72}$ | 492 | 55.81 | 3.62±0.18 | 4.4±0.22 | 3.33±0.17 |
| Hexatriacontane | $C_{36}H_{74}$ | 507 | 56.9 | 1.75±0.09 | 3.95±0.2 | 2.44±0.12 |

The wax-oil product from the tube reactor showed the presence of oxygenated compounds in addition to hydrocarbons (Table 3.6). The mixture was dominated by oxygenated compounds (~71% at 550 °C) with the most abundant compound being levoglucosan, and its concentration increased with pyrolysis temperature (Figure 3.6). This is consistent with the Py-GCMS experiments and the pyrolysis of CCB [40]. Other oxygenated compounds such as furans (e.g., furfural), aldehyde/ketones, and acids were also present in the mixture, consistent with previous findings for lignocellulosic pyrolysis oils [72]. What is evident from the pyrolysis experiments is the product distributions between the auger and tube reactor were quite different and warrant further investigation.
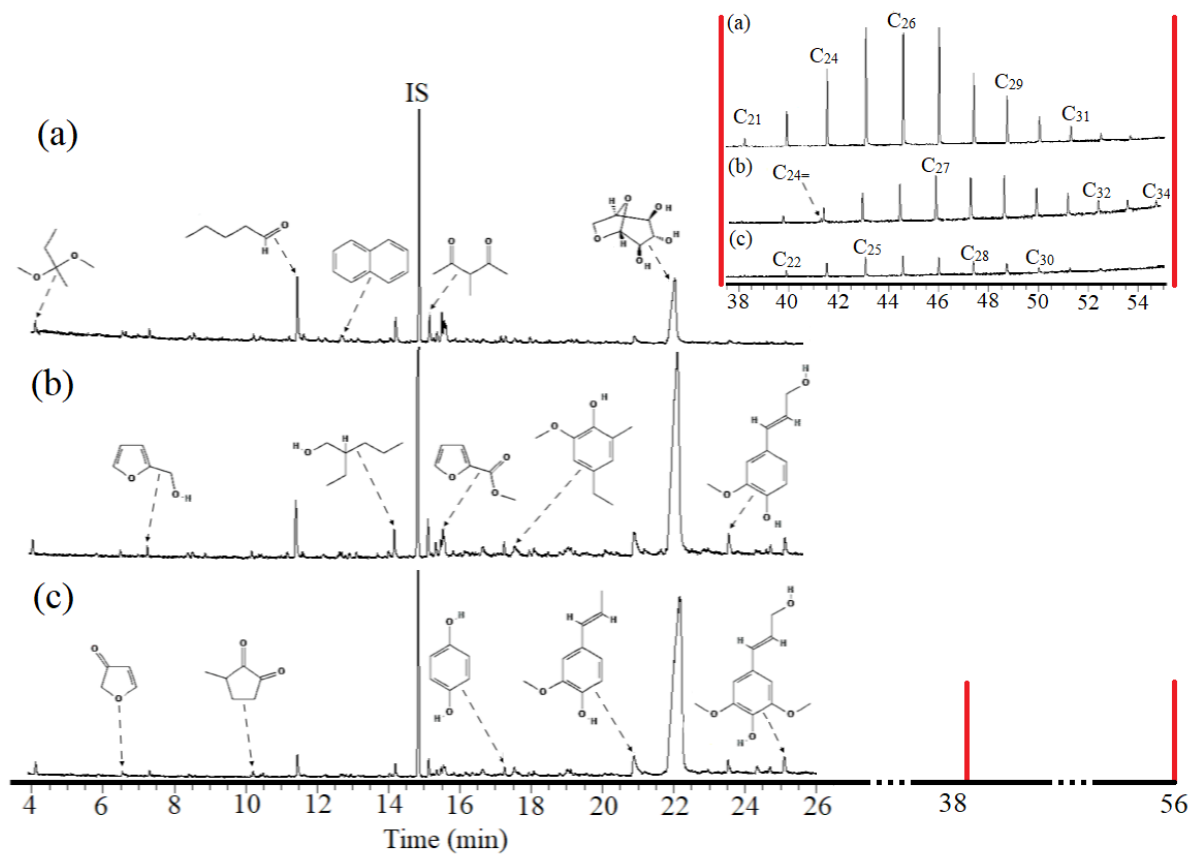


Figure 3.6.  GC-MS Chromatograms of (a) WCCB450, (b) WCCB500, and (c) WCCB550 pyrolysis wax-oil samples collected from the tube reactor. No significant peaks were detected between 26 and 38 minutes.

Table 3.6. Compounds identified in wax corrugated cardboard (WCCB) fresh wax-oil obtained from the tube reactor by GC-MS.

| Compound | Formula | M+ | RT | WCCB450 µg/ml | WCCB500 µg/ml | WCCB550 µg/ml |
|---|---|---|---|---|---|---|
| 2,2-Dimethoxybutane | $C_6H_{14}O_2$ | 118 | 4.1 | 0.61 ± 0.03 | 1.01 ± 0.05 | 0.84 ± 0.04 |
| 3(2H)-Furanone | $C_4H_4O_2$ | 84 | 6.53 | 0.49 ± 0.02 | 0.43 ± 0.02 | 0.33 ± 0.02 |
| 2-Furfuryl alcohol | $C_5H_6O_2$ | 98 | 7.3 | 0.58 ± 0.03 | 0.77 ± 0.04 | 0.41 ± 0.02 |
| 5-Methylfurfural | $C_6H_6O_2$ | 110 | 8.41 | - | 0.49 ± 0.02 | 0.31 ± 0.02 |
| 2-Propenal | $C_3H_6O$ | 58 | 8.92 | 0.39 ± 0.02 | 0.42 ± 0.02 | 0.17 ± 0.01 |
| 1,2-Cyclopentanedione, 3-methyl- | $C_6H_8O_2$ | 112 | 10.21 | 0.4 ± 0.02 | 0.54 ± 0.03 | 0.61 ± 0.03 |
| 1-Acetyloxypropane-2-one | $C_5H_8O_3$ | 116 | 10.42 | 0.24 ± 0.01 | 4.53 ± 0.23 | - |
| Pentanal | $C_5H_{10}O$ | 86 | 11.45 | 5.00 ± 0.25 | - | 1.64 ± 0.08 |
| Naphthalene | $C_{10}H_8$ | 128 | 12.93 | 1.13 ± 0.06 | 0.53 ± 0.03 | 0.22 ± 0.01 |
| Vanillin | $C_8H_8O_3$ | 152 | 13.15 | - | - | 0.21 ± 0.01 |
| Syringol | $C_8H_{10}O_3$ | 154 | 13.73 | - | - | 0.24 ± 0.01 |
| 2-ethyl-1-Pentanol | $C_7H_{16}O$ | 116 | 14.19 | 2.0 ± 0.1 | 2.45 ± 0.12 | 0.93 ± 0.05 |
| 3-Methyl-2,4-pentanedione | $C_6H_{10}O_2$ | 114 | 15.13 | 2.14 ± 0.11 | 3.01 ± 0.15 | 1.27 ± 0.06 |
| 1,4:3,6-Dianhydro-α-d-glucopyranose | $C_6H_8O_4$ | 144 | 15.35 | - | 1.03 ± 0.05 | 0.37 ± 0.02 |
| Catechol | $C_6H_6O_2$ | 110 | 15.48 | 2.12 ± 0.11 | 0.92 ± 0.05 | 0.50 ± 0.02 |
| 5-Hydroxymethylfurfural | $C_6H_6O_3$ | 110 | 15.55 | 1.11 ± 0.06 | 1.56 ± 0.08 | 1.31 ± 0.07 |
| Methyl 2-furoate | $C_6H_6O_3$ | 126 | 15.6 | 1.33 ± 0.07 | 1.33 ± 0.07 | - |
| Alpha-d-xylopyranose | $C_5H_{10}O_5$ | 150 | 16.34 | - | - | 0.33 ± 0.02 |
| Dodecane | $C_{12}H_{26}$ | 170 | 16.64 | - | - | 0.74 ± 0.04 |
| 3-Methylcatechol | $C_7H_8O_2$ | 124 | 17.14 | 0.40 ± 0.02 | - | - |
| 1,4-Benzenediol | $C_6H_6O_2$ | 110 | 17.25 | 0.53 ± 0.03 | 0.95 ± 0.05 | 0.62 ± 0.03 |
| Phenol, 4-ethyl-2-methoxy- | $C_9H_{12}O_2$ | 152 | 17.53 | 0.74 ± 0.04 | 2.73 ± 0.14 | 0.81 ± 0.04 |
| 4-Methylcatechol | $C_7H_8O2$ | 124 | 17.94 | 0.44 ± 0.02 | 0.45 ± 0.02 | 0.22 ± 0.01 |
| 4-vinyl-guaiacol | $C_9H_{10}O_2$ | 150 | 19.01 | 0.17 ± 0.01 | 1.72 ± 0.09 | 0.98 ± 0.05 |
| Vanillin | $C_8H_8O_3$ | 152 | 20.06 | 0.34 ± 0.02 | 0.98 ± 0.05 | 0.26 ± 0.01 |
| Isoeugenol | $C_{10}H_{12}O_2$ | 164 | 20.89 | 1.19 ± 0.06 | 4.89 ± 0.24 | 4.44 ± 0.22 |
| Tetradecane | $C_{14}H_{30}$ | 198 | 21.18 | - | - | 0.43 ± 0.02 |
| Levoglucosan | $C_6H_{10}O_5$ | 162 | 22.17 | 17.86 ± 0.89 | 67.64 ± 3.4 | 71.72 ± 3.59 |
| Coniferyl alcohol | $C_{10}H_{12}O_3$ | 180 | 23.52 | - | 2.65 ± 0.13 | 1.13 ± 0.06 |
| Pentadecane | $C_{15}H_{32}$ | 212 | 24.33 | - | - | 1.02 ± 0.05 |
| L-Glucose | $C_6H_{12}O_6$ | 180 | 24.7 | - | 0.93 ± 0.05 | 0.72 ± 0.04 |
| Sinapyl alcohol | $C_{11}H_{14}O_4$ | 210 | 25.09 | - | 2.19 ± 0.11 | 1.56 ± 0.08 |
| isomer-Eicosane | $C_{20}H_{42}$ | 282 | 36.49 | 0.19 ± 0.01 | - | - |
| Heneicosane | $C_{21}H_{44}$ | 296 | 38.25 | 3.36 ± 0.17 | - | 0.83 ± 0.04 |
| Docosene | $C_{22}H_{44}$ | 308 | 39.91 | 7.73 ± 0.39 | 1.25 ± 0.06 | 0.66 ± 0.03 |
| 1-Tetracosene | $C_{24}H_{48}$ | 336 | 41.44 | - | 0.66 ± 0.03 | 1.34 ± 0.07 |
| Tetracosane | $C_{24}H_{50}$ | 338 | 41.53 | 12.36 ± 0.62 | 2.09 ± 0.1 | 2.21 ± 0.11 |
| Pentacosane | $C_{25}H_{52}$ | 352 | 43.07 | 10.91 ± 0.55 | 3.13 ± 0.16 | 2.10 ± 0.10 |
| Hexacosane | $C_{26}H_{54}$ | 366 | 44.56 | 10.69 ± 0.53 | 4.21 ± 0.21 | 2.23 ± 0.11 |

| | | | | | | |
|---|---|---|---|---|---|---|
| Heptacosane | $C_{27}H_{56}$ | 380 | 46 | $7.37 \pm 0.37$ | $5.08 \pm 0.25$ | $1.57 \pm 0.08$ |
| Octacosane | $C_{28}H_{58}$ | 394 | 47.39 | $5.06 \pm 0.25$ | $5.51 \pm 0.28$ | $1.54 \pm 0.08$ |
| Nonacosane | $C_{29}H_{60}$ | 408 | 48.73 | $2.89 \pm 0.14$ | $5.52 \pm 0.28$ | $0.71 \pm 0.04$ |
| Triacontane | $C_{30}H_{62}$ | 422 | 50.01 | $1.84 \pm 0.09$ | $4.23 \pm 0.21$ | $0.63 \pm 0.03$ |
| Hentriacontane | $C_{31}H_{64}$ | 436 | 51.26 | $0.95 \pm 0.05$ | $3.54 \pm 0.18$ | $0.52 \pm 0.03$ |
| Dotriacontane | $C_{32}H_{66}$ | 450 | 52.46 | $0.49 \pm 0.02$ | $2.04 \pm 0.10$ | $0.24 \pm 0.01$ |
| Tritriacontane | $C_{33}H_{68}$ | 464 | 53.62 | $0.27 \pm 0.01$ | $1.51 \pm 0.08$ | - |
| Tetracosane, 11-decyl- | $C_{34}H_{70}$ | 478 | 54.81 | - | $1.45 \pm 0.07$ | - |
| Pentatriacontane | $C_{35}H_{72}$ | 492 | 55.93 | - | $1.51 \pm 0.08$ | - |

### 3.4.7 WCCB char characterization

The char samples obtained from the auger pyrolysis of WCCB were characterized by proximate and ultimate analyses, calorific value, density, and surface area (Table 3.1). Consistent with previous findings for char characteristics [104], %C (45-51%), FC (27-62%), and calorific values (27-30 MJ kg$^{-1}$) all increased with pyrolysis temperature. The calorific values are slightly higher (30 MJ kg$^{-1}$) than those reported for cardboard by Phan et al. [35] and Ghorbel et al. [74], likely due to the presence of wax. The BET surface areas were low (<1 m$^2$ g$^{-1}$) for all char samples and consistent with values found for other lignocellulosic biomass chars [23]. The density of WCCB and chars were between 1.2 and 1.4 g cm$^{-3}$. The SEM micrographs (Figure 3.7) shows the progressive changes of char fibers with temperatures. The average fiber length was decreased from 650 µm in the original WCCB to 200 µm upon pyrolysis at 550 °C. These char fibers could be used in plastic composite materials to improve their mechanical and in-service performance [106].
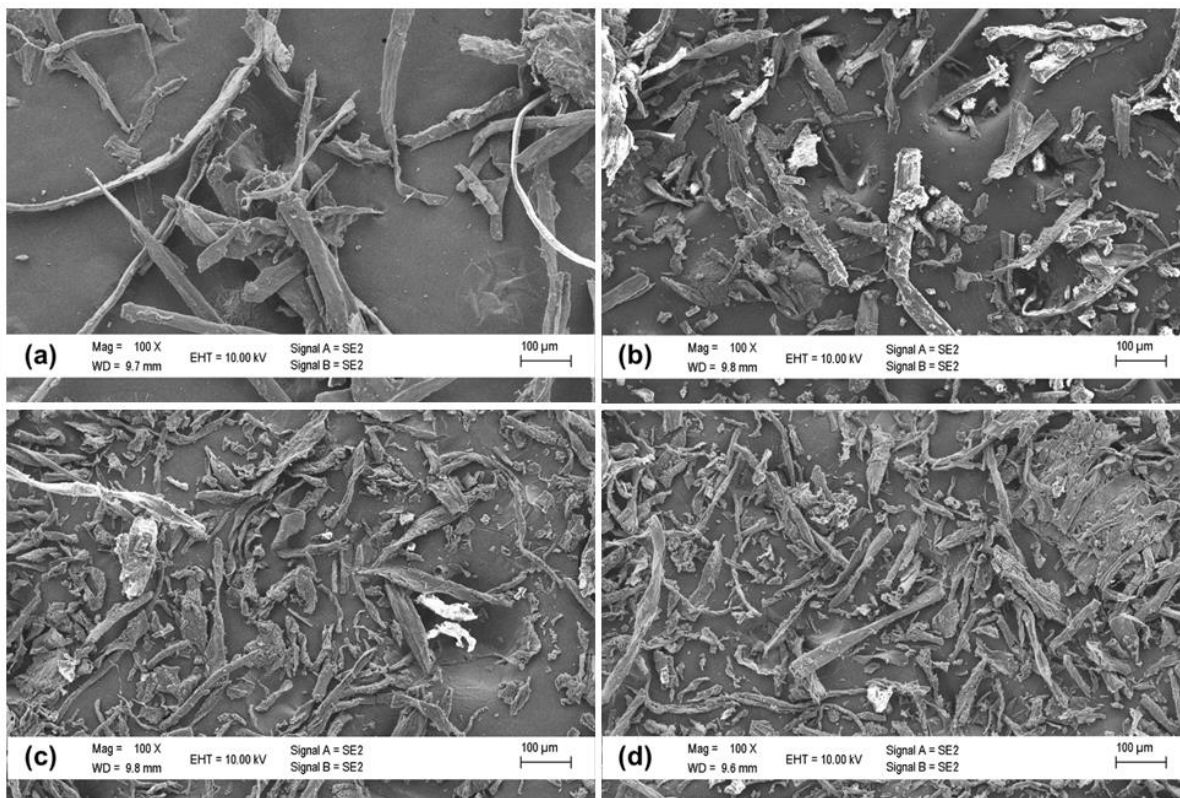
Figure 3.7. Scanning electron micrographs of (a) waxed corrugated cardboard (WCCB), (b) WCCB450 char, (c) WCCB500 char, and (d) WCCB550 char from the auger reactor at 100× magnification.

### 3.4.7.1  FTIR Spectroscopy

FTIR analysis was performed to obtain chemical group information of WCCB, char, and wax-oil samples from the auger reactor (Figure 3.8). Paraffin was also run as a standard for comparison of wax-oil samples (Figure 3.8 e). All spectra were normalized with respect to the band at 2917 cm$^{-1}$. Band assignments for all samples are based on the literature [107], [114] and are given in Table 3.7 [67]. For the WCCB, char, and oil samples, the broad band at 3600-3200 cm$^{-1}$ is attributed to O-H stretching vibrations in alcohol [107]. Expectedly, the O-H band is absent for paraffin (Figure 3.8 a), confirming that the compounds contributing to this band were in the cardboard itself and not the wax coating. The bands between 2930 cm$^{-1}$ and 2850 cm$^{-1}$ in all samples (WCCB, char, and wax-oil) confirm the existence of asymmetric and symmetric C-H stretching for aliphatic functional groups. In the char samples, the bands in this area decrease in intensity with temperatures, suggesting a high degree of wax removal. The bands at about 1600 cm$^{-1}$ and 1507 cm$^{-1}$ were assigned to

aromatic skeletal stretching associated with lignin [112]. This band was absent in the oil spectra, confirming that most of the lignin in WCCB was converted to char. The bands between 650 and 875 cm$^{-1}$ were associated with aromatic C-H stretching vibrations and indicated the presence of lignin in chars; these bands were absent in the oil samples [115]. One observable trend in the spectra of char samples is that with increased temperatures, not only was there a reduction in the relative intensity of the bands associated with the wax coating, but there was also an increase in the relative intensity of the C-H deformation bands. This was an indication of a high degree of decomposition and increased wax extraction. The FTIR spectra of the wax-oil sample (Figure 3.8 f-h) show a high degree of similarity to that of the paraffin sample (Figure 3.8 e).
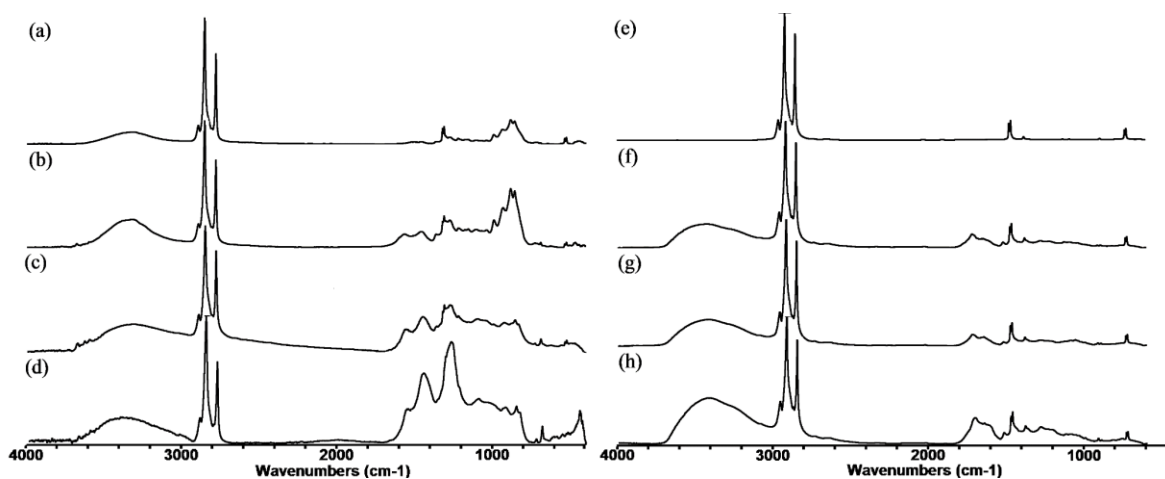
Figure 3.8. FTIR spectra of (a) waxed corrugated cardboard (WCCB), (b) WCCB450 char, (c) WCCB500 char, (d) WCCB550 char, (e) paraffin, (f) WCCB450 wax-oil, (g) WCCB500 wax-oil, and (h) WCCB550 wax-oil samples from the auger reactor.

Table 3.7. FTIR spectra assignments for WCCB and char samples, paraffin (standard), and wax-oil samples from the auger reactor [62]– [65], [77]– [81].

| Band assignment | WCCB | WCCB450 | WCCB500 | WCCB550 | Paraffin | WCCB450 | WCCB500 | WCCB550 |
| --- | --- | --- | --- | --- | --- | --- | --- | --- |
| | | Char | | | | Wax-Oil | | |
| | | | | Wavenumber (cm$^{-1}$) | | | | |
| O–H stretching vibration, H–bonded, (alcohols, phenols) | 3349 | 3349 | 3348 | 3437 | | 3424 | 3403 | 3411 |
| C–H stretch (Alkanes) | 2956 | 2956 | 2956 | 2956 | 2956 | 2955 | 2955 | 2956 |
| C–H (CH$_3$, CH$_2$) stretching vibration | 2917 | 2916 | 2916 | 2917 | 2915 | 2915 | 2915 | 2915 |
| CH$_2$ Symmetric stretch | 2848 | 2848 | 2849 | 2849 | 2850 | 2850 | 2850 | 2850 |
| C=O stretch, α, β– unsaturated esters | | | | | | 1715 | 1715 | 1703 |
| Aromatic skeletal vibration (C=C) in lignin | | 1600 | 1598 | 1594 | | | | |
| Aromatic skeletal vibration (C=C) | 1472 | | | | 1472 | 1472 | 1472 | 1472 |
| C–H deformation | 1462 | 1462 | 1462 | | 1462 | 1462 | 1462 | 1462 |
| Deformation of CH, CH$_3$, and CH$_2$ | | | | 1428 | | | | |
| CH$_3$ Symmetric bending | | | | | | | | 1377 |
| C–O Stretching and O–H bending | 1058 | 1160 | | 1262 | | | | 1278 |
| C–O stretching | | 1033 | 1033 | 1032 | | | | |
| Aliphatic CH$_2$ rocking Aliphatic | | | | | 729 | 729 | 729 | 729 |
| Adjacent aromatic C–H deformation | 719 | | | | 719 | 719 | 719 | 719 |
| –C≡C–H: C–H bend (alkynes) | | | | 647 | | | | |

The relative changes in hydroxyl, carbonyl, and cellulose indices that occurred during pyrolysis were analyzed by calculating HI, CI, and CeI, according to the method outlined by Zinchik et al. [79]. The HI increased for all char samples (from 0.22 to 2.06) and wax-oil samples (from 0.19 to 0.37) with increased temperature (Table 3.8). The CeI decreased from

0.45 to 0.24 in char samples, suggesting the reduction in cellulose content due to dehydration and degradation reactions [40]. Expectedly, due to a lack of cellulose in the wax portion of WCCB, the CeI did not show a significant change in the oil samples. These results support that the reduction in cellulose content was due to dehydration and degradation reactions [148]. The CI showed an upward trend for both char samples and the oil-samples due to oxidation with an increase in pyrolysis temperature.

Table 3.8. Cellulose index (CeI), carbonyl index (CI), and hydroxyl index (HI) of WCCB, chars, and wax-oils obtained from the auger reactor.

| Parameter | WCCB | WCCB 450 | WCCB 500 | WCCB 550 | Paraffin | WCCB 450 | WCCB 500 | WCCB 550 |
|---|---|---|---|---|---|---|---|---|
| | | | Char | | | | Wax-Oil | |
| Carbonyl index (CI) | 0.01 | 0.11 | 0.18 | 0.27 | 0.14 | 0.11 | 0.11 | 0.21 |
| Cellulose index (CeI) | 0.18 | 0.45 | 0.25 | 0.24 | 0.00 | 0.04 | 0.04 | 0.08 |
| Hydroxyl index (HI) | 0.10 | 0.22 | 0.22 | 2.06 | 0.00 | 0.19 | 0.21 | 0.37 |

### 3.4.7.2  X-Ray Diffraction

XRD analysis is used to determine the crystalline component in semi-crystalline biomass, paraffin, and polymeric samples [149]. The XRD diffractograms of WCCB and char samples from the auger reactor are shown in Figure 3.9. The diffractograms of WCCB (Figure 3.9 a) shows a long-range-ordering peak (peaks in the 2θ range of 2-8°) at 4.6° (004) confirming the presence of wax in the WCCB. The diffractogram also shows peaks at about 15.2 and 22.5° assigned respectively to 101, and 200, which are attributed to cellulose. Three peaks associated with wax are apparent at 004 (at 4.6°), 110 (at 21.5°) and 020 (at 23.8°) [150] [151], [152]. The broad peak is attributed to amorphous components from cellulose, hemicellulose, lignin, and wax [153]. With an increase in the pyrolysis temperature, the intensity of cellulose-based peaks at 101 and 200 gradually decreased and eventually disappeared completely at 550 °C due to the removal of crystalline regions (Figure 3.9 b-d). Jiajin et al. [154], in their study of pyrolysis-induced structural changes, reported that cellulose depolymerization started at 300 °C. The intensity of wax-based peaks decreased with an increase in pyrolysis temperature.
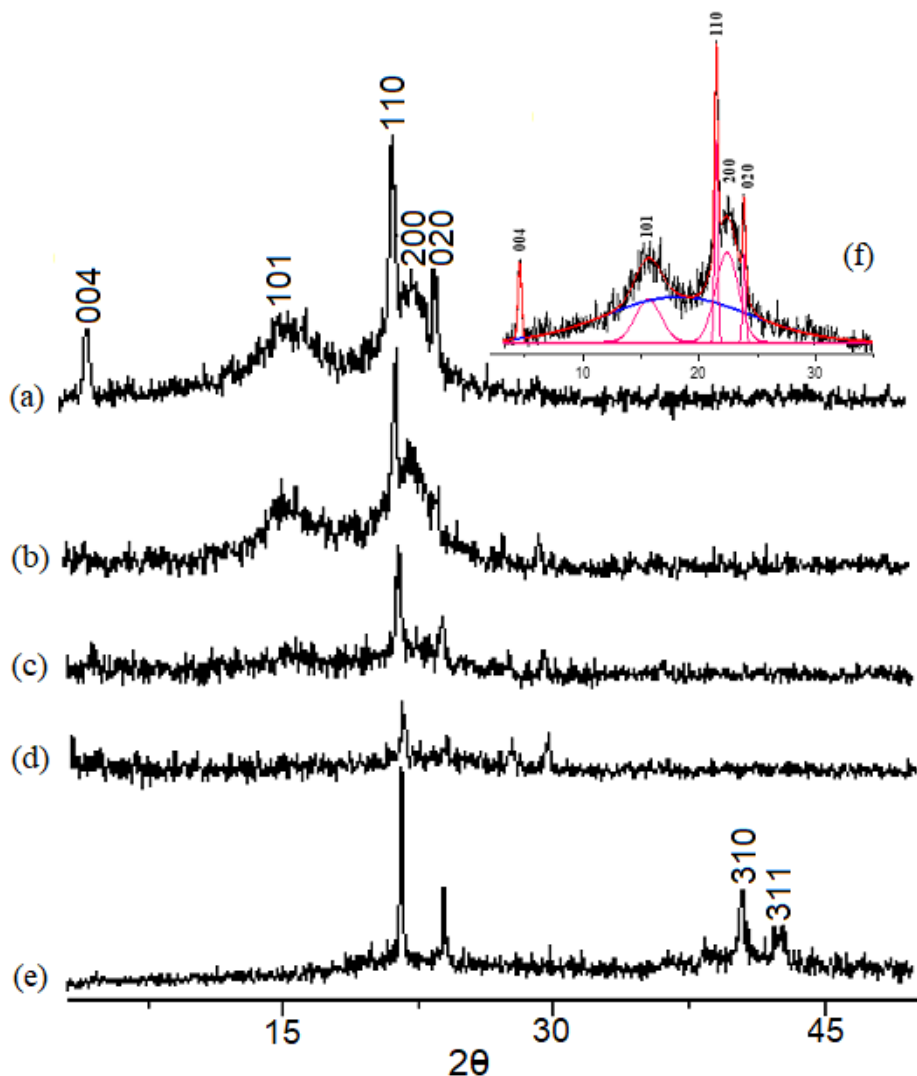
Figure 3.9. X-ray diffractograms of (a) waxed corrugated cardboard (WCCB), (b) WCCB450 char, (c) WCCB500 char, (d) WCCB550 char, and (e) extracted wax, (f) peak fitting for WCCB (right).

The diffractogram of extracted wax (Figure 3.9 e) showed four peaks at $2\theta$s of 21.6, 23.9, 40.4, and 42.7°, which are attributed to the typical diffractions of the 110, 020, 310, and 311, respectively. The presence of 110 and 020 at 21.6 and 23.9° shows the wax exhibiting standard orthorhombic structure [155]. Additionally, two broad peaks were detected at $2\theta \approx$ 18-25° and 35-45°, indicating the presence of amorphous content in the extracted wax. A comparison of diffractograms of WCCB with extracted wax suggests that the disappearance of the 004 peaks in extracted wax could be associated with the solubilizing effect of non-

polar solvent [156]. The absence of peaks at 310 and 311 in WCCB could be attributed to the effect of pyrolysis temperature. The diffractogram of the extracted wax is similar to that of petroleum wax [155]. The CIc and CIw for WCCB and char samples, calculated based on Equation 1, are summarized in Table 3.9.

Table 3.9. CI analysis of WCCB extracted wax from WCCB and chars.

| Crystallinity index | WCCB | WCCB450 Char | WCCB500 | WCCB550 | Ext Wax |
|---|---|---|---|---|---|
| CIc (%) | 33.8 | 28.4 | 12.9 | 0 | 0 |
| CIw (%) | 13.0 | 7.0 | 6.6 | 4.1 | 34.8 |
| Total (%) | 46.8 | 35.4 | 19.5 | 4.1 | 34.8 |

The CIc of WCCB was found to be 33.8%. About 16% of the crystalline fraction of WCCB was disrupted at 500 °C and became completely amorphous at 550 °C, confirming the structural change of cellulose microfibrils upon increasing the temperature [157]. Only about half of crystallinity was solubilized at 550 °C for the wax. The total crystallinity of WCCB, which depends on the proportion of wax and cellulosic material, was found higher than the crystallinity of extracted wax.

## 3.5 Conclusion

In this work, unrecyclable waxed cardboard (WCCB) was pyrolyzed at three temperatures (450, 500, and 550 °C) and the pyrolysis products (wax-oil and char) were obtained successfully. An increase in pyrolysis temperatures resulted in a decrease in char and an increase in wax-oil yields. Pyrolysis is a promising technology for solvent-free wax extraction/recovery. Higher pyrolysis temperatures resulted in increase cracking resulting in a higher proportion of smaller hydrocarbon fragments. The recovered wax can be catalytically upgraded to produce transportation fuels. The recovered char fiber size was temperature-dependent, and these fibers could be used in composite products.

The absence of oxygenated compounds, such as levoglucosan, in the GC-MS results of the wax-oil samples, prompted the authors to design and build a small tubular batch reactor to collect the wax-oil in multiple stages and analyze the oil. The oil collected from the small reactor prior to the condensation of long hydrocarbon chains contained an abundance of oxygenated compounds, most notably levoglucosan.

# Chapter 4. Catalytic upgrading of pyrolysis wax-oil obtained from waxed corrugated cardboard using zeolite Y catalyst

"Catalytic upgrading of pyrolysis wax-oil obtained from waxed corrugated cardboard using zeolite Y catalyst." Submitted to the Journal *Energy and Fuels*

## 4.1    Abstract

About 5% of all corrugated cardboard is coated with wax to enhance performance under humid conditions. Waxed cardboard is unrecyclable. The authors have previously shown that the wax can be effectively recovered using pyrolysis. The main compounds found in wax-oil obtained from pyrolysis of waxed cardboard were alkanes, alkenes, and dienes ($C_9$ to $C_{36}$). In this work, recovered wax and wax-oil samples were thermally and catalytically pyrolyzed on a custom-made small tubular batch reactor, and the resultant liquid products were analyzed (GCMS, FTIR, ESI-MS) against gasoline to evaluate their performance as a transport fuel. The products of thermal pyrolysis of the samples are mainly comprised of dienes and short-chain olefins, oxygenated compounds, and minor amounts of aromatic compounds. Their functional groups resembled those found in paraffin. The analyses revealed that the liquid products of catalytic pyrolysis had chemical and functional group profiles similar to those of gasoline (e.g., methyl benzenes). The addition of zeolite Y as the catalyst facilitated the conversion of long-chain hydrocarbons to short-chain alkanes and aromatics. The monomer to oligomer ratio of the liquid products also increased significantly after catalytic pyrolysis.

## 4.2    Introduction

An increase in urban population is expected to result in a two-fold increase in the generation of municipal solid waste (MSW) to an astonishing 30 million tons per year by 2033 [57]. The Environmental Protection Agency has reported that paper products and corrugated cardboard comprise a significant 25% of the generated MSW [4], of which 5% is coated with wax (waxed corrugated cardboard) to enhance their performance under humid/wet conditions for produce packaging [5]. Severe environmental, health, and economic consequences can arise from the mismanagement of  MSW [2]. The management becomes crucially important when it comes to unrecyclable materials that are not readily biodegradable such as waxed cardboard. The addition of coated cardboard such as Tetrapak[TM] and waxed cardboard to

landfills is particularly troublesome because of the plastic nature of their coatings [5]. This issue necessitates the development of alternative solutions for recovering value from coated cardboard and eliminating the environmental risks.

In their earlier work [158], the authors have successfully obtained wax-oil via pyrolysis of waxed cardboard at three temperatures of 450, 500, and 550 °C. The process was found to be effective for solvent-free wax recovery from the cardboard. The pyrolysis wax-oil products contained mainly alkanes, alkenes, and dienes ($C_9$ to $C_{36}$), and chain length decreased with pyrolysis temperature. The results suggested that this wax fraction could be recovered and used as bunker fuel ($C_{12}$-$C_{40}$) or further converted to diesel ($C_{10}$-$C_{20}$) via catalytic (hydrocracking) upgrading [158].

Pyrolysis is among the energy recovery technologies that have been extensively used for plastic waste [125], [127][37] [41]–[46]. There are concerns about the economic and energy consumption feasibility of the pyrolysis process. Moreover, quite often, the pyrolysis process produces liquid oil that contains large carbon chain compounds [47]. The oil is also of lower quality because of its low octane number and presence of solid residues [48], [159] and impurities such as sulfur, nitrogen, chlorine, and phosphorous [49]. To overcome these issues, catalytic pyrolysis of plastics has become a topic of interest in the past decade [50]. Various catalysts have been utilized, such as red mud (bauxite residue) and ZSM-5 [50], fluid catalytic cracking (FCC) [51], HZSM-5 [52], zeolite Y [53], $Fe_2O_3$ [54], and natural zeolite [55], to improve the quality of the obtained oil in catalytic pyrolysis. The reported findings in the literature [50]–[55], along with the authors' earlier confirmation of the plastic-like nature of wax-oil suggest that a catalytic pyrolysis is a viable option for upgrading the wax-oil samples to liquid fuel.

In catalytic pyrolysis processes, the primary function of the catalysts is to increase the proportion of lighter hydrocarbons in the oil through cracking reactions [56] and improve the overall process energy efficiency [50] (i.e., achieving higher quality products at lower temperatures). The first step in catalytic pyrolysis is the thermal cracking on the external surface of the catalyst. The porous structure inside the catalyst works as channels for selective movement and breakdown of large hydrocarbon chains into smaller chains [51]. Generally, the degradation of heavier alkenes occurs in the outer surface of the catalyst, and

further degradation and product selectivity take place in the internal pores of the catalyst [57]. The catalyst can be mixed with feedstock in the reactor or with organic vapors produced in a separate catalyst chamber. Lopez et al. [50] and Chen et al. [43] have reported that a liquid phase or direct contact with feedstock improves the cracking process by reducing the reaction temperature and retention time. However, in the case of direct contact, it is difficult to recover the catalyst due to the sticky nature of plastic feedstock [55]. Various catalysts such as zeolite Y and ZSM-5 [50] were used with vapor phase contact with promising results.

The three main types of catalysts used in catalytic pyrolysis include FCC, silica-alumina catalysts, and zeolites [57]. FCC catalysts are mainly used in the petroleum refineries for cracking of heavy oil into gasoline and liquid oil petroleum and have been successfully used in the pyrolysis process [57]. Silica-alumina catalysts are amorphous catalysts that have Lewis acid sites as electron acceptors and Brønsted acid sites with ionizable hydrogen atoms [57]. Zeolite catalysts are crystalline alumino-silicates sieves that have a 3D framework consisting of cavities and channels. The main characteristic of these catalysts is their ion-exchange capabilities and open pores. Different ratios of $SiO_2/Al_2O_3$ in zeolites determine their reactivity and affect the final products of the pyrolysis process[53], [160]. Zeolite catalysts generally increase volatile hydrocarbon production and have a low rate of deactivation. The introduction of zeolite materials in FCC catalyst formulations (e.g., zeolite Y) resulted in a drastic increase in the gasoline yield in the 1970s and 1980s [60].

Miandad et al. have reported that natural and synthetic zeolite catalysts can be used for catalytic pyrolysis of four major types of plastic wastes such as polyethylene, polystyrene, polypropylene and poly(ethylene-terephthalate) [37]. Their resultant liquid oils had high higher heating value (HHV) (40.2–45 MJ/kg), which is similar to conventional diesel [62]. Syamsiro et al. have used zeolite Y and natural zeolite catalysts for sequential pyrolysis and catalytic reforming of municipal plastic wastes and produced high-quality liquid products and higher heating value solid products than those of biomass and low-rank coal [55]. Lee used multiple zeolite catalysts, including zeolite Y, for the upgrading of pyrolysis wax oil (obtained from municipal plastic waste) in a continuous plug flow reactor at 450 °C [53]. Furthermore, he also reported that the catalyst pore dimensions played a vital role in the

conversion of wax into light hydrocarbon, and catalysts with more than one dimension, such as zeolite Y, showed high conversion of wax into light hydrocarbon.

While the literature is rich on catalytic pyrolysis of various types of plastic waste, there is a gap for waxed cardboard that we aim to address with this work. Zeolite Y was chosen for the catalytic pyrolysis process due to its suitability and the main cracking component of FCC. Since zeolite Y contains an internal porous structure this can convert longer-chain hydrocarbons to smaller molecules through the formation of carbonium ions via proton transfers in the hydrocarbon's Brønsted and Lewis acid sites [160], [161]. Furthermore, since the pores of zeolite Y are small (7.3 Å), the larger molecules in the wax-oil will need to be thermally cracked first before passing through the pores. In this study, chemically extracted wax and pyrolysis wax-oil products of waxed cardboard were subjected to thermal and catalytic pyrolysis in a tube reactor, and the products were analyzed, characterized and the results discussed.

## 4.3 Materials and methods

### 4.3.1 Materials

Milled waxed cardboard (4.0 g) was Soxhlet extracted in duplicate using $CH_2Cl_2$ (150 mL) for 16 h, and wax was collected using a rotary evaporator. The wax-oil samples were the products of waxed cardboard pyrolysis at three different temperatures of 450, 500, and 550 °C in an auger reactor. The details of the pyrolysis and solvent extraction process are outlined in the authors' previous work [158]. The wax-oil samples were named WO450, WO500, and WO550 according to their original pyrolysis temperature (450, 500, and 550 °C). Regular gasoline (Conoco gas station in Moscow, ID) and Paraffin (J. T. Baker Chemicals) were used as reference standards. Zeolite Y (hydrogen form, powder, $SiO_2/Al_2O_3 = 30$, (Alfa Aesar) was used as received.

### 4.3.2 Differential Scanning Calorimetry (DSC)

DSC analysis of the wax-oil samples, paraffin wax, and extracted wax were conducted in duplicates using a Perkin Elmer DSC-7 instrument (Shelton, CT, USA). Approximately 6 mg of sample was scanned from 25 °C to 100 °C at a heating rate of 10 °C min⁻¹, under nitrogen (20 ml min⁻¹), and data were analyzed using the Pyris v.13.3.1 software. Percent crystallinity of the wax was determined using the equation below:

Equation 2

$$X_c = \frac{\Delta H_m}{\Delta H_0} \; x \; 100\%$$

$X_c$ is the percent crystallinity of the wax, $\Delta H_m$ is the melting enthalpy or enthalpy of fusion calculated from the area under the peak, and $\Delta H_0$ is the theoretical enthalpy of fusion for paraffin wax (210 J g⁻¹).

### 4.3.3 Thermogravimetric Analysis (TGA)

TGA was performed on a Perkin–Elmer TGA-7 instrument (Shelton, CT, USA) to determine the thermal stability and effect of the catalyst on the thermal breakdown of wax-oil samples. Experiments with catalysts were a (9:1) mixed blend of wax and zeolite Y catalyst. Approximately 5 mg of sample was heated from 30 °C to 900 °C at 10 °C min⁻¹ under nitrogen (30 mL min⁻¹). Data were analyzed using the Pyris v13.3 software.

### 4.3.4 Pyrolysis and Catalytic Pyrolysis

Pyrolysis and catalytic pyrolysis experiments were performed on a small quartz tube (20 mm ID x 300 mm) reactor with an $N_2$ purge (60 ml min⁻¹) using a mass flow controller (Dakota Instruments) (Figure 4.1). During pyrolysis, extracted wax and wax-oil (0.50 g each) was placed inside a glass tube (14 mm OD x 125 mm) and secured by glass wool on both sides. For catalytic pyrolysis experiments, the sample was sandwiched between glass wool and zeolite Y plus sand mixture (1:1 ratio) on both sides (1 g each side) and the end secured with glass wool (Figure 4.1). The tube was then inserted inside the heated zone (150 mm). A single-stage cooling U-tube submerged in liquid nitrogen was used to condense the vapors. An impinger that contained 10 ml of dichloromethane was used at the very end to trap the lighter hydrocarbons that had escaped the U-tube. The yields of the trapped products and solid residue were determined gravimetrically. A second series of experiments were

performed using the extracted wax and wax samples with recovered zeolite Y catalyst (heated to 600°C for 1 h) to establish the potential for using recovered catalyst.
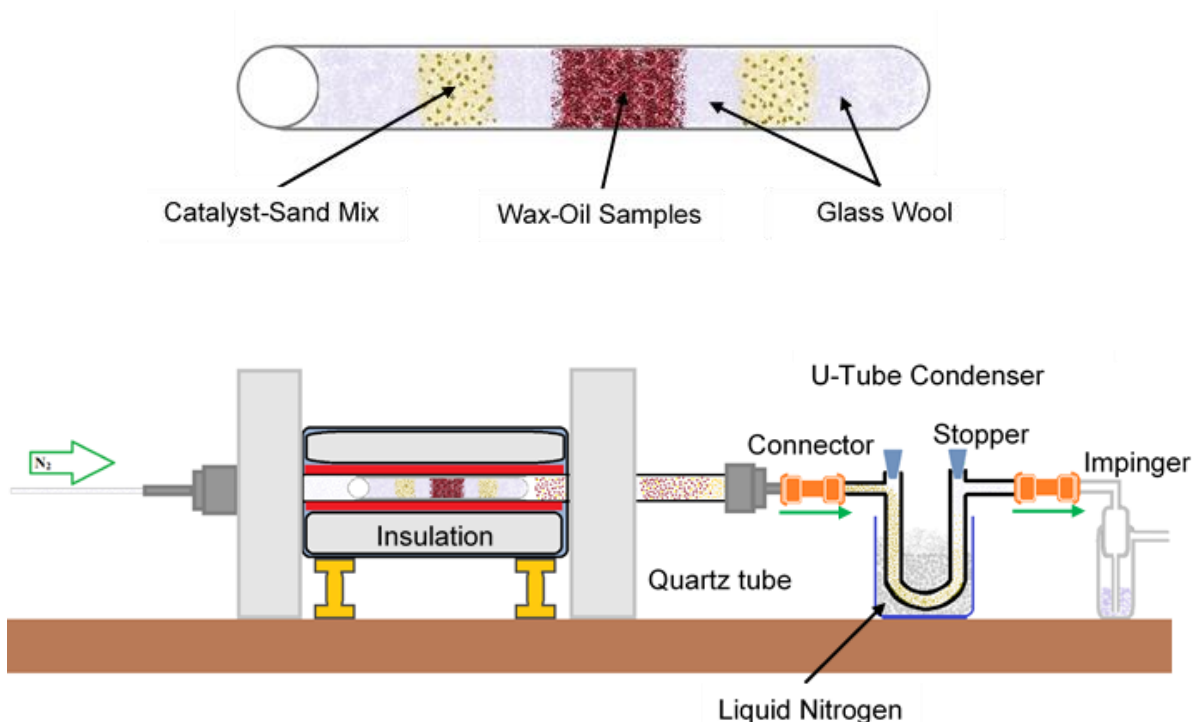


Figure 4.1. Figure showing the carrier tube and tube furnace reactor and traps set up.

### 4.3.5 Gas Chromatography-Mass Spectrometry (GC-MS)

The pyrolysis and catalytic pyrolysis products (1 mg in $CH_2Cl_2$ (1 mL) containing 1,2,4-trichlorobenzene as an internal standard) were analyzed in duplicate by GC-MS (Trace 1300-ISQ, ThermoScientific). The compounds were separated using a ZB-5 capillary column (30 m × 0.25 mm Ø, Phenomenex) using a temperature program of 40 °C (1 min) to 320 °C (10 min) at 5 °C min$^{-1}$.

#### 4.3.5.1 Fourier Transform InfraRed Spectroscopy (FTIR)

FTIR spectra were obtained, in quadruplicate, for gasoline, paraffin, and resultant pyrolysis and catalytic pyrolysis products using a Thermo-Nicolet iS5 spectrometer equipped with a ZnSe attenuated total reflection (iD5 ATR) accessory. FTIR spectra were baseline corrected and averaged using the Omnic v9 software (Thermo-Nicolet).

### 4.3.6 Electrospray Ionization Mass Spectrometry (ESI-MS)

The molar mass of products of pyrolysis and catalytic pyrolysis were determined using a Finnigan LCQ-Deca instrument (ThermoQuest). The resultant samples (1 mg mL$^{-1}$) were

dissolved in dichloromethane (50%), methanol (49%), and acetic (1%) acid solution and subjected to negative ion ESI–MS ($m/z$ 100–2,000) at a flow rate of 20 μL min$^{-1}$. The ion source and capillary voltages were 4.5 kV and 50 V at 275°C, respectively. The number average molar mass ($M_n$) was calculated as $M_n = \sum N_i M_i / \sum N_i$ and the weight average molar mass ($M_w$) as $M_w = \sum N_i M_i^2 / \sum N_i M_i$ where, $N_i$ is the intensity of ions, and $M_i$ is the mass after accounting for the charge.

## 4.4    Results and discussion

### 4.4.1    Differential Scanning Calorimetry

DSC was performed to determine the melt characteristics of the wax samples [162]. DSC thermograms of the paraffin reference, extracted wax, wax-oil samples obtained at different pyrolysis temperatures are shown in Figure 4.2 . The peak temperatures and crystallinity values for the samples are given in Table 4.1. Two endothermic melting peaks, a major and minor peak, are observed for all thermograms with clearly segregated peaks for paraffin and broader merging peaks for the wax-oil samples. The two peaks observed for each sample can be attributed to the molecular fractions of the waxes with distinct molar masses melting at different temperatures [163]. Paraffin is a petroleum product that mostly contains long-chain hydrocarbons that melt completely at higher temperatures [164]. Compared to the melting range for the paraffin reference (35-60 °C), those of the extracted wax and wax-oil samples were lower (32-55 °C). The average minor and major melting peak temperatures for paraffin were 46 °C and 61 °C, respectively. Gonen et al. observed comparable melting peak temperatures, 39 °C (minor) and 57 °C (major), in their study of the effect of zinc stearate on paraffin wax thermal degradation [164]. The minor and major peaks also depict the solid-solid phase and solid-liquid phase transition for the wax-oil samples, respectively [162], [165]. An increase in the pyrolysis temperature from 450 °C to 500 °C resulted in a slight increase in wax-oil major melting peak temperature from 51.3°C to 52.2 °C. The melting peak temperature decreased to 47.7 °C for WO550 yielding  shorter-chain hydrocarbons, which have a lower melting point [158]. Shorter-chain hydrocarbons exhibit a higher melting enthalpy and lower melting temperature [166], [167]. This is consistent with studies that show the melting point of waxes decreases with a decreased number of carbon atoms [168].
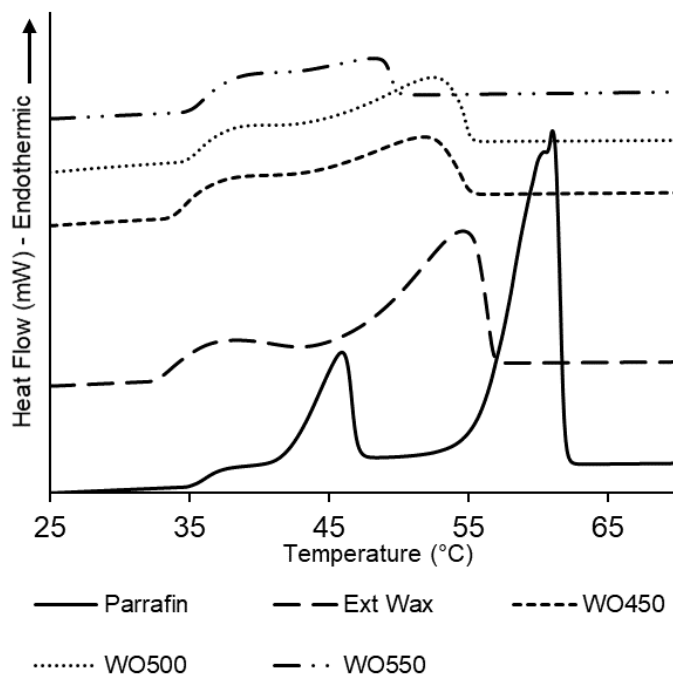
Figure 4.2. DSC thermograms showing the melt transitions of paraffin reference, solvent extracted wax, and WO450, WO500, and WO550.

Table 4.1. Average DSC melting peaks and percent crystallization of paraffin, extracted wax, and wax-oil samples obtained previously from pyrolysis of waxed cardboard at 450, 500, and 550 °C.

| Samples | Major Peak- $T_m$ (°C) | $\Delta H_m$ (J/g) | $X_c$ (%) |
|---|---|---|---|
| Paraffin reference | $61.0 \pm 0.09$ | $235.3 \pm 0.78$ | $74 \pm 0.19$ |
| Solvent Extracted Wax | $54.7 \pm 0.04$ | $191.3 \pm 3.01$ | $57 \pm 1.90$ |
| WO450 | $51.3 \pm 0.47$ | $102.3 \pm 7.10$ | $49 \pm 3.38$ |
| WO500 | $52.2 \pm 0.25$ | $113.2 \pm 2.47$ | $54 \pm 1.18$ |
| WO550 | $47.7 \pm 1.17$ | $123.4 \pm 11.36$ | $59 \pm 5.41$ |

The crystallinity of paraffin reference was 74%, while that of the solvent extracted wax was 57%. Similar crystallinity of paraffin wax was recorded by Stranding et al. at 80% [162]. Crystallinity values for wax in the wax-oil mixtures increased from 49% to 59% with an increase in pyrolysis temperature due to the increased presence of crystals in shorter-chain hydrocarbons. Since enthalpy is proportional to crystallinity, higher enthalpy of fusion values is relative to the increased heat needed to break more crystalline structures in the mixture [169]. Al Maadeed et al. also recorded a reduction in crystallinity of polyolefin blends HDPE and LLDPE due to the increased wax addition in their study. This conforms to the high wax yield and low crystallinity seen in previous studies and in the DSC results [158], [169]. The presence of shorter chain hydrocarbons obtained at higher pyrolysis temperatures suggested that the wax-oil samples might be viable options for producing cleaner fuels [170], [171].

### 4.4.2   Thermogravimetric Analysis

Thermal degradation of the wax-oil samples without and with 10% catalyst was determined by TGA (Figure 4.3 a). Differential thermogravimetric (DTG) curves are shown in Figure 4.3 b. The thermal decomposition onset, major peak, and final decomposition temperatures are given in Table 4.2. Thermal degradation behavior determined by TGA of wax-oil samples WO450, WO500, and WO550 and with zeolite Y catalyst.

Table 4.2. Thermal degradation behavior determined by TGA of wax-oil samples WO450, WO500, and WO550 and with zeolite Y catalyst.

| Samples | Onset (°C) | Major Peak (°C) | Final decomposition (°C) |
|---|---|---|---|
| WO450 | 243 | 331 | 354 |
| WO450 + 10% catalyst | 80 | 307 | 372 |
| WO500 | 75 | 340 | 364 |
| WO500 + 10% catalyst | 70 | 315 | 367 |
| WO550 | 98 | 336 | 370 |
| WO550 + 10% catalyst | 63 | 305 | 384 |
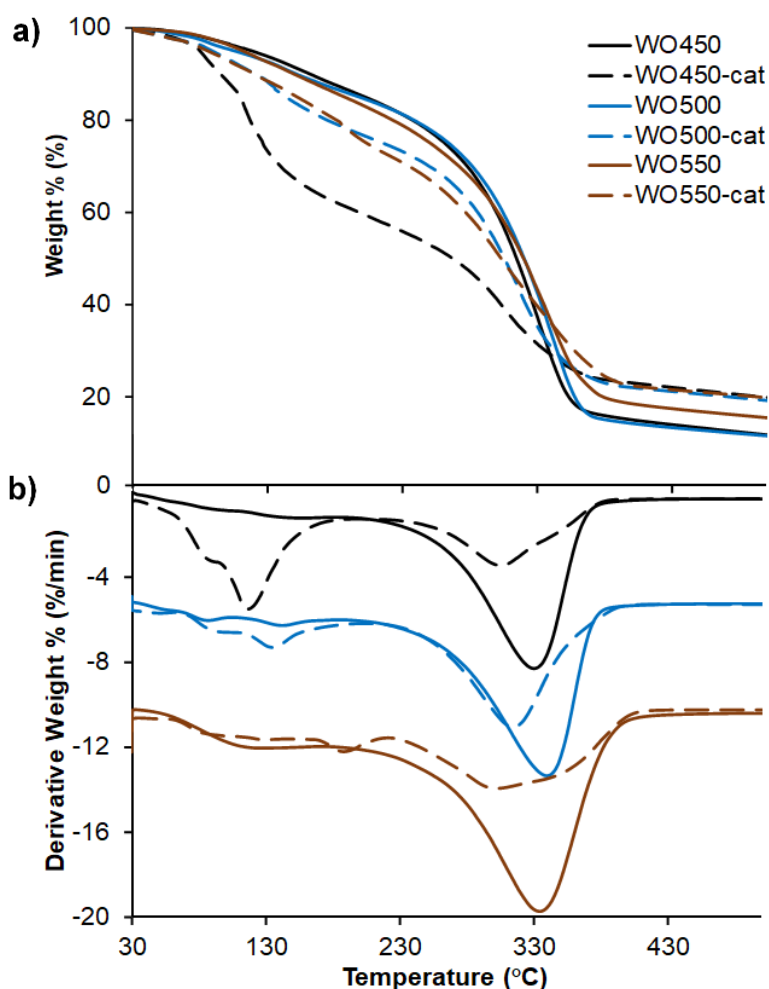
Figure 4.3. a) Thermogravimetric analysis (TGA) and b) differential thermogravimetric (DTG) thermograms for wax-oil samples (WO450, WO500, and WO550) and with the addition of 10% zeolite Y catalyst.

Onset temperatures for catalyzed wax-oils blends occurred at lower temperatures compared to wax-oil alone and likely resulting from catalytic breakdown [172]. Small peak shoulders observed <100 °C in the wax oil samples are likely due to water evaporation. The final weight loss temperatures for WO450, WO500, and WO550 were 354 °C, 364 °C, and 370 °C, respectively. The presence of the catalyst in wax-oil samples caused an increase in the final decomposition temperatures showing the thermal stability of the waxes present. An approximate 15% solid residue was observed for the catalyzed samples associated with the weight of the catalyst.

At low temperatures, the DTG thermograms of non-catalyzed samples display narrow peaks. The broad decomposition peaks of the catalyzed wax-oil samples indicated the effective

breakdown of lower molecular weight alkanes [173]. Catalytic pyrolysis of WO450 exhibited optimum yield potential for small chain hydrocarbons.

Major degradation peaks ranged from 330 °C to 340 °C in uncatalyzed reactions and 305 °C to 315 °C in catalyzed reactions [174]. Major DTG peaks decreased in size in the presence of catalysts due to the increased degradation of low molecular weight alkanes at lower temperatures. Studies show that the presence of highly acidic zeolite catalysts increases the rate of polymeric breakdown into more gaseous fractions and shorter hydrocarbons [175], [176]. Zeolites have an increased acidity and a high affinity for water and carbon formation [177]. Their crystalline structure promotes hydrogen transfer reactions causing high conversions in thermal conversion processes [178], [179]. TGA is a useful tool for establishing suitable operating temperatures for a catalytic pyrolysis process.

### 4.4.3  Pyrolysis process and product yield

Solvent extracted wax and wax-oil samples previously obtained from pyrolysis were subjected to thermal and catalytic pyrolysis to obtain lower molar mass products. The liquid products were collected in the U-tube condenser and the impinger that had been designed to trap volatile compounds. The product yields are shown in Figure 4.4. In the thermal pyrolysis process, the WO550 sample achieved the maximum total liquid product yield at 38%, and the extracted wax sample exhibited the highest impinger yield at 2.6%. In the catalytic pyrolysis process, WO550 once again achieved the maximum total liquid product yield at 60%. Significantly more liquid product (on average 3-fold more) was collected from the impinger in the catalytic pyrolysis process compared to the thermal pyrolysis process. Specifically, the catalytically pyrolyzed solvent extracted wax sample resulted in an 11% impinger yield, more than four times that of the thermally-pyrolyzed extracted wax. This suggests a significant increase in the production of lighter hydrocarbons during the catalytic pyrolysis process. In general, more total liquid products were obtained from the catalytic pyrolysis process (on average 70%). These results are consistent with what has been reported in the literature for catalytic pyrolysis products of plastic waste: Miandad et al. [62] reported a maximum liquid product yield of 54% for catalytic pyrolysis of polystyrene using natural zeolites, and Syamsiro et al. [55] reported a 52% liquid product yield for catalytic pyrolysis

of municipal solid plastic waste using zeolite Y. The addition of the impinger collection stage may have contributed to the slightly higher yield values in this work.

To establish if the catalyst could be reused, all wax-oil samples (WO450, WO500 and WO550) were catalytically pyrolyzed with recovered catalyst (used 5 times) and no significant difference was found between the product yields of the samples compared to new zeolite Y. All yield values were within the values reported ± 5% in Figure 4.4.
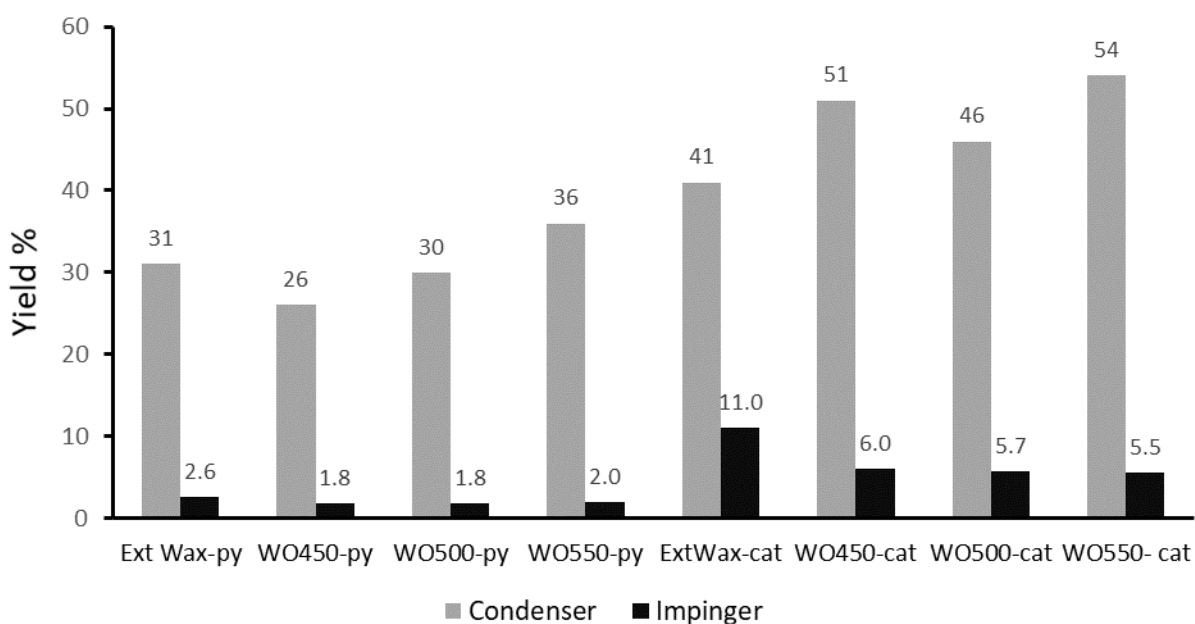


Figure 4.4. Product yields of thermal pyrolysis (py) and catalytic pyrolysis (cat) of solvent extracted wax and pyrolysis wax-oil samples (WO450, WO500, and WO550).

### 4.4.4   Gas Chromatography Mass Spectrometry

The liquid products of thermal and catalytic pyrolysis of the extracted wax and wax-oil samples were analyzed by GC-MS. The authors have reported in their earlier work that the wax-oil samples were mixtures of long-chain alkanes, alkenes, and dienes, as well as oxygenated compounds such as levoglucosan [158]. The thermal pyrolysis process resulted in a mixture of alkanes and olefins with varying chain length ($C_6$-$C_{39}$) and a small proportion of aromatic hydrocarbons (0.0-5.4%) (Figure 4.5 and Figure 4.6; Table 4.3 and Table 4.4). A considerable number of oxygenated compounds were still present (2.9-13.9%). The most

abundant compounds collected from the condenser were long-chain alkanes and alkenes ($C_{22}$-$C_{28}$), which suggest that in the absence of the catalyst, the conversion was incomplete. The most abundant impinger-collected compounds were short-chain alkenes ($C_7$-$C_{10}$). While the thermal pyrolysis partially cracked the compounds in the extracted wax and wax-oil samples and decreased the average chain length of the compounds [158], the presence of oxygenated compounds and absence of aromatics were discouraging factors as both significantly reduce the quality of the liquid product.

The catalytic pyrolysis products of extracted wax and wax-oil samples had a chemical composition profile that resembled that of gasoline closely [180] (Figure 4.7 and Figure 4.8; Table 4.5 and Table 4.6). The samples contained a mixture of short-chain alkanes and aromatics ($C_6$-$C_{15}$). Compounds most abundantly found in gasoline (e.g., pentanes and hexanes, xylene, and toluene) were also found in significant amounts in all samples. Overall, the percentages of alkanes, olefins, and aromatics were very close to those found for the characterized gasoline samples, with WO450 and WO500 products having percentage values within 1% of gasoline (Table 4.7). As expected, the impinger-collected products having shorter carbon chain lengths than those collected from the U-tube condenser. The most abundant compound was 2-methyl hexane that was also abundantly found in gasoline. Methyl benzenes such as toluene and xylene were also present. A significant improvement over the thermal pyrolysis products was the absence of oxygenated compounds and the presence of aromatic compounds. The aromatic compound profile of the products of catalytic pyrolysis in this work was similar to those reported by Bagri et al. [181] for liquid products obtained from catalytic pyrolysis of polyethylene using zeolite Y. The addition of zeolite Y in the catalytic pyrolysis process has been shown to increase the aromatic compounds. Zeolite Y's 3D structure plays a vital role in the conversion of wax into light hydrocarbons [53]. The zeolite Y used in the catalytic pyrolysis process facilitated the conversion of long-chain hydrocarbons to lighter hydrocarbons and aromatics, much like those found in gasoline.
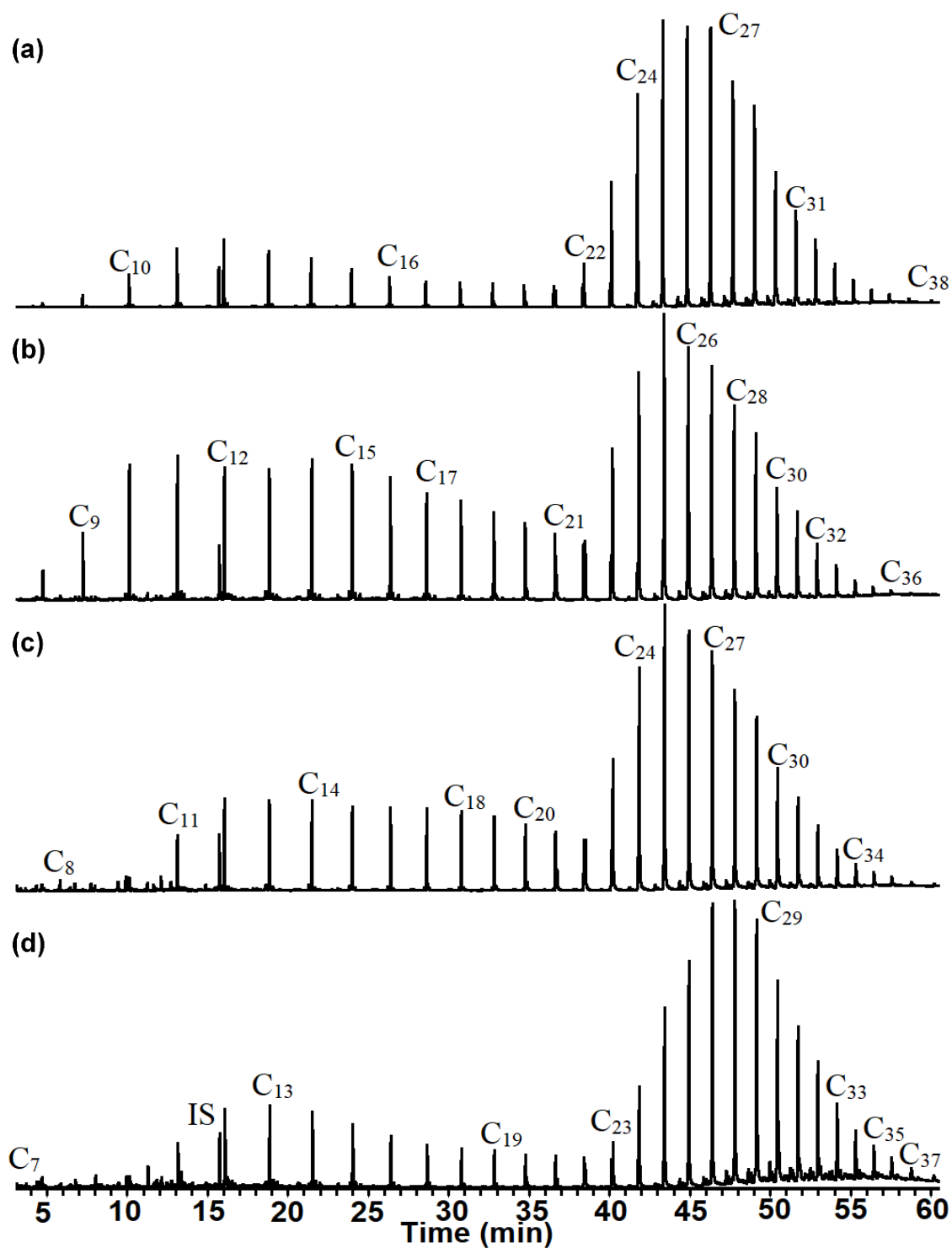
Figure 4.5. GC-MS Chromatograms of thermal pyrolysis products of (a) solvent extracted wax-py, (b) WO450-py, (c) WO500-py, and (d) WO550-py collected from the U-tube.

Table 4.3. Identified compounds in the liquid products of thermal pyrolysis of solvent extracted wax and wax-oil samples collected from the U-tube.

| Compound Name | M+ | Formula | RT min | ExtWax mg/g | WO450 mg/g | WO500 mg/g | WO550 mg/g |
|---|---|---|---|---|---|---|---|
| 1-Methylpentyl cyclopropane | 126 | $C_9H_{18}$ | 3.06 | 0.12 | - | - | - |
| Propanoic acid | 74 | $C_3H_6O_2$ | 3.14 | - | 0.47 | 0.57 | 2.32 |
| Acetic acid, hydroxy-, methyl ester | 90 | $C_3H_6O_3$ | 3.25 | - | 0.07 | 0.34 | - |
| Acetoin | 88 | $C_4H_8O_2$ | 3.41 | - | 0.17 | 0.19 | 0.46 |
| 1-Propanol | 60 | $C_3H_8O$ | 3.72 | - | 0.44 | 0.42 | 0.51 |
| Propanoic acid, 2-methyl- | 88 | $C_4H_8O_2$ | 4.1 | - | - | - | 0.23 |
| 2,2-Dimethoxybutane | 118 | $C_6H_{14}O_2$ | 4.2 | 0.20 | 0.26 | 0.64 | 0.53 |
| Cyclobutene, 2-propenylidene- | 92 | $C_7H_8$ | 4.35 | - | 0.70 | 0.41 | 1.03 |
| Toluene | 92 | $C_7H_8$ | 4.41 | - | 0.89 | 1.10 | 0.36 |
| Cyclopentanol | 86 | $C_5H_{10}O$ | 4.69 | - | 1.96 | 2.76 | 3.04 |
| Cyclopropane, pentyl- | 112 | $C_8H_{16}$ | 4.8 | 1.45 | - | - | - |
| 1-Methyl-2-methylenecyclohexane | 110 | $C_8H_{14}$ | 4.86 | - | 0.33 | - | 1.00 |
| 3,3-Dimethylcyclohexanol | 128 | $C_8H_{16}O$ | 5.06 | - | 0.34 | - | - |
| Cyclopropane, pentyl- | 112 | $C_8H_{16}$ | 5.58 | - | 0.50 | 0.18 | 0.65 |
| 1,4-Cyclohexanediol, trans- | 116 | $C_6H_{12}O_2$ | 5.89 | - | 0.48 | 0.43 | 2.26 |
| 1,2-Ethanediol, monoacetate | 104 | $C_4H_8O_3$ | 6.29 | - | 0.24 | - | - |
| 3-Furanmethanol | 98 | $C_5H_6O_2$ | 6.42 | - | 0.33 | 0.19 | 0.35 |
| 2-Butanone | 72 | $C_4H_8O$ | 6.49 | - | 0.52 | 0.55 | 0.78 |
| 2-Propanone, 1-(acetyloxy)- | 116 | $C_5H_8O_3$ | 6.77 | - | 1.11 | 0.07 | 1.63 |
| p-Xylene | 106 | $C_8H_{10}$ | 6.81 | - | 0.28 | 0.14 | - |
| 1-Nonene | 126 | $C_9H_{18}$ | 7.29 | 3.77 | 0.15 | - | 0.41 |
| Nonane | 128 | $C_9H_{20}$ | 7.52 | 0.25 | 0.28 | 0.25 | - |
| 1,2,3-Cyclopentanetriol | 118 | $C_5H_{10}O_3$ | 7.69 | - | - | - | 0.24 |
| 2-Cyclopenten-1-one, 2-methyl- | 96 | $C_6H_8O$ | 7.79 | - | - | - | 1.61 |
| 2-Methyl-2-cyclopentenone | 96 | $C_6H_8O$ | 7.82 | - | 0.29 | 0.33 | - |
| Ethanone, 1-(2-furanyl)- | 110 | $C_6H_6O_2$ | 7.93 | - | 0.25 | 0.17 | 0.52 |
| Acetylfuran | 110 | $C_6H_6O_2$ | 8.05 | - | 3.32 | 1.22 | 1.48 |
| 2-Cyclopenten-1-one, 2-hydroxy- | 98 | $C_5H_6O_2$ | 8.28 | - | 0.46 | 0.15 | - |
| 2,5-Hexanedione | 114 | $C_6H_{10}O_2$ | 8.42 | - | 0.43 | 0.12 | 0.42 |
| 2-Cyclohexen-1-one | 96 | $C_6H_8O$ | 8.52 | 9.50 | 0.16 | - | 0.30 |
| 2(5H)-Furanone, 5-methyl- | 98 | $C_5H_6O_2$ | 8.77 | 0.50 | 0.24 | 0.14 | 0.19 |
| 2(3H)-Furanone, dihydro-5-methyl- | 100 | $C_5H_8O_2$ | 9.18 | - | 0.28 | - | 0.12 |
| 2-Cyclopenten-1-one, 3-methyl- | 96 | $C_6H_8O$ | 9.47 | - | 1.40 | - | 3.74 |
| 5-Methyl furfural | 110 | $C_6H_6O_2$ | 9.53 | - | - | 1.17 | - |
| Phenol | 94 | $C_6H_6O$ | 9.97 | - | 2.48 | 1.30 | 4.06 |
| 1-Decene | 140 | $C_{10}H_{20}$ | 10.18 | - | 1.59 | 0.92 | 3.24 |
| Cyclohexanol, 2,3-dimethyl- | 128 | $C_8H_{16}O$ | 10.26 | - | 0.49 | 0.22 | 0.52 |

| Compound Name | M+ | Formula | RT min | ExtWax mg/g | WO450 mg/g | WO500 mg/g | WO550 mg/g |
|---|---|---|---|---|---|---|---|
| Decane | 142 | $C_{10}H_{22}$ | 10.44 | - | - | - | - |
| Octanal | 128 | $C_8H_{16}O$ | 10.58 | 17.87 | 0.48 | 0.35 | 0.44 |
| 2-Cyclohexen-1-one, 4,4-dimethyl- | 124 | $C_8H_{12}O$ | 11 | - | - | - | 0.30 |
| 2,4-Hexadiene, 2,5-dimethyl- | 110 | $C_8H_{14}$ | 11.16 | - | - | - | 0.39 |
| 1,2-Cyclopentanedione, 3-methyl- | 112 | $C_6H_8O_2$ | 11.32 | 1.07 | 3.85 | 3.84 | 2.06 |
| 2-Cyclopenten-1-one, 2,3-dimethyl- | 110 | $C_7H_{10}O$ | 11.68 | - | 0.82 | 0.56 | 1.58 |
| 1,4-Cyclohex-2-enedione | 110 | $C_6H_6O_2$ | 11.87 | - | 1.44 | 1.92 | 0.51 |
| 3-Methyl-3-buten-1-ol | 86 | $C_5H_{10}O$ | 11.95 | - | - | - | 0.34 |
| Phenol, 2-methyl- | 108 | $C_7H_8O$ | 12.15 | - | 2.16 | 1.55 | 4.30 |
| 2-Furanol, tetrahydro-2-methyl- | 102 | $C_5H_{10}O_2$ | 12.47 | 13.17 | 1.06 | 0.09 | 0.41 |
| Acetophenone | 120 | $C_8H_8O$ | 12.53 | - | - | - | 0.51 |
| Phenol, 3-methyl- | 108 | $C_7H_8O$ | 12.77 | 0.44 | 1.53 | 0.13 | 3.54 |
| 1,10-Undecadiene | 152 | $C_{11}H_{20}$ | 12.94 | 20.58 | 0.42 | 1.11 | 0.34 |
| 1-Undecene | 154 | $C_{11}H_{22}$ | 13.18 | - | 9.44 | 0.39 | 0.29 |
| Undecane | 156 | $C_{11}H_{24}$ | 13.42 | 1.12 | 3.44 | 4.98 | 14.43 |
| 2-Propylcyclohexanol | 142 | $C_9H_{18}O$ | 13.59 | - | - | - | 0.85 |
| Nonanal | 142 | $C_9H_{18}O$ | 13.61 | - | 0.85 | 1.13 | 0.91 |
| Phenol, 2,3-dimethyl- | 122 | $C_8H_{10}O$ | 13.7 | - | - | - | 0.81 |
| Maltol | 126 | $C_6H_6O_3$ | 13.89 | - | 0.72 | 0.41 | 0.46 |
| 2-Cyclopenten-1-one, 3-ethyl-2-hydroxy- | 126 | $C_7H_{10}O_2$ | 14.05 | - | 0.61 | 0.56 | 0.37 |
| Phenol, 2,4-dimethyl- | 122 | $C_8H_{10}O$ | 14.62 | - | - | - | 0.46 |
| Phenol, 3,5-dimethyl- | 122 | $C_8H_{10}O$ | 15.06 | 0.53 | 1.12 | 0.12 | 1.24 |
| Phenol, 2-ethyl- | 122 | $C_8H_{10}O$ | 15.53 | - | 0.45 | 0.82 | 2.43 |
| 1,11-Dodecadiene | 166 | $C_{12}H_{22}$ | 15.86 | 0.97 | - | - | 1.18 |
| 1-Dodecene | 168 | $C_{12}H_{24}$ | 16.1 | - | 13.12 | 7.06 | 21.88 |
| 3-Dodecene, (Z)- | 168 | $C_{12}H_{24}$ | 16.25 | 0.64 | 1.40 | 1.50 | 0.79 |
| Dodecane | 170 | $C_{12}H_{26}$ | 16.34 | 15.54 | 0.97 | 0.53 | 0.72 |
| Catechol | 110 | $C_6H_6O_2$ | 16.41 | - | - | - | 0.26 |
| Decanal | 156 | $C_{10}H_{20}O$ | 16.55 | 0.77 | 1.03 | - | - |
| 1,4:3,6-Dianhydro-α-d-glucopyranose | 144 | $C_6H_8O_4$ | 16.75 | - | 0.68 | 0.91 | 0.21 |
| 3,4-Anhydro-d-galactosan | 144 | $C_6H_8O_4$ | 17.08 | - | - | 0.47 | - |
| 2,3-Anhydro-d-mannosan | 144 | $C_6H_8O_4$ | 17.24 | - | - | 0.99 | - |
| Benzene, 1-ethyl-4-methoxy- | 136 | $C_9H_{12}O$ | 17.49 | - | - | - | 0.36 |
| Dihydrocarveol | 154 | $C_{10}H_{18}O$ | 18.09 | - | - | - | 0.75 |
| (3E)-Trideca-1,3-diene | 180 | $C_{13}H_{24}$ | 18.68 | - | 0.83 | 0.94 | 1.15 |
| 1-Tridecene | 182 | $C_{13}H_{26}$ | 18.89 | 0.25 | 13.90 | 12.04 | 21.55 |
| 2-Undecanone, 6,10-dimethyl- | 198 | $C_{13}H_{26}O$ | 18.97 | - | 0.53 | - | - |
| Tridecane | 184 | $C_{13}H_{28}$ | 19.11 | 12.19 | 1.13 | 0.82 | 1.11 |
| Undecanal | 170 | $C_{11}H_{22}O$ | 19.37 | 0.78 | 0.89 | 0.16 | - |

| Compound Name | M+ | Formula | RT min | ExtWax mg/g | WO450 mg/g | WO500 mg/g | WO550 mg/g |
|---|---|---|---|---|---|---|---|
| Phenol, 2,6-dimethoxy- | 154 | $C_8H_{10}O_3$ | 20.63 | - | 0.50 | 0.12 | - |
| 2,3-Dimethoxyphenol | 154 | $C_8H_{10}O_3$ | 20.66 | - | - | 0.27 | - |
| Phenol, 2-methoxy-4-(1-propenyl)- | 164 | $C_{10}H_{12}O_2$ | 20.77 | - | 0.41 | 0.37 | - |
| 1,13-Tetradecadiene | 194 | $C_{14}H_{26}$ | 21.35 | 0.27 | 0.63 | 0.41 | 1.31 |
| 1-Tetradecene | 196 | $C_{14}H_{28}$ | 21.55 | 9.79 | 13.41 | 15.10 | 22.00 |
| 2-Dodecanone | 184 | $C_{12}H_{24}O$ | 21.67 | 0.51 | 0.44 | - | - |
| Tetradecane | 198 | $C_{14}H_{30}$ | 21.75 | - | 0.85 | 0.67 | 0.75 |
| Dodecanal | 184 | $C_{12}H_{24}O$ | 22.03 | - | 0.70 | 0.68 | - |
| Isoeugenol | 164 | $C_{10}H_{12}O_2$ | 23.16 | - | 0.91 | 4.74 | 0.70 |
| Pentadecadiene | 208 | $C_{15}H_{28}$ | 23.88 | 0.22 | 1.20 | 13.60 | 1.55 |
| 1-Pentadecene | 210 | $C_{15}H_{30}$ | 24.06 | 8.42 | 10.79 | 0.86 | 22.12 |
| Pentadecane | 212 | $C_{15}H_{32}$ | 24.24 | 0.54 | 1.05 | 0.49 | 0.70 |
| Tridecanal | 198 | $C_{13}H_{26}O$ | 24.55 | - | 0.63 | - | - |
| (Z)6-Pentadecen-1-ol | 226 | $C_{15}H_{30}O$ | 25.33 | 0.16 | 0.33 | - | 0.44 |
| Hexadecadiene | 222 | $C_{16}H_{30}$ | 26.27 | 8.14 | 0.60 | - | 1.11 |
| 1-Hexadecene | 224 | $C_{16}H_{32}$ | 26.44 | 0.53 | 8.77 | 10.20 | 21.05 |
| Hexadecane | 226 | $C_{16}H_{34}$ | 26.6 | 0.13 | 1.17 | 0.57 | 0.57 |
| Pentadecanal | 226 | $C_{15}H_{30}O$ | 26.94 | 7.81 | 0.40 | - | - |
| 13-Heptadecyn-1-ol | 252 | $C_{17}H_{32}O$ | 27.73 | 0.84 | 0.63 | - | - |
| 1-Hexadecanol | 242 | $C_{16}H_{34}O$ | 27.88 | 7.57 | - | - | - |
| n-Heptadecadiene | 236 | $C_{17}H_{32}$ | 28.54 | 1.80 | 0.65 | - | 0.97 |
| 1-Heptadecene | 238 | $C_{17}H_{34}$ | 28.69 | 7.16 | 7.67 | 8.38 | 21.02 |
| Heptadecane | 240 | $C_{17}H_{36}$ | 28.84 | 5.49 | 0.88 | 0.64 | 0.69 |
| Oxirane, tetradecyl- | 240 | $C_{16}H_{32}O$ | 29.21 | 6.61 | 0.34 | - | - |
| Octadecadiene-1,17 | 250 | $C_{18}H_{34}$ | 30.7 | 16.26 | 0.23 | - | 0.65 |
| 1-Octadecene | 252 | $C_{18}H_{36}$ | 30.83 | 5.78 | 7.39 | 7.24 | 21.60 |
| Octadecane | 254 | $C_{18}H_{38}$ | 30.98 | 45.84 | 0.69 | 0.57 | 0.65 |
| 8,11-Nonadecadiene | 264 | $C_{19}H_{36}$ | 32.75 | 4.94 | 0.19 | - | 0.82 |
| 1-Nonadecene | 266 | $C_{19}H_{38}$ | 32.87 | 82.66 | 7.02 | 6.55 | 19.87 |
| Nonadecane | 268 | $C_{19}H_{40}$ | 33 | 109.92 | 0.90 | 0.87 | 1.39 |
| 1-Eicosene | 280 | $C_{20}H_{40}$ | 34.83 | 3.24 | 6.66 | 5.81 | 19.14 |
| Eicosane | 282 | $C_{20}H_{42}$ | 34.94 | 106.88 | 1.04 | 2.41 | 2.36 |
| 1-Heneicosene | 294 | $C_{21}H_{42}$ | 36.69 | 2.38 | 6.18 | 5.22 | 16.49 |
| Heneicosane | 296 | $C_{21}H_{44}$ | 36.79 | 1.24 | 1.95 | 6.96 | 6.14 |
| 1-Docosene | 308 | $C_{22}H_{44}$ | 38.47 | 116.06 | 5.96 | 4.61 | 13.77 |
| Docosane | 310 | $C_{22}H_{46}$ | 38.57 | 3.52 | 4.23 | 18.70 | 16.85 |
| 1-Tricosene | 322 | $C_{23}H_{46}$ | 40.17 | 1.41 | 5.51 | 3.93 | 11.33 |
| Tricosane | 324 | $C_{23}H_{48}$ | 40.28 | 96.59 | 10.21 | 48.74 | 41.47 |
| 1-Tetracosene | 336 | $C_{24}H_{48}$ | 41.82 | 3.34 | 5.33 | 3.03 | 8.21 |

| Compound Name | M+ | Formula | RT min | ExtWax mg/g | WO450 mg/g | WO500 mg/g | WO550 mg/g |
|---|---|---|---|---|---|---|---|
| Tetracosane | 338 | $C_{24}H_{50}$ | 41.91 | 2.28 | 22.20 | 84.48 | 70.34 |
| 6,9-Pentacosadiene | 348 | $C_{25}H_{48}$ | 42.89 | - | - | - | 1.36 |
| 9-Pentacosene | 350 | $C_{25}H_{50}$ | 43.4 | - | - | - | 6.15 |
| 2-Methyltetracosane | 352 | $C_{25}H_{52}$ | 43.49 | 81.62 | 41.77 | 118.95 | 91.96 |
| 9,10-Hexacosadiene | 362 | $C_{26}H_{50}$ | 44.42 | 3.38 | 1.02 | 3.85 | 2.66 |
| 1-Hexacosene | 364 | $C_{26}H_{52}$ | 45 | 1.24 | 51.99 | 108.41 | 91.54 |
| 2-Methylhexacosane | 380 | $C_{27}H_{56}$ | 45.89 | - | 1.26 | 3.39 | 1.95 |
| Heptacosadiene | 376 | $C_{27}H_{52}$ | 46.05 | 61.97 | 1.96 | 3.39 | 1.44 |
| 1-Heptacosene | 378 | $C_{27}H_{54}$ | 46.25 | 2.43 | 1.61 | 1.69 | 0.93 |
| Heptacosane | 380 | $C_{27}H_{56}$ | 46.46 | 1.31 | 70.91 | 110.21 | 86.41 |
| Octacosadiene | 390 | $C_{28}H_{58}$ | 47.33 | 42.06 | 3.85 | 4.18 | 2.39 |
| 1-Octacosene | 392 | $C_{28}H_{58}$ | 47.7 | 2.98 | - | 1.78 | 1.13 |
| Octacosane | 394 | $C_{28}H_{58}$ | 47.86 | 2.36 | 74.87 | 93.85 | 67.46 |
| Nonacosadiene | 404 | $C_{29}H_{56}$ | 48.69 | 28.20 | 4.28 | 3.77 | 1.88 |
| 1-Nonacosene | 406 | $C_{29}H_{58}$ | 48.85 | 17.63 | 3.47 | 2.97 | 1.07 |
| Nonacosane | 408 | $C_{29}H_{60}$ | 49.21 | 0.75 | 69.98 | 85.44 | 57.61 |
| Triacontadiene | 418 | $C_{30}H_{60}$ | 50.02 | 0.59 | 4.68 | 3.63 | 1.78 |
| 1-Triacontene | 420 | $C_{30}H_{60}$ | 50.17 | 12.17 | 2.37 | 2.43 | - |
| Triacontane | 422 | $C_{30}H_{62}$ | 50.51 | 7.42 | 52.80 | 64.21 | 44.58 |
| Hentriaconta-1,3-diene | 432 | $C_{31}H_{60}$ | 51.31 | 4.81 | 3.93 | 3.28 | 1.32 |
| 1-Hentriacontene | 434 | $C_{31}H_{62}$ | 51.46 | 2.10 | - | 2.83 | 0.95 |
| Hentriacontane | 436 | $C_{31}H_{64}$ | 51.78 | 1.22 | 41.02 | 46.30 | 32.66 |
| Dotriacontadiene | 446 | $C_{32}H_{62}$ | 51.92 | - | 5.89 | - | - |
| 1-Dotriacontene | 448 | $C_{32}H_{64}$ | 52.56 | - | 4.70 | 3.99 | - |
| Dotriacontane | 450 | $C_{32}H_{66}$ | 53.02 | - | 30.73 | 34.25 | - |
| 1-Tritriacontene | 462 | $C_{33}H_{66}$ | 54.21 | - | 2.66 | 24.01 | - |
| Tritriacontane | 464 | $C_{33}H_{68}$ | 54.42 | - | 21.43 | - | 0.95 |
| 1-Tetratriacontene | 476 | $C_{34}H_{68}$ | 55.08 | - | 2.29 | 0.82 | 0.71 |
| Tetratriacontane | 478 | $C_{34}H_{70}$ | 55.37 | - | 14.40 | 16.80 | 7.28 |
| Pentatriacontane | 492 | $C_{35}H_{72}$ | 56.5 | - | 10.48 | 11.40 | - |
| Hexatriacontane | 507 | $C_{36}H_{74}$ | 57.6 | - | 6.50 | 8.78 | 5.33 |
| Heptatriacontane | 521 | $C_{37}H_{76}$ | 58.84 | - | 4.53 | 5.65 | 2.38 |
| Octatriacontane | 535 | $C_{38}H_{78}$ | 60.23 | - | 2.55 | 3.01 | 1.46 |
| 13,25-Dimethylheptatriacontane | 549 | $C_{39}H_{80}$ | 61.84 | - | 1.33 | 1.39 | - |
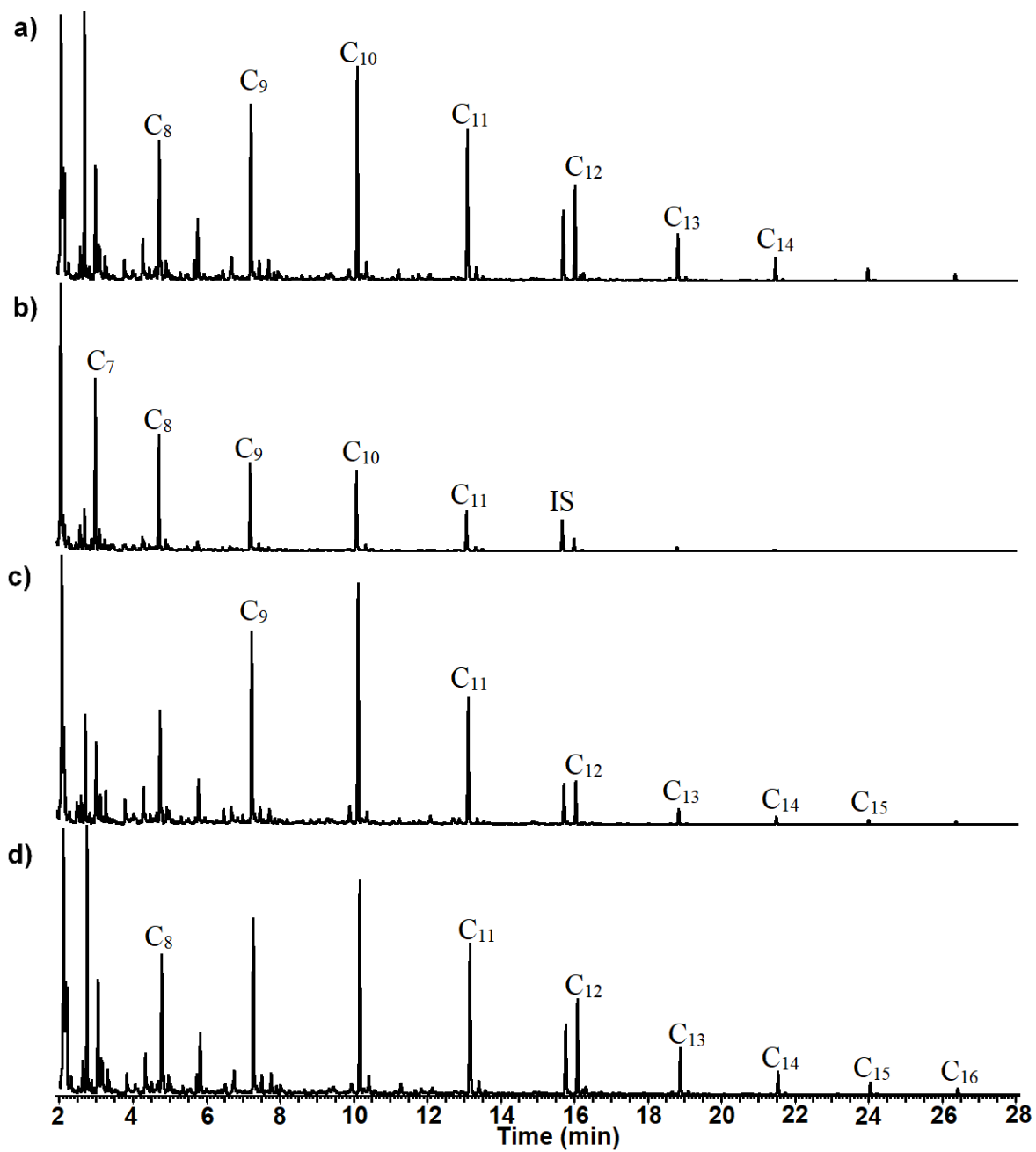
Figure 4.6. GC-MS Chromatograms of thermal pyrolysis products of (a) solvent extracted wax-py, (b) WO450-py, (c) WO500-py, and (d) WO550-py collected from the impinger.

Table 4.4. Identified compounds in the liquid products of thermal pyrolysis of solvent extracted wax and wax-oil samples collected from the impinger.

| Compound Name | M+ | Formula | RT min | ExtWax mg/g | WO450 mg/g | WO500 mg/g | WO550 mg/g |
|---|---|---|---|---|---|---|---|
| 1-Hexene | 84 | $C_6H_{12}$ | 2.1 | - | 237.60 | 201.66 | 117.74 |
| 2-Hexanone, 3,4-dimethyl- | 128 | $C_8H_{16}O$ | 2.16 | - | 16.60 | 32.99 | 30.92 |
| Furan, 3-methyl- | 82 | $C_5H_6O$ | 2.2 | - | 13.40 | 26.74 | 10.43 |
| Cyclopentene, 3-methyl- | 82 | $C_6H_{10}$ | 2.63 | - | 20.97 | 6.68 | 5.49 |
| Acetic anhydride | 102 | $C_4H_6O_3$ | 2.75 | - | 27.14 | 45.83 | 38.59 |
| Cyclohexene | 82 | $C_6H_{10}$ | 2.94 | - | 9.66 | 9.36 | 8.62 |
| 1-Heptene | 98 | $C_7H_{14}$ | 3.06 | 193.37 | 133.04 | 72.83 | 51.18 |
| Hexane, 3-methyl- | 100 | $C_7H_{16}$ | 3.18 | 12.06 | 16.14 | 19.03 | 20.53 |
| 1,3-Pentadiene, 2,3-dimethyl- | 96 | $C_7H_{12}$ | 3.24 | 3.08 | 2.77 | 2.83 | 2.62 |
| 2-Heptene | 98 | $C_7H_{14}$ | 3.28 | 3.32 | 5.21 | 3.15 | 2.11 |
| Cyclopentane, 1-methyl-2-methylene- | 96 | $C_7H_{12}$ | 3.36 | 1.59 | - | 6.84 | 15.45 |
| 2,3-Dimethyl-1,3-pentadiene | 96 | $C_7H_{12}$ | 3.4 | 2.66 | - | 3.35 | 1.68 |
| Cyclohexene, 1-methyl- | 96 | $C_7H_{12}$ | 3.5 | 3.99 | 4.52 | - | 11.08 |
| Cyclohexane, methyl- | 98 | $C_7H_{14}$ | 3.55 | 3.13 | 5.83 | - | 3.67 |
| Vinylcyclopentane | 96 | $C_7H_{12}$ | 3.58 | 1.55 | - | - | 2.75 |
| Cyclohexene, 3-methyl- | 96 | $C_7H_{12}$ | 3.83 | 7.06 | 10.56 | - | 16.30 |
| Methylenecyclohexane | 96 | $C_7H_{12}$ | 3.88 | 5.18 | 7.81 | 7.96 | 7.22 |
| 1-Undecyne | 152 | $C_{11}H_{20}$ | 4.12 | 6.23 | - | - | - |
| Toluene | 92 | $C_7H_8$ | 4.35 | 6.65 | 10.62 | 19.38 | 23.67 |
| 1-Methylcyclohexene | 96 | $C_7H_{12}$ | 4.39 | 6.55 | 6.77 | - | - |
| 2,4-Hexadiene | 82 | $C_6H_{10}$ | 4.49 | 3.20 | - | 3.84 | 4.02 |
| 1,4-Octadiene | 110 | $C_8H_{14}$ | 4.62 | 6.45 | - | 6.78 | 5.94 |
| Heptane, 3-methylene- | 112 | $C_8H_{16}$ | 4.76 | 66.29 | 89.23 | 57.45 | 54.56 |
| Cyclopropane, pentyl- | 112 | $C_8H_{16}$ | 4.8 | 165.70 | 114.24 | 6.08 | 6.09 |
| Hexane, 3-ethyl- | 114 | $C_8H_{18}$ | 4.98 | 12.56 | 6.16 | 5.14 | 7.93 |
| 2-Octene, (Z)- | 112 | $C_8H_{16}$ | 5.14 | 5.65 | 3.33 | - | - |
| 2-Hexene, 3,5-dimethyl- | 112 | $C_8H_{16}$ | 5.21 | 2.51 | 0.89 | 2.64 | - |
| cis-1-Butyl-2-methylcyclopropane | 112 | $C_8H_{16}$ | 5.32 | 1.99 | 1.11 | - | 3.90 |
| Vinylcyclohexane | 110 | $C_8H_{14}$ | 5.51 | 2.22 | 3.70 | 1.94 | - |
| 1-Methyl-2-methylenecyclohexane | 110 | $C_8H_{14}$ | 5.57 | 4.73 | 1.54 | 2.60 | 3.96 |
| 3-Isopropylcyclopentene | 110 | $C_8H_{14}$ | 6.13 | 0.84 | 0.70 | 8.22 | 4.61 |
| Ethylidenecyclohexane | 110 | $C_8H_{14}$ | 6.21 | 1.84 | 1.79 | 23.88 | 23.81 |
| 7-Methyl-1-octene | 126 | $C_9H_{18}$ | 6.33 | 3.15 | 3.41 | 2.84 | 2.36 |
| Ethylbenzene | 106 | $C_8H_{10}$ | 6.53 | 2.80 | 2.84 | 4.86 | 8.24 |
| p-Xylene | 106 | $C_8H_{10}$ | 6.73 | 1.82 | 2.82 | 13.39 | 13.18 |
| Cyclohexane, 2-propenyl- | 124 | $C_9H_{16}$ | 6.91 | 3.81 | 0.87 | - | 2.16 |
| 1,8-Nonadiene | 124 | $C_9H_{16}$ | 7.05 | 5.09 | 1.16 | 2.03 | 4.90 |

| Compound Name | M+ | Formula | RT min | ExtWax mg/g | WO450 mg/g | WO500 mg/g | WO550 mg/g |
|---|---|---|---|---|---|---|---|
| 1-Nonene | 126 | $C_9H_{18}$ | 7.28 | 160.02 | 73.67 | 76.82 | 110.92 |
| Nonane | 128 | $C_9H_{20}$ | 7.51 | 9.43 | 5.95 | 7.88 | 9.17 |
| 2-Nonene, (E)- | 128 | $C_9H_{20}$ | 7.69 | 1.57 | 1.91 | 1.67 | 1.37 |
| Cyclopentane, 1-methyl-2-(2-propenyl)- | 124 | $C_9H_{16}$ | 7.8 | 2.35 | 1.21 | 9.07 | 9.88 |
| cis-2-Nonene | 126 | $C_9H_{18}$ | 7.92 | 0.70 | 3.36 | 3.13 | 2.60 |
| Allylcyclohexane | 124 | $C_9H_{16}$ | 8.11 | 1.95 | 1.01 | 1.94 | 3.06 |
| 1-Butylcyclopentene | 124 | $C_9H_{16}$ | 8.9 | 1.70 | 1.48 | 1.99 | 2.20 |
| 4-Dodecene, (E)- | 168 | $C_{12}H_{24}$ | 9.06 | 0.89 | 1.14 | 2.02 | 3.08 |
| 4-Nonene, 2-methyl- | 140 | $C_{10}H_{20}$ | 9.13 | 2.41 | 0.96 | 3.14 | 2.86 |
| 1-Methyl-2-(3-methylpentyl) cyclopropane | 140 | $C_{10}H_{20}$ | 9.31 | 1.77 | 1.31 | 3.56 | 5.47 |
| 1,11-Dodecadiene | 166 | $C_{12}H_{22}$ | 9.76 | 1.27 | 1.01 | 7.13 | 4.67 |
| Bicyclo[3.3.1]nonan-2-one | 138 | $C_9H_{14}O$ | 9.93 | - | - | - | 15.55 |
| 1-Decene | 140 | $C_{10}H_{20}$ | 10.18 | 130.92 | 71.77 | 89.19 | 141.42 |
| Mesitylene | 120 | $C_9H_{12}$ | 10.27 | - | - | 2.99 | - |
| Decane | 140 | $C_{10}H_{20}$ | 10.43 | 6.05 | 5.06 | 8.83 | 8.84 |
| 4-Decene | 140 | $C_{10}H_{20}$ | 10.6 | 1.47 | 0.22 | 2.68 | 3.02 |
| Cyclohexane, 1-methyl-2-propyl- | 140 | $C_{10}H_{20}$ | 10.86 | 1.34 | 0.72 | 0.83 | 1.48 |
| Bicyclo[6.1.0]nonane | 124 | $C_9H_{16}$ | 11.14 | 1.01 | 0.56 | 2.18 | 2.04 |
| Cyclotene | 112 | $C_6H_8O_2$ | 11.27 | - | - | - | 3.87 |
| 2-Cyclopenten-1-one, 2,3-dimethyl- | 110 | $C_7H_{10}O$ | 11.67 | - | - | - | 1.60 |
| 1,10-Undecadiene | 152 | $C_{11}H_{20}$ | 12.09 | 0.89 | 0.58 | 3.59 | 1.18 |
| Phenol, 2-methyl- | 108 | $C_7H_8O$ | 12.13 | - | - | - | 4.36 |
| p-Cresol | 108 | $C_7H_8O$ | 12.75 | - | - | - | 4.77 |
| 1-Dodecene | 168 | $C_{12}H_{24}$ | 13.17 | 60.01 | 36.77 | 70.82 | 76.11 |
| Tetradecane | 198 | $C_{14}H_{30}$ | 13.41 | 2.90 | 3.24 | 6.66 | 3.20 |
| Nonanal | 142 | $C_9H_{18}O$ | 13.57 | - | 1.76 | 2.01 | 1.77 |
| 2-Cyclopenten-1-one, 3-ethyl-2-hydroxy- | 126 | $C_7H_{10}O_2$ | 14.06 | - | - | - | 0.40 |
| Benzene, (1-methylene-2-propenyl)- | 130 | $C_{10}H_{10}$ | 14.93 | - | - | - | 2.92 |
| Dodecane | 170 | $C_{12}H_{26}$ | 16.09 | 23.35 | 11.86 | 43.44 | 25.33 |
| 3-Dodecene, (Z)- | 168 | $C_{12}H_{24}$ | 16.23 | - | 0.93 | 2.57 | 1.02 |
| Phenol, 4-ethyl-2-methoxy- | 152 | $C_9H_{12}O2$ | 18.66 | - | 1.58 | 1.34 | 1.04 |
| 1-Tridecene | 182 | $C_{13}H_{26}$ | 18.89 | 11.53 | 3.51 | 21.33 | 17.52 |
| 2-n-Propyl-1-heptanol | 158 | $C_{10}H_{22}O$ | 19.09 | - | 0.31 | 1.46 | 0.60 |
| 1-Tetradecene | 196 | $C_{14}H_{28}$ | 21.55 | 9.61 | 1.44 | 10.37 | 4.84 |
| 1-Pentadecene | 210 | $C_{15}H_{30}$ | 24.05 | 8.16 | 0.67 | 0.67 | 2.81 |
| 1-Hexadecene | 224 | $C_{16}H_{32}$ | 26.43 | 6.05 | 0.34 | 5.83 | 1.71 |
| 1-Heptadecene | 238 | $C_{17}H_{34}$ | 28.69 | 3.81 | 3.22 | 3.02 | 1.17 |
| 1-Octadecene | 252 | $C_{18}H_{36}$ | 30.83 | 1.75 | - | 1.52 | 0.42 |
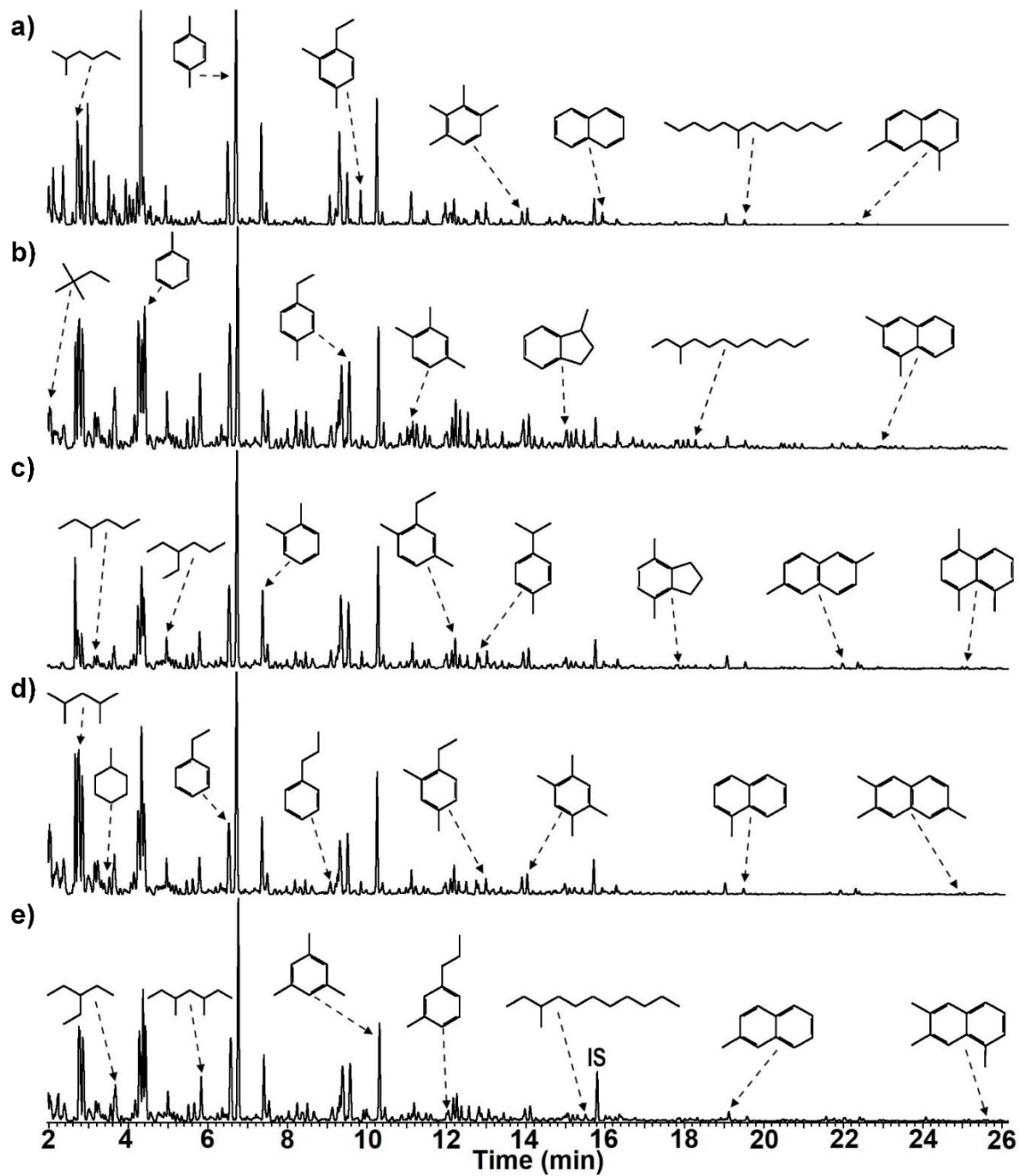
Figure 4.7. GC-MS Chromatograms of (a) gasoline and U-tube condenser trapped liquid products of catalytic pyrolysis of (b) solvent extracted wax-cat (c) WO450-cat, (d) WO500-cat, and (e) WO550-cat.

Table 4.5. Identified compounds in gasoline and the liquid products of catalytic pyrolysis of solvent extracted wax and wax-oil samples collected from the U-tube.

| Compound Name | M+ | Formula | RT min | Gasoline mg/g | Ext Wax mg/g | WO450 mg/g | WO500 mg/g | WO550 mg/g |
|---|---|---|---|---|---|---|---|---|
| 2,2-Dimethylbutane | 86 | $C_6H_{14}$ | 1.99 | 19.71 | - | - | - | - |
| Pentane, 3-methylene- | 84 | $C_6H_{12}$ | 2.1 | 29.60 | 57.96 | - | 16.50 | 54.30 |
| 2-Pentene, 3-methyl-, (E)- | 84 | $C_6H_{12}$ | 2.15 | - | 35.58 | - | - | 57.28 |
| Cyclopentane, methyl- | 84 | $C_6H_{12}$ | 2.35 | 32.38 | - | 61.67 | - | 41.13 |
| Cyclopropane, 1,1,2,3-tetramethyl- | 98 | $C_7H_{14}$ | 2.62 | - | 81.08 | 434.13 | - | 8.30 |
| Pentane, 2,4-dimethyl- | 100 | $C_7H_{16}$ | 2.71 | 73.92 | - | 193.96 | - | - |
| Hexane, 2-methyl- | 100 | $C_7H_{16}$ | 2.76 | 163.85 | - | - | 22.55 | 226.27 |
| Pentane, 3-ethyl- | 100 | $C_7H_{16}$ | 2.81 | 32.31 | 132.51 | 145.11 | 19.98 | 152.47 |
| 2,2,3,3-Tetramethylbutane | 114 | $C_8H_{18}$ | 2.97 | 65.80 | - | - | 2.78 | 39.74 |
| 1-Heptene, 4-methyl- | 112 | $C_8H_{16}$ | 3.01 | - | 28.32 | - | - | - |
| Hexane, 3-methyl- | 100 | $C_7H_{16}$ | 3.13 | 25.18 | 35.47 | 53.86 | 7.34 | 33.21 |
| 1,4-Pentadiene, 3,3-dimethyl- | 96 | $C_7H_{12}$ | 3.2 | 6.79 | - | - | - | - |
| 4-Methyl-2-hexene, c&t | 98 | $C_7H_{14}$ | 3.23 | - | 36.60 | 79.83 | 1.67 | 38.57 |
| 2-Hexene, 3-methyl-, (Z)- | 98 | $C_7H_{14}$ | 3.33 | - | 8.26 | 22.83 | - | 7.01 |
| 3-Heptene | 98 | $C_7H_{14}$ | 3.4 | - | 8.76 | 22.92 | - | 8.22 |
| Cyclohexane, methyl- | 95 | $C_7H_{14}$ | 3.5 | 23.12 | 18.94 | 35.60 | 4.59 | 30.67 |
| Hexane, 2,5-dimethyl- | 114 | $C_8H_{18}$ | 3.59 | 6.46 | - | - | - | - |
| Hexane, 2,4-dimethyl- | 114 | $C_8H_{18}$ | 3.63 | 11.61 | 86.04 | 149.51 | 10.16 | 21.92 |
| Cyclopentane, 1,2,4-trimethyl- | 112 | $C_8H_{18}$ | 3.77 | 4.72 | - | - | 20.05 | 64.83 |
| 2-Pentene, 3-ethyl-2-methyl- | 112 | $C_8H_{16}$ | 3.8 | - | 7.10 | - | 2.66 | 10.89 |
| 3-Ethylpentane | 100 | $C_7H_{16}$ | 3.92 | 19.68 | - | - | - | - |
| 2,3,3-Trimethylpentane | 114 | $C_8H_{18}$ | 4.02 | 14.22 | 9.24 | 31.50 | - | 12.44 |
| 2,3-Dimethylhexane | 114 | $C_8H_{18}$ | 4.11 | 9.73 | 36.76 | 59.07 | 15.78 | 29.45 |
| 2-Methylheptane | 114 | $C_8H_{18}$ | 4.22 | 21.50 | 150.61 | 335.92 | 85.31 | 190.80 |
| Toluene | 92 | $C_7H_8$ | 4.31 | 103.69 | 99.20 | 487.31 | - | 150.31 |
| 3-Methylheptane | 114 | $C_8H_{18}$ | 4.37 | 21.92 | 139.17 | 333.77 | 35.33 | - |
| Cyclohexane, 1,3-dimethyl-, trans- | 112 | $C_8H_{16}$ | 4.49 | 6.27 | 13.43 | 56.72 | 78.97 | 137.63 |
| 2,2,4-Trimethylhexane | 128 | $C_9H_{20}$ | 4.55 | 7.25 | - | - | 5.40 | 18.64 |
| Ethylcyclohexane | 112 | $C_8H_{16}$ | 4.69 | 3.27 | 10.85 | - | - | - |
| 3-Ethylhexane | 114 | $C_8H_{18}$ | 4.93 | 17.64 | 41.27 | 122.98 | 24.48 | 38.09 |
| 1,4-Dimethylcyclohexane | 112 | $C_8H_{16}$ | 5.07 | 4.13 | 7.06 | 52.34 | - | 13.82 |
| Cyclohexane, 1,4-dimethyl-, cis- | 112 | $C_8H_{16}$ | 5.18 | 3.21 | 12.52 | 40.87 | 6.43 | 13.95 |
| 2-Hexene, 3,5-dimethyl- | 112 | $C_8H_{18}$ | 5.21 | - | 10.50 | - | 4.20 | 11.08 |
| 2,3-Dimethylheptane | 128 | $C_9H_{20}$ | 5.28 | 1.85 | - | 20.97 | 4.64 | 7.76 |
| Heptane, 2,4-dimethyl- | 128 | $C_9H_{20}$ | 5.45 | 3.39 | 25.81 | 61.97 | 20.83 | 27.13 |
| 2-Methyloctane | 128 | $C_9H_{20}$ | 5.6 | 4.00 | 28.45 | 77.10 | 23.92 | 28.05 |
| 3,5-Dimethylheptane | 128 | $C_9H_{20}$ | 5.76 | 9.34 | 75.70 | 191.91 | 68.35 | 76.12 |

| Compound Name | M+ | Formula | RT min | Gasoline mg/g | Ext Wax mg/g | WO450 mg/g | WO500 mg/g | WO550 mg/g |
|---|---|---|---|---|---|---|---|---|
| 1,2,4-Trimethylcyclohexane | 126 | $C_9H_{18}$ | 6.18 | 1.68 | 10.21 | 44.99 | 5.53 | 10.57 |
| 3-Ethyl-2,4-dimethylpentane | 128 | $C_9H_{20}$ | 6.3 | 2.66 | 19.51 | 41.69 | 12.88 | 15.18 |
| Ethylbenzene | 106 | $C_8H_{10}$ | 6.49 | 48.49 | 154.15 | - | 3.22 | 3.66 |
| Octane, 2-methyl- | 128 | $C_9H_{20}$ | 6.53 | - | - | 491.01 | 156.50 | 188.43 |
| p-Xylene | 106 | $C_8H_{10}$ | 6.71 | 129.08 | 240.12 | 1168.48 | 272.02 | 386.58 |
| 2,2,3-Trimethyldecane | 184 | $C_{13}H_{28}$ | 6.86 | 3.11 | - | - | - | - |
| 2,2-Dimethyloctane | 142 | $C_{10}H_{22}$ | 7.05 | 4.00 | - | - | - | 4.89 |
| Cyclohexane, 1-ethyl-2-methyl-, cis- | 126 | $C_9H_{18}$ | 7.14 | 2.54 | - | - | - | - |
| o-Xylene | 106 | $C_8H_{10}$ | 7.34 | 49.38 | 64.92 | 400.10 | 66.58 | 107.22 |
| 1-Nonene | 126 | $C_9H_{18}$ | 7.47 | 9.35 | 39.44 | 129.53 | 29.03 | 29.85 |
| Cyclohexane, 1-ethyl-2-methyl- | 128 | $C_9H_{20}$ | 7.67 | 2.19 | - | 54.50 | - | 9.88 |
| Nonane | 128 | $C_9H_{20}$ | 7.73 | - | 11.35 | - | 7.86 | - |
| 2,3-Dimethyloctane | 142 | $C_{10}H_{22}$ | 7.91 | 1.70 | 8.98 | - | 9.67 | 12.91 |
| 2,4,6-Trimethylheptane | 142 | $C_{10}H_{22}$ | 7.96 | 1.33 | 21.51 | 36.03 | 14.84 | 12.26 |
| 4-Methylnonane | 142 | $C_{10}H_{22}$ | 8.18 | 2.14 | - | 87.88 | - | - |
| Cumene | 120 | $C_9H_{12}$ | 8.22 | 3.41 | 41.72 | - | 39.17 | 25.91 |
| Octane, 2,3-dimethyl- | 142 | $C_{10}H_{22}$ | 8.34 | - | 27.02 | 67.17 | 22.86 | 19.55 |
| 2,6-Dimethyloctane | 142 | $C_{10}H_{22}$ | 8.43 | 3.73 | 31.91 | 85.18 | 29.53 | 26.23 |
| Heptane, 3,4,5-trimethyl- | 142 | $C_{10}H_{22}$ | 8.6 | 1.63 | 28.98 | - | - | - |
| 3-Ethyl-2-methylheptane | 142 | $C_{10}H_{22}$ | 8.65 | 0.91 | - | 88.69 | 24.15 | 20.70 |
| Propylbenzene | 120 | $C_9H_{12}$ | 9.07 | 15.00 | - | - | - | - |
| Nonane, 4-methyl- | 142 | $C_{10}H_{22}$ | 9.11 | - | 32.73 | 111.53 | 30.83 | 28.72 |
| 2,2,6-Trimethyloctane | 156 | $C_{11}H_{24}$ | 9.21 | 9.50 | 21.45 | 55.28 | 15.95 | 17.06 |
| Benzene, 1-ethyl-3-methyl- | 120 | $C_9H_{12}$ | 9.3 | 64.52 | 39.43 | 82.02 | 33.82 | 20.81 |
| Nonane, 2-methyl- | 142 | $C_{10}H_{22}$ | 9.37 | - | 103.56 | 450.18 | 113.41 | 118.76 |
| Benzene, 1-ethyl-4-methyl- | 120 | $C_9H_{12}$ | 9.5 | 26.55 | 8.51 | 349.45 | 4.99 | 5.97 |
| Benzene, 1,2,4-trimethyl- | 120 | $C_9H_{12}$ | 9.56 | - | 102.96 | - | 106.69 | 107.58 |
| Benzene, 1-ethyl-2-methyl- | 120 | $C_9H_{12}$ | 9.84 | 16.27 | 11.12 | 67.23 | 23.37 | 14.79 |
| 5-Decene, (E)- | 140 | $C_{10}H_{20}$ | 10.02 | - | 6.02 | 25.54 | 12.35 | 14.38 |
| Mesitylene | 120 | $C_9H_{12}$ | 10.25 | 63.98 | 117.92 | 552.83 | 143.14 | 156.26 |
| Decane | 142 | $C_{10}H_{22}$ | 10.39 | 6.14 | 23.63 | 57.42 | 17.63 | 18.88 |
| cis-3-Decene | 140 | $C_{10}H_{20}$ | 10.59 | - | - | 48.63 | 6.08 | 5.30 |
| Isobutylbenzene | 134 | $C_{10}H_{14}$ | 10.65 | 1.25 | - | - | - | - |
| Sec-butylbenzene | 134 | $C_{10}H_{14}$ | 10.75 | 1.84 | - | - | - | - |
| Octane, 5-ethyl-2-methyl- | 156 | $C_{11}H_{24}$ | 10.84 | - | 18.12 | 45.62 | 14.76 | 11.54 |
| Nonane, 2,5-dimethyl- | 156 | $C_{11}H_{24}$ | 11.03 | - | 16.69 | 27.65 | 14.73 | 11.72 |
| 1,2,4-Trimethylbenzene | 120 | $C_9H_{12}$ | 11.11 | 17.86 | 34.19 | 99.44 | 10.70 | 32.74 |
| Decane, 3,7-dimethyl- | 170 | $C_{12}H_{26}$ | 11.27 | - | 28.12 | 46.09 | 21.05 | 16.60 |

| Compound Name | M+ | Formula | RT min | Gasoline mg/g | Ext Wax mg/g | WO450 mg/g | WO500 mg/g | WO550 mg/g |
|---|---|---|---|---|---|---|---|---|
| Allylbenzene | 118 | $C_9H_{10}$ | 11.42 | 2.02 | 22.57 | 33.27 | 17.45 | 11.46 |
| Indane | 118 | $C_9H_{10}$ | 11.52 | 7.15 | 15.40 | 54.07 | 11.40 | 12.94 |
| 1,3-Diethylbenzene | 134 | $C_{10}H_{14}$ | 11.92 | 3.75 | 31.12 | - | 9.24 | 3.31 |
| 1-Methyl-3-propylbenzene | 134 | $C_{10}H_{14}$ | 11.97 | 12.38 | - | 102.85 | 16.55 | 10.51 |
| Bicyclo[3.1.0]hex-2-ene, 4-methylene-1-(1-methylethyl)- | 134 | $C_{10}H_{14}$ | 12.11 | 9.98 | 27.38 | 83.76 | 24.65 | 17.55 |
| 2-Ethyl-p-xylene | 134 | $C_{10}H_{14}$ | 12.19 | 12.22 | 45.00 | 118.67 | 42.33 | 37.08 |
| 2-Methyldecane | 156 | $C_{11}H_{24}$ | 12.3 | 4.04 | 33.17 | 52.47 | 25.05 | 41.12 |
| 1-Methyl-2-propylbenzene | 134 | $C_{10}H_{14}$ | 12.44 | 3.05 | - | 10.51 | - | 20.72 |
| 3-Methyldecane | 156 | $C_{11}H_{24}$ | 12.5 | 1.90 | 31.56 | 49.78 | 24.24 | 22.90 |
| 1-Ethyl-2,4-dimethylbenzene | 134 | $C_{10}H_{14}$ | 12.75 | 6.58 | - | 68.20 | - | 33.98 |
| Benzene, 4-ethyl-1,2-dimethyl- | 134 | $C_{10}H_{14}$ | 12.8 | 5.60 | 17.82 | 40.43 | 17.86 | 10.58 |
| 4-Allyltoluene | 132 | $C_{10}H_{12}$ | 12.87 | 0.99 | 9.98 | - | 10.92 | - |
| p-Cymene | 134 | $C_{10}H_{14}$ | 12.99 | 13.78 | 18.79 | 88.67 | 22.54 | 7.35 |
| O-Cymene | 134 | $C_{10}H_{14}$ | 13.2 | 0.70 | 3.29 | 49.51 | 4.28 | 8.42 |
| Undecane | 156 | $C_{11}H_{24}$ | 13.38 | 3.15 | 17.13 | 45.15 | - | - |
| Benzene, 1-methyl-4-(2-methylpropyl)- | 148 | $C_{11}H_{16}$ | 13.46 | 0.86 | 2.85 | - | 10.95 | 15.02 |
| Benzene, (1,1-dimethylpropyl)- | 148 | $C_{11}H_{16}$ | 13.55 | 0.91 | 5.18 | 26.03 | 4.94 | 1.38 |
| 1-Ethyl-3,5-dimethylbenzene | 134 | $C_{10}H_{14}$ | 13.63 | 2.30 | 4.64 | 13.70 | 3.56 | 5.45 |
| trans-4a-Methyl-decahydronaphthalene | 152 | $C_{11}H_{20}$ | 13.72 | 0.52 | 3.38 | - | - | 5.24 |
| 1,2,3,4-Tetramethylbenzene, | 134 | $C_{10}H_{14}$ | 13.95 | - | 39.79 | 90.86 | 2.38 | 24.53 |
| 1,2,4,5-Tetramethylbenzene | 134 | $C_{10}H_{14}$ | 14.04 | 9.34 | 38.86 | 101.41 | 34.32 | 28.27 |
| 3,7-Dimethyldecane | 170 | $C_{12}H_{26}$ | 14.18 | 0.69 | 14.85 | 13.06 | 36.89 | 5.30 |
| 1-Methyl-4-(1-methylpropyl)-benzene | 148 | $C_{11}H_{16}$ | 14.52 | 1.71 | 12.34 | 12.11 | 10.73 | 4.54 |
| 5-Methylindan | 132 | $C_{10}H_{12}$ | 14.6 | 4.01 | 8.92 | 11.28 | 8.31 | 8.92 |
| 1,3-Diethyl-4-methylbenzene | 148 | $C_{11}H_{16}$ | 14.71 | 1.52 | - | 26.93 | 7.30 | 2.67 |
| 3,5-Diethyltoluene | 148 | $C_{11}H_{16}$ | 14.75 | 2.18 | 5.12 | 13.81 | 5.47 | 1.94 |
| Benzene, 1-methyl-4-(1-methylpropyl)- | 148 | $C_{11}H_{16}$ | 14.88 | - | 3.89 | 26.37 | 2.00 | - |
| 1-Methylindan | 132 | $C_{10}H_{12}$ | 14.93 | 5.06 | - | 9.78 | 4.04 | 7.13 |
| 1,4-Diethylbenzene | 132 | $C_{10}H_{12}$ | 14.98 | 4.55 | 30.59 | 64.26 | 28.53 | 13.32 |
| Isopentylbenzene | 148 | $C_{11}H_{16}$ | 15.12 | 2.20 | 14.01 | 29.26 | 11.71 | 9.35 |
| Benzene, 2,4-dimethyl-1-(1-methylethyl)- | 148 | $C_{11}H_{16}$ | 15.28 | 3.08 | 19.10 | 33.68 | 15.60 | 9.69 |
| 1,4-Diethyl-2-methylbenzene | 148 | $C_{11}H_{16}$ | 15.36 | 0.76 | - | - | - | - |
| 3-Methylundecane | 170 | $C_{12}H_{26}$ | 15.45 | 0.98 | 15.40 | 27.36 | 13.04 | 15.10 |

| Compound Name | M+ | Formula | RT min | Gasoline mg/g | Ext Wax mg/g | WO450 mg/g | WO500 mg/g | WO550 mg/g |
|---|---|---|---|---|---|---|---|---|
| Undecane, 3-methyl- | 170 | $C_{12}H_{26}$ | 15.68 | - | 4.81 | 12.84 | 4.86 | 4.79 |
| Benzene, 1-methyl-4-(1-methyl-2-propenyl)- | 146 | $C_{11}H_{14}$ | 15.87 | 0.59 | - | - | - | - |
| Naphthalene | 128 | $C_{10}H_8$ | 15.99 | 6.45 | 3.20 | 26.52 | 2.58 | 9.58 |
| 1,1-Dimethylindan | 146 | $C_{11}H_{14}$ | 16 | 1.79 | 4.98 | 17.14 | 4.87 | 3.71 |
| 2,2-Dimethylindene, 2,3-dihydro- | 146 | $C_{11}H_{14}$ | 16.07 | 0.95 | - | 16.20 | 3.16 | 10.05 |
| Benzene, pentamethyl- | 148 | $C_{11}H_{16}$ | 16.3 | 3.68 | 20.30 | 40.77 | 15.76 | 5.66 |
| Benzene, 1,4-diethyl-2-methyl- | 148 | $C_{11}H_{16}$ | 16.39 | - | - | 12.19 | 4.77 | 8.34 |
| Benzene, 1,3-dimethyl-5-(1-methylethyl)- | 148 | $C_{11}H_{16}$ | 16.66 | - | - | 16.32 | 15.23 | 18.35 |
| Dodecane | 170 | $C_{12}H_{26}$ | 16.73 | - | 15.87 | 15.34 | 2.04 | 2.30 |
| Decane, 3,3,6-trimethyl- | 184 | $C_{13}H_{28}$ | 16.95 | - | 5.39 | 10.30 | 5.90 | 3.15 |
| Undecane, 3,8-dimethyl- | 184 | $C_{13}H_{28}$ | 17.14 | - | 7.87 | 10.43 | 6.91 | 2.31 |
| Undecane, 2,9-dimethyl- | 184 | $C_{13}H_{28}$ | 17.29 | - | 4.89 | 4.85 | 4.93 | 2.86 |
| 4,7-Dimethylindan | 146 | $C_{11}H_{14}$ | 17.78 | 2.42 | - | - | 2.70 | 2.51 |
| Dodecane, 6-methyl- | 184 | $C_{13}H_{28}$ | 17.81 | - | 6.39 | - | 5.08 | 4.91 |
| Undecane, 2,4-dimethyl- | 184 | $C_{13}H_{28}$ | 17.85 | - | 6.92 | 33.12 | 6.33 | 4.83 |
| Dodecane, 4-methyl- | 184 | $C_{13}H_{28}$ | 17.99 | - | 5.99 | 10.90 | 5.28 | 3.28 |
| Dodecane, 2-methyl- | 184 | $C_{13}H_{28}$ | 18.12 | - | 7.26 | 14.14 | 5.38 | 5.78 |
| 1,6-Dimethylindan | 146 | $C_{11}H_{14}$ | 18.17 | 1.04 | - | - | - | - |
| Dodecane, 3-methyl- | 184 | $C_{13}H_{28}$ | 18.3 | - | 6.58 | 14.30 | 5.04 | 5.35 |
| 3,4-Dimethylcumene | 148 | $C_{11}H_{16}$ | 18.68 | - | 5.77 | 26.82 | 5.43 | 3.65 |
| Naphthalene, 2-methyl- | 142 | $C_{11}H_{10}$ | 19.05 | 6.92 | 8.14 | 69.08 | 10.75 | 20.02 |
| Naphthalene, 1-methyl- | 142 | $C_{11}H_{10}$ | 19.51 | 2.94 | 12.52 | 36.25 | 6.66 | 11.57 |
| Tridecane, 6-methyl- | 198 | $C_{14}H_{30}$ | 20.46 | - | 4.91 | 7.81 | 3.40 | 3.52 |
| Tridecane, 5-methyl- | 198 | $C_{14}H_{30}$ | 20.54 | - | 3.51 | 3.38 | 2.22 | 1.19 |
| Tridecane, 4-methyl- | 198 | $C_{14}H_{30}$ | 20.67 | - | 3.51 | 3.29 | 1.90 | 2.45 |
| Tridecane, 2-methyl- | 198 | $C_{14}H_{30}$ | 20.8 | - | 4.54 | 7.31 | 2.74 | 2.27 |
| Tridecane, 3-methyl- | 198 | $C_{14}H_{30}$ | 20.98 | - | 4.33 | 10.86 | 2.83 | 3.15 |
| Naphthalene, 2-ethyl- | 156 | $C_{12}H_{12}$ | 21.71 | 0.68 | - | 13.02 | 1.01 | 6.84 |
| Tetradecane | 198 | $C_{14}H_{30}$ | 21.75 | - | 5.54 | 37.34 | 4.17 | 7.49 |
| Naphthalene, 2,6-dimethyl- | 156 | $C_{12}H_{12}$ | 21.97 | 0.84 | 8.89 | 28.47 | 7.75 | 9.91 |
| Naphthalene, 1,7-dimethyl- | 156 | $C_{12}H_{12}$ | 22.35 | 0.91 | 5.07 | 16.89 | 4.40 | 6.81 |
| Naphthalene, 1,5-dimethyl- | 156 | $C_{12}H_{12}$ | 22.44 | 0.45 | 3.25 | 10.98 | 2.77 | 3.90 |
| Naphthalene, 1,3-dimethyl- | 156 | $C_{12}H_{12}$ | 22.99 | - | 3.05 | 7.39 | 1.50 | 1.73 |
| Tetradecane, 4-methyl- | 212 | $C_{15}H_{32}$ | 23.21 | - | 1.80 | 4.59 | 1.99 | 2.62 |
| Tetradecane, 2-methyl- | 212 | $C_{15}H_{32}$ | 23.34 | - | 2.83 | 8.57 | 2.00 | 2.23 |
| Tetradecane, 3-methyl- | 212 | $C_{15}H_{32}$ | 23.52 | - | 2.07 | 4.95 | 1.47 | 5.52 |
| Pentadecane | 212 | $C_{15}H_{32}$ | 24.24 | - | 2.63 | 4.46 | 1.86 | 3.00 |

| Compound Name | M+ | Formula | RT min | Gasoline mg/g | Ext Wax mg/g | WO450 mg/g | WO500 mg/g | WO550 mg/g |
|---|---|---|---|---|---|---|---|---|
| Naphthalene, 2,3,6-trimethyl- | 170 | $C_{13}H_{14}$ | 25.02 | - | 2.58 | 9.54 | 2.45 | 2.27 |
| Naphthalene, 1,4,5-trimethyl- | 170 | $C_{13}H_{14}$ | 25.13 | - | 2.65 | 10.85 | 1.84 | 2.91 |
| Naphthalene, 1,6,7-trimethyl- | 170 | $C_{13}H_{14}$ | 25.52 | - | 2.54 | 10.29 | 2.15 | 2.92 |
| Naphthalene, 1,4,6-trimethyl- | 170 | $C_{13}H_{14}$ | 25.92 | - | 3.22 | 13.69 | 2.50 | 2.85 |
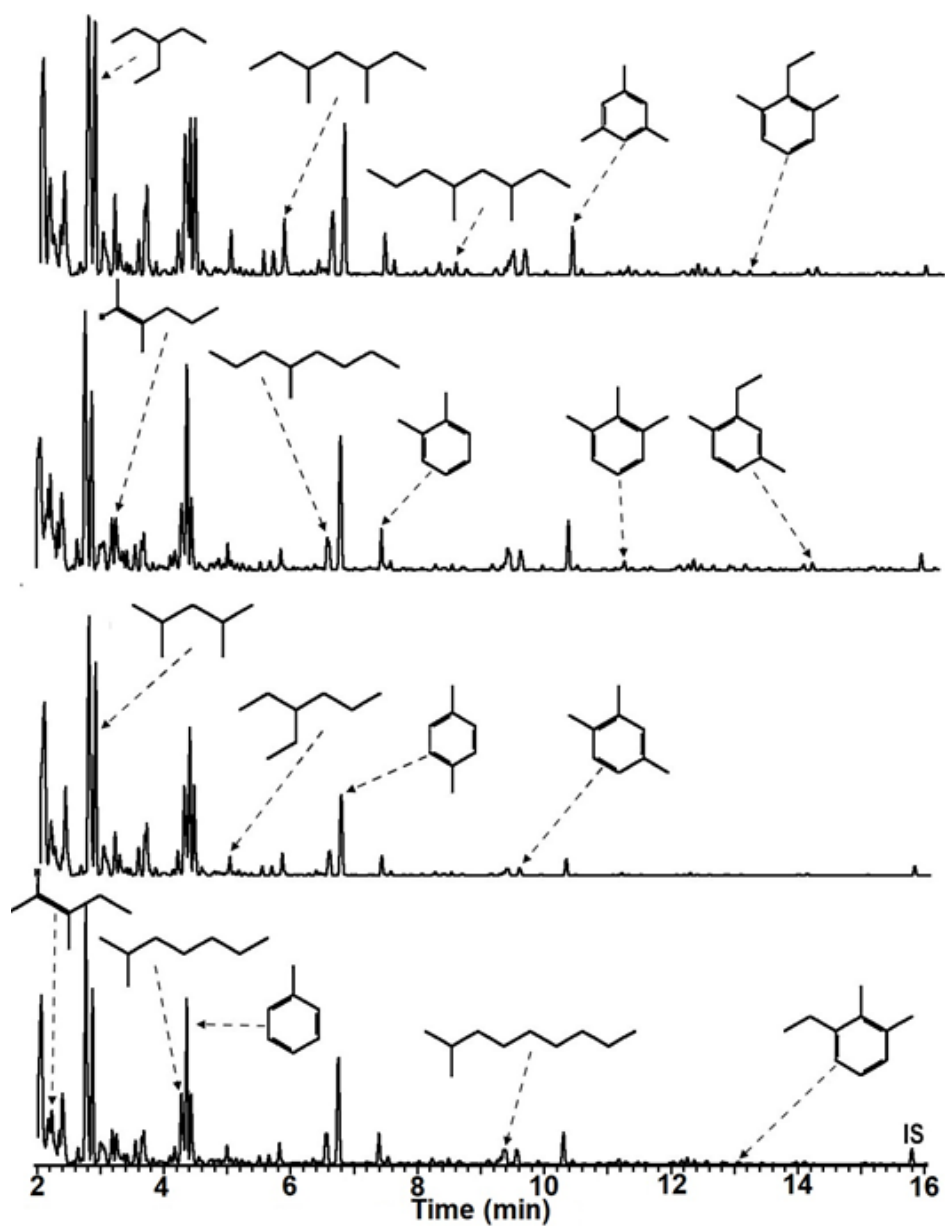
Figure 4.8. GC-MS Chromatograms of impinger trapped liquid products of catalytic pyrolysis of (a) solvent extracted wax-cat (b) WO450-cat, (c) WO500-cat, and (d) WO550-cat.

Table 4.6. Identified compounds in gasoline and the liquid products of catalytic pyrolysis of solvent extracted wax and wax-oil samples collected from the impinger.

| Compound Name | M+ | Formula | RT | Ext Wax mg/g | WO450 mg/g | WO500 mg/g | WO 550 mg/g |
|---|---|---|---|---|---|---|---|
| Pentane, 3-methyl- | 86 | $C_6H_{14}$ | 2.05 | 103.48 | 54.84 | 96.39 | 106.75 |
| 1-Hexene | 84 | $C_6H_{12}$ | 2.16 | 48.07 | 17.75 | 35.28 | 18.60 |
| 2-Pentene, 3-methyl- | 84 | $C_6H_{12}$ | 2.21 | - | 29.01 | 14.78 | 20.57 |
| Butane, 2,2,3-trimethyl- | 100 | $C_7H_{16}$ | 2.32 | 11.07 | 14.48 | 6.71 | 11.43 |
| Pentane, 2,4-dimethyl- | 100 | $C_7H_{16}$ | 2.38 | 42.75 | 44.38 | 56.13 | 36.56 |
| Cyclopropane, 1,1,2,3-tetramethyl- | 98 | $C_7H_{14}$ | 2.63 | 3.93 | 11.96 | 4.56 | 9.23 |
| Hexane, 2-methyl- | 100 | $C_7H_{16}$ | 2.75 | 126.58 | 150.24 | 166.22 | 158.87 |
| Pentane, 3-ethyl- | 100 | $C_7H_{16}$ | 2.85 | 90.95 | 81.43 | 107.92 | 90.78 |
| 1-Heptene, 4-methyl- | 112 | $C_8H_{16}$ | 2.98 | 24.57 | 10.65 | 28.10 | 15.86 |
| Cyclopentane, 1,2-dimethyl-, cis- | 98 | $C_7H_{14}$ | 3.04 | - | 16.12 | 5.37 | 17.10 |
| Heptane | 100 | $C_7H_{16}$ | 3.16 | 25.22 | 23.28 | 20.41 | 6.82 |
| 3-Hexene, 3-methyl-, (Z)- | 98 | $C_7H_{14}$ | 3.23 | 9.71 | 24.86 | 10.47 | 15.49 |
| 2-Hexene, 3-methyl-, (Z)- | 98 | $C_7H_{14}$ | 3.34 | 2.75 | 5.31 | 2.20 | 2.28 |
| 2-Pentene, 3,4-dimethyl-, (E)- | 98 | $C_7H_{14}$ | 3.4 | 2.62 | 7.96 | 2.36 | 3.73 |
| Cyclohexane, methyl- | 98 | $C_7H_{14}$ | 3.53 | 11.81 | 12.59 | 14.08 | 12.84 |
| Hexane, 2,5-dimethyl- | 114 | $C_8H_{18}$ | 3.62 | 16.60 | 9.73 | 13.05 | 11.01 |
| Hexane, 2,4-dimethyl- | 114 | $C_8H_{18}$ | 3.66 | 24.86 | 13.81 | 21.00 | 13.41 |
| Cyclopentane, 1,2,4-trimethyl- | 112 | $C_8H_{16}$ | 3.8 | 3.37 | 3.14 | 2.94 | 6.87 |
| 2-Pentene, 3-ethyl-2-methyl- | 112 | $C_8H_{16}$ | 4.07 | 2.52 | 5.91 | 2.32 | 3.75 |
| Hexane, 2,3-dimethyl- | 114 | $C_8H_{18}$ | 4.14 | 15.05 | 8.48 | 10.82 | 8.30 |
| Heptane, 2-methyl- | 114 | $C_8H_{18}$ | 4.25 | 60.89 | 34.11 | 48.03 | 40.40 |
| Toluene | 92 | $C_7H_8$ | 4.33 | 43.43 | 83.16 | 61.05 | 68.21 |
| Heptane, 3-methyl- | 114 | $C_8H_{18}$ | 4.41 | 52.59 | 33.32 | 43.63 | 35.26 |
| Cyclohexane, 1,3-dimethyl-, trans- | 112 | $C_8H_{16}$ | 4.52 | 5.61 | 2.74 | 4.00 | 4.33 |
| 2-Heptene, 6-methyl- | 112 | $C_8H_{16}$ | 4.7 | - | 2.40 | - | - |
| Cyclopentane, 1-ethyl-3-methyl-, cis | 112 | $C_8H_{16}$ | 4.72 | - | 1.32 | 0.74 | 3.57 |
| Cyclopentane, 1-ethyl-3-methyl-, trans- | 112 | $C_8H_{16}$ | 4.79 | - | 2.40 | 1.28 | 1.80 |
| Heptane, 4-methylene- | 112 | $C_8H_{16}$ | 4.83 | - | 3.77 | 1.43 | 1.70 |
| 3-Octene, (Z)- | 112 | $C_8H_{16}$ | 4.9 | - | 2.38 | 0.95 | 0.89 |
| Hexane, 3-ethyl- | 114 | $C_8H_{18}$ | 4.96 | 12.04 | 9.11 | 7.43 | 7.60 |
| 2-Methyl-2-heptene | 112 | $C_8H_{16}$ | 5.03 | 1.60 | 3.39 | 1.60 | 2.40 |
| Cyclohexane, 1,4-dimethyl- | 112 | $C_8H_{16}$ | 5.1 | 2.40 | 3.45 | 2.10 | 1.72 |
| 4-Octene, (E)- | 112 | $C_8H_{16}$ | 5.19 | 1.59 | 3.58 | 1.75 | 3.07 |
| Hexane, 2,3,5-trimethyl- | 128 | $C_9H_{20}$ | 5.3 | 1.29 | 1.79 | 0.99 | 2.48 |
| Heptane, 2,4-dimethyl- | 128 | $C_9H_{20}$ | 5.47 | 7.02 | 3.94 | 4.30 | 3.93 |
| Octane, 2-methyl- | 128 | $C_9H_{20}$ | 5.62 | 7.39 | 3.84 | 4.57 | 4.62 |
| Heptane, 3,5-dimethyl- | 128 | $C_9H_{20}$ | 5.79 | 19.62 | 9.57 | 11.70 | 11.89 |
| Hexane, 3-ethyl-2-methyl- | 128 | $C_9H_{20}$ | 6.08 | 0.98 | 1.07 | 51.84 | 0.62 |
| Cyclohexane, 1,2,4-trimethyl- | 126 | $C_9H_{18}$ | 6.21 | 1.02 | - | - | 2.68 |

| Compound Name | M+ | Formula | RT | Ext Wax mg/g | WO450 mg/g | WO500 mg/g | WO 550 mg/g |
|---|---|---|---|---|---|---|---|
| Heptane, 2,3-dimethyl- | 128 | $C_9H_{20}$ | 6.32 | 3.71 | - | 2.20 | 0.70 |
| Octane, 4-methyl- | 128 | $C_9H_{20}$ | 6.55 | 30.53 | 24.96 | 19.46 | 27.30 |
| p-Xylene | 106 | $C_8H_{10}$ | 6.73 | 54.97 | 68.21 | 44.73 | 63.50 |
| o-Xylene | 106 | $C_8H_{10}$ | 7.36 | 12.57 | 17.32 | 9.82 | 16.63 |
| Nonane | 128 | $C_9H_{20}$ | 7.5 | 4.35 | 4.69 | 2.33 | 4.39 |
| Cyclohexane, 1-ethyl-2-methyl-, cis- | 126 | $C_9H_{18}$ | 7.71 | 0.76 | 1.87 | 0.54 | 1.45 |
| Octane, 4-ethyl- | 142 | $C_{10}H_{22}$ | 7.83 | 1.25 | - | - | - |
| Heptane, 2,4,6-trimethyl- | 142 | $C_{10}H_{22}$ | 7.99 | 2.12 | 0.87 | 0.88 | 1.38 |
| Octane, 3,5-dimethyl- | 142 | $C_{10}H_{22}$ | 8.2 | 5.20 | 2.62 | 2.03 | 3.63 |
| Octane, 2,7-dimethyl- | 143 | $C_{10}H_{23}$ | 8.32 | 1.37 | 0.81 | 0.45 | 0.54 |
| Octane, 3-ethyl- | 144 | $C_{10}H_{24}$ | 8.35 | 1.49 | 0.96 | 1.28 | 2.89 |
| Octane, 2,6-dimethyl- | 142 | $C_{10}H_{22}$ | 8.46 | 3.69 | 2.51 | 1.62 | 3.53 |
| Nonane, 3-methyl- | 143 | $C_{10}H_{23}$ | 8.62 | 2.96 | 2.34 | 1.27 | 3.07 |
| Octane, 2,3-dimethyl- | 142 | $C_{10}H_{22}$ | 9.09 | 3.48 | 3.55 | 1.45 | 3.39 |
| Nonane, 5-methyl- | 142 | $C_{10}H_{22}$ | 9.23 | 1.87 | 0.90 | 0.76 | 1.65 |
| Nonane, 4-methyl- | 142 | $C_{10}H_{22}$ | 9.27 | 3.67 | 7.18 | 1.32 | 2.12 |
| Nonane, 2-methyl- | 142 | $C_{10}H_{22}$ | 9.36 | 12.50 | 6.44 | 6.22 | 14.78 |
| Benzene, 1,2,4-trimethyl- | 120 | $C_9H_{12}$ | 9.52 | 12.20 | 12.41 | 5.65 | 11.63 |
| Benzene, 1-ethyl-3-methyl- | 121 | $C_9H_{13}$ | 9.87 | 1.41 | 2.36 | 0.71 | 1.87 |
| Cyclodecane | 140 | $C_{10}H_{20}$ | 10 | 0.20 | 0.31 | 0.22 | 0.87 |
| Mesitylene | 120 | $C_9H_{12}$ | 10.27 | 15.95 | 25.56 | 8.81 | 18.16 |
| Decane | 140 | $C_{10}H_{20}$ | 10.41 | 1.88 | 2.56 | 0.68 | 2.23 |
| 5-Decene | 140 | $C_{10}H_{20}$ | 10.59 | - | 1.19 | - | 0.99 |
| Octane, 5-ethyl-2-methyl- | 156 | $C_{11}H_{24}$ | 10.82 | 1.25 | 1.18 | 0.43 | 1.18 |
| Decane, 4-methyl- | 156 | $C_{11}H_{24}$ | 11.01 | 1.20 | 1.07 | 0.40 | 1.02 |
| Nonane, 2,5-dimethyl- | 157 | $C_{11}H_{25}$ | 11.09 | 1.02 | - | 1.51 | 2.64 |
| Benzene, 1,2,3-trimethyl- | 120 | $C_9H_{12}$ | 11.14 | 2.53 | 5.04 | 2.83 | 6.30 |
| Nonane, 3,7-dimethyl- | 156 | $C_{11}H_{24}$ | 11.24 | 2.03 | 1.71 | 0.65 | 1.89 |
| Decane, 2,9-dimethyl- | 170 | $C_{12}H_{26}$ | 11.44 | 1.59 | 1.59 | 0.55 | 1.56 |
| Decane, 3-methyl- | 156 | $C_{11}H_{24}$ | 11.57 | 1.08 | 2.27 | 0.44 | 1.25 |
| Benzene, 1-methyl-3-propyl- | 134 | $C_{10}H_{14}$ | 12 | 1.40 | 2.43 | 1.64 | 3.75 |
| Decane, 5-methyl- | 156 | $C_{11}H_{24}$ | 12.13 | 2.07 | 2.89 | 0.74 | 1.40 |
| Benzene, 2-ethyl-1,4-dimethyl- | 134 | $C_{10}H_{14}$ | 12.22 | 3.73 | 5.22 | 1.42 | 2.46 |
| Decane, 2-methyl- | 156 | $C_{11}H_{24}$ | 12.33 | 2.09 | 2.48 | - | 3.87 |
| Undecane, 4-methyl- | 170 | $C_{12}H_{26}$ | 12.41 | 0.25 | 0.46 | 0.70 | 2.04 |
| 1-Undecene, 4-methyl- | 168 | $C_{12}H_{24}$ | 12.53 | 2.08 | 2.25 | 0.67 | 0.23 |
| o-Cymene | 134 | $C_{10}H_{14}$ | 12.78 | 1.34 | 2.58 | 0.52 | 2.06 |
| Benzene, 4-ethyl-1,2-dimethyl- | 134 | $C_{10}H_{14}$ | 12.83 | 0.93 | 1.59 | 0.40 | 1.22 |
| Benzene, 2-ethyl-1,3-dimethyl- | 134 | $C_{10}H_{14}$ | 13.02 | 1.69 | 3.79 | 0.67 | 0.95 |
| Undecane | 156 | $C_{11}H_{24}$ | 13.4 | 0.97 | 1.18 | 0.30 | 0.82 |
| Cyclopropane, 1-pentyl-2-propyl- | 154 | $C_{11}H_{22}$ | 13.57 | - | 1.31 | - | 1.76 |

| Compound Name | M+ | Formula | RT | Ext Wax mg/g | WO450 mg/g | WO500 mg/g | WO 550 mg/g |
|---|---|---|---|---|---|---|---|
| Benzene, 1,2,4,5-tetramethyl- | 134 | $C_{10}H_{14}$ | 13.93 | 2.69 | 3.47 | 1.07 | 2.00 |
| Benzene, 1-ethyl-3,5-dimethyl- | 134 | $C_{10}H_{14}$ | 14.06 | 2.86 | 4.15 | 1.05 | 0.52 |
| Benzene, 2-ethenyl-1,4-dimethyl- | 132 | $C_{10}H_{12}$ | 14.96 | - | 1.15 | 0.24 | 0.35 |
| Benzene, 1-ethyl-2,3-dimethyl- | 134 | $C_{10}H_{14}$ | 15.01 | 1.76 | 2.63 | 0.75 | 1.67 |
| 2,3-Dimethyldecane | 170 | $C_{12}H_{26}$ | 15.15 | 0.81 | 1.38 | 0.27 | 0.50 |
| Undecane, 2-methyl- | 170 | $C_{12}H_{26}$ | 15.27 | 1.11 | 1.33 | 0.40 | 0.55 |
| Undecane, 3-methyl- | 170 | $C_{12}H_{26}$ | 15.47 | 0.84 | 1.18 | 0.33 | 0.48 |
| Benzene, 1-methyl-4-(1-methylpropyl)- | 148 | $C_{11}H_{16}$ | 15.66 | - | 0.54 | 0.66 | 1.83 |
| 1H-Indene, 1-methylene- | 128 | $C_{10}H_8$ | 15.98 | - | 1.17 | - | - |
| Benzene, pentamethyl- | 148 | $C_{11}H_{16}$ | 16.32 | 1.20 | 1.95 | 0.44 | 1.59 |
| 1H-Indene, 1-ethylidene- | 142 | $C_{11}H_{10}$ | 19.08 | - | 1.13 | - | - |

Table 4.7. Yields (g/100g) of alkanes, olefins, aromatics, and oxygenated compounds in the pyrolysis (catalytic and non-catalytic) products from solvent extracted wax and wax-oil samples (WO450, WO500, WO550). The proportions are also shown for gasoline as a basis of comparison.

| | | | Alkanes (g/100 g) | Olefins (g/100 g) | Aromatics (g/100 g) | Oxygenated (g/100 g) |
|---|---|---|---|---|---|---|
| | | Gasoline | 47.37 | 4.00 | 48.64 | - |
| Catalytic Pyrolysis | U-Tube | ExtWax | 48.56 | 8.45 | 42.99 | - |
| | | WO450 | 48.08 | 4.26 | 47.65 | - |
| | | WO500 | 48.79 | 4.14 | 47.07 | - |
| | | WO550 | 53.05 | 7.05 | 39.90 | - |
| | Impinger | ExtWax | 74.38 | 9.55 | 16.07 | - |
| | | WO450 | 63.30 | 12.01 | 24.70 | - |
| | | WO500 | 75.53 | 10.18 | 14.29 | - |
| | | WO550 | 70.47 | 8.93 | 20.60 | - |
| Thermal Pyrolysis | U-Tube | ExtWax | 47.67 | 44.83 | - | 6.54 |
| | | WO450 | 65.10 | 29.50 | 0.15 | 5.24 |
| | | WO500 | 71.13 | 25.90 | 0.11 | 2.86 |
| | | WO550 | 56.92 | 37.96 | 0.04 | 5.08 |
| | Impinger | ExtWax | 24.52 | 71.05 | 1.13 | 4.25 |
| | | WO450 | 22.74 | 67.15 | 2.14 | 7.97 |
| | | WO500 | 14.97 | 66.11 | 5.09 | 13.82 |
| | | WO550 | 13.94 | 67.71 | 5.44 | 12.91 |

The liquid products of catalytic pyrolysis of solvent extracted wax, WO450, WO500 and WO550 with reused catalyst were near identical to those obtained using new zeolite Y (Figure 4.9-Figure 4.12). These findings confirm that the catalyst can effectively be reused to upgrade wax via catalytic pyrolysis.
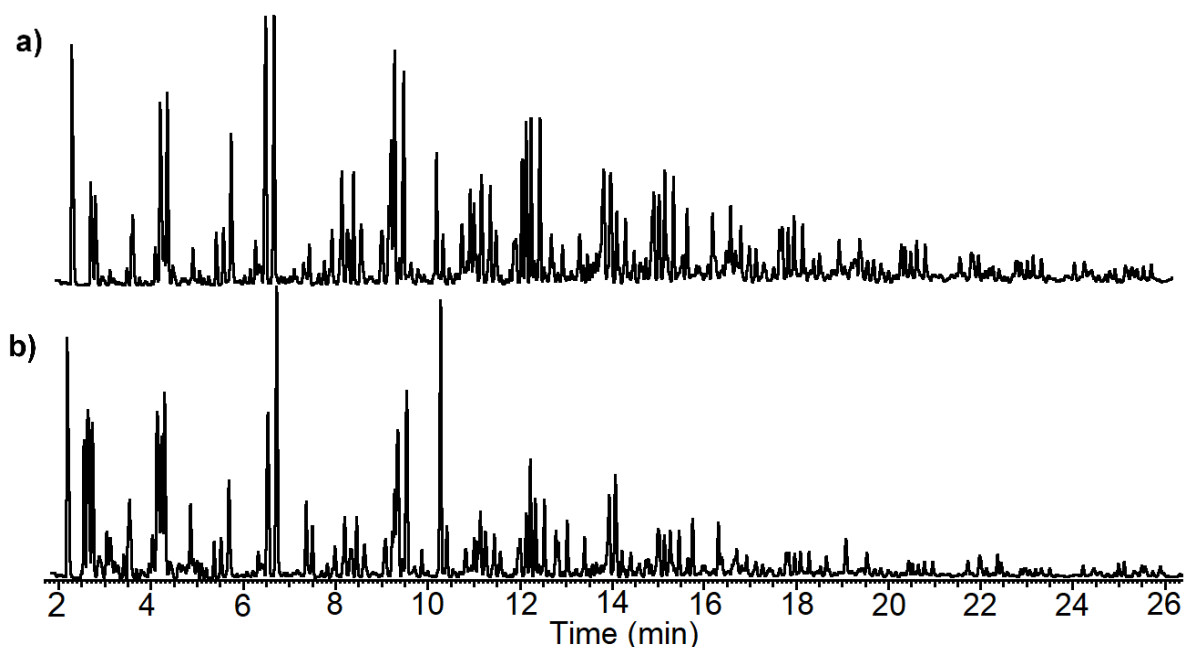


Figure 4.9. GC-MS Chromatograms of catalytic pyrolysis products of (a) solvent extracted wax-cat virgin, (b) solvent extracted wax-cat used.
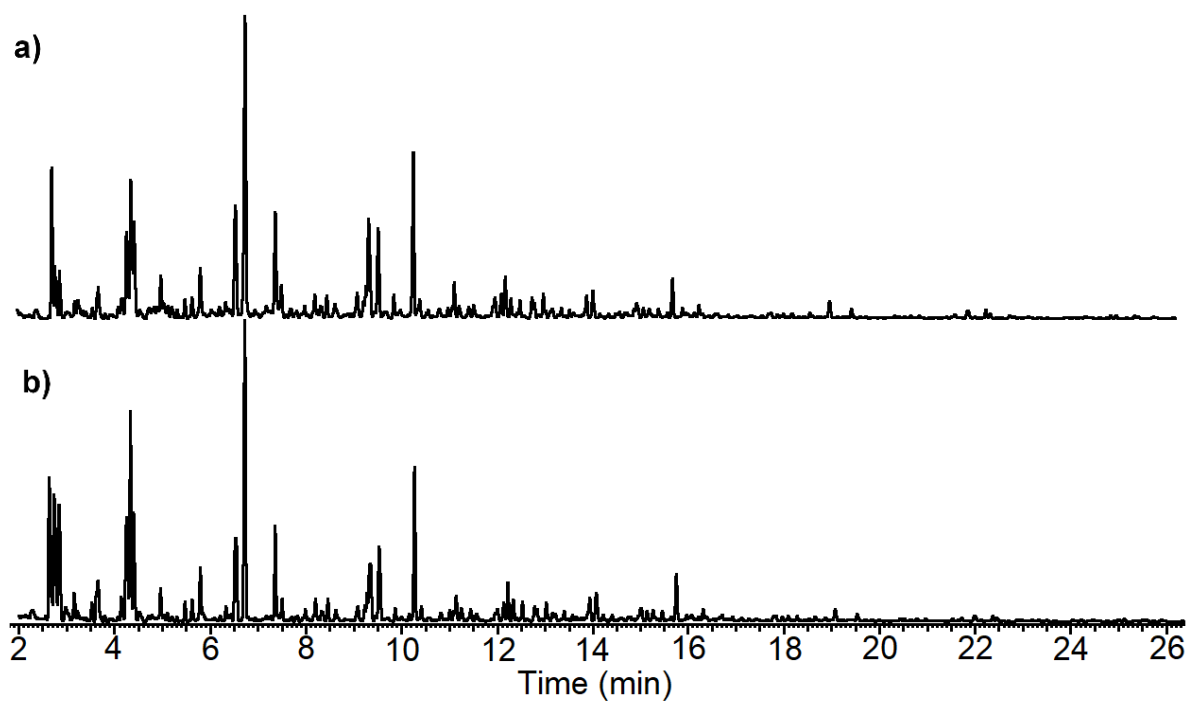
Figure 4.10. GC-MS Chromatograms of catalytic pyrolysis products of (a) WO450-cat virgin, (b) WO450-cat used.
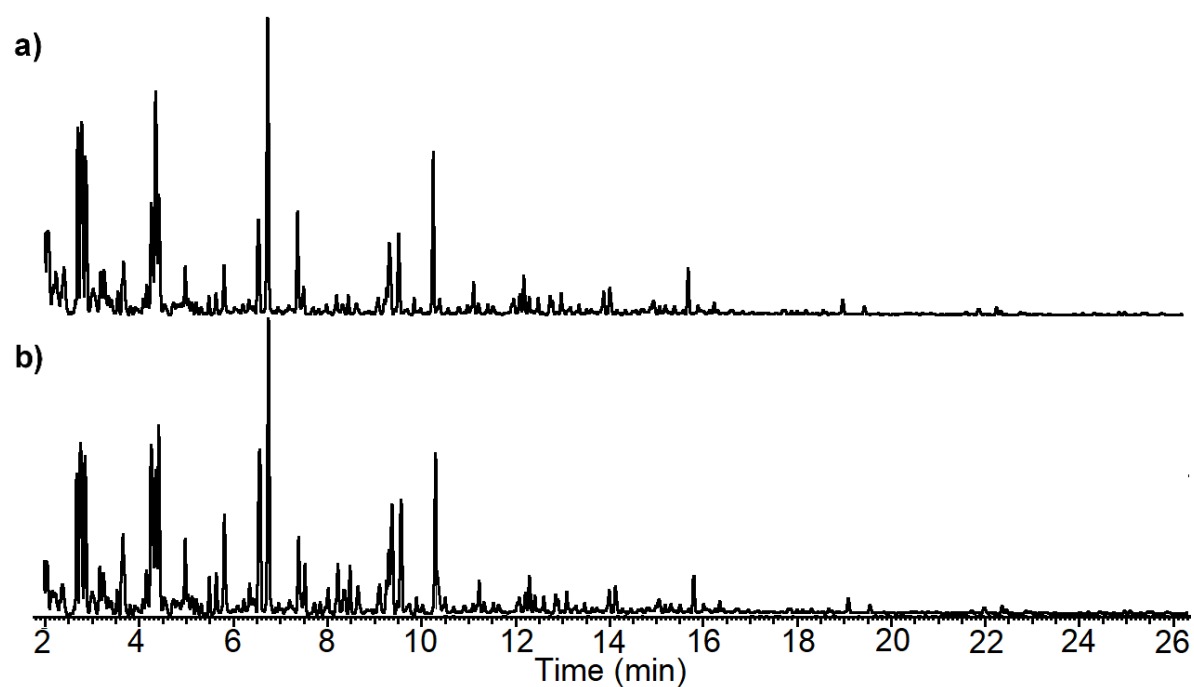


Figure 4.11. GC-MS Chromatograms of catalytic pyrolysis products of (a) WO500-cat virgin, (b) WO500-cat used.
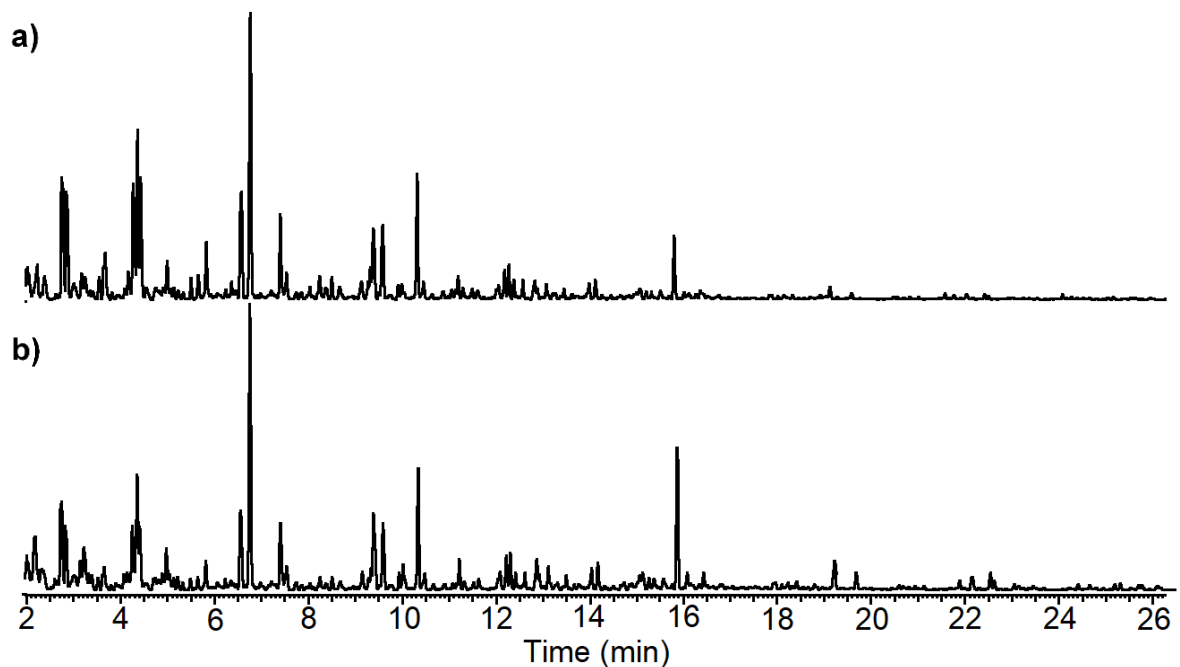
Figure 4.12. GC-MS Chromatograms of catalytic pyrolysis products of (a) WO550-cat virgin, (b) WO500-cat used.

### 4.4.5    Fourier Transform InfraRed Spectroscopy

FTIR analysis was performed to obtain chemical group information of the thermal and catalytic pyrolysis products of solvent-extracted wax and wax-oil samples (Figure 4.13). Band assignments for all samples are based on the literature and are given in Table 4.8. [182]–[188]. The authors had previously established that the wax-oil obtained from pyrolysis of waxed cardboard was similar in structure and chemical composition to paraffin [158]. FTIR spectra of thermal pyrolysis products (Figure 4.13 f-j) remained similar to that of paraffin, and the second round of thermal pyrolysis did not change the spectra. It appears that the thermal pyrolysis process has resulted in the disappearance of the O-H stretching vibrations (3600-3200 $cm^{-1}$) in all samples [107]. The bands around 2915 $cm^{-1}$ and 2847 $cm^{-1}$ in all samples confirm the existence of asymmetric and symmetric C-H stretching for aliphatic functional groups.

FTIR analysis of the liquid products of catalytic pyrolysis of solvent extracted wax and wax-oil samples revealed a high degree of similarity in chemical groups between the liquid products and gasoline (Figure 4.13 a-e). The bands present around 2960 $cm^{-1}$ and 2925 $cm^{-1}$

in gasoline and all liquid products are due to the asymmetric stretching of methyl (CH$_3$) and methylene (CH$_2$), respectively. While the intensity of the two bands is about the same for gasoline, the liquid product bands tend to be more intense for methylene stretching. The vibration band from 2875 to 2850 cm$^{-1}$ can be attributed to the coupled vibrations of symmetric stretching of the methyl and methylene groups. These bands are present in all liquid products at a higher intensity and with a small shoulder (for methylene stretches) compared to the one present in gasoline. The liquid products had lower intensities for all bands between 1375 to 1610 cm$^{-1}$. The band present around 1465 cm$^{-1}$ can be assigned to C-H deformations. The band at 1375 cm$^{-1}$ can be attributed to CH$_3$ symmetrical deformations, and the bands observed around 1608 cm$^{-1}$ can be attributed to aromatic C–C stretching vibrations [182], [186], [189]. Finally, the bands between 720 and 840 cm$^{-1}$ that have higher intensity in gasoline can mostly be attributed to the aromatic CH out of plane bending [186]. In contrast to the liquid products of catalytic pyrolysis, thermal pyrolysis products of extracted wax and wax-oil samples showed little resemblance in chemical groups to gasoline.
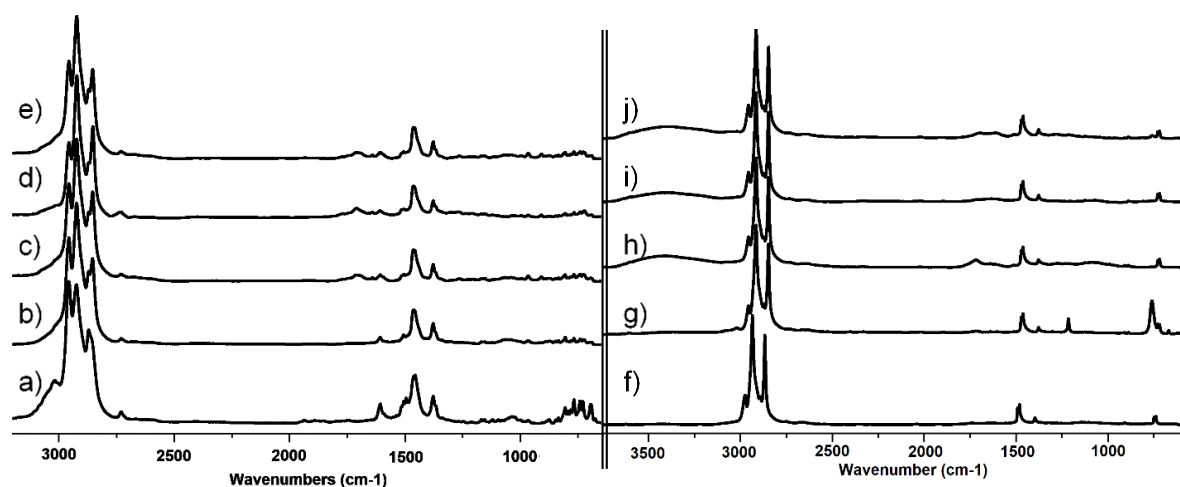


Figure 4.13. FTIR spectra of a) gasoline and liquid products of catalytic pyrolysis of b) extracted wax-cat, c) WO450-cat, d) WO500-cat, e) WO550-cat, f) paraffin and liquid products of thermal pyrolysis of g) solvent extracted wax- py, h) WO450-py, i) WO500-py, j) WO550-py.

Table 4.8. FTIR spectra band assignments for the products of thermal and catalytic pyrolysis of extracted wax and wax-oil samples (WO450, WO500, WO550) and gasoline and paraffin as bases of comparison.

| Bond/ Functional Group | Gasoline | Catalytic Pyrolysis | | | | Thermal Pyrolysis | | | | Paraffin |
|---|---|---|---|---|---|---|---|---|---|---|
| | | ExtWax | WO450 | WO500 | WO550 | ExtWax | WO450 | WO500 | WO550 | |
| Wavenumber ($cm^{-1}$) | | | | | | | | | | |
| =C-H Bend (Alkene) | | | | | | 719 | 719 | 719 | 719 | 719 |
| Aliphatic CH2 Rocking | 728 | 726 | 721 | 722 | 727 | 729 | 729 | 729 | 729 | 729 |
| =C-H Bend (Alkene) | 742 | 741 | 743 | 741 | 741 | | | | | |
| C-H "oop" aromatics | 768 | 768 | 768 | 768 | 768 | 761 | | | | |
| Aromatic C–H out of plane bending | 782 | 782 | 785 | 782 | 782 | | | | | |
| =C-H Bending Alkene | 795 | 795 | | 764 | 795 | | | | | |
| Aromatic C–H out of plane bending | 806 | 806 | 807 | 806 | 806 | | | | | |
| Aromatic C–H out of plane bending | 835 | 834 | 836 | 834 | 834 | | | | | |
| C H in-plane bending | | | | | | 1217 | | | | |
| CH$_3$ Symmetric bending | 1377 | 1378 | 1378 | 1378 | 1378 | 1378 | 1377 | 1378 | 1378 | 1377 |
| CH$_3$ asymmetric deformation | 1456 | 1463 | 1463 | 1464 | 1463 | 1462 | 1462 | 1462 | 1463 | 1462 |
| Aromatic skeletal vibration (C=C) | | | | | | 1472 | 1473 | 1472 | 1472 | 1472 |
| Aromatic skeletal vibration C–C | 1607 | 1608 | 1608 | 1608 | 1607 | | | | | |
| H–C=O: C–H stretch aldehydes | 2730 | 2730 | 2733 | 2735 | 2730 | | | | | |
| Aliphatic CH$_2$ Symmetric stretch | | 2854 | 2852 | 2853 | 2854 | 2847 | 2847 | 2847 | 2847 | 2847 |
| Aliphatic CH$_3$ Symmetric stretch | 2871 | 2872 | 2874 | 2871 | 2871 | | | | | |
| Aliphatic CH$_2$ Asymmetric Stretching | 2924 | 2923 | 2922 | 2922 | 2923 | 2915 | 2915 | 2915 | 2915 | 2915 |
| Aliphatic CH$_3$ Asymmetric Stretching | 2956 | 2956 | 2956 | 2956 | 2956 | 2956 | 2955 | 2956 | 2956 | 2956 |

### 4.4.6   Electrospray Ionization Mass Spectrometry

Negative ion ESI-MS was carried out to measure the molar mass distribution of compounds (volatile and non-volatile) in the liquid products obtained from thermal and catalytic pyrolysis of extracted wax and wax-oil samples (Figure 4.14). The calculated $M_w$ and $M_n$ obtained in duplicate for all samples are given in Table 4.9. In the thermal pyrolysis products, significant [M-H]$^-$ peaks were observed at 123, 137, 149, 161, 163, 177, 191 $m/z$ (tentatively assigned to guaiacol, creosol, vinyl guaiacol, levoglucosan, eugenol/isoeugenol, coniferyl aldehyde, and $C_{11}H_{12}O_3$, respectively). These compounds are derived from the cardboard portion of the original waxed cardboard and remained in the chemical composition of the wax-oil samples after the second round of pyrolysis [40], [147], [158]. A closer look at the

spectra for $100 < m/z < 300$ revealed the presence of series of ions ($m/z$ 14 apart) corresponding to hydrocarbon dienes from $C_8$ ($m/z$= 109) to $C_{19}$ ($m/z = 263$); alkenes from $C_8$ ($m/z$= 111) to $C_{21}$ ($m/z = 293$); and alkanes from $C_9$ ($m/z$= 125) to $C_{21}$ ($m/z = 295$) were also detected. The results are similar to those reported by the authors for pyrolysis products of waxed cardboard [158]. In contrast to the products of thermal pyrolysis, products of catalytic pyrolysis did not have any peaks for oxygenated compounds or dienes. Instead, in the $100 < m/z < 300$ range, the products had significant peaks in a series for aromatics from $C_8$ ($m/z$= 105) to $C_{13}$ ($m/z = 175$); alkanes $C_7$ ($m/z$= 101) to $C_{15}$ ($m/z = 211$); and alkenes from $C_8$ ($m/z$= 111) to $C_{10}$ ($m/z = 139$). It should be noted that some important compounds, such as benzene and toluene, fall below the $100 < m/z$ range analyzed. The ESI-MS data confirmed that catalytic pyrolysis resulted in a more drastic breakdown of aliphatic compounds into short-chain hydrocarbons and aromatics compared to thermal pyrolysis.

The $M_w$, $M_n$, and monomer to oligomer ratio of thermal and catalytic pyrolysis products are reported in Table 4.9. It should be noted that the $M_w$ and $M_n$ values of samples WO450, WO500, and WO550 (before pyrolysis) were from a previous study [158]. The $M_n$ of all samples decreased by an average of 13% and 19% after thermal and catalytic pyrolysis, respectively. A decrease in average molar mass is the result of thermal degradation and samples' reaction with the catalyst [67]. An estimate of monomer ($\Sigma$ $m/z$ 100-300) to oligomer ($\Sigma$ $m/z$ 301-2000) compounds was calculated from ion intensities (Table 4.9). The ranges were arbitrarily decided as indicative of low and high molar mass [40]. The difference between thermal and catalytic pyrolysis products was more pronounced for the change in monomer to oligomer ratio. While thermal pyrolysis products' monomer to oligomer ratio increased by about 30%, catalytic pyrolysis products' ratio increased more than twice as much by 68%. This higher ratio is the result of the extensive breakdown of larger hydrocarbons to short-chain alkanes and small aromatic compounds facilitated by zeolite Y during catalytic pyrolysis.

Table 4.9. Weight (Mw) and number average molar mass (Mn) of thermal pyrolysis and catalytic pyrolysis of extracted wax and wax-oil samples (WO450, WO500, WO550) determined from negative ion ESI-MS data.

| Sample | Original material [158] | | | After Thermal Pyrolysis | | | After Catalytic Pyrolysis | | |
|---|---|---|---|---|---|---|---|---|---|
| | $M_n$ (g mol$^{-1}$) | $M_w$ (g mol$^{-1}$) | Monomer /Oligomer | $M_n$ (g mol$^{-1}$) | $M_w$ (g mol$^{-1}$) | Monomer /Oligomer | $M_n$ (g mol$^{-1}$) | $M_w$ (g mol$^{-1}$) | Monomer /Oligomer |
| Extracted Wax | 850 | 1077 | 0.11 | 858 | 1086 | 0.11 | 833 | 1055 | 0.12 |
| WO450 | 733 | 975 | 0.22 | 659 | 909 | 0.22 | 547 | 762 | 0.34 |
| WO500 | 731 | 971 | 0.22 | 572 | 819 | 0.36 | 558 | 813 | 0.44 |
| WO550 | 693 | 948 | 0.31 | 557 | 843 | 0.49 | 522 | 797 | 0.64 |
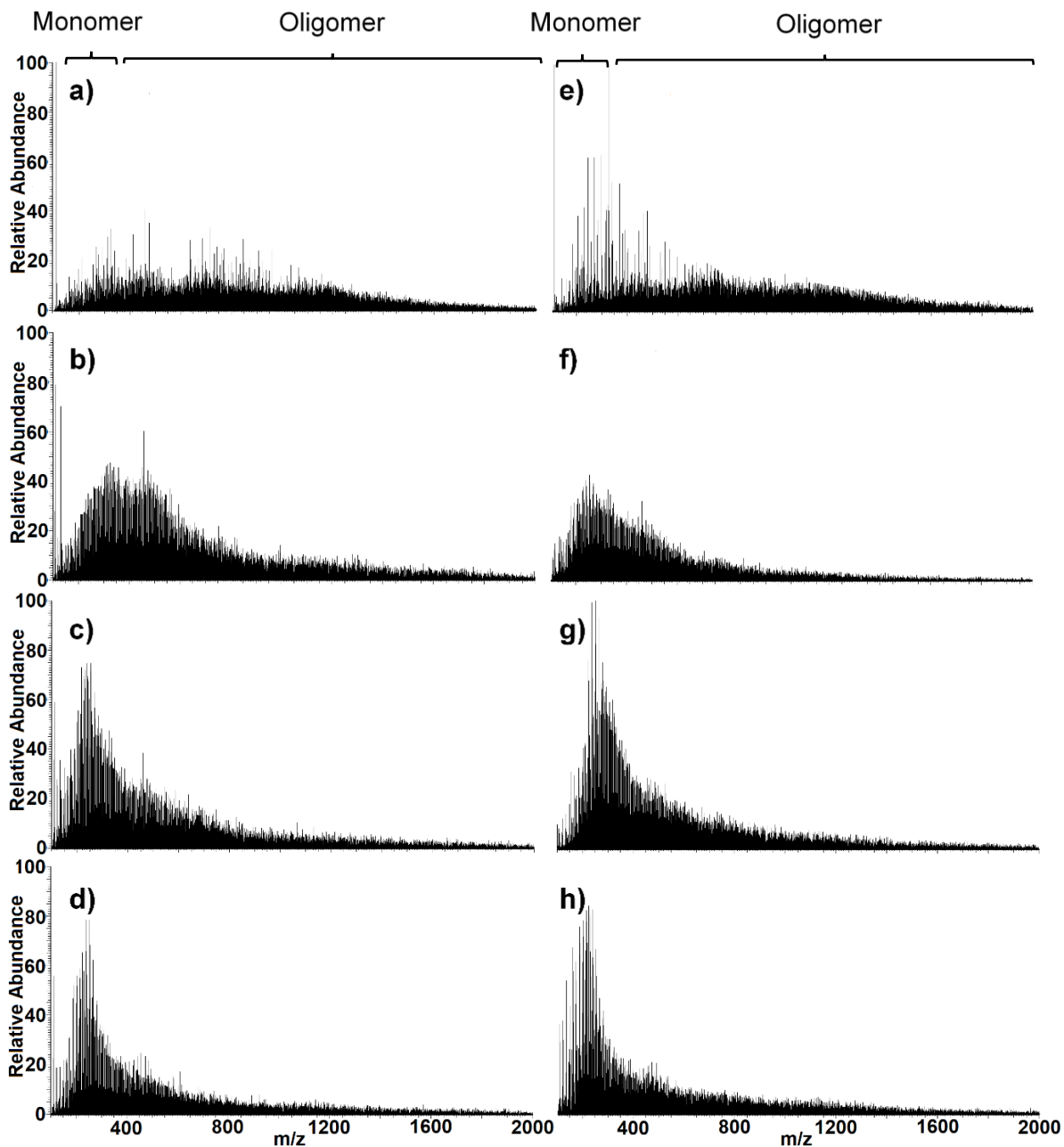
Figure 4.14. Negative-ion ESI-MS spectra of the products of thermal pyrolysis of (a) solvent extracted wax-py, (b) WO450-py, (c) WO500-py, (d) WO550-py, and liquid products of catalytic pyrolysis of (e) solvent extracted wax-cat, (f) WO450-cat, (g) WO500-cat, (h) WO550-cat.

## 4.5    Conclusion

Wax-oil was successfully obtained by pyrolysis of unrecyclable waxed corrugated cardboard and subsequently upgraded catalytically and non-catalytically to produce a liquid fuel. A small tubular batch reactor was employed to screen process conditions (temperature, addition of catalyst, and reuse of catalyst) and thermally and catalytically pyrolyze solvent-extracted wax and wax-oil samples obtained from waxed cardboard. The resultant liquid products were then characterized and analyzed against gasoline to evaluate their performance as a transport fuel. Thermal pyrolysis liquid products contained an abundance of dienes and short-chain olefins. Their functional groups remained similar to those found in paraffin. The absence of aromatic compounds and the presence of oxygenated compounds made them less desirable for consideration as a liquid fuel, except as bunker fuel. The catalytic pyrolysis liquid products were similar to gasoline in chemical composition and functional groups and could be used as a "drop in" fuel. The addition of zeolite Y as the catalyst facilitated the conversion of long-chain hydrocarbons to short-chain alkanes and aromatics. The catalyst was able to be recovered and reused and this is an important feature for industrial use in catalytic pyrolysis.

## Chapter 5. Conclusion

### 5.1 Summary

The rapid growth of the human population necessitates the development of novel ways to process massive amounts of municipal solid waste (MSW) created every day and to harvest products and energy where possible to ensure sufficient energy sources for the future. Cardboard products, including waxed cardboard, comprise a substantial portion of landfilled municipal solid waste and have great value creation potential. In this dissertation, we developed laboratory-scale "waste-to-product" and "waste-to-energy" pathways using pyrolysis for cardboard and waxed cardboard.

We collected cardboard samples from the University of Idaho recycling center, pyrolyzed them at various temperatures on an auger reactor, and characterized the products. The liquid products found were oxygenated and acidic and more suitable to be used as a heating oil. The pyrolysis process resulted in the generation of many compounds such as acids, alcohols, levoglucosan and phenols, which may be refined. For example, the abundantly found levoglucosan could be isolated and used as a tracer compound to determine smoke distribution or fermented into bio-ethanol. The cardboard biochar had low levels of nitrogen and ash. The biochar hydrophobicity and thermal stability make it a viable candidate for use as a reinforcing fiber in composite materials or use as a soil amendment (Figure 5.1).

Many studies had shown that co-pyrolysis of lignocellulosic biomass and polymers resulted in higher quality liquid pyrolysis products. Using non-recyclable waxed cardboard, a rich feedstock in hydrocarbons, it was postulated that the wax could be recovered by pyrolysis, a solvent free extraction process. Studies had shown that wax could be effectively recovered, and pyrolysis is a promising technology for wax extraction/recovery. Higher pyrolysis temperatures resulted in increased cracking, and subsequently in a higher proportion of smaller hydrocarbon fragments. Since the char was mostly the product of the lignocellulosic
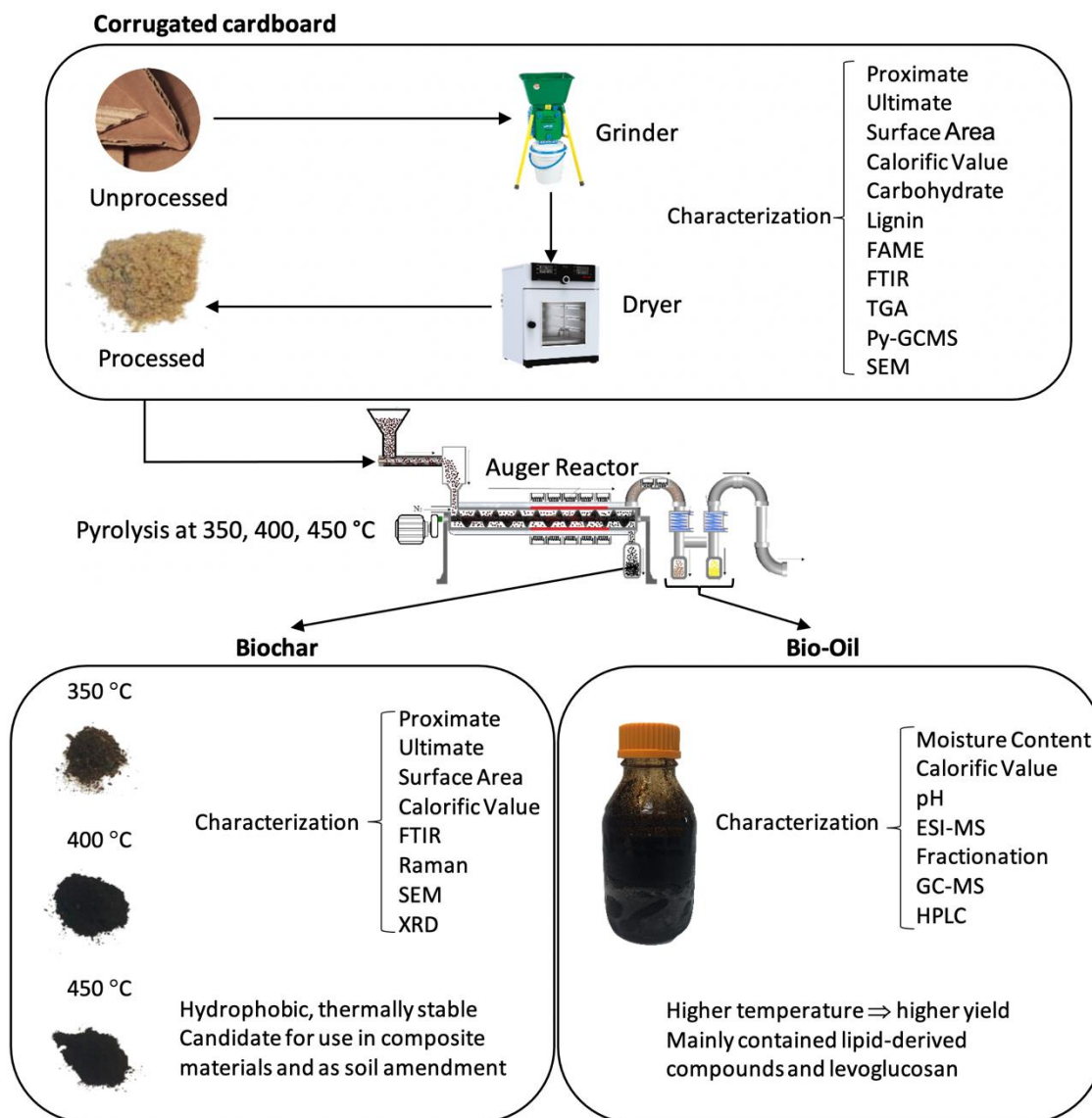
Figure 5.1. Summary of Chapter 2: corrugated cardboard processing.

portion of our feedstock, we found the fibers suitable for use in composite products. The recovered wax composition and structure was similar to those of paraffin and showed great potential for catalytic upgrading to produce transportation fuels (Figure 5.2).

Finally, the recovered wax from WCCB was evaluated as a feedstock for producing liquid transportation fuel. A custom-built tubular batch reactor was used to screen process conditions (temperature) during the thermal and catalytic pyrolysis. The characterized liquid products were dienes and short-chain olefins from pyrolysis. The absence of aromatic compounds and the presence of oxygenated compounds made them less desirable for

consideration as a liquid fuel but suitable for use as bunker fuel. The products from catalytic pyrolysis using zeolite Y included aromatics and were similar to those found gasoline. The liquid product could potentially be used as a "drop in" fuel. The addition of zeolite Y as the catalyst facilitated the conversion of long-chain hydrocarbons to short-chain alkanes and aromatics. We were able to recover the catalyst and reuse it multiple times to generate the same products. This is an important feature for industrial use in catalytic pyrolysis (Figure 5.2).

## 5.2  Future Work

This study has proven the feasibility of the pyrolysis process for recovering products and energy from cardboard and waxed cardboard in laboratory-scale. Future work will focus on designing and building a reactor that can accomplish similar results in large scale. The results suggest that a large-scale, efficient reactor may be able to recover high-quality liquid fuel from waxed cardboard through a series of pyrolysis processes (thermal and catalytic). Plastic waste is also a viable feedstock that needs to be investigated since it has a high carbon content. The resultant fuel can then be evaluated on engine combustion and ignition properties, such as high heating value, and emission characteristics. This system could be set up in distributed facilities to produce fuel locally from local waste streams.

It is, however, important that the life cycle of the process be assessed properly and the technoeconomics analyzed to evaluate the economic and environmental impacts as well as the feasibility of a processing plant.
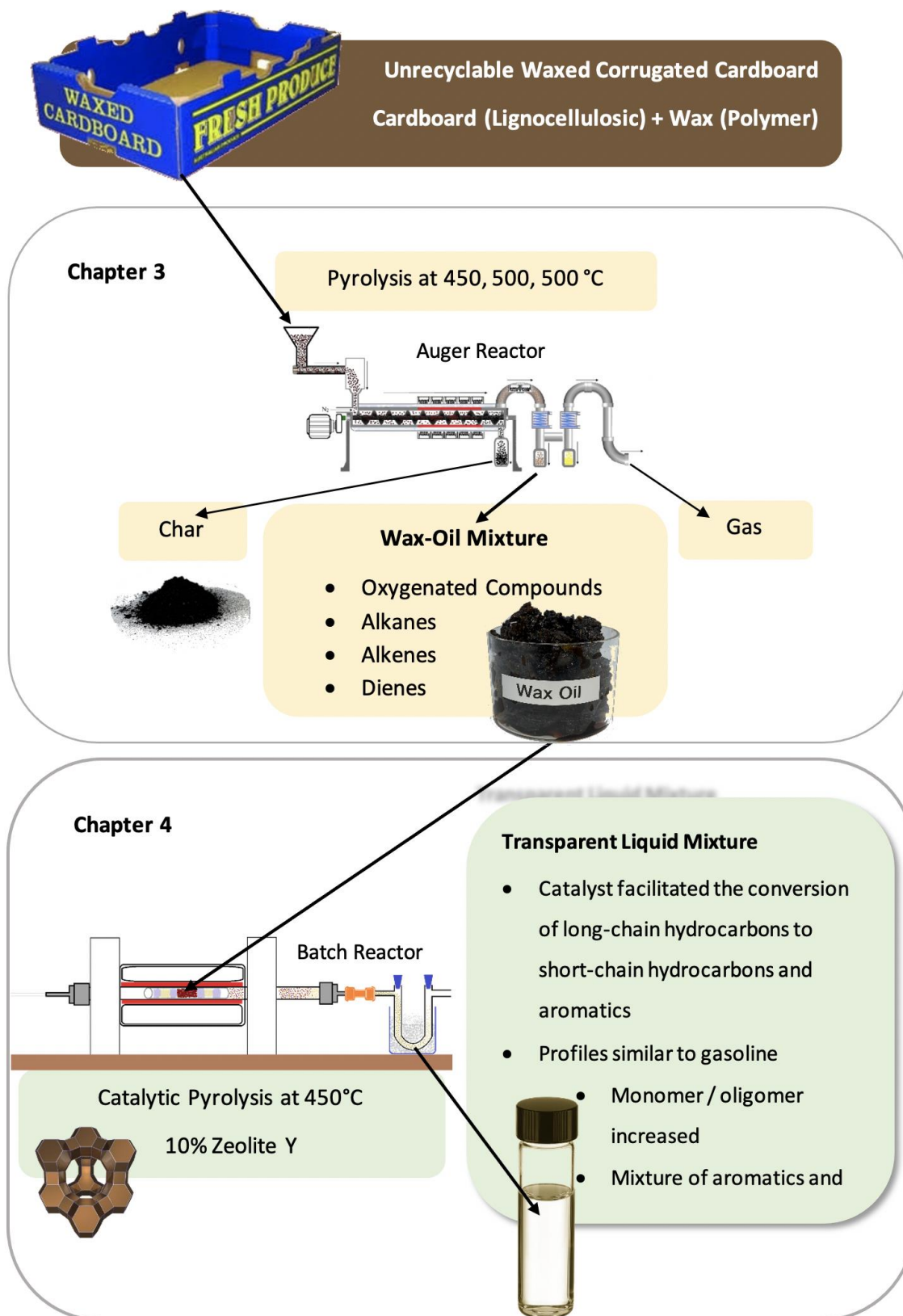
Figure 5.2. Summary of Chapters 3 and 4: waxed cardboard processing and catalytic upgrading.

# References

[1]     K. O. Zacho, M. Mosgaard, and H. Riisgaard, "Capturing uncaptured values — A Danish case study on municipal preparation for reuse and recycling of waste," *Resources, Conservation and Recycling*, vol. 136, pp. 297–305, 2018, doi: https://doi.org/10.1016/j.resconrec.2018.04.031.

[2]     A. S. Nizami *et al.*, "Developing waste biorefinery in Makkah: A way forward to convert urban waste into renewable energy," *Applied Energy*, vol. 186, pp. 189–196, Jan. 2017, doi: 10.1016/j.apenergy.2016.04.116.

[3]     L. Sørum, M. G. Grønli, and J. E. Hustad, "Pyrolysis characteristics and kinetics of municipal solid wastes," *Fuel*, vol. 80, no. 9, pp. 1217–1227, Jul. 2001, doi: 10.1016/S0016-2361(00)00218-0.

[4]     O. US EPA, "Paper and Paperboard: Material-Specific Data," *US EPA*, Sep. 07, 2017. https://www.epa.gov/facts-and-figures-about-materials-waste-and-recycling/paper-and-paperboard-material-specific-data (accessed Feb. 08, 2020).

[5]     "PAPER RECYCLING SUPPLEMENT - Unwelcome Wax," *Recycling Today*. https://www.recyclingtoday.com/article/paper-recycling-supplement---unwelcome-wax/ (accessed Feb. 08, 2020).

[6]     "How to Recycle Waxed Cardboard," *Earth 911*. https://earth911.com/recycling-guide/how-to-recycle-waxed-cardboard/ (accessed Mar. 13, 2021).

[7]     "IGI Wax: - Packaging Wax and Corrugated Wax Manufacturer and Supplier," *The International Group*. https://igiwax.com/packaging-corrugated-wax/ (accessed Mar. 01, 2020).

[8]     N. Touze-Foltz, H. Xie, and G. Stoltz, "Performance issues of barrier systems for landfills: A review," *Geotextiles and Geomembranes*, vol. 49, no. 2, pp. 475–488, Apr. 2021, doi: 10.1016/j.geotexmem.2020.10.016.

[9]     "EIA projects nearly 50% increase in world energy usage by 2050, led by growth in Asia - Today in Energy - U.S. Energy Information Administration (EIA)." https://www.eia.gov/todayinenergy/detail.php?id=41433 (accessed Mar. 13, 2021).

[10]    E. S. Shuba and D. Kifle, "Microalgae to biofuels: 'Promising' alternative and renewable energy, review," *Renewable and Sustainable Energy Reviews*, vol. 81, no. Part 1, pp. 743–755, 2018, doi: https://doi.org/10.1016/j.rser.2017.08.042.

[11] "Waste-to-Energy," *Energy.gov*. https://www.energy.gov/eere/bioenergy/waste-energy (accessed Mar. 13, 2021).

[12] "Waste to Energy Projects | Sindicatum." https://sindicatum.com/sindicatum-renewable-energy/waste-to-energy-projects/ (accessed Mar. 13, 2021).

[13] "Types of Cardboard and Cardboard Box Material." https://www.thomasnet.com/articles/materials-handling/types-of-cardboard-and-corrugated-boxes (accessed Mar. 13, 2021).

[14] M. Ioelovich, "Waste Paper as Promising Feedstock for Production of Biofuel," *Journal of Scientific Research and Reports*, vol. 3. Feb. 22, 2014, doi: 10.9734/JSRR/2014/8025.

[15] D. Glushkov, K. Paushkina, D. Shabardin, and P. Strizhak, "Environmental aspects of converting municipal solid waste into energy as part of composite fuels," *Journal of Cleaner Production*, vol. 201, pp. 1029–1042, 2018, doi: https://doi.org/10.1016/j.jclepro.2018.08.126.

[16] S. V. Vassilev, C. G. Vassileva, and V. S. Vassilev, "Advantages and disadvantages of composition and properties of biomass in comparison with coal: An overview," *Fuel*, vol. 158, pp. 330–350, Oct. 2015, doi: 10.1016/j.fuel.2015.05.050.

[17] M. Mladenović, M. Paprika, and A. Marinković, "Denitrification techniques for biomass combustion," *Renewable and Sustainable Energy Reviews*, vol. 82, pp. 3350–3364, Feb. 2018, doi: 10.1016/j.rser.2017.10.054.

[18] E. Houshfar *et al.*, "NOx emission reduction by staged combustion in grate combustion of biomass fuels and fuel mixtures," *Fuel*, vol. 98, pp. 29–40, Aug. 2012, doi: 10.1016/j.fuel.2012.03.044.

[19] H. Gu, Y. Tang, J. Yao, and F. Chen, "Study on biomass gasification under various operating conditions," *Journal of the Energy Institute*, Oct. 2018, doi: 10.1016/j.joei.2018.10.002.

[20] J. Karl and T. Pröll, "Steam gasification of biomass in dual fluidized bed gasifiers: A review," *Renewable and Sustainable Energy Reviews*, vol. 98, pp. 64–78, Dec. 2018, doi: 10.1016/j.rser.2018.09.010.

[21] A. Seçer, N. Küçet, E. Fakı, and A. Hasanoğlu, "Comparison of co–gasification efficiencies of coal, lignocellulosic biomass and biomass hydrolysate for high yield hydrogen production," *International Journal of Hydrogen Energy*, Oct. 2018, doi: 10.1016/j.ijhydene.2018.09.144.

[22] D. Saebea, P. Ruengrit, A. Arpornwichanop, and Y. Patcharavorachot, "Gasification of plastic waste for synthesis gas production," *Energy Reports*, vol. 6, pp. 202–207, Feb. 2020, doi: 10.1016/j.egyr.2019.08.043.

[23] G. Chen *et al.*, "Gasification of lignocellulosic biomass pretreated by anaerobic digestion (AD) process: An experimental study," *Fuel*, vol. 247, pp. 324–333, Jul. 2019, doi: 10.1016/j.fuel.2019.03.002.

[24] A. R. K. Gollakota, N. Kishore, and S. Gu, "A review on hydrothermal liquefaction of biomass," *Renewable and Sustainable Energy Reviews*, vol. 81, pp. 1378–1392, Jan. 2018, doi: 10.1016/j.rser.2017.05.178.

[25] S. S. Toor, L. Rosendahl, and A. Rudolf, "Hydrothermal liquefaction of biomass: A review of subcritical water technologies," *Energy*, vol. 36, no. 5, pp. 2328–2342, May 2011, doi: 10.1016/j.energy.2011.03.013.

[26] B. de Caprariis, P. De Filippis, A. Petrullo, and M. Scarsella, "Hydrothermal liquefaction of biomass: Influence of temperature and biomass composition on the bio-oil production," *Fuel*, vol. 208, pp. 618–625, Nov. 2017, doi: 10.1016/j.fuel.2017.07.054.

[27] M. S. Seshasayee and P. E. Savage, "Oil from plastic via hydrothermal liquefaction: Production and characterization," *Applied Energy*, vol. 278, p. 115673, Nov. 2020, doi: 10.1016/j.apenergy.2020.115673.

[28] X. Miao, Q. Wu, and C. Yang, "Fast pyrolysis of microalgae to produce renewable fuels," *Journal of Analytical and Applied Pyrolysis*, vol. 71, no. 2, pp. 855–863, 2004, doi: https://doi.org/10.1016/j.jaap.2003.11.004.

[29] L. Ma, T. Wang, Q. Liu, X. Zhang, W. Ma, and Q. Zhang, "A review of thermal–chemical conversion of lignocellulosic biomass in China," *Biotechnology Advances*, vol. 30, no. 4, pp. 859–873, Jul. 2012, doi: 10.1016/j.biotechadv.2012.01.016.

[30] E. S. Shuba and D. Kifle, "Microalgae to biofuels: 'Promising' alternative and renewable energy, review," *Renewable and Sustainable Energy Reviews*, vol. 81, pp. 743–755, Jan. 2018, doi: 10.1016/j.rser.2017.08.042.

[31] "Production and characterization of bio-oil and biochar from the pyrolysis of residual bacterial biomass from a polyhydroxyalkanoate production process - ScienceDirect." https://www.sciencedirect.com/science/article/pii/S0165237015301091 (accessed Oct. 20, 2018).

[32] C. Zhou, W. Yang, and W. Blasiak, "Characteristics of waste printing paper and cardboard in a reactor pyrolyzed by preheated agents," *Fuel Processing Technology*, vol. 116, pp. 63–71, 2013, doi: https://doi.org/10.1016/j.fuproc.2013.04.023.

[33] P. Rutkowski, "Characteristics of bio-oil obtained by catalytic pyrolysis of beverage carton packaging waste," *Journal of Analytical and Applied Pyrolysis*, vol. 104, pp. 609–617, 2013, doi: https://doi.org/10.1016/j.jaap.2013.05.006.

[34] H. Raclavská *et al.*, "Possibilities of the utilization of char from the pyrolysis of tetrapak," *Journal of Environmental Management*, vol. 219, pp. 231–238, 2018, doi: https://doi.org/10.1016/j.jenvman.2018.05.002.

[35] A. N. Phan, C. Ryu, V. N. Sharifi, and J. Swithenbank, "Characterisation of slow pyrolysis products from segregated wastes for energy production," *Journal of Analytical and Applied Pyrolysis*, vol. 81, no. 1, pp. 65–71, Jan. 2008, doi: 10.1016/j.jaap.2007.09.001.

[36] X. Wang, Z. Yu, and A. G. McDonald, "Effect of Different Reinforcing Fillers on Properties, Interfacial Compatibility and Weatherability of Wood-plastic Composites," *J Bionic Eng*, vol. 16, no. 2, pp. 337–353, Mar. 2019, doi: 10.1007/s42235-019-0029-0.

[37] R. Miandad, M. Rehan, A.-S. Nizami, M. A. El-Fetouh Barakat, and I. M. Ismail, "The Energy and Value-Added Products from Pyrolysis of Waste Plastics," in *Recycling of Solid Waste for Biofuels and Bio-chemicals*, O. P. Karthikeyan, K. Heimann, and S. S. Muthu, Eds. Singapore: Springer, 2016, pp. 333–355.

[38] W. Chen, S. Shi, J. Zhang, M. Chen, and X. Zhou, "Co-pyrolysis of waste newspaper with high-density polyethylene: Synergistic effect and oil characterization," *Energy Conversion and Management*, vol. 112, pp. 41–48, Mar. 2016, doi: 10.1016/j.enconman.2016.01.005.

[39] F. Paradela, F. Pinto, A. M. Ramos, I. Gulyurtlu, and I. Cabrita, "Study of the slow batch pyrolysis of mixtures of plastics, tyres and forestry biomass wastes," *Journal of Analytical and Applied Pyrolysis*, vol. 85, no. 1, pp. 392–398, May 2009, doi: 10.1016/j.jaap.2008.09.003.

[40] F. Sotoudehnia, A. Baba Rabiu, A. Alayat, and A. G. McDonald, "Characterization of bio-oil and biochar from pyrolysis of waste corrugated cardboard," *Journal of Analytical and Applied Pyrolysis*, vol. 145, p. 104722, Jan. 2020, doi: 10.1016/j.jaap.2019.104722.

[41]  N. Borsodi, N. Miskolczi, A. Angyal, L. Bartha, and A. Lengyel, "Hydrocarbons obtained by pyrolysis of contaminated waste plastics," p. 10, 2011.

[42]  D. S. Achilias, C. Roupakias, P. Megalokonomos, A. A. Lappas, and E. V. Antonakou, "Chemical recycling of plastic wastes made from polyethylene (LDPE and HDPE) and polypropylene (PP)," *Journal of Hazardous Materials*, vol. 149, no. 3, pp. 536–542, Nov. 2007, doi: 10.1016/j.jhazmat.2007.06.076.

[43]  D. Chen, L. Yin, H. Wang, and P. He, "Pyrolysis technologies for municipal solid waste: A review," *Waste Management*, vol. 34, no. 12, pp. 2466–2486, Dec. 2014, doi: 10.1016/j.wasman.2014.08.004.

[44]  I. Velghe, R. Carleer, J. Yperman, and S. Schreurs, "Study of the pyrolysis of municipal solid waste for the production of valuable products," *Journal of Analytical and Applied Pyrolysis*, vol. 92, no. 2, pp. 366–375, Nov. 2011, doi: 10.1016/j.jaap.2011.07.011.

[45]  W. K. Buah, A. M. Cunliffe, and P. T. Williams, "Characterization of Products from the Pyrolysis of Municipal Solid Waste," *Process Safety and Environmental Protection*, vol. 85, no. 5, pp. 450–457, Jan. 2007, doi: 10.1205/psep07024.

[46]  K. Murata, K. Sato, and Y. Sakata, "Effect of pressure on thermal degradation of polyethylene," *Journal of Analytical and Applied Pyrolysis*, vol. 71, no. 2, pp. 569–589, Jun. 2004, doi: 10.1016/j.jaap.2003.08.010.

[47]  "Influence of time and temperature on pyrolysis of plastic wastes in a semi-batch reactor - ScienceDirect." https://www.sciencedirect.com/science/article/pii/S1385894711008643 (accessed Jul. 04, 2020).

[48]  S.-S. Kim and S. Kim, "Pyrolysis characteristics of polystyrene and polypropylene in a stirred batch reactor," *Chemical Engineering Journal*, vol. 98, no. 1, pp. 53–60, Mar. 2004, doi: 10.1016/S1385-8947(03)00184-0.

[49]  N. Miskolczi, A. Angyal, L. Bartha, and I. Valkai, "Fuels by pyrolysis of waste plastics from agricultural and packaging sectors in a pilot scale reactor," *Fuel Processing Technology*, vol. 90, no. 7, pp. 1032–1040, Jul. 2009, doi: 10.1016/j.fuproc.2009.04.019.

[50]  A. López, I. de Marco, B. M. Caballero, M. F. Laresgoiti, A. Adrados, and A. Aranzabal, "Catalytic pyrolysis of plastic wastes with two different types of catalysts: ZSM-5 zeolite and Red Mud," *Applied Catalysis B: Environmental*, vol. 104, no. 3, pp. 211–219, May 2011, doi: 10.1016/j.apcatb.2011.03.030.

[51] K.-H. Lee, "Thermal and catalytic degradation of pyrolytic oil from pyrolysis of municipal plastic wastes," *Journal of Analytical and Applied Pyrolysis*, vol. 85, no. 1, pp. 372–379, May 2009, doi: 10.1016/j.jaap.2008.11.032.

[52] M. del R. Hernández, A. Gómez, Á. N. García, J. Agulló, and A. Marcilla, "Effect of the temperature in the nature and extension of the primary and secondary reactions in the thermal and HZSM-5 catalytic pyrolysis of HDPE," *Applied Catalysis A: General*, vol. 317, no. 2, pp. 183–194, Feb. 2007, doi: 10.1016/j.apcata.2006.10.017.

[53] K.-H. Lee, "Effects of the types of zeolites on catalytic upgrading of pyrolysis wax oil," *Journal of Analytical and Applied Pyrolysis*, vol. 94, pp. 209–214, Mar. 2012, doi: 10.1016/j.jaap.2011.12.015.

[54] M. Sarker and M. M. Rashid, "Waste Plastics Mixture of Polystyrene and Polypropylene into Light Grade Fuel using Fe2O3 Catalyst," vol. 2, no. 1, p. 13, 2013.

[55] M. Syamsiro *et al.*, "Fuel Oil Production from Municipal Plastic Wastes in Sequential Pyrolysis and Catalytic Reforming Reactors," *Energy Procedia*, vol. 47, pp. 180–188, Jan. 2014, doi: 10.1016/j.egypro.2014.01.212.

[56] L. C. Lerici, M. S. Renzini, and L. B. Pierella, "Chemical Catalyzed Recycling of Polymers: Catalytic Conversion of PE, PP and PS into Fuels and Chemicals over H-Y," *Procedia Materials Science*, vol. 8, pp. 297–303, Jan. 2015, doi: 10.1016/j.mspro.2015.04.076.

[57] R. Miandad, M. A. Barakat, A. S. Aburiazaiza, M. Rehan, and A. S. Nizami, "Catalytic pyrolysis of plastic waste: A review," *Process Safety and Environmental Protection*, vol. 102, pp. 822–838, Jul. 2016, doi: 10.1016/j.psep.2016.06.022.

[58] Y. Sakata, M. A. Uddin, K. Koizumi, and K. Murata, "Thermal degradation of polyethylene mixed with poly(vinyl chloride) and poly(ethyleneterephthalate)," *Polymer Degradation and Stability*, vol. 53, no. 1, pp. 111–117, Jan. 1996, doi: 10.1016/0141-3910(96)00077-8.

[59] S. D. Anuar Sharuddin, F. Abnisa, W. M. A. Wan Daud, and M. K. Aroua, "A review on pyrolysis of plastic wastes," *Energy Conversion and Management*, vol. 115, pp. 308–326, May 2016, doi: 10.1016/j.enconman.2016.02.037.

[60] E. T. C. Vogt and B. M. Weckhuysen, "Fluid catalytic cracking: recent developments on the grand old lady of zeolite catalysis," *Chem. Soc. Rev.*, vol. 44, no. 20, pp. 7342–7370, Oct. 2015, doi: 10.1039/C5CS00376H.

[61] R. Yuan and Y. Shen, "Catalytic pyrolysis of biomass-plastic wastes in the presence of MgO and MgCO3 for hydrocarbon-rich oils production," *Bioresource Technology*, vol. 293, p. 122076, Dec. 2019, doi: 10.1016/j.biortech.2019.122076.

[62] R. Miandad, M. A. Barakat, M. Rehan, A. S. Aburiazaiza, I. M. I. Ismail, and A. S. Nizami, "Plastic waste to liquid oil through catalytic pyrolysis using natural and synthetic zeolite catalysts," *Waste Management*, vol. 69, pp. 66–78, Nov. 2017, doi: 10.1016/j.wasman.2017.08.032.

[63] L. Sokka, R. Antikainen, and P. E. Kauppi, "Municipal solid waste production and composition in Finland—Changes in the period 1960–2002 and prospects until 2020," *Resources, Conservation & Recycling*, vol. 50, no. 4, pp. 475–488, 2007, doi: 10.1016/j.resconrec.2007.01.011.

[64] S. Grierson, V. Strezov, G. Ellem, R. Mcgregor, and J. Herbertson, "Thermal characterisation of microalgae under slow pyrolysis conditions," *Journal of Analytical and Applied Pyrolysis*, vol. 85, no. 1, pp. 118–123, 2009, doi: https://doi.org/10.1016/j.jaap.2008.10.003.

[65] C. David, S. Salvador, J. L. Dirion, and M. Quintard, "Determination of a reaction scheme for cardboard thermal degradation using thermal gravimetric analysis," *Journal of Analytical and Applied Pyrolysis*, vol. 67, no. 2, pp. 307–323, 2003, doi: https://doi.org/10.1016/S0165-2370(02)00070-0.

[66] P. J. Mitchell, T. S. L. Dalley, and R. J. Helleur, "Preliminary laboratory production and characterization of biochars from lignocellulosic municipal waste," *Journal of Analytical and Applied Pyrolysis*, vol. 99, pp. 71–78, 2013, doi: https://doi.org/10.1016/j.jaap.2012.10.025.

[67] F. Sotoudehniakarani, A. Alayat, and A. G. McDonald, "Characterization and comparison of pyrolysis products from fast pyrolysis of commercial Chlorella vulgaris and cultivated microalgae," *Journal of Analytical and Applied Pyrolysis*, vol. 139, pp. 258–273, May 2019, doi: 10.1016/j.jaap.2019.02.014.

[68] J. A. Conesa, JoséA. Caballero, A. Marcilla, and R. Font, "Analysis of different kinetic models in the dynamic pyrolysis of cellulose," *Thermochimica Acta*, vol. 254, pp. 175–192, 1995, doi: https://doi.org/10.1016/0040-6031(94)02102-T.

[69] C. Wu, Z. Wang, J. Huang, and P. T. Williams, "Pyrolysis/gasification of cellulose, hemicellulose and lignin for hydrogen production in the presence of various nickel-based catalysts," *Fuel*, vol. 106, pp. 697–706, Apr. 2013, doi: 10.1016/J.FUEL.2012.10.064.

[70]   R. Ragucci, P. Giudicianni, and A. Cavaliere, "Cellulose slow pyrolysis products in a pressurized steam flow reactor," *Fuel*, vol. 107, pp. 122–130, May 2013, doi: 10.1016/J.FUEL.2013.01.057.

[71]   H. Yang, R. Yan, H. Chen, D. H. Lee, and C. Zheng, "Characteristics of hemicellulose, cellulose and lignin pyrolysis," vol. 86, no. 12–13, pp. 1781–1788, 2007, doi: 10.1016/j.fuel.2006.12.013.

[72]   S. Wang, X. Guo, T. Liang, Y. Zhou, and Z. Luo, "Mechanism research on cellulose pyrolysis by Py-GC/MS and subsequent density functional theory studies," *Bioresource Technology*, vol. 104, pp. 722–728, 2012, doi: https://doi.org/10.1016/j.biortech.2011.10.078.

[73]   X. Zhang, W. Yang, and W. Blasiak, "Thermal decomposition mechanism of levoglucosan during cellulose pyrolysis," *Journal of Analytical and Applied Pyrolysis*, vol. 96, pp. 110–119, Jul. 2012, doi: 10.1016/J.JAAP.2012.03.012.

[74]   L. Ghorbel, T. Rouissi, S. K. Brar, D. López-González, A. A. Ramirez, and S. Godbout, "Value-added performance of processed cardboard and farm breeding compost by pyrolysis," *Waste Management*, vol. 38, pp. 164–173, 2015, doi: https://doi.org/10.1016/j.wasman.2015.01.009.

[75]   A. G. Schoning, "Absorptiometric determination of acid-soluble lignin in semichemical bisulfite pulps and in some woods and plants," 1965.

[76]   A. O. Balogun, F. Sotoudehniakarani, and A. G. McDonald, "Thermo-kinetic, spectroscopic study of brewer's spent grains and characterisation of their pyrolysis products," *Journal of Analytical and Applied Pyrolysis*, vol. 127, pp. 8–16, Sep. 2017, doi: 10.1016/j.jaap.2017.09.009.

[77]   K. Iiyama and A. F. A. Wallis, "An improved acetyl bromide procedure for determining lignin in woods and wood pulps," *Wood Sci.Technol.*, vol. 22, no. 3, pp. 271–280, Sep. 1988, doi: 10.1007/BF00386022.

[78]   T. R. Green and R. Popa, "A Simple Assay for Monitoring Cellulose in Paper-Spiked Soil," *J Polym Environ*, vol. 18, no. 4, pp. 634–637, Dec. 2010, doi: 10.1007/s10924-010-0239-3.

[79]   Z. Xu *et al.*, "Properties of Torrefied U.S. Waste Blends," *Frontiers in Energy Research*, vol. 6, Jul. 2018, doi: 10.3389/fenrg.2018.00065.

[80]   A. O. Balogun, O. A. Lasode, and A. G. McDonald, "Thermochemical and pyrolytic analyses of Musa spp. residues from the rainforest belt of Nigeria," *Environmental*

*Progress & Sustainable Energy*, vol. 37, no. 6, pp. 1932–1941, 2018, doi: 10.1002/ep.12869.

[81] A. M. Alayat, F. Sotoudehniakarani, and A. G. McDonald, "Fermentation of Apple Pomace Using Mixed Microbial Culture to Organic Acids," p. 15, 2019.

[82] B. Lela, M. Barišić, and S. Nižetić, "Cardboard/sawdust briquettes as biomass fuel: Physical–mechanical and thermal characteristics," *Waste Management*, vol. 47, pp. 236–245, 2016, doi: https://doi.org/10.1016/j.wasman.2015.10.035.

[83] K. Ding, Z. Zhong, J. Wang, B. Zhang, M. Addy, and R. Ruan, "Effects of alkali-treated hierarchical HZSM-5 zeolites on the production of aromatic hydrocarbons from catalytic fast pyrolysis of waste cardboard," *Journal of Analytical and Applied Pyrolysis*, vol. 125, pp. 153–161, 2017, doi: https://doi.org/10.1016/j.jaap.2017.04.006.

[84] V. Dhyani and T. Bhaskar, "A comprehensive review on the pyrolysis of lignocellulosic biomass," *Renewable Energy*, vol. 129, pp. 695–716, Dec. 2018, doi: 10.1016/j.renene.2017.04.035.

[85] P. Grammelis, P. Basinas, A. Malliopoulou, and G. Sakellaropoulos, "Pyrolysis kinetics and combustion characteristics of waste recovered fuels," *Fuel*, vol. 88, no. 1, pp. 195–205, Jan. 2009, doi: 10.1016/j.fuel.2008.02.002.

[86] P. Nowicki, M. Supłat, J. Przepiórski, and R. Pietrzak, "NO2 removal on adsorbents obtained by pyrolysis and physical activation of corrugated cardboard," *Chemical Engineering Journal*, vol. 195–196, pp. 7–14, Jul. 2012, doi: 10.1016/j.cej.2012.04.073.

[87] D. Czajczyńska *et al.*, "Potentials of pyrolysis processes in the waste management sector," *Energy Procedia*, vol. 123, pp. 387–394, 2017, doi: https://doi.org/10.1016/j.egypro.2017.07.275.

[88] G. Leyssens, G. Trouvé, I. Caplain, C. Schönnenbeck, and F. Cazier, "Energetic performances and environmental impact of the combustion of cardboard/sawdust in a domestic boiler," *Fuel*, vol. 122, pp. 21–27, 2014, doi: https://doi.org/10.1016/j.fuel.2014.01.034.

[89] R. Yáñez, J. L. Alonso, and J. C. Parajó, "Production of hemicellulosic sugars and glucose from residual corrugated cardboard," *Process Biochemistry*, vol. 39, no. 11, pp. 1543–1551, Jul. 2004, doi: 10.1016/S0032-9592(03)00283-8.

[90] J. Young Jung, M. Suk Choi, and J.-K. Yang, "Optimization of Concentrated Acid Hydrolysis of Waste Paper Using Response Surface Methodology," *Journal of the Korean Wood Science and Technology*, vol. 41, Mar. 2013, doi: 10.5658/WOOD.2013.41.2.87.

[91] A. Patel, D. K. Sindhu, N. Arora, R. P. Singh, V. Pruthi, and P. A. Pruthi, "Biodiesel production from non-edible lignocellulosic biomass of Cassia fistula L. fruit pulp using oleaginous yeast Rhodosporidium kratochvilovae HIMPA1," *Bioresource Technology*, vol. 197, pp. 91–98, Dec. 2015, doi: 10.1016/j.biortech.2015.08.039.

[92] K. Raveendran, A. Ganesh, and K. C. Khilar, "Pyrolysis characteristics of biomass and biomass components," *Fuel*, vol. 75, no. 8, pp. 987–998, 1996, doi: https://doi.org/10.1016/0016-2361(96)00030-0.

[93] M. Hu *et al.*, "Thermogravimetric kinetics of lignocellulosic biomass slow pyrolysis using distributed activation energy model, Fraser–Suzuki deconvolution, and iso-conversional method," *Energy Conversion and Management*, vol. 118, pp. 1–11, Jun. 2016, doi: 10.1016/j.enconman.2016.03.058.

[94] W. Jin, K. Singh, and J. Zondlo, "Pyrolysis Kinetics of Physical Components of Wood and Wood-Polymers Using Isoconversion Method," *Agriculture*, vol. 3, no. 1, pp. 12–32, 2013, doi: 10.3390/agriculture3010012.

[95] L. Sanchez-Silva, D. López-González, J. Villaseñor, P. Sánchez, and J. L. Valverde, "Thermogravimetric–mass spectrometric analysis of lignocellulosic and marine biomass pyrolysis," *Bioresource Technology*, vol. 109, pp. 163–172, 2012, doi: https://doi.org/10.1016/j.biortech.2012.01.001.

[96] S. Wang, Q. Liu, Z. Luo, L. Wen, and K. Cen, "Mechanism study on cellulose pyrolysis using thermogravimetric analysis coupled with infrared spectroscopy," *Front. Energy Power Eng. China*, vol. 1, no. 4, pp. 413–419, Oct. 2007, doi: 10.1007/s11708-007-0060-8.

[97] L. M. Alvarenga, T. P. Xavier, M. A. S. Barrozo, M. S. Bacelos, and T. S. Lira, "Determination of activation energy of pyrolysis of carton packaging wastes and its pure components using thermogravimetry," *Waste Management*, vol. 53, pp. 68–75, 2016, doi: https://doi.org/10.1016/j.wasman.2016.04.015.

[98] J. Y. Yeo, B. L. F. Chin, J. K. Tan, and Y. S. Loh, "Comparative studies on the pyrolysis of cellulose, hemicellulose, and lignin based on combined kinetics," *Journal of the Energy Institute*, vol. 92, no. 1, pp. 27–37, Feb. 2019, doi: 10.1016/j.joei.2017.12.003.

[99]    F. Shafizadeh, R. H. Furneaux, T. G. Cochran, J. P. Scholl, and Y. Sakai, "Production of levoglucosan and glucose from pyrolysis of cellulosic materials," *Journal of Applied Polymer Science*, vol. 23, no. 12, pp. 3525–3539, 1979, doi: 10.1002/app.1979.070231209.

[100]   J. Piskorz, D. Radlein, and D. S. Scott, "On the mechanism of the rapid pyrolysis of cellulose," *Journal of Analytical and Applied Pyrolysis*, vol. 9, no. 2, pp. 121–137, Jan. 1986, doi: 10.1016/0165-2370(86)85003-3.

[101]   B. R. T. Simoneit *et al.*, "Levoglucosan, a tracer for cellulose in biomass burning and atmospheric particles," *Atmospheric Environment*, vol. 33, no. 2, pp. 173–182, Jan. 1999, doi: 10.1016/S1352-2310(98)00145-9.

[102]   J. Wang, Q. Wei, J. Zheng, and M. Zhu, "Effect of pyrolysis conditions on levoglucosan yield from cotton straw and optimization of levoglucosan extraction from bio-oil," *Journal of Analytical and Applied Pyrolysis*, vol. 122, pp. 294–303, Nov. 2016, doi: 10.1016/j.jaap.2016.09.013.

[103]   Y. B. Yang, A. N. Phan, C. Ryu, V. Sharifi, and J. Swithenbank, "Mathematical modelling of slow pyrolysis of segregated solid wastes in a packed-bed pyrolyser," *Fuel*, vol. 86, no. 1, pp. 169–180, Jan. 2007, doi: 10.1016/j.fuel.2006.07.012.

[104]   C. E. Brewer, "Biochar characterization and engineering," Iowa State University, 2012.

[105]   A. Amin, A. Gadallah, A. K. El Morsi, N. N. El-Ibiari, and G. I. El-Diwani, "Experimental and empirical study of diesel and castor biodiesel blending effect, on kinematic viscosity, density and calorific value," *Egyptian Journal of Petroleum*, vol. 25, no. 4, pp. 509–514, Dec. 2016, doi: 10.1016/j.ejpe.2015.11.002.

[106]   X. Wang, F. Sotoudehniakarani, Z. Yu, J. J. Morrell, J. Cappellazzi, and A. G. McDonald, "Evaluation of corrugated cardboard biochar as reinforcing fiber on properties, biodegradability and weatherability of wood-plastic composites," *Polymer Degradation and Stability*, vol. 168, p. 108955, Oct. 2019, doi: 10.1016/j.polymdegradstab.2019.108955.

[107]   I. Fonts, M. Azuara, G. Gea, and M. B. Murillo, "Study of the pyrolysis liquids obtained from different sewage sludge," *Journal of Analytical and Applied Pyrolysis*, vol. 85, no. 1, pp. 184–191, 2009, doi: https://doi.org/10.1016/j.jaap.2008.11.003.

[108]   H. Lu, W. Zhang, S. Wang, L. Zhuang, Y. Yang, and R. Qiu, "Characterization of sewage sludge-derived biochars from different feedstocks and pyrolysis temperatures,"

*Journal of Analytical and Applied Pyrolysis*, vol. 102, pp. 137–143, 2013, doi: https://doi.org/10.1016/j.jaap.2013.03.004.

[109] M. K. Hossain, V. Strezov, K. Y. Chan, A. Ziolkowski, and P. F. Nelson, "Influence of pyrolysis temperature on production and nutrient properties of wastewater sludge biochar," *Journal of Environmental Management*, vol. 92, no. 1, pp. 223–228, 2011, doi: https://doi.org/10.1016/j.jenvman.2010.09.008.

[110] K. B. Cantrell, P. G. Hunt, M. Uchimiya, J. M. Novak, and K. S. Ro, "Impact of pyrolysis temperature and manure source on physicochemical characteristics of biochar," *Bioresource Technology*, vol. 107, pp. 419–428, 2012, doi: https://doi.org/10.1016/j.biortech.2011.11.084.

[111] M. Uchimiya, L. H. Wartelle, K. T. Klasson, C. A. Fortier, and I. M. Lima, "Influence of Pyrolysis Temperature on Biochar Property and Function as a Heavy Metal Sorbent in Soil," *Journal of Agricultural and Food Chemistry*, vol. 59, no. 6, pp. 2501–2510, 2011, doi: 10.1021/jf104206c.

[112] K. L. Iroba and Tabil, "Photoacoustic Spectroscopy in the Assessment of the Quantitative Composition of the Biomass — Barley Straw," *Biofuels - Status and Perspective*, Sep. 2015, doi: 10.5772/59225.

[113] H. Yuan, T. Lu, Y. Wang, H. Huang, and Y. Chen, "Influence of pyrolysis temperature and holding time on properties of biochar derived from medicinal herb (radix isatidis) residue and its effect on soil CO2 emission," *Journal of Analytical and Applied Pyrolysis*, vol. 110, pp. 277–284, 2014, doi: https://doi.org/10.1016/j.jaap.2014.09.016.

[114] G. Zhang, Q. Zhang, K. Sun, X. Liu, W. Zheng, and Y. Zhao, "Sorption of simazine to corn straw biochars prepared at different pyrolytic temperatures," *Environmental Pollution*, vol. 159, no. 10, pp. 2594–2601, 2011, doi: https://doi.org/10.1016/j.envpol.2011.06.012.

[115] D. Angın, "Effect of pyrolysis temperature and heating rate on biochar obtained from pyrolysis of safflower seed press cake," *Bioresource Technology*, vol. 128, pp. 593–597, 2013, doi: https://doi.org/10.1016/j.biortech.2012.10.150.

[116] J. McDonald-Wharry, M. Manley-Harris, and K. Pickering, "Carbonisation of biomass-derived chars and the thermal reduction of a graphene oxide sample studied using Raman spectroscopy," *Carbon*, vol. 59, pp. 383–405, Aug. 2013, doi: 10.1016/j.carbon.2013.03.033.

[117] L. Zhao, X. Cao, O. Mašek, and A. Zimmerman, "Heterogeneity of biochar properties as a function of feedstock sources and production temperatures," *Journal of Hazardous Materials*, vol. 256–257, pp. 1–9, Jul. 2013, doi: 10.1016/j.jhazmat.2013.04.015.

[118] Y.-K. Park *et al.*, "Wild reed of Suncheon Bay: Potential bio-energy source," *Renewable Energy*, vol. 42, pp. 168–172, Jun. 2012, doi: 10.1016/j.renene.2011.08.025.

[119] R. Xiao and W. Yang, "Influence of temperature on organic structure of biomass pyrolysis products," *Renewable Energy*, vol. 50, pp. 136–141, Feb. 2013, doi: 10.1016/j.renene.2012.06.028.

[120] H. S. Heo *et al.*, "Bio-oil production from fast pyrolysis of waste furniture sawdust in a fluidized bed," *Bioresource Technology*, vol. 101, no. 1, Supplement, pp. S91–S96, Jan. 2010, doi: 10.1016/j.biortech.2009.06.003.

[121] L. Wei *et al.*, "Production and characterization of bio-oil and biochar from the pyrolysis of residual bacterial biomass from a polyhydroxyalkanoate production process," *Journal of Analytical and Applied Pyrolysis*, vol. 115, pp. 268–278, Sep. 2015, doi: 10.1016/j.jaap.2015.08.005.

[122] Z. Hu, Y. Zheng, F. Yan, B. Xiao, and S. Liu, "Bio-oil production through pyrolysis of blue-green algae blooms (BGAB): Product distribution and bio-oil characterization," *Energy*, vol. 52, no. Supplement C, pp. 119–125, 2013, doi: https://doi.org/10.1016/j.energy.2013.01.059.

[123] H. N. Almeida *et al.*, "Characterization and pyrolysis of Chlorella vulgaris and Arthrospira platensis: potential of bio-oil and chemical production by Py-GC/MS analysis," *Environmental Science and Pollution Research*, vol. 24, no. 16, pp. 14142–14150, Jun. 2017, doi: 10.1007/s11356-017-9009-2.

[124] "I. Chemical, Crystallographical and Physical Properties of Liquid Paraffins and Paraffin Waxes," *Developments in Petroleum Science*, vol. 14, pp. 13–140, Jan. 1982, doi: 10.1016/S0376-7361(08)70146-8.

[125] E. Önal, B. B. Uzun, and A. E. Pütün, "Bio-oil production via co-pyrolysis of almond shell as biomass and high density polyethylene," *Energy Conversion and Management*, vol. 78, pp. 704–710, Feb. 2014, doi: 10.1016/j.enconman.2013.11.022.

[126] B. Biswal, S. Kumar, and R. K. Singh, "Production of Hydrocarbon Liquid by Thermal Pyrolysis of Paper Cup Waste," *Journal of Waste Management*, 2013. https://www.hindawi.com/journals/jwm/2013/731858/ (accessed May 25, 2020).

[127] J. F. Mastral, C. Berrueco, and J. Ceamanos, "Theoretical prediction of product distribution of the pyrolysis of high density polyethylene," *Journal of Analytical and Applied Pyrolysis*, vol. 80, no. 2, pp. 427–438, Oct. 2007, doi: 10.1016/j.jaap.2006.07.009.

[128] A. Pattiya, "Bio-oil production via fast pyrolysis of biomass residues from cassava plants in a fluidised-bed reactor," *Bioresource Technology*, vol. 102, no. 2, pp. 1959–1967, Jan. 2011, doi: 10.1016/j.biortech.2010.08.117.

[129] M. Brebu, S. Ucar, C. Vasile, and J. Yanik, "Co-pyrolysis of pine cone with synthetic polymers," *Fuel*, vol. 89, no. 8, pp. 1911–1918, Aug. 2010, doi: 10.1016/j.fuel.2010.01.029.

[130] C. Dong, Y. Yang, B. Jin, and M. Horio, "The pyrolysis of sawdust and polyethylene in TG and U-shape tube reactor," *Waste Management*, vol. 27, no. 11, pp. 1557–1561, Jan. 2007, doi: 10.1016/j.wasman.2006.10.021.

[131] F. Abnisa and W. M. A. Wan Daud, "A review on co-pyrolysis of biomass: An optional technique to obtain a high-grade pyrolysis oil," *Energy Conversion and Management*, vol. 87, pp. 71–85, Nov. 2014, doi: 10.1016/j.enconman.2014.07.007.

[132] P. Rutkowski and A. Kubacki, "Influence of polystyrene addition to cellulose on chemical structure and properties of bio-oil obtained during pyrolysis," *Energy Conversion and Management*, vol. 47, no. 6, pp. 716–731, Apr. 2006, doi: 10.1016/j.enconman.2005.05.017.

[133] T. Cornelissen, J. Yperman, G. Reggers, S. Schreurs, and R. Carleer, "Flash co-pyrolysis of biomass with polylactic acid. Part 1: Influence on bio-oil yield and heating value," *Fuel*, vol. 87, no. 7, pp. 1031–1041, Jun. 2008, doi: 10.1016/j.fuel.2007.07.019.

[134] M. K. D. Rambo, M. M. C. Ferreira, M. K. D. Rambo, and M. M. C. Ferreira, "Determination of Cellulose Crystallinity of Banana Residues Using Near Infrared Spectroscopy and Multivariate Analysis," *Journal of the Brazilian Chemical Society*, vol. 26, no. 7, pp. 1491–1499, Jul. 2015, doi: 10.5935/0103-5053.20150118.

[135] K. Karimi and M. J. Taherzadeh, "A critical review of analytical methods in pretreatment of lignocelluloses: Composition, imaging, and crystallinity," *Bioresource Technology*, vol. 200, pp. 1008–1018, Jan. 2016, doi: 10.1016/j.biortech.2015.11.022.

[136] J. H. Flynn, "The isoconversional method for determination of energy of activation at constant heating rates," *Journal of thermal analysis*, vol. 27, no. 1, pp. 95–102, May 1983, doi: 10.1007/BF01907325.

[137] C. D. DOYLE, "Series Approximations to the Equation of Thermogravimetric Data," *Nature*, vol. 207, p. 290, Jul. 1965.

[138] Ö. Çepelioğullar and A. E. Pütün, "Thermal and kinetic behaviors of biomass and plastic wastes in co-pyrolysis," *Energy Conversion and Management*, vol. 75, pp. 263–270, Nov. 2013, doi: 10.1016/j.enconman.2013.06.036.

[139] B. L. F. Chin, S. Yusup, A. Al Shoaibi, P. Kannan, C. Srinivasakannan, and S. A. Sulaiman, "Kinetic studies of co-pyrolysis of rubber seed shell with high density polyethylene," *Energy Conversion and Management*, vol. 87, pp. 746–753, Nov. 2014, doi: 10.1016/j.enconman.2014.07.043.

[140] M. Brebu and C. Vasile, "Thermal Degredation of Lignin - A Review," p. 11.

[141] A. Aboulkas, K. El harfi, and A. El Bouadili, "Thermal degradation behaviors of polyethylene and polypropylene. Part I: Pyrolysis kinetics and mechanisms," *Energy Conversion and Management*, vol. 51, no. 7, pp. 1363–1369, Jul. 2010, doi: 10.1016/j.enconman.2009.12.017.

[142] Y. Wang, S.-T. Zhang, Y.-F. Zhang, and N. Deng, "Gas formation characteristics during low temperature pyrolysis of municipal household garbage," *Ranliao Huaxue Xuebao/Journal of Fuel Chemistry and Technology*, vol. 33, pp. 62–67, Feb. 2005.

[143] A. López, I. de Marco, B. M. Caballero, M. F. Laresgoiti, and A. Adrados, "Pyrolysis of municipal plastic wastes: Influence of raw material composition," *Waste Management*, vol. 30, no. 4, pp. 620–627, Apr. 2010, doi: 10.1016/j.wasman.2009.10.014.

[144] E. M. Grieco and G. Baldi, "Pyrolysis of polyethylene mixed with paper and wood: Interaction effects on tar, char and gas yields," *Waste Management*, vol. 32, no. 5, pp. 833–839, May 2012, doi: 10.1016/j.wasman.2011.12.014.

[145] M. Arabiourrutia, G. Elordi, G. Lopez, E. Borsella, J. Bilbao, and M. Olazar, "Characterization of the waxes obtained by the pyrolysis of polyolefin plastics in a conical spouted bed reactor," *Journal of Analytical and Applied Pyrolysis*, vol. 94, pp. 230–237, Mar. 2012, doi: 10.1016/j.jaap.2011.12.012.

[146] S. Adhikari, H. Nam, and J. P. Chakraborty, "Chapter 8 - Conversion of Solid Wastes to Fuels and Chemicals Through Pyrolysis," in *Waste Biorefinery*, T. Bhaskar, A. Pandey, S. V. Mohan, D.-J. Lee, and S. K. Khanal, Eds. Elsevier, 2018, pp. 239–263.

[147] S. Liang, Y. Han, L. Wei, and A. G. McDonald, "Production and characterization of bio-oil and bio-char from pyrolysis of potato peel wastes," *Biomass Conv. Bioref.*, vol. 5, no. 3, pp. 237–246, Sep. 2015, doi: 10.1007/s13399-014-0130-x.

[148] Z. Wang *et al.*, "Effect of Cellulose Crystallinity on Solid/Liquid Phase Reactions Responsible for the Formation of Carbonaceous Residues during Pyrolysis," Feb. 10, 2014. https://pubs.acs.org/doi/pdf/10.1021/ie4014259 (accessed Apr. 19, 2020).

[149] S. H. Kim, C. M. Lee, and K. Kafle, "Characterization of crystalline cellulose in biomass: Basic principles, applications, and limitations of XRD, NMR, IR, Raman, and SFG," *Korean J. Chem. Eng.*, vol. 30, no. 12, pp. 2127–2141, Dec. 2013, doi: 10.1007/s11814-013-0162-0.

[150] C. Mukarakate *et al.*, "Influence of Crystal Allomorph and Crystallinity on the Products and Behavior of Cellulose during Fast Pyrolysis," *ACS Sustainable Chem. Eng.*, vol. 4, no. 9, pp. 4662–4674, Sep. 2016, doi: 10.1021/acssuschemeng.6b00812.

[151] L. M. Flórez Pardo, J. G. Salcedo Mendoza, and J. E. López Galán, "INFLUENCE OF PRETREATMENTS ON CRYSTALLINITY AND ENZYMATIC HYDROLYSIS IN SUGAR CANE RESIDUES," *Brazilian Journal of Chemical Engineering*, vol. 36, no. 1, pp. 131–141, Mar. 2019, doi: 10.1590/0104-6632.20190361s20180093.

[152] "Unraveling variations of crystalline cellulose induced by ionic liquid and their effects on enzymatic hydrolysis | Scientific Reports." https://www.nature.com/articles/s41598-017-09885-9 (accessed Feb. 29, 2020).

[153] S. Darmawan, N. J. Wistara, G. Pari, A. Maddu, and W. Syafii, "Characterization of Lignocellulosic Biomass as Raw Material for the Production of Porous Carbon-based Materials," *BioResources*, vol. 11, no. 2, Art. no. 2, Feb. 2016.

[154] J. Liang, J. Chen, S. Wu, C. Liu, and M. Lei, "Comprehensive insights into cellulose structure evolution via multi-perspective analysis during a slow pyrolysis process," *Sustainable Energy Fuels*, vol. 2, no. 8, pp. 1855–1862, Jul. 2018, doi: 10.1039/C8SE00166A.

[155] M. Sahai, A. Kumar, and S. Kumar, "Crystal structure of fractionally crystallized waxes isolated from crude oil," *J Appl Cryst*, vol. 50, no. 2, Art. no. 2, Apr. 2017, doi: 10.1107/S1600576717000711.

[156] J. Yiming *et al.*, "A new bio-based organogel for the removal of wax coating from indoor bronze surfaces," *Herit Sci*, vol. 7, no. 1, p. 34, May 2019, doi: 10.1186/s40494-019-0276-8.

[157] M. Poletto, H. L. Ornaghi, and A. J. Zattera, "Native Cellulose: Structure, Characterization and Thermal Properties," *Materials (Basel)*, vol. 7, no. 9, pp. 6105–6119, Aug. 2014, doi: 10.3390/ma7096105.

[158] F. Sotoudehnia, E. Mengistie, A. Alayat, and A. G. McDonald, "Valorization of waste waxed corrugated cardboard via pyrolysis for recovering wax," *Environmental Progress & Sustainable Energy*, 11.25.2020, issue e13566, doi.org/10.1002/ep.13566.

[159] E. Stauffer, J. A. Dolan, and R. Newman, *Fire Debris Analysis*. Academic Press, 2007.

[160] A. Galadima and O. Muraza, "Zeolite catalysts in upgrading of bioethanol to fuels range hydrocarbons: A review," *Journal of Industrial and Engineering Chemistry*, vol. 31, pp. 1–14, Nov. 2015, doi: 10.1016/j.jiec.2015.07.015.

[161] J. Agullo *et al.*, "Catalytic pyrolysis of low density polyethylene over H-β, H-Y, H-Mordenite, and H-Ferrierite zeolite catalysts: Influence of acidity and structures," 2007, doi: 10.1134/S002315840704009X.

[162] T. Standring, S. Blackburn, and P. Wilson, "Investigation into Paraffin Wax and Ethylene Vinyl Acetate Blends for Use as a Carrier Vehicle in Ceramic Injection Molding," *Polymer-Plastics Technology and Engineering*, vol. 55, no. 8, pp. 802–817, May 2016, doi: 10.1080/03602559.2015.1132434.

[163] W. Ciesińska, B. Liszyńska, and J. Zieliński, "Selected thermal properties of polyethylene waxes," *J Therm Anal Calorim*, vol. 125, no. 3, pp. 1439–1443, Sep. 2016, doi: 10.1007/s10973-016-5706-1.

[164] H.-S. Hwang, S. Kim, M. Singh, J. K. Winkler-Moser, and S. X. Liu, "Organogel Formation of Soybean Oil with Waxes," *J Am Oil Chem Soc*, vol. 89, no. 4, pp. 639–647, Apr. 2012, doi: 10.1007/s11746-011-1953-2.

[165] M. Gönen, D. Balköse, F. İnal, and S. Ülkü, "The effect of zinc stearate on thermal degradation of paraffin wax," *J Therm Anal Calorim*, vol. 94, no. 3, pp. 737–742, Dec. 2008, doi: 10.1007/s10973-008-9365-8.

[166] R. Aguado, M. Olazar, San José María J., B. Gaisán, and J. Bilbao, "Wax Formation in the Pyrolysis of Polyolefins in a Conical Spouted Bed Reactor," *Energy Fuels*, vol. 16, no. 6, pp. 1429–1437, Nov. 2002, doi: 10.1021/ef020043w.

[167] C. Vélez, M. Khayet, and J. M. Ortiz de Zárate, "Temperature-dependent thermal properties of solid/liquid phase change even-numbered n-alkanes: n-Hexadecane, n-octadecane and n-eicosane," *Applied Energy*, vol. 143, pp. 383–394, Apr. 2015, doi: 10.1016/j.apenergy.2015.01.054.

[168] N. Ukrainczyk, S. Kurajica, and J. Sipusic, "Thermophysical Comparison of Five Commercial Paraffin Waxes as Latent Heat Storage Materials," *Chemical and Biochemical Engineering Quarterly*, vol. 24, Jul. 2010, doi: 10.15255/CABEQ.2014.240.

[169] M. A. AlMaadeed, S. Labidi, I. Krupa, and M. Ouederni, "Effect of waste wax and chain structure on the mechanical and physical properties of polyethylene," *Arabian Journal of Chemistry*, vol. 8, no. 3, pp. 388–399, May 2015, doi: 10.1016/j.arabjc.2014.01.006.

[170] Z. Wu, W. Zhou, X. Hao, and X. Zhang, "Plasma reforming of n-pentane as a simulated gasoline to hydrogen and cleaner carbon-based fuels," *Energy*, vol. 189, p. 116265, Dec. 2019, doi: 10.1016/j.energy.2019.116265.

[171] Y. Shitao, X. Cao, S. Wu, Q. Chen, L. Li, and H. Li, "Effective pyrolysis of waste cooking oils into hydrocarbon rich biofuel on novel mesoporous catalyst with acid and alkali coexisting," *Industrial Crops and Products*, vol. 150, p. 112362, Aug. 2020, doi: 10.1016/j.indcrop.2020.112362.

[172] A. Hassani, "Pyrolysis of plastic waste into green fuels–experimental study," Master's Thesis, Universitetet i Sørøst-Norge, 2018.

[173] N. Mishra, N. Patra, S. Pandey, M. Salerno, M. Sharon, and M. Sharon, "Taguchi method optimization of wax production from pyrolysis of waste polypropylene," *Journal of Thermal Analysis & Calorimetry*, vol. 117, no. 2, pp. 885–892, Aug. 2014, doi: 10.1007/s10973-014-3793-4.

[174] A. R. Chowdhury, G. Sabat, N. Gouda, and A. K. Panda, "Production of hydrocarbon rich fuel from abandoned beehive by pyrolysis," *Environmental Progress & Sustainable Energy*, vol. 40, no. 1, p. e13472, Jan. 2021, doi: 10.1002/ep.13472.

[175] A. López, I. de Marco, B. M. Caballero, M. F. Laresgoiti, A. Adrados, and A. Torres, "Pyrolysis of municipal plastic wastes II: Influence of raw material composition under catalytic conditions," *Waste Management*, vol. 31, no. 9, pp. 1973–1983, Sep. 2011, doi: 10.1016/j.wasman.2011.05.021.

[176] T. Sangpatch, N. Supakata, V. Kanokkantapong, and B. Jongsomjit, "Fuel oil generated from the cogon grass-derived Al–Si (Imperata cylindrica (L.) Beauv) catalysed pyrolysis of waste plastics," *Heliyon*, vol. 5, no. 8, Aug. 2019, doi: 10.1016/j.heliyon.2019.e02324.

[177] L. Zhang, Z. Bao, S. Xia, Q. Lu, and K. B. Walters, "Catalytic Pyrolysis of Biomass and Polymer Wastes," *Catalysts*, vol. 8, no. 12, Art. no. 12, Dec. 2018, doi: 10.3390/catal8120659.

[178] X. Li, B. Shen, Q. Guo, and J. Gao, "Effects of large pore zeolite additions in the catalytic pyrolysis catalyst on the light olefins production," *Catalysis Today*, vol. 125, no. 3, pp. 270–277, Jul. 2007, doi: 10.1016/j.cattod.2007.03.021.

[179] J. F. Mastral, C. Berrueco, M. Gea, and J. Ceamanos, "Catalytic degradation of high density polyethylene over nanocrystalline HZSM-5 zeolite," *Polymer Degradation and Stability*, vol. 91, no. 12, pp. 3330–3338, Dec. 2006, doi: 10.1016/j.polymdegradstab.2006.06.009.

[180] G. Luo and A. G. McDonald, "Conversion of Methanol and Glycerol into Gasoline via ZSM-5 Catalysis," *Energy Fuels*, vol. 28, no. 1, pp. 600–606, Jan. 2014, doi: 10.1021/ef401993x.

[181] R. Bagri and P. T. Williams, "Catalytic pyrolysis of polyethylene," *Journal of Analytical and Applied Pyrolysis*, vol. 63, no. 1, pp. 29–41, Mar. 2002, doi: 10.1016/S0165-2370(01)00139-5.

[182] E. Calabrò and S. Magazù, "FTIR Spectroscopy Analysis of Molecular Vibrations in Gasoline Fuel Under 200 mT Static Magnetic Field Highlighted Structural Changes of Hydrocarbons Chains," *Petroleum Science and Technology*, vol. 33, no. 19, pp. 1676–1684, Oct. 2015, doi: 10.1080/10916466.2015.1089282.

[183] K. B. Beć and C. W. Huck, "Breakthrough Potential in Near-Infrared Spectroscopy: Spectra Simulation. A Review of Recent Developments," *Front Chem*, vol. 7, Feb. 2019, doi: 10.3389/fchem.2019.00048.

[184] S. Corsetti, F. M. Zehentbauer, D. McGloin, and J. Kiefer, "Characterization of gasoline/ethanol blends by infrared and excess infrared spectroscopy," *Fuel*, vol. 141, pp. 136–142, Feb. 2015, doi: 10.1016/j.fuel.2014.10.025.

[185] A. Asghari, M. K. Khorrami, and A. B. Garmarudi, "Comparison between partial least square and support vector regression with a genetic algorithm wavelength selection method for the simultaneous determination of some oxygenate compounds in gasoline by FTIR spectroscopy," *Infrared Physics & Technology*, vol. 105, p. 103177, Mar. 2020, doi: 10.1016/j.infrared.2019.103177.

[186] M. A. Al-Ghouti, Y. S. Al-Degs, and M. Amer, "Determination of motor gasoline adulteration using FTIR spectroscopy and multivariate calibration," *Talanta*, vol. 76, no. 5, pp. 1105–1112, Sep. 2008, doi: 10.1016/j.talanta.2008.05.024.

[187] A. Iob, R. Buenafe, and N. M. Abbas, "Determination of oxygenates in gasoline by FTIR," *Fuel*, vol. 77, no. 15, pp. 1861–1864, Dec. 1998, doi: 10.1016/S0016-2361(98)00103-3.

[188] M. K. Trivedi, A. Branton, D. Trivedi, G. Nayak, K. Bairwa, and S. Jana, "Impact of Biofield Treatment on Spectroscopic and Physicochemical Properties of p-Nitroaniline," *Insights in Analytical Electrochemistry*, vol. 1, no. 1, Sep. 2015, Accessed: Feb. 19, 2021. [Online]. Available: https://hal.archives-ouvertes.fr/hal-01435927.

[189] J. Dadson, S. Pandam, and N. Asiedu, "Modeling the characteristics and quantification of adulterants in gasoline using FTIR spectroscopy and chemometric calibrations," *Cogent Chemistry*, vol. 4, no. 1, p. 1482637, Jan. 2018, doi: 10.1080/23312009.2018.1482637.

## Appendix: Analytical Methods

**Calorific value**

The calorific values samples (in duplicate) were determined by bomb calorimetry using a Parr oxygen bomb calorimeter (model no. 1261) in accordance with ASTM D5865-04. A Carver Laboratory hydraulic press (1,500 MPa) was utilized to press pre-dried samples (1.0 g) into pellets (6 mm Ø) for analysis.

**Differential Scanning Calorimetry (DSC)**

DSC analysis of the wax-oil samples, paraffin wax, and extracted wax were conducted in duplicates using a Perkin Elmer DSC-7 instrument (Shelton, CT, USA). Approximately 6 mg of sample was scanned from 25 °C to 100 °C at a heating rate of 10 °C min$^{-1}$, under nitrogen (20 ml min$^{-1}$), and data were analyzed using the Pyris v.13.3.1 software. Percent crystallinity of the wax was determined using the equation below:

Equation 3

$$X_c = \frac{\Delta H_m}{\Delta H_0} \ x \ 100\%$$

$X_c$ is the percent crystallinity of the wax, $\Delta H_m$ is the melting enthalpy or enthalpy of fusion calculated from the area under the peak, and $\Delta H_0$ is the theoretical enthalpy of fusion for paraffin wax (210 J g$^{-1}$).

**Electrospray Ionization-Mass Spectrometry (ESI-MS)**

Negative ion ESI-MS was used to determine the molar mass of samples using a Finnigan LCQ-Deca instrument (ThermoQuest). The samples (1 mg mL$^{-1}$) in methanol containing 1% acetic acid and were subjected to ESI–MS (*m/z* 100–2,000) for 3 mins at a flow rate of 10 μL min$^{-1}$. The ion source and capillary voltages were optimized using a reserpine standard and the instrument autotune function at 4.5 kV and -20 V at 275°C, respectively. The MS data (averaged over 3 min run) were analyzed using the Xcalibur software (v2.2) and transferred to Microsoft Excel$^{TM}$ to calculate the number average molar mass (*M$_n$*) as $M_n =$

$\sum N_i M_i / \sum N_i$ and the weight average molar mass ($M_w$) as $M_w = \sum N_i M_i^2 / \sum N_i M_i$ where $N_i$ is the intensity of ions and $M_i$ is the mass after accounting for the charge.

**Fatty Acid Methyl Ester (FAME) analysis**

Lipids were identified using their FAME derivatives. The samples (2 mg) were heated in a sealed 5 mL reacti-vial[TM] for 90 min at 90 °C in a mixture of methanol/sulfuric acid/chloroform (1.7:0.3:2.0 v/v/v, 2 mL) to convert to their FAME derivatives. Chloroform contained 1-naphthaleneacetic acid as an internal standard (200 µg mL^{-1}). Water was then added to the cooled vial, and after vigorous shaking, the organic layer was collected and dried over anhydrous sodium sulfate. The FAME compounds were analyzed by gas chromatography-mass spectrometry (GC–MS) using a FOCUS-ISQ (ThermoScientific) system at a temperature gradient of 40 °C (1 min) to 320 °C at 5 °C min^{-1} equipped with a ZB-5 (30 m x 0.25 mmØ, 0.25 µm coating, Phenomenex) capillary column. The eluted compounds were identified with authentic $C_{12}$ to $C_{20}$ fatty acid standards and by spectral matching with the 2017 NIST mass spectral library.

**Fourier Transform InfraRed (FTIR) spectroscopy**

FTIR spectra were obtained, in quadruplicate, for the original, biochar, and bio-oil samples using a Thermo-Nicolet iS5 spectrometer equipped with a ZnSe attenuated total reflection (iD5 ATR) accessory. FTIR spectra were baseline corrected and averaged using the Omnic v9 software (Thermo-Nicolet).

**Gas Chromatography-Mass Spectrometry (GC-MS)**

The fresh bio-oils (1 mg in dichloromethane (1 mL) containing anthracene or trichlorobenzene (100 µg mL^{-1}) as an internal standard) were analyzed in duplicate by GC-MS (Focus-ISQ, ThermoScientific). Separation was achieved on ZB-5 capillary column (30 m × 0.25 mm Ø, 0.25 µm coating, Phenomenex) using a temperature program of 40 °C (1 min) to 320 °C at 5 °C min^{-1}.

**High-Performance Liquid Chromatography (HPLC)**

The fresh bio-oils were analyzed for organic acids and anhydro-sugars by HPLC, in triplicate, using a Rezex ROA organic acid column (7.8 × 30 cm, Phenomenex) equipped with a differential refractive index detector (Shodex SE31), on elution with 0.005 N aqueous sulfuric acid (0.5 mL min$^{-1}$) at 65 °C. The identity of the compounds was determined by retention time against authentic standards (formic acid, acetic acid, propionic acid, methanol, levoglucosan, furfurol, furfural, hydroxymethyfurfural, glycerol, glucose, and xylose).

Lignin and carbohydrate analysis

The extractive free samples were analyzed for lignin and carbohydrate contents. Klason and acid soluble lignin were determined by digesting extractive-free CCB (200 mg) with sulphuric acid (2 ml, 72%) for 60 min at 30 ºC, followed by secondary hydrolysis (4% sulfuric acid, 30 min, 121ºC) in an autoclave according to ASTM D 1106-96. Klason lignin content was determined gravimetrically after filtration. Acid soluble lignin was determined by absorbance at 205 nm of the filtered hydrolysate (made up to 250 mL) using an absorption coefficient of 110 L g-1 cm-1 (Biomate 5, Thermoelectron) [75]. Carbohydrate analysis was performed on the hydrolysis filtrate (5 mL) according to ASTM E 1758-01. The monosaccharides were quantified by HPLC (two Rezex RPM columns, 7.8 mm x 300 mm, Phenomenex) at 85 ºC on elution with water (0.5 mL min-1) using differential refractive index detection (Waters model 2414) [76]. Total lignin was also determined, in duplicate, using acetyl bromide / UV absorbance method [77]. Oven-dry and extractive-free CCB (5 mg) was incubated with acetyl bromide (25% w/w) in acetic acid (5 mL) together with perchloric acid (0.2 mL, 70%) at 70 °C for 60 min. The solutions were made up to 100 mL containing 2M sodium hydroxide (10 mL) and acetic acid (25 mL). Absorbance at 280 nm was measured (Biomate 5, ThermoElectron) and lignin content was determined using an absorptivity of lignin (ε) of 20.09 L g-1 cm-1. Total carbohydrate content was also determined, in duplicate, using a modified phenol-sulfuric acid colorimetric method [78]. Oven-dry CCB (10 mg) and cellulose standard (Sigmacell type 101, 2 to 10 mg) were incubated in sulfuric acid (100 µL, 77%) and then phenol in water (1 mL, 5%) and subsequently concentrated sulfuric acid (5 mL) were added. Absorbance at 490 nm was measured (Biomate 5, Thermoelectron).

**Moisture content (solid)**

The moisture content of the CCB was determined prior to the extraction using Mettler Toledo moisture analyzer. About 4 grams of samples were Soxhlet extracted using dichloromethane (150 mL) for 16 h and lipid (extractives) content was determined gravimetrically, according to ASTM D1108-96.

**pH, moisture content (liquid)**

The pH value of the pyrolysis bio-oil was measured with a portable pH meter (Orion-3-Star). The water content of the bio-oils was determined on a Mettler model V30 Karl Fischer titrator.

**Proximate and ultimate analysis**

Proximate analysis was performed on samples following ASTM E870-82 to identify ash, volatile matter (VM), and fixed carbon (FC) contents. For FC and VM, samples were combusted at 950 °C in a muffle furnace for 7 min. The ash content was determined after furnacing at 600 °C for at least 16 h. A Costech ESC 4010 elemental analyzer was used to determine carbon (C), nitrogen (N), and hydrogen (H) contents.

**Py-GCMS analysis**

Analytical pyrolysis was performed on samples at 500 °C (in duplicate) using a Pyrojector II unit (SGE Analytical Science) coupled to a GC-MS (Focus-ISQ, Thermo Scientific). The compounds were separated on the ZB-5 capillary column (30 m × 0.25 mm Ø, 0.25 µm coating, Phenomenex) from 50 (1 min) to 250 °C (10 min) at 5°C min$^{-1}$. The eluted compounds were identified by their mass spectra, authentic standards, and NIST 2017 library matching. The abundance of each compound was calculated relative to the carbon dioxide peak.

**Raman spectroscopy**

Raman spectra (3 replicates) were recorded on an Alpha 300R Raman microscope (Witec) at 532 nm excitation and the spectra averaged and baseline corrected. The ratio of D

(disordered, 1355 cm$^{-1}$)/G (graphitic, 1580 cm$^{-1}$) band intensities ($I_D/I_G$) was used to calculate an estimation of disordered carbon in the biochar [67].

**Scanning Electron Microscopy (SEM)**

SEM was performed on carbon-coated samples using a Zeiss Supra 55 VP-FEG instrument [Carl Zeiss LLC, White Plains, NY] at either 5 or 10 kV. The average fiber length and width were determined using at least 50 values obtained from the fibers present in each image.

**Surface area analyses**

The specific surface areas ($S_{BET}$) of all degassed char samples (0.25 g, in duplicate) were measured on a Micromeritics FlowSorb 2300 instrument according to ASTM D6556-10.

**ThermoGravimetric Analysis (TGA)**

TGA was performed on samples (5-6 mg) using a PerkinElmer TGA-7 instrument from 30 to 900 ºC at heating rates (β) of 5, 10, 15, 20, and 25 °C min$^{-1}$ under nitrogen (30 mL min$^{-1}$) to determine activation energy (*E*) and thermal degradation behavior [28][29]. The TGA and differential thermogravimetric (DTG) data were analyzed using Pyris v11 software.

The *E* was calculated using a model-free technique (Flynn-Wall-Ozawa's (FWO) method [136], [137]) that relied on TGA data. Isothermal TGA was also used to estimate the char mass yield of samples during pyrolysis at given temperatures. The temperature was ramped from 30 °C to 450, 500 and 550 °C at 200 °C min$^{-1}$ and then maintained for 60 min.

**Wax extraction**

The WCCB sample (4.0 g) was Soxhlet extracted in duplicate using $CH_2Cl_2$ (150 mL) for 16 h, and wax content was determined gravimetrically, according to ASTM D1108-96.

**X-Ray Diffraction (XRD)**

Carbonyl index (CI), cellulose index (CeI), and hydroxyl index (HI) were calculated as the ratio of the band intensity (absorbance) at 1,720, 1,024, and 3,342 cm$^{-1}$, respectively, to the band 2,916 cm$^{-1}$ for the -$CH_2$- group [79]. The cellulose crystallinity index (CCI) was determined from the XRD (Siemens D5000 diffractometer; 5 to 55º using 0.05º steps). CCI

was determined from the ratio of the integral intensities, after peak fitting and amorphous baseline subtraction using IgorPro v8 software, of crystalline portions to the total intensity of sample according to $CCI = (1 - (I_{am}/I_{002}))$, where $I_{am}$ is the intensity of the peak at $2\theta = 16°$ and $I_{002}$ is the maximum intensity of the (002) plane diffraction at $2\theta = 22°$ [80], [81].

XRD analysis on wax-free WCCB and char were performed on a Siemens D5000 diffractometer using Cu-Ka radiation (wavelength of 0.1542 nm) from $2\theta = 2$ to $80°$ at $0.01°$ steps. The crystallinity index (CI) for cellulose (CIc) and wax (CIw) were determined using the adjusted deconvolution method [134][135].

Equation 4

$$CI = \left(\frac{\sum A_{cry}}{\sum A_{cry} + \sum A_{am}}\right) x\ 100$$

Where $A_{cry}$ is the adjusted crystalline peak area, and $A_{am}$ is the adjusted broad peak area of the amorphous component. Crystalline peaks for cellulose are found at 101 and 200, and peaks for wax are found at 004, 011, 020, 310, and 311.